

## EUROPEAN ORGANIZATION FOR NUCLEAR RESEARCH

LEPEWWG/2003-01  
ALEPH 2003-006 PHYSIC 2003-003  
DELPHI 2003-08 PHYS 930  
L3 Note 2797  
OPAL TN 735  
8 April 2003

# A Combination of Preliminary Electroweak Measurements and Constraints on the Standard Model

The LEP Collaborations\* ALEPH, DELPHI, L3, OPAL,  
the LEP Electroweak Working Group<sup>†</sup>  
and the SLD Heavy Flavour Group<sup>‡</sup>

Prepared from Contributions of the LEP and SLD Experiments  
to the 2003 Winter Conferences.

---

\*The LEP Collaborations each take responsibility for the preliminary results of their own experiment.

<sup>†</sup>WWW access at <http://www.cern.ch/LEPEWWG>

The members of the LEP Electroweak Working Group who contributed significantly to this note are:  
D. Abbaneo, J. Alcaraz, P. Antilogus, A. Bajo-Vaquero, P. Bambade, E. Barberio, A. Blondel, S. Blyth, D. Bourilkov,  
P. Checchia, R. Chierici, R. Clare, B. de la Cruz, G. Della Ricca, E. Delmeire, M. Dierckxsens, D. Duchesneau, G. Duck-  
eck, M. Elsing, P. Garcia-Abia, C. Goy, M.W. Grunewald, A. Gurtu, J.B. Hansen, R. Hawkings, J. Holt, St. Jezequel,  
R.W.L. Jones, T. Kawamoto, B. Kersevan, W. Kittel, N. Kjaer, E. Lançon, W. Liebig, L. Malgeri, C. Mariotti, M. Mar-  
tinez, F. Matorras, C. Matteuzzi, S. Mele, E. Migliore, M.N. Minard, K. Mönig, C. Parkes, U. Parzefall, P. Perez,  
M. Pepe-Altarelli, B. Pietrzyk, G. Quast, P. Renton, S. Riemann, K. Sachs, T. Schoerner-Sadenius, A. Straessner,  
D. Strom, R. Tenchini, F. Teubert, S. Todorova-Nova, E. Tournefier, A. Valassi, A. Venturi, C.P. Ward, N.K. Watson,  
St. Wynhoff.

<sup>‡</sup>N. de Groot, P.C. Rowson, B. Schumm, D. Su.

## Abstract

This note presents a combination of published and preliminary electroweak results from the four LEP collaborations and the SLD collaboration which were prepared for the 2003 winter conferences. Averages from Z resonance results are derived for hadronic and leptonic cross sections, the leptonic forward-backward asymmetries, the  $\tau$  polarisation asymmetries, the  $b\bar{b}$  and  $c\bar{c}$  partial widths and forward-backward asymmetries and the  $q\bar{q}$  charge asymmetry. Above the Z resonance, averages are derived for di-fermion cross sections and forward-backward asymmetries, photon-pair, W-pair, Z-pair, single-W and single-Z cross sections, electroweak gauge boson couplings, W mass and width and W decay branching ratios. Also, an investigation of the interference of photon and Z-boson exchange is presented, and colour reconnection and Bose-Einstein correlation analyses in W-pair production are combined. The main changes with respect to the experimental results presented in summer 2002 are updates to the mass of the W boson measured at LEP-2.

The results are compared with precise electroweak measurements from other experiments, notably the recent final result on the electroweak mixing angle determined in neutrino-nucleon scattering by the NuTeV collaboration and the new result in atomic parity violation in Caesium. The parameters of the Standard Model are evaluated, first using the combined LEP electroweak measurements, and then using the full set of electroweak results.

# Chapter 1

## Introduction

This paper presents an update of combined results on electroweak parameters by the four LEP experiments and SLD using published and preliminary measurements, superseding previous analyses [1]. Results derived from the Z resonance are based on data recorded until the end of 1995 for the LEP experiments and 1998 for SLD. Since 1996 LEP has run at energies above the W-pair production threshold. In 2000, the final year of data taking at LEP, the total delivered luminosity was as high as in 1999; the maximum centre-of-mass energy attained was close to 209 GeV although most of the data taken in 2000 was collected at 205 and 207 GeV. By the end of LEP-II operation, a total integrated luminosity of approximately  $700\text{pb}^{-1}$  per experiment has been recorded above the Z resonance.

The LEP-I (1990-1995) Z-pole measurements consist of the hadronic and leptonic cross sections, the leptonic forward-backward asymmetries, the  $\tau$  polarisation asymmetries, the  $b\bar{b}$  and  $c\bar{c}$  partial widths and forward-backward asymmetries and the  $q\bar{q}$  charge asymmetry. The measurements of the left-right cross section asymmetry, the  $b\bar{b}$  and  $c\bar{c}$  partial widths and left-right-forward-backward asymmetries for b and c quarks from SLD are treated consistently with the LEP data. Many technical aspects of their combination are described in References 2, 3 and references therein.

The LEP-II (1996-2000) measurements are di-fermion cross sections and forward-backward asymmetries; di-photon production, W-pair, Z-pair, single-W and single-Z production cross sections, and electroweak gauge boson self couplings. W boson properties, like mass, width and decay branching ratios are also measured. New studies on photon/Z interference in fermion-pair production as well as on colour reconnection and Bose-Einstein correlations in W-pair production are presented.

Several measurements included in the combinations are still preliminary.

This note is organised as follows:

**Chapter 2** Z line shape and leptonic forward-backward asymmetries;

**Chapter 3**  $\tau$  polarisation;

**Chapter 4** Measurement of polarised asymmetries at SLD;

**Chapter 5** Heavy flavour analyses;

**Chapter 6** Inclusive hadronic charge asymmetry;

**Chapter 7** Photon-pair production at energies above the Z;

- Chapter 8** Fermion-pair production at energies above the Z;
- Chapter 9** Photon/Z-boson interference;
- Chapter 10** W and four-fermion production;
- Chapter 11** Electroweak gauge boson self couplings;
- Chapter 12** Colour reconnection in W-pair events;
- Chapter 13** Bose-Einstein correlations in W-pair events;
- Chapter 14** W-boson mass and width;
- Chapter 15** Interpretation of the Z-pole results in terms of effective couplings of the neutral weak current;
- Chapter 16** Interpretation of all results, also including results from neutrino interaction and atomic parity violation experiments as well as from CDF and DØ in terms of constraints on the Standard Model
- Chapter 17** Conclusions including prospects for the future.

To allow a quick assessment, a box highlighting the updates is given at the beginning of each chapter.

## Chapter 2

# Z Lineshape and Lepton Forward-Backward Asymmetries

### Updates with respect to summer 2002:

Unchanged w.r.t. summer 2000: All experiments have published final results which enter in the combination. The final combination procedure is used, the obtained averages are final.

The results presented here are based on the full LEP-I data set. This includes the data taken during the energy scans in 1990 and 1991 in the range<sup>1</sup>  $|\sqrt{s} - m_Z| < 3$  GeV, the data collected at the Z peak in 1992 and 1994 and the precise energy scans in 1993 and 1995 ( $|\sqrt{s} - m_Z| < 1.8$  GeV). The total event statistics are given in Table 2.1. Details of the individual analyses can be found in References 4–7.

$q\bar{q}$						$\ell^+\ell^-$					
year	A	D	L	O	all	year	A	D	L	O	all
'90/91	433	357	416	454	1660	'90/91	53	36	39	58	186
'92	633	697	678	733	2741	'92	77	70	59	88	294
'93	630	682	646	649	2607	'93	78	75	64	79	296
'94	1640	1310	1359	1601	5910	'94	202	137	127	191	657
'95	735	659	526	659	2579	'95	90	66	54	81	291
total	4071	3705	3625	4096	15497	total	500	384	343	497	1724

Table 2.1: The  $q\bar{q}$  and  $\ell^+\ell^-$  event statistics, in units of  $10^3$ , used for the analysis of the Z line shape and lepton forward-backward asymmetries by the experiments ALEPH (A), DELPHI (D), L3 (L) and OPAL (O).

For the averaging of results the LEP experiments provide a standard set of 9 parameters describing the information contained in hadronic and leptonic cross sections and leptonic forward-backward asymmetries. These parameters are convenient for fitting and averaging since they have small correlations. They are:

- The mass  $m_Z$  and total width  $\Gamma_Z$  of the Z boson, where the definition is based on the Breit-Wigner denominator ( $s - m_Z^2 + is\Gamma_Z/m_Z$ ) with  $s$ -dependent width [8].

<sup>1</sup>In this note  $\hbar = c = 1$ .

- The hadronic pole cross section of Z exchange:

$$\sigma_h^0 \equiv \frac{12\pi}{m_Z^2} \frac{\Gamma_{ee}\Gamma_{\text{had}}}{\Gamma_Z^2}. \quad (2.1)$$

Here  $\Gamma_{ee}$  and  $\Gamma_{\text{had}}$  are the partial widths of the Z for decays into electrons and hadrons.

- The ratios:

$$R_e^0 \equiv \Gamma_{\text{had}}/\Gamma_{ee}, \quad R_\mu^0 \equiv \Gamma_{\text{had}}/\Gamma_{\mu\mu} \text{ and } R_\tau^0 \equiv \Gamma_{\text{had}}/\Gamma_{\tau\tau}. \quad (2.2)$$

Here  $\Gamma_{\mu\mu}$  and  $\Gamma_{\tau\tau}$  are the partial widths of the Z for the decays  $Z \rightarrow \mu^+\mu^-$  and  $Z \rightarrow \tau^+\tau^-$ . Due to the mass of the  $\tau$  lepton, a difference of 0.2% is expected between the values for  $R_e^0$  and  $R_\mu^0$ , and the value for  $R_\tau^0$ , even under the assumption of lepton universality [9].

- The pole asymmetries,  $A_{\text{FB}}^{0,e}$ ,  $A_{\text{FB}}^{0,\mu}$  and  $A_{\text{FB}}^{0,\tau}$ , for the processes  $e^+e^- \rightarrow e^+e^-$ ,  $e^+e^- \rightarrow \mu^+\mu^-$  and  $e^+e^- \rightarrow \tau^+\tau^-$ . In terms of the real parts of the effective vector and axial-vector neutral current couplings of fermions,  $g_{Vf}$  and  $g_{Af}$ , the pole asymmetries are expressed as

$$A_{\text{FB}}^{0,f} \equiv \frac{3}{4} \mathcal{A}_e \mathcal{A}_f \quad (2.3)$$

with

$$\mathcal{A}_f \equiv \frac{2g_{Vf}g_{Af}}{g_{Vf}^2 + g_{Af}^2} = 2 \frac{g_{Vf}/g_{Af}}{1 + (g_{Vf}/g_{Af})^2}. \quad (2.4)$$

The imaginary parts of the vector and axial-vector coupling constants as well as real and imaginary parts of the photon vacuum polarisation are taken into account explicitly in the fitting formulae and are fixed to their Standard Model values. The fitting procedure takes into account the effects of initial-state radiation [8] to  $\mathcal{O}(\alpha^3)$  [10–12], as well as the  $t$ -channel and the  $s$ - $t$  interference contributions in the case of  $e^+e^-$  final states.

The set of 9 parameters does not describe hadron and lepton-pair production completely, because it does not include the interference of the  $s$ -channel Z exchange with the  $s$ -channel  $\gamma$  exchange. For the results presented in this section and used in the rest of the note, the  $\gamma$ -exchange contributions and the hadronic  $\gamma$ Z interference terms are fixed to their Standard Model values. The leptonic  $\gamma$ Z interference terms are expressed in terms of the effective couplings.

The four sets of nine parameters provided by the LEP experiments are presented in Table 2.2. For performing the average over these four sets of nine parameters, the overall covariance matrix is constructed from the covariance matrices of the individual LEP experiments and taking into account common systematic errors [2]. The common systematic errors include theoretical errors as well as errors arising from the uncertainty in the LEP beam energy. The beam energy uncertainty contributes an uncertainty of  $\pm 1.7$  MeV to  $m_Z$  and  $\pm 1.2$  MeV to  $\Gamma_Z$ . In addition, the uncertainty in the centre-of-mass energy spread of about  $\pm 1$  MeV contributes  $\pm 0.2$  MeV to  $\Gamma_Z$ . The theoretical error on calculations of the small-angle Bhabha cross section is  $\pm 0.054\%$  [13] for OPAL and  $\pm 0.061\%$  [14] for all other experiments, and results in the largest common systematic uncertainty on  $\sigma_h^0$ . QED radiation, dominated by photon radiation from the initial state electrons, contributes a common uncertainty of  $\pm 0.02\%$  on  $\sigma_h^0$ , of  $\pm 0.3$  MeV on  $m_Z$  and of  $\pm 0.2$  MeV on  $\Gamma_Z$ . The contribution of  $t$ -channel diagrams and the  $s$ - $t$  interference in  $Z \rightarrow e^+e^-$  leads to an additional theoretical uncertainty estimated to be  $\pm 0.024$  on  $R_e^0$  and  $\pm 0.0014$  on  $A_{\text{FB}}^{0,e}$ , which are fully anti-correlated. Uncertainties from the model-independent parameterisation of the energy dependence of the cross section are almost negligible, if the definitions of Reference [15] are applied. Through unavoidable remaining Standard Model

		correlations								
		$m_Z$	$\Gamma_Z$	$\sigma_h^0$	$R_e^0$	$R_\mu^0$	$R_\tau^0$	$A_{\text{FB}}^{0,e}$	$A_{\text{FB}}^{0,\mu}$	$A_{\text{FB}}^{0,\tau}$
$\chi^2/N_{\text{df}} = 169/176$		ALEPH								
$m_Z$ [GeV]	$91.1891 \pm 0.0031$	1.00								
$\Gamma_Z$ [GeV]	$2.4959 \pm 0.0043$	.038	1.00							
$\sigma_h^0$ [nb]	$41.558 \pm 0.057$	-.091	-.383	1.00						
$R_e^0$	$20.690 \pm 0.075$	.102	.004	.134	1.00					
$R_\mu^0$	$20.801 \pm 0.056$	-.003	.012	.167	.083	1.00				
$R_\tau^0$	$20.708 \pm 0.062$	-.003	.004	.152	.067	.093	1.00			
$A_{\text{FB}}^{0,e}$	$0.0184 \pm 0.0034$	-.047	.000	-.003	-.388	.000	.000	1.00		
$A_{\text{FB}}^{0,\mu}$	$0.0172 \pm 0.0024$	.072	.002	.002	.019	.013	.000	-.008	1.00	
$A_{\text{FB}}^{0,\tau}$	$0.0170 \pm 0.0028$	.061	.002	.002	.017	.000	.011	-.007	.016	1.00
$\chi^2/N_{\text{df}} = 177/168$		DELPHI								
$m_Z$ [GeV]	$91.1864 \pm 0.0028$	1.00								
$\Gamma_Z$ [GeV]	$2.4876 \pm 0.0041$	.047	1.00							
$\sigma_h^0$ [nb]	$41.578 \pm 0.069$	-.070	-.270	1.00						
$R_e^0$	$20.88 \pm 0.12$	.063	.000	.120	1.00					
$R_\mu^0$	$20.650 \pm 0.076$	-.003	-.007	.191	.054	1.00				
$R_\tau^0$	$20.84 \pm 0.13$	.001	-.001	.113	.033	.051	1.00			
$A_{\text{FB}}^{0,e}$	$0.0171 \pm 0.0049$	.057	.001	-.006	-.106	.000	-.001	1.00		
$A_{\text{FB}}^{0,\mu}$	$0.0165 \pm 0.0025$	.064	.006	-.002	.025	.008	.000	-.016	1.00	
$A_{\text{FB}}^{0,\tau}$	$0.0241 \pm 0.0037$	.043	.003	-.002	.015	.000	.012	-.015	.014	1.00
$\chi^2/N_{\text{df}} = 158/166$		L3								
$m_Z$ [GeV]	$91.1897 \pm 0.0030$	1.00								
$\Gamma_Z$ [GeV]	$2.5025 \pm 0.0041$	.065	1.00							
$\sigma_h^0$ [nb]	$41.535 \pm 0.054$	.009	-.343	1.00						
$R_e^0$	$20.815 \pm 0.089$	.108	-.007	.075	1.00					
$R_\mu^0$	$20.861 \pm 0.097$	-.001	.002	.077	.030	1.00				
$R_\tau^0$	$20.79 \pm 0.13$	.002	.005	.053	.024	.020	1.00			
$A_{\text{FB}}^{0,e}$	$0.0107 \pm 0.0058$	-.045	.055	-.006	-.146	-.001	-.003	1.00		
$A_{\text{FB}}^{0,\mu}$	$0.0188 \pm 0.0033$	.052	.004	.005	.017	.005	.000	.011	1.00	
$A_{\text{FB}}^{0,\tau}$	$0.0260 \pm 0.0047$	.034	.004	.003	.012	.000	.007	-.008	.006	1.00
$\chi^2/N_{\text{df}} = 155/194$		OPAL								
$m_Z$ [GeV]	$91.1858 \pm 0.0030$	1.00								
$\Gamma_Z$ [GeV]	$2.4948 \pm 0.0041$	.049	1.00							
$\sigma_h^0$ [nb]	$41.501 \pm 0.055$	.031	-.352	1.00						
$R_e^0$	$20.901 \pm 0.084$	.108	.011	.155	1.00					
$R_\mu^0$	$20.811 \pm 0.058$	.001	.020	.222	.093	1.00				
$R_\tau^0$	$20.832 \pm 0.091$	.001	.013	.137	.039	.051	1.00			
$A_{\text{FB}}^{0,e}$	$0.0089 \pm 0.0045$	-.053	-.005	.011	-.222	-.001	.005	1.00		
$A_{\text{FB}}^{0,\mu}$	$0.0159 \pm 0.0023$	.077	-.002	.011	.031	.018	.004	-.012	1.00	
$A_{\text{FB}}^{0,\tau}$	$0.0145 \pm 0.0030$	.059	-.003	.003	.015	-.010	.007	-.010	.013	1.00

Table 2.2: Line Shape and asymmetry parameters from fits to the data of the four LEP experiments and their correlation coefficients.

assumptions, dominated by the need to fix the  $\gamma$ -Z interference contribution in the  $q\bar{q}$  channel, there is some small dependence of  $\pm 0.2$  MeV of  $m_Z$  on the Higgs mass,  $m_H$  (in the range 100 GeV to 1000 GeV) and the value of the electromagnetic coupling constant. Such “parametric” errors are negligible for the other results. The combined parameter set and its correlation matrix are given in Table 2.3.

If lepton universality is assumed, the set of 9 parameters is reduced to a set of 5 parameters.

without lepton universality		correlations								
$\chi^2/N_{\text{df}} = 32.6/27$		$m_Z$	$\Gamma_Z$	$\sigma_h^0$	$R_e^0$	$R_\mu^0$	$R_\tau^0$	$A_{\text{FB}}^{0,e}$	$A_{\text{FB}}^{0,\mu}$	$A_{\text{FB}}^{0,\tau}$
$m_Z$ [GeV]	$91.1876 \pm 0.0021$	1.00								
$\Gamma_Z$ [GeV]	$2.4952 \pm 0.0023$	-.024	1.00							
$\sigma_h^0$ [nb]	$41.541 \pm 0.037$	-.044	-.297	1.00						
$R_e^0$	$20.804 \pm 0.050$	.078	-.011	.105	1.00					
$R_\mu^0$	$20.785 \pm 0.033$	.000	.008	.131	.069	1.00				
$R_\tau^0$	$20.764 \pm 0.045$	.002	.006	.092	.046	.069	1.00			
$A_{\text{FB}}^{0,e}$	$0.0145 \pm 0.0025$	-.014	.007	.001	-.371	.001	.003	1.00		
$A_{\text{FB}}^{0,\mu}$	$0.0169 \pm 0.0013$	.046	.002	.003	.020	.012	.001	-.024	1.00	
$A_{\text{FB}}^{0,\tau}$	$0.0188 \pm 0.0017$	.035	.001	.002	.013	-.003	.009	-.020	.046	1.00
with lepton universality										
$\chi^2/N_{\text{df}} = 36.5/31$		$m_Z$	$\Gamma_Z$	$\sigma_h^0$	$R_\ell^0$	$A_{\text{FB}}^{0,\ell}$				
$m_Z$ [GeV]	$91.1875 \pm 0.0021$	1.00								
$\Gamma_Z$ [GeV]	$2.4952 \pm 0.0023$	-.023	1.00							
$\sigma_h^0$ [nb]	$41.540 \pm 0.037$	-.045	-.297	1.00						
$R_\ell^0$	$20.767 \pm 0.025$	.033	.004	.183	1.00					
$A_{\text{FB}}^{0,\ell}$	$0.0171 \pm 0.0010$	.055	.003	.006	-.056	1.00				

Table 2.3: Average line shape and asymmetry parameters from the data of the four LEP experiments, without and with the assumption of lepton universality.

$R_\ell^0$  is defined as  $R_\ell^0 \equiv \Gamma_{\text{had}}/\Gamma_{\ell\ell}$ , where  $\Gamma_{\ell\ell}$  refers to the partial Z width for the decay into a pair of massless charged leptons. The data of each of the four LEP experiments are consistent with lepton universality (the difference in  $\chi^2$  over the difference in d.o.f. with and without the assumption of lepton universality is 3/4, 6/4, 5/4 and 3/4 for ALEPH, DELPHI, L3 and OPAL, respectively). The lower part of Table 2.3 gives the combined result and the corresponding correlation matrix. Figure 2.1 shows, for each lepton species and for the combination assuming lepton universality, the resulting 68% probability contours in the  $R_\ell^0$ - $A_{\text{FB}}^{0,\ell}$  plane. Good agreement is observed.

For completeness the partial decay widths of the Z boson are listed in Table 2.4, although they are more correlated than the ratios given in Table 2.3. The leptonic pole cross-section,  $\sigma_\ell^0$ , defined as

$$\sigma_\ell^0 \equiv \frac{12\pi}{m_Z^2} \frac{\Gamma_{\ell\ell}^2}{\Gamma_Z^2}, \quad (2.5)$$

in analogy to  $\sigma_h^0$ , is shown in the last line of the Table. Because QCD final state corrections appear twice in the denominator via  $\Gamma_Z$ ,  $\sigma_\ell^0$  has a higher sensitivity to  $\alpha_s$  than  $\sigma_h^0$  or  $R_\ell^0$ , where the dependence on QCD corrections is only linear.

## 2.1 Number of Neutrino Species

An important aspect of our measurement concerns the information related to Z decays into invisible channels. Using the results of Table 2.3, the ratio of the Z decay width into invisible particles and the leptonic decay width is determined:

$$\Gamma_{\text{inv}}/\Gamma_{\ell\ell} = 5.942 \pm 0.016. \quad (2.6)$$



without lepton universality		correlations			
		$\Gamma_{\text{had}}$	$\Gamma_{ee}$	$\Gamma_{\mu\mu}$	$\Gamma_{\tau\tau}$
$\Gamma_{\text{had}}$ [MeV]	$1745.8 \pm 2.7$	1.00			
$\Gamma_{ee}$ [MeV]	$83.92 \pm 0.12$	-0.29	1.00		
$\Gamma_{\mu\mu}$ [MeV]	$83.99 \pm 0.18$	0.66	-0.20	1.00	
$\Gamma_{\tau\tau}$ [MeV]	$84.08 \pm 0.22$	0.54	-0.17	0.39	1.00
with lepton universality		correlations			
		$\Gamma_{\text{inv}}$	$\Gamma_{\text{had}}$	$\Gamma_{\ell\ell}$	
$\Gamma_{\text{inv}}$ [MeV]	$499.0 \pm 1.5$	1.00			
$\Gamma_{\text{had}}$ [MeV]	$1744.4 \pm 2.0$	-0.29	1.00		
$\Gamma_{\ell\ell}$ [MeV]	$83.984 \pm 0.086$	0.49	0.39	1.00	
$\Gamma_{\text{inv}}/\Gamma_{\ell\ell}$	$5.942 \pm 0.016$				
$\sigma_\ell^0$ [nb]	$2.0003 \pm 0.0027$				

Table 2.4: Partial decay widths of the Z boson, derived from the results of the 9-parameter averages in Table 2.3. In the case of lepton universality,  $\Gamma_{\ell\ell}$  refers to the partial Z width for the decay into a pair of massless charged leptons.

The Standard Model value for the ratio of the partial widths to neutrinos and charged leptons is:

$$(\Gamma_{\nu\nu}/\Gamma_{\ell\ell})_{\text{SM}} = 1.9912 \pm 0.0012. \quad (2.7)$$

The central value is evaluated for  $m_Z = 91.1875$  GeV and the error quoted accounts for a variation of  $m_t$  in the range  $m_t = 174.3 \pm 5.1$  GeV and a variation of  $m_H$  in the range  $100 \text{ GeV} \leq m_H \leq 1000 \text{ GeV}$ . The number of light neutrino species is given by the ratio of the two expressions listed above:

$$N_\nu = 2.9841 \pm 0.0083, \quad (2.8)$$

which is two standard deviations below the value of 3 expected from 3 observed fermion families.

Alternatively, one can assume 3 neutrino species and determine the width from additional invisible decays of the Z. This yields

$$\Delta\Gamma_{\text{inv}} = -2.7 \pm 1.6 \text{ MeV}. \quad (2.9)$$

The measured total width is below the Standard Model expectation. If a conservative approach is taken to limit the result to only positive values of  $\Delta\Gamma_{\text{inv}}$  and normalising the probability for  $\Delta\Gamma_{\text{inv}} \geq 0$  to be unity, then the resulting 95% CL upper limit on additional invisible decays of the Z is

$$\Delta\Gamma_{\text{inv}} < 2.0 \text{ MeV}. \quad (2.10)$$

The theoretical error on the luminosity [14] constitutes a large part of the uncertainties on  $N_\nu$  and  $\Delta\Gamma_{\text{inv}}$ .

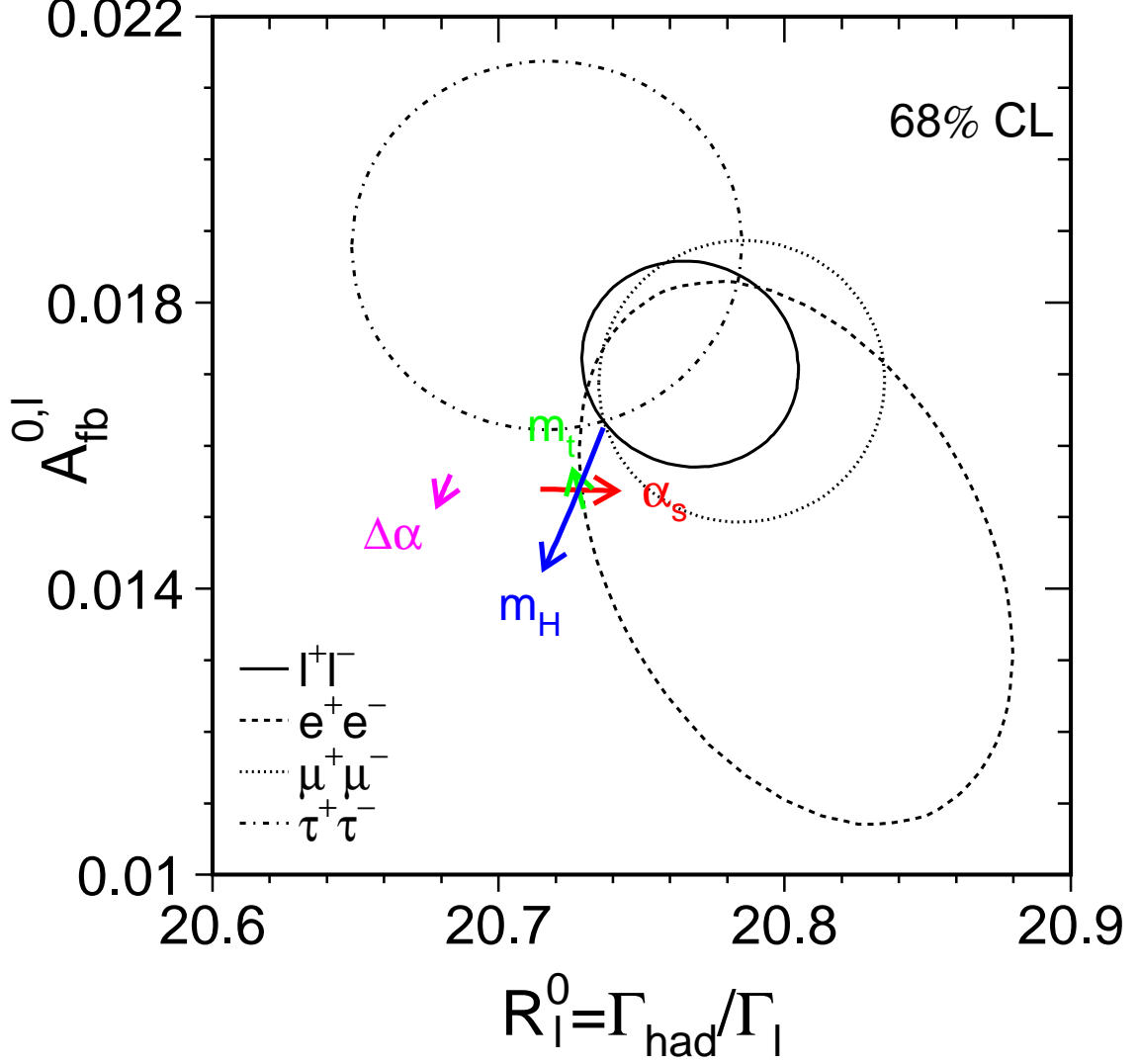


Figure 2.1: Contours of 68% probability in the  $R_\ell^0 - A_{\text{FB}}^{0,\ell}$  plane. For better comparison the results for the  $\tau$  lepton are corrected to correspond to the massless case. The Standard Model prediction for  $m_Z = 91.1875$  GeV,  $m_t = 174.3$  GeV,  $m_H = 300$  GeV, and  $\alpha_S(m_Z^2) = 0.118$  is also shown. The lines with arrows correspond to the variation of the Standard Model prediction when  $m_t$ ,  $m_H$ ,  $\alpha_S(m_Z^2)$  and  $\Delta\alpha_{\text{had}}^{(5)}(m_Z^2)$  are varied in the intervals  $m_t = 174.3 \pm 5.1$  GeV,  $m_H = 300_{-186}^{+700}$  GeV,  $\alpha_S(m_Z^2) = 0.118 \pm 0.002$  and  $\Delta\alpha_{\text{had}}^{(5)}(m_Z^2) = 0.02761 \pm 0.00036$ , respectively. The arrows point in the direction of increasing values of  $m_t$ ,  $m_H$ ,  $\alpha_S$  and  $\Delta\alpha_{\text{had}}^{(5)}(m_Z^2)$ .

# Chapter 3

## The $\tau$ Polarisation

### Updates with respect to summer 2002:

Unchanged w.r.t. summer 2002: All experiments have published final results which enter the combination. The final combination procedure is used, the obtained averages are final.

The longitudinal  $\tau$  polarisation  $\mathcal{P}_\tau$  of  $\tau$  pairs produced in Z decays is defined as

$$\mathcal{P}_\tau \equiv \frac{\sigma_R - \sigma_L}{\sigma_R + \sigma_L}, \quad (3.1)$$

where  $\sigma_R$  and  $\sigma_L$  are the  $\tau$ -pair cross sections for the production of a right-handed and left-handed  $\tau^-$ , respectively. The distribution of  $\mathcal{P}_\tau$  as a function of the polar scattering angle  $\theta$  between the  $e^-$  and the  $\tau^-$ , at  $\sqrt{s} = m_Z$ , is given by

$$\mathcal{P}_\tau(\cos \theta) = -\frac{\mathcal{A}_\tau(1 + \cos^2 \theta) + 2\mathcal{A}_e \cos \theta}{1 + \cos^2 \theta + 2\mathcal{A}_\tau \mathcal{A}_e \cos \theta}, \quad (3.2)$$

with  $\mathcal{A}_e$  and  $\mathcal{A}_\tau$  as defined in Equation (2.4). Equation (3.2) is valid for pure Z exchange. The effects of  $\gamma$  exchange,  $\gamma$ -Z interference and electromagnetic radiative corrections in the initial and final states are taken into account in the experimental analyses. In particular, these corrections account for the  $\sqrt{s}$  dependence of the  $\tau$  polarisation, which is important because the off-peak data are included in the event samples for all experiments. When averaged over all production angles  $\mathcal{P}_\tau$  is a measurement of  $\mathcal{A}_\tau$ . As a function of  $\cos \theta$ ,  $\mathcal{P}_\tau(\cos \theta)$  provides nearly independent determinations of both  $\mathcal{A}_\tau$  and  $\mathcal{A}_e$ , thus allowing a test of the universality of the couplings of the Z to e and  $\tau$ .

Each experiment makes separate  $\mathcal{P}_\tau$  measurements using the five  $\tau$  decay modes  $e\nu\bar{\nu}$ ,  $\mu\nu\bar{\nu}$ ,  $\pi\nu$ ,  $\rho\nu$  and  $a_1\nu$  [16–19]. The  $\rho\nu$  and  $\pi\nu$  are the most sensitive channels, contributing weights of about 40% each in the average. DELPHI and L3 also use an inclusive hadronic analysis. The combination is made using the results from each experiment already averaged over the  $\tau$  decay modes.

### 3.1 Results

Tables 3.1 and 3.2 show the most recent results for  $\mathcal{A}_\tau$  and  $\mathcal{A}_e$  obtained by the four LEP collaborations [16–19] and their combination. Although the sizes of the event samples used by the four experiments are roughly equal, smaller errors are quoted by ALEPH. This is largely associated with the higher angular granularity of the ALEPH electromagnetic calorimeter. Common systematic errors arise from

uncertainties in radiative corrections (decay radiation) in the  $\pi\nu$  and  $\rho\nu$  channels, and in the modelling of the  $a_1$  decays [20]. These errors and their correlations need further investigation, but are already taken into account in the combination (see also Reference 18). The statistical correlation between the extracted values of  $\mathcal{A}_\tau$  and  $\mathcal{A}_e$  is small ( $\leq 5\%$ ).

The average values for  $\mathcal{A}_\tau$  and  $\mathcal{A}_e$ :

$$\mathcal{A}_\tau = 0.1439 \pm 0.0043 \quad (3.3)$$

$$\mathcal{A}_e = 0.1498 \pm 0.0049, \quad (3.4)$$

with a correlation of 0.012, are compatible, in good agreement with neutral-current lepton universality. This combination is performed including the small common systematic errors between  $\mathcal{A}_\tau$  and  $\mathcal{A}_e$  within each experiment and between experiments. Assuming e- $\tau$  universality, the values for  $\mathcal{A}_\tau$  and  $\mathcal{A}_e$  can be combined. The combined result of  $\mathcal{A}_\tau$  and  $\mathcal{A}_e$  is:

$$\mathcal{A}_\ell = 0.1465 \pm 0.0033, \quad (3.5)$$

where the error includes a systematic component of 0.0016.

Experiment		$\mathcal{A}_\tau$
ALEPH	(90 - 95), final	$0.1451 \pm 0.0052 \pm 0.0029$
DELPHI	(90 - 95), final	$0.1359 \pm 0.0079 \pm 0.0055$
L3	(90 - 95), final	$0.1476 \pm 0.0088 \pm 0.0062$
OPAL	(90 - 95), final	$0.1456 \pm 0.0076 \pm 0.0057$
LEP Average	final	$0.1439 \pm 0.0035 \pm 0.0026$

Table 3.1: LEP results for  $\mathcal{A}_\tau$ . The first error is statistical and the second systematic.

Experiment		$\mathcal{A}_e$
ALEPH	(90 - 95), final	$0.1504 \pm 0.0068 \pm 0.0008$
DELPHI	(90 - 95), final	$0.1382 \pm 0.0116 \pm 0.0005$
L3	(90 - 95), final	$0.1678 \pm 0.0127 \pm 0.0030$
OPAL	(90 - 95), final	$0.1454 \pm 0.0108 \pm 0.0036$
LEP Average	final	$0.1498 \pm 0.0048 \pm 0.0009$

Table 3.2: LEP results for  $\mathcal{A}_e$ . The first error is statistical and the second systematic.

## Chapter 4

# Measurement of polarised lepton asymmetries at SLC

**Updates with respect to summer 2002:**

Unchanged w.r.t. summer 2000: SLD has published final results for  $A_{LR}$  and the leptonic left-right forward-backward asymmetries.

The measurement of the left-right cross section asymmetry ( $A_{LR}$ ) by SLD [21] at the SLC provides a systematically precise, statistics-dominated determination of the coupling  $\mathcal{A}_e$ , and is presently the most precise single measurement, with the smallest systematic error, of this quantity. In principle the analysis is straightforward: one counts the numbers of Z bosons produced by left and right longitudinally polarised electrons, forms an asymmetry, and then divides by the luminosity-weighted  $e^-$  beam polarisation magnitude (the  $e^+$  beam is not polarised):

$$A_{LR} = \frac{N_L - N_R}{N_L + N_R} \frac{1}{P_e}. \quad (4.1)$$

Since the advent of high polarisation “strained lattice” GaAs photo-cathodes (1994), the average electron polarisation at the interaction point has been in the range 73% to 77%. The method requires no detailed final state event identification ( $e^+e^-$  final state events are removed, as are non-Z backgrounds) and is insensitive to all acceptance and efficiency effects. The small total systematic error of 0.64% relative is dominated by the 0.50% relative systematic error in the determination of the  $e^-$  polarisation. The relative statistical error on  $A_{LR}$  is about 1.3%.

The precision Compton polarimeter detects beam electrons that are scattered by photons from a circularly polarised laser. Two additional polarimeters that are sensitive to the Compton-scattered photons and which are operated in the absence of positron beam, have verified the precision polarimeter result and are used to set a calibration uncertainty of 0.4% relative. In 1998, a dedicated experiment was performed in order to test directly the expectation that accidental polarisation of the positron beam was negligible; the  $e^+$  polarisation was found to be consistent with zero ( $-0.02 \pm 0.07$ )%.

The  $A_{LR}$  analysis includes several very small corrections. The polarimeter result is corrected for higher order QED and accelerator related effects, a total of  $(-0.22 \pm 0.15)$ % relative for 1997/98 data. The event asymmetry is corrected for backgrounds and accelerator asymmetries, a total of  $(+0.15 \pm 0.07)$ % relative, for 1997/98 data.

The translation of the  $A_{LR}$  result to a “pole” value is a  $(-2.5 \pm 0.4)$ % relative shift, where the uncertainty arises from the precision of the centre-of-mass energy determination. This small error due

to the beam energy measurement reflects the results of a scan of the Z peak used to calibrate the energy spectrometers to  $m_Z$  from LEP data. The pole value,  $A_{\text{LR}}^0$ , is equivalent to a measurement of  $\mathcal{A}_e$ .

The 2000 result is included in a running average of all of the SLD  $A_{\text{LR}}$  measurements (1992, 1993, 1994/1995, 1996, 1997 and 1998). This updated result for  $A_{\text{LR}}^0$  ( $\mathcal{A}_e$ ) is  $0.1514 \pm 0.0022$ . In addition, the left-right forward-backward asymmetries for leptonic final states are measured [22]. From these, the parameters  $\mathcal{A}_e$ ,  $\mathcal{A}_\mu$  and  $\mathcal{A}_\tau$  can be determined. The results are  $\mathcal{A}_e = 0.1544 \pm 0.0060$ ,  $\mathcal{A}_\mu = 0.142 \pm 0.015$  and  $\mathcal{A}_\tau = 0.136 \pm 0.015$ . The lepton-based result for  $\mathcal{A}_e$  can be combined with the  $A_{\text{LR}}^0$  result to yield  $\mathcal{A}_e = 0.1516 \pm 0.0021$ , including small correlations in the systematic errors. The correlation of this measurement with  $\mathcal{A}_\mu$  and  $\mathcal{A}_\tau$  is indicated in Table 4.1.

Assuming lepton universality, the  $A_{\text{LR}}$  result and the results on the leptonic left-right forward-backward asymmetries can be combined, while accounting for small correlated systematic errors, yielding

$$\mathcal{A}_\ell = 0.1513 \pm 0.0021. \quad (4.2)$$

	$\mathcal{A}_e$	$\mathcal{A}_\mu$	$\mathcal{A}_\tau$
$\mathcal{A}_e$	1.000		
$\mathcal{A}_\mu$	0.038	1.000	
$\mathcal{A}_\tau$	0.033	0.007	1.000

Table 4.1: Correlation coefficients between  $\mathcal{A}_e$ ,  $\mathcal{A}_\mu$  and  $\mathcal{A}_\tau$

# Chapter 5

## Results from b and c Quarks

**Updates with respect to summer 2002:**

Unchanged w.r.t. summer 2002: Several results are still preliminary.

### 5.1 Introduction

The relevant quantities in the heavy quark sector at LEP-I/SLD which are currently determined by the combination procedure are:

- The ratios of the b and c quark partial widths of the Z to its total hadronic partial width:  $R_b^0 \equiv \Gamma_{b\bar{b}}/\Gamma_{\text{had}}$  and  $R_c^0 \equiv \Gamma_{c\bar{c}}/\Gamma_{\text{had}}$ . (The symbols  $R_b, R_c$  are used to denote the experimentally measured ratios of event rates or cross sections.)
- The forward-backward asymmetries,  $A_{\text{FB}}^{b\bar{b}}$  and  $A_{\text{FB}}^{c\bar{c}}$ .
- The final state coupling parameters  $\mathcal{A}_b, \mathcal{A}_c$  obtained from the left-right-forward-backward asymmetry at SLD.
- The semileptonic branching ratios,  $\text{BR}(b \rightarrow \ell^-)$ ,  $\text{BR}(b \rightarrow c \rightarrow \ell^+)$  and  $\text{BR}(c \rightarrow \ell^+)$ , and the average time-integrated  $B^0\bar{B}^0$  mixing parameter,  $\bar{\chi}$ . These are often determined at the same time or with similar methods as the asymmetries. Including them in the combination greatly reduces the errors. For example  $\bar{\chi}$  parameterises the probability that a b-quark decays into a negative lepton which is the charge tagging efficiency in the asymmetry analyses. For this reason the errors coming from the mixture of different lepton sources in  $b\bar{b}$  events cancel largely in the asymmetries if they are analysed together with  $\bar{\chi}$ .
- The probability that a c quark produces a  $D^+$ ,  $D_s$ ,  $D^{*+}$  meson<sup>1</sup> or a charmed baryon. The probability that a c quark fragments into a  $D^0$  is calculated from the constraint that the probabilities for the weakly decaying charmed hadrons add up to one.

A full description of the averaging procedure is published in [3]; the main motivations for the procedure are outlined here. Several analyses measure more than one parameter simultaneously, for example the

---

<sup>1</sup>Actually the product  $P(c \rightarrow D^{*+}) \times \text{BR}(D^{*+} \rightarrow \pi^+ D^0)$  is fitted because this quantity is needed and measured by the LEP experiments.

asymmetry measurements with leptons or D mesons. Some of the measurements of electroweak parameters depend explicitly on the values of other parameters, for example  $R_b$  depends on  $R_c$ . The common tagging and analysis techniques lead to common sources of systematic uncertainty, in particular for the double-tag measurements of  $R_b$ . The starting point for the combination is to ensure that all the analyses use a common set of assumptions for input parameters which give rise to systematic uncertainties. The input parameters are updated and extended [23] to accommodate new analyses and more recent measurements. The correlations and interdependencies of the input measurements are then taken into account in a  $\chi^2$  minimisation which results in the combined electroweak parameters and their correlation matrix.

## 5.2 Summary of Measurements and Averaging Procedure

All measurements are presented by the LEP and SLD collaborations in a consistent manner for the purpose of combination. The tables prepared by the experiments include a detailed breakdown of the systematic error of each measurement and its dependence on other electroweak parameters. Where necessary, the experiments apply small corrections to their results in order to use agreed values and ranges for the input parameters to calculate systematic errors. The measurements, corrected where necessary, are summarised in Appendix A in Tables A.1–A.20, where the statistical and systematic errors are quoted separately. The correlated systematic entries are from physics sources shared with one or more other results in the tables and are derived from the full breakdown of common systematic uncertainties. The uncorrelated systematic entries come from the remaining sources.

### 5.2.1 Averaging Procedure

A  $\chi^2$  minimisation procedure is used to derive the values of the heavy-flavour electroweak parameters, following the procedure described in Reference 3. The full statistical and systematic covariance matrix for all measurements is calculated. This correlation matrix takes into account correlations between different measurements of one experiment and between different experiments. The explicit dependence of each measurement on the other parameters is also accounted for.

Since c-quark events form the main background in the  $R_b$  analyses, the value of  $R_b$  depends on the value of  $R_c$ . If  $R_b$  and  $R_c$  were measured in the same analysis, this would be reflected in the correlation matrix for the results. However the analyses do not determine  $R_b$  and  $R_c$  simultaneously but instead measure  $R_b$  for an assumed value of  $R_c$ . In this case the dependence is parameterised as

$$R_b = R_b^{\text{meas}} + a(R_c) \frac{(R_c - R_c^{\text{used}})}{R_c}. \quad (5.1)$$

In this expression,  $R_b^{\text{meas}}$  is the result of the analysis assuming a value of  $R_c = R_c^{\text{used}}$ . The values of  $R_c^{\text{used}}$  and the coefficients  $a(R_c)$  are given in Table A.1 where appropriate. The dependence of all other measurements on other electroweak parameters is treated in the same way, with coefficients  $a(x)$  describing the dependence on parameter  $x$ .

### 5.2.2 Partial Width Measurements

The measurements of  $R_b$  and  $R_c$  fall into two categories. In the first, called a single-tag measurement, a method to select b or c events is devised, and the number of tagged events is counted. This number



must then be corrected for backgrounds from other flavours and for the tagging efficiency to calculate the true fraction of hadronic  $Z$  decays of that flavour. The dominant systematic errors come from understanding the branching ratios and detection efficiencies which give the overall tagging efficiency. For the second technique, called a double-tag measurement, each event is divided into two hemispheres. With  $N_t$  being the number of tagged hemispheres,  $N_{tt}$  the number of events with both hemispheres tagged and  $N_{\text{had}}$  the total number of hadronic  $Z$  decays one has

$$\frac{N_t}{2N_{\text{had}}} = \varepsilon_b R_b + \varepsilon_c R_c + \varepsilon_{\text{uds}}(1 - R_b - R_c), \quad (5.2)$$

$$\frac{N_{tt}}{N_{\text{had}}} = \mathcal{C}_b \varepsilon_b^2 R_b + \mathcal{C}_c \varepsilon_c^2 R_c + \mathcal{C}_{\text{uds}} \varepsilon_{\text{uds}}^2 (1 - R_b - R_c), \quad (5.3)$$

where  $\varepsilon_b$ ,  $\varepsilon_c$  and  $\varepsilon_{\text{uds}}$  are the tagging efficiencies per hemisphere for b, c and light-quark events, and  $\mathcal{C}_q \neq 1$  accounts for the fact that the tagging efficiencies between the hemispheres may be correlated. In the case of  $R_b$  one has  $\varepsilon_b \gg \varepsilon_c \gg \varepsilon_{\text{uds}}$ ,  $\mathcal{C}_b \approx 1$ . The correlations for the other flavours can be neglected. These equations can be solved to give  $R_b$  and  $\varepsilon_b$ . Neglecting the c and uds backgrounds and the correlations, they are approximately given by

$$\varepsilon_b \approx 2N_{tt}/N_t, \quad (5.4)$$

$$R_b \approx N_t^2/(4N_{tt}N_{\text{had}}). \quad (5.5)$$

The double-tagging method has the advantage that the b tagging efficiency is derived from the data, reducing the systematic error. The residual background of other flavours in the sample, and the evaluation of the correlation between the tagging efficiencies in the two hemispheres of the event are the main sources of systematic uncertainty in such an analysis.

In the standard approach each hemisphere is simply tagged as b or non-b. This method can be enhanced by using more tags. All additional efficiencies can be determined from the data, reducing the statistical uncertainties without adding new systematic uncertainties.

Small corrections must be applied to the results to obtain the partial width ratios  $R_b^0$  and  $R_c^0$  from the cross section ratios  $R_b$  and  $R_c$ . These corrections depend slightly on the invariant mass cutoff of the simulations used by the experiments; they are applied by the collaborations before the combination.

The partial width measurements included are:

- Lifetime (and lepton) double-tag measurements for  $R_b$  from ALEPH [24], DELPHI [25], L3 [26], OPAL [27] and SLD [28]. These are the most precise determinations of  $R_b$ . Since they completely dominate the combined result, no other  $R_b$  measurements are used at present. The basic features of the double-tag technique are discussed above. In the ALEPH, DELPHI, OPAL and SLD measurements the charm rejection is enhanced by using the invariant mass information. DELPHI, OPAL and SLD also add kinematic information from the particles at the secondary vertex. The ALEPH and DELPHI measurements make use of several different tags, which reduces largely the statistical error. This allows to cut harder in the primary b-tag so that, due to the higher b-purity, also the systematic uncertainties are reduced.
- Analyses with  $D/D^{*\pm}$  mesons to measure  $R_c$  from ALEPH, DELPHI and OPAL. All measurements are constructed in such a way that no assumptions about charm fragmentation are necessary as these are determined from the LEP-I data. The available measurements can be divided into three groups:

- inclusive/exclusive double tag (ALEPH [29], DELPHI [30,31], OPAL [32]): In a first step  $D^{*\pm}$  mesons are reconstructed in several decay channels and their production rate is measured, which depends on the product  $R_c \times P(c \rightarrow D^{*+}) \times BR(D^{*+} \rightarrow \pi^+ D^0)$ . This sample of  $c\bar{c}$  (and  $b\bar{b}$ ) events is then used to measure  $P(c \rightarrow D^{*+}) \times BR(D^{*+} \rightarrow \pi^+ D^0)$  using a slow pion tag in the opposite hemisphere. In the ALEPH measurement only  $R_c$  is given and no explicit  $P(c \rightarrow D^{*+}) \times BR(D^{*+} \rightarrow \pi^+ D^0)$  is available.
- exclusive double tag (ALEPH [29]): This analysis uses exclusively reconstructed  $D^{*+}$ ,  $D^0$  and  $D^+$  mesons in different decay channels. It has lower statistics but better purity than the inclusive analyses.
- reconstruction of all weakly decaying charmed states (ALEPH [33], DELPHI [31], OPAL [34]): These analyses make the assumption that the production fractions of  $D^0$ ,  $D^+$ ,  $D_s$  and  $\Lambda_c$  in c-quark jets of  $c\bar{c}$  events add up to one with small corrections due to unmeasured charm strange baryons. This is a single tag measurement, relying only on knowing the decay branching ratios of the charm hadrons. These analyses are also used to measure the c hadron production ratios which are needed for the  $R_b$  analyses.
- A lifetime plus mass double tag from SLD to measure  $R_c$  [35]. This analysis uses the same tagging algorithm as the SLD  $R_b$  analysis, but with the neural net tuned to tag charm. Although the charm tag has a purity of about 84%, most of the background is from b which can be measured with high precision from the b/c mixed tag rate.
- A measurement of  $R_c$  using single leptons assuming  $BR(c \rightarrow \ell^+)$  from ALEPH [29].

To avoid effects from nonlinearities in the fit, for the inclusive/exclusive single/double tag and for the charm-counting analyses, the products  $R_c P(c \rightarrow D^{*+}) \times BR(D^{*+} \rightarrow \pi^+ D^0)$ ,  $R_c f_{D^0}$ ,  $R_c f_{D^+}$ ,  $R_c f_{D_s}$  and  $R_c f_{\Lambda_c}$  that are actually measured in the analyses are directly used as inputs to the fit. The measurements of the production rates of weakly decaying charmed hadrons, especially  $R_c f_{D_s}$  and  $R_c f_{\Lambda_c}$  have substantial errors due to the uncertainties in the branching ratios of the decay mode used. These errors are relative so that the absolute errors are smaller when the measurements fluctuate downwards, leading to a potential bias towards lower averages. To avoid this bias, for the production rates of weakly decaying charmed hadrons the logarithm of the production rates instead of the rates themselves are input to the fit. For  $R_c f_{D^0}$  and  $R_c f_{D^+}$  the difference between the results using the logarithm or the value itself is negligible. For  $R_c f_{D_s}$  and  $R_c f_{\Lambda_c}$  the difference in the extracted value of  $R_c$  is about one tenth of a standard deviation.

### 5.2.3 Asymmetry Measurements

All b and c asymmetries given by the experiments correspond to full acceptance.

The QCD corrections to the forward-backward asymmetries depend strongly on the experimental analyses. For this reason the numbers given by the collaborations are also corrected for QCD effects. A detailed description of the procedure can be found in [36] with updates reported in [23].

For the heavy-flavour combinations described in this chapter, the LEP peak and off-peak asymmetries are corrected to  $\sqrt{s} = 91.26$  GeV using the predicted dependence from ZFITTER [37]. The slope of the asymmetry around  $m_Z$  depends only on the axial coupling and the charge of the initial and final state fermions and is thus independent of the value of the asymmetry itself, i.e., the effective electroweak mixing angle.

After calculating the overall averages, the quark pole asymmetries  $A_{\text{FB}}^{0,q}$ , defined in terms of effective couplings, are derived from the measured asymmetries by applying corrections as listed in Table 5.1. These corrections are due to the energy shift from 91.26 GeV to  $m_Z$ , initial state radiation,  $\gamma$  exchange and  $\gamma$ -Z interference. A very small correction due to the nonzero value of the b quark mass is included in the last correction. All corrections are calculated using ZFITTER.

Source	$\delta A_{\text{FB}}^b$	$\delta A_{\text{FB}}^c$
$\sqrt{s} = m_Z$	-0.0013	-0.0034
QED corrections	+0.0041	+0.0104
$\gamma$ , $\gamma$ -Z, mass	-0.0003	-0.0008
Total	+0.0025	+0.0062

Table 5.1: Corrections to be applied to the quark asymmetries as  $A_{\text{FB}}^0 = A_{\text{FB}}^{\text{meas}} + \delta A_{\text{FB}}$ .

The SLD left-right-forward-backward asymmetries are also corrected for all radiative effects and are directly presented in terms of  $\mathcal{A}_b$  and  $\mathcal{A}_c$ .

The measurements used are:

- Measurements of  $A_{\text{FB}}^{b\bar{b}}$  and  $A_{\text{FB}}^{c\bar{c}}$  using leptons from ALEPH [38], DELPHI [39], L3 [40] and OPAL [41]. These analyses measure either  $A_{\text{FB}}^{b\bar{b}}$  only from a high  $p_t$  lepton sample or they obtain  $A_{\text{FB}}^{b\bar{b}}$  and  $A_{\text{FB}}^{c\bar{c}}$  from a fit to the lepton spectra. In the case of OPAL the lepton information is combined with hadronic variables in a neural net. DELPHI uses in addition lifetime information and jet-charge in the hemisphere opposite to the lepton to separate the different lepton sources. Some asymmetry analyses also measure  $\bar{\chi}$ .
- Measurements of  $A_{\text{FB}}^{b\bar{b}}$  based on lifetime tagged events with a hemisphere charge measurement from ALEPH [42], DELPHI [43, 44], L3 [45] and OPAL [46]. These measurements dominate the combined result.
- Analyses with D mesons to measure  $A_{\text{FB}}^{c\bar{c}}$  from ALEPH [47] or  $A_{\text{FB}}^{c\bar{c}}$  and  $A_{\text{FB}}^{b\bar{b}}$  from DELPHI [48] and OPAL [49].
- Measurements of  $\mathcal{A}_b$  and  $\mathcal{A}_c$  from SLD. These results include measurements using lepton [50], D meson [51] and vertex mass plus hemisphere charge [52] tags, which have similar sources of systematic errors as the LEP asymmetry measurements. SLD also uses vertex mass for bottom or charm tagging in conjunction with a kaon tag or a vertex charge tag for both  $\mathcal{A}_b$  and  $\mathcal{A}_c$  measurements [53–55].

## 5.2.4 Other Measurements

The measurements of the charmed hadron fractions  $P(c \rightarrow D^{*+}) \times \text{BR}(D^{*+} \rightarrow \pi^+ D^0)$ ,  $f(D^+)$ ,  $f(D_s)$  and  $f(c_{\text{baryon}})$  are included in the  $R_c$  measurements and are described there.

ALEPH [56], DELPHI [57], L3 [26, 58] and OPAL [59] measure  $\text{BR}(b \rightarrow \ell^-)$ ,  $\text{BR}(b \rightarrow c \rightarrow \ell^+)$  and  $\bar{\chi}$  or a subset of them from a sample of leptons opposite to a b-tagged hemisphere and from a double lepton sample. DELPHI [30] and OPAL [60] measure  $\text{BR}(c \rightarrow \ell^+)$  from a sample opposite to a high energy  $D^{*\pm}$ .

## 5.3 Results

In a first fit the asymmetry measurements on peak, above peak and below peak are corrected to three common centre-of-mass energies and are then combined at each energy point. The results of this fit, including the SLD results, are given in Appendix B. The dependence of the average asymmetries on centre-of-mass energy agrees with the prediction of the Standard Model, as shown in Figure 5.1. A second fit is made to derive the pole asymmetries  $A_{\text{FB}}^{0,q}$  from the measured quark asymmetries, in which all the off-peak asymmetry measurements are corrected to the peak energy before combining. This fit determines a total of 14 parameters: the two partial widths, two LEP asymmetries, two coupling parameters from SLD, three semileptonic branching ratios, the average mixing parameter and the probabilities for c quark to fragment into a  $D^+$ , a  $D_s$ , a  $D^{*+}$ , or a charmed baryon. If the SLD measurements are excluded from the fit there are 12 parameters to be determined. Results for the non-electroweak parameters are independent of the treatment of the off-peak asymmetries and the SLD data.

### 5.3.1 Results of the 12-Parameter Fit to the LEP Data

Using the full averaging procedure gives the following combined results for the electroweak parameters:

$$\begin{aligned} R_b^0 &= 0.21648 \pm 0.00073 \\ R_c^0 &= 0.1687 \pm 0.0047 \\ A_{\text{FB}}^{0,b} &= 0.0994 \pm 0.0017 \\ A_{\text{FB}}^{0,c} &= 0.0709 \pm 0.0036, \end{aligned} \tag{5.6}$$

where all corrections to the asymmetries and partial widths are applied. The  $\chi^2/\text{d.o.f.}$  is  $45/(96 - 12)$ . The corresponding correlation matrix is given in Table 5.2.

	$R_b^0$	$R_c^0$	$A_{\text{FB}}^{0,b}$	$A_{\text{FB}}^{0,c}$
$R_b^0$	1.00	-0.17	-0.08	0.07
$R_c^0$	-0.17	1.00	0.08	-0.06
$A_{\text{FB}}^{0,b}$	-0.08	0.08	1.00	0.14
$A_{\text{FB}}^{0,c}$	0.07	-0.06	0.14	1.00

Table 5.2: The correlation matrix for the four electroweak parameters from the 12-parameter fit.

### 5.3.2 Results of the 14-Parameter Fit to LEP and SLD Data

Including the SLD results for  $R_b$ ,  $R_c$ ,  $\mathcal{A}_b$  and  $\mathcal{A}_c$  into the fit the following results are obtained:

$$\begin{aligned} R_b^0 &= 0.21644 \pm 0.00065, \\ R_c^0 &= 0.1718 \pm 0.0031, \\ A_{\text{FB}}^{0,b} &= 0.0995 \pm 0.0017, \\ A_{\text{FB}}^{0,c} &= 0.0713 \pm 0.0036, \\ \mathcal{A}_b &= 0.922 \pm 0.020, \\ \mathcal{A}_c &= 0.670 \pm 0.026, \end{aligned} \tag{5.7}$$

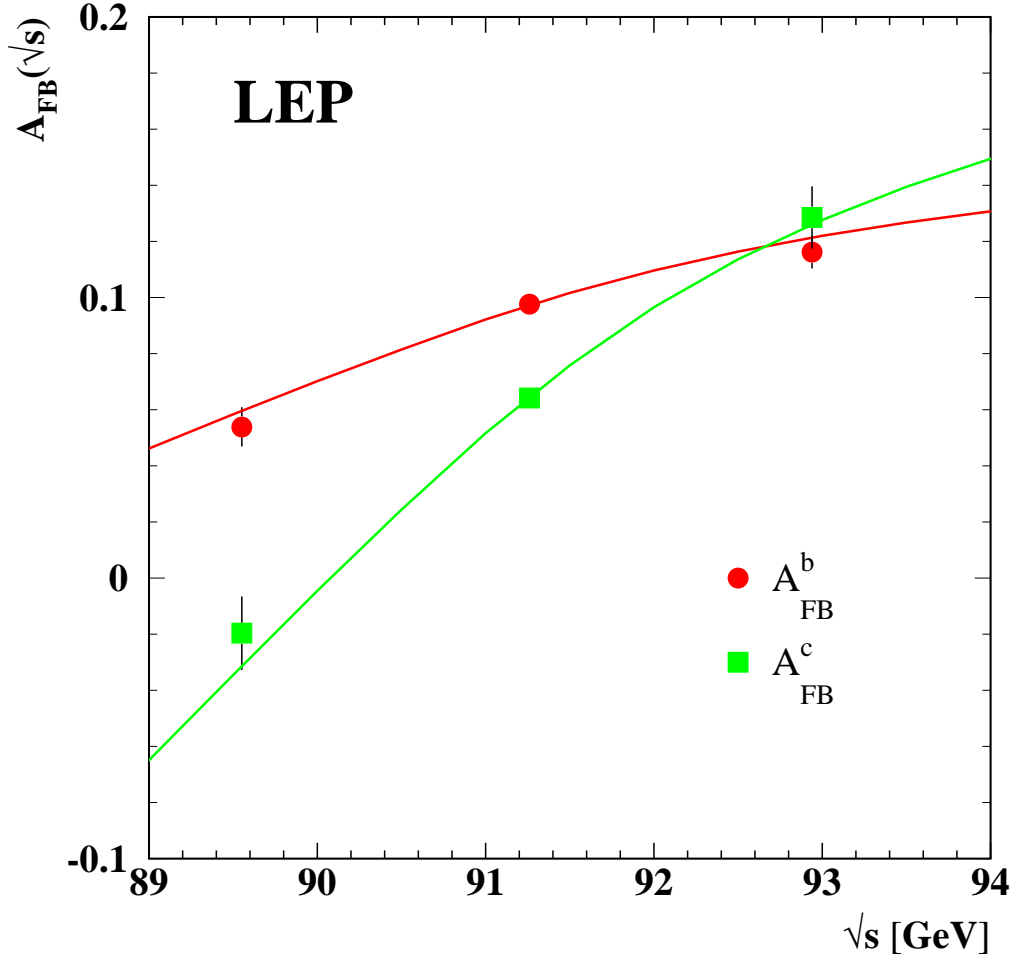


Figure 5.1: Measured asymmetries for b and c quark final states as a function of the centre-of-mass energy. The Standard-Model expectations are shown as the lines calculated for  $m_t = 175$  GeV and  $m_H = 300$  GeV.

with a  $\chi^2/\text{d.o.f.}$  of  $48/(105 - 14)$ . The corresponding correlation matrix is given in Table 5.3 and the largest errors for the electroweak parameters are listed in Table 5.4. If only statistical errors are used in the fit the  $\chi^2/\text{d.o.f.}$  is  $85/(105 - 14)$ . This indicates that the data fluctuate towards a very small  $\chi^2$  and that probably systematic uncertainties are estimated in a conservative way.

In deriving these results the parameters  $\mathcal{A}_b$  and  $\mathcal{A}_c$  are treated as independent of the forward-backward asymmetries  $A_{FB}^{0,b}$  and  $A_{FB}^{0,c}$  (but see Section 15.1 for a joint analysis). In Figure 5.2 the results for  $R_b^0$  and  $R_c^0$  are shown compared with the Standard Model expectation.

Amongst the non-electroweak observables the B semileptonic branching fraction ( $\text{BR}(b \rightarrow \ell^-) = 0.1062 \pm 0.0021$ ) is of special interest. The dominant error source on this quantity is the dependence on the semileptonic decay models  $b \rightarrow \ell^-$ ,  $c \rightarrow \ell^+$  with

$$\Delta \text{BR}(b \rightarrow \ell^-)_{b \rightarrow \ell^- - \text{modelling}} = 0.0012. \quad (5.8)$$

	$R_b^0$	$R_c^0$	$A_{\text{FB}}^{0,b}$	$A_{\text{FB}}^{0,c}$	$\mathcal{A}_b$	$\mathcal{A}_c$
$R_b^0$	1.00	-0.14	-0.07	0.07	-0.07	0.05
$R_c^0$	-0.14	1.00	0.05	-0.05	0.04	-0.05
$A_{\text{FB}}^{0,b}$	-0.07	0.05	1.00	0.14	0.02	0.00
$A_{\text{FB}}^{0,c}$	0.07	-0.05	0.14	1.00	-0.02	0.04
$\mathcal{A}_b$	-0.07	0.04	0.02	-0.02	1.00	0.13
$\mathcal{A}_c$	0.05	-0.05	0.00	0.04	0.13	1.00

Table 5.3: The correlation matrix for the six electroweak parameters from the 14-parameter fit.

	$R_b^0$ ( $10^{-3}$ )	$R_c^0$ ( $10^{-3}$ )	$A_{\text{FB}}^{0,b}$ ( $10^{-3}$ )	$A_{\text{FB}}^{0,c}$ ( $10^{-3}$ )	$\mathcal{A}_b$ ( $10^{-2}$ )	$\mathcal{A}_c$ ( $10^{-2}$ )
statistics	0.43	2.4	1.5	3.1	1.5	2.1
internal systematics	0.28	1.4	0.5	1.5	1.4	1.6
QCD effects	0.18	0.1	0.4	0.1	0.3	0.2
semil. B,D decay model	0.01	0.1	0.1	0.6	0.1	0.1
BR(D $\rightarrow$ neut.)	0.14	0.3	0	0	0	0
D decay multiplicity	0.13	0.3	0	0.2	0	0
BR(D <sup>+</sup> $\rightarrow$ K <sup>-</sup> $\pi^+\pi^+$ )	0.09	0.2	0	0.2	0	0
BR(D <sub>s</sub> $\rightarrow$ $\phi\pi^+$ )	0.02	0.5	0	0	0	0
BR( $\Lambda_c \rightarrow$ p K <sup>-</sup> $\pi^+$ )	0.06	0.5	0	0.2	0	0
D lifetimes	0.06	0.1	0	0.2	0	0
gluon splitting	0.22	0.1	0.1	0.2	0.1	0.1
c fragmentation	0.10	0.2	0	0.1	0.1	0.1
light quarks	0.07	0.2	0	0	0	0
beam polarisation	0	0	0	0	0.5	0.4
total	0.65	3.1	1.7	3.6	2.0	2.6

Table 5.4: The dominant error sources for the electroweak parameters from the 14-parameter fit.

Extensive studies have been made to understand the size of this error. Amongst the electroweak quantities the quark asymmetries with leptons depend also on the assumptions on the decay model while the asymmetries using other methods usually do not. The fit implicitly requires that the different methods give consistent results. This effectively constrains the decay model and thus reduces the error from this source in the fit result for BR(b  $\rightarrow \ell^-$ ).

To get a conservative estimate of the modelling error in BR(b  $\rightarrow \ell^-$ ) the fit is repeated removing all asymmetry measurements. The result of this fit is

$$\text{BR}(b \rightarrow \ell^-) = 0.1065 \pm 0.0023 \quad (5.9)$$

with

$$\Delta\text{BR}(b \rightarrow \ell^-)_{b \rightarrow \ell^- - \text{modelling}} = 0.0014. \quad (5.10)$$

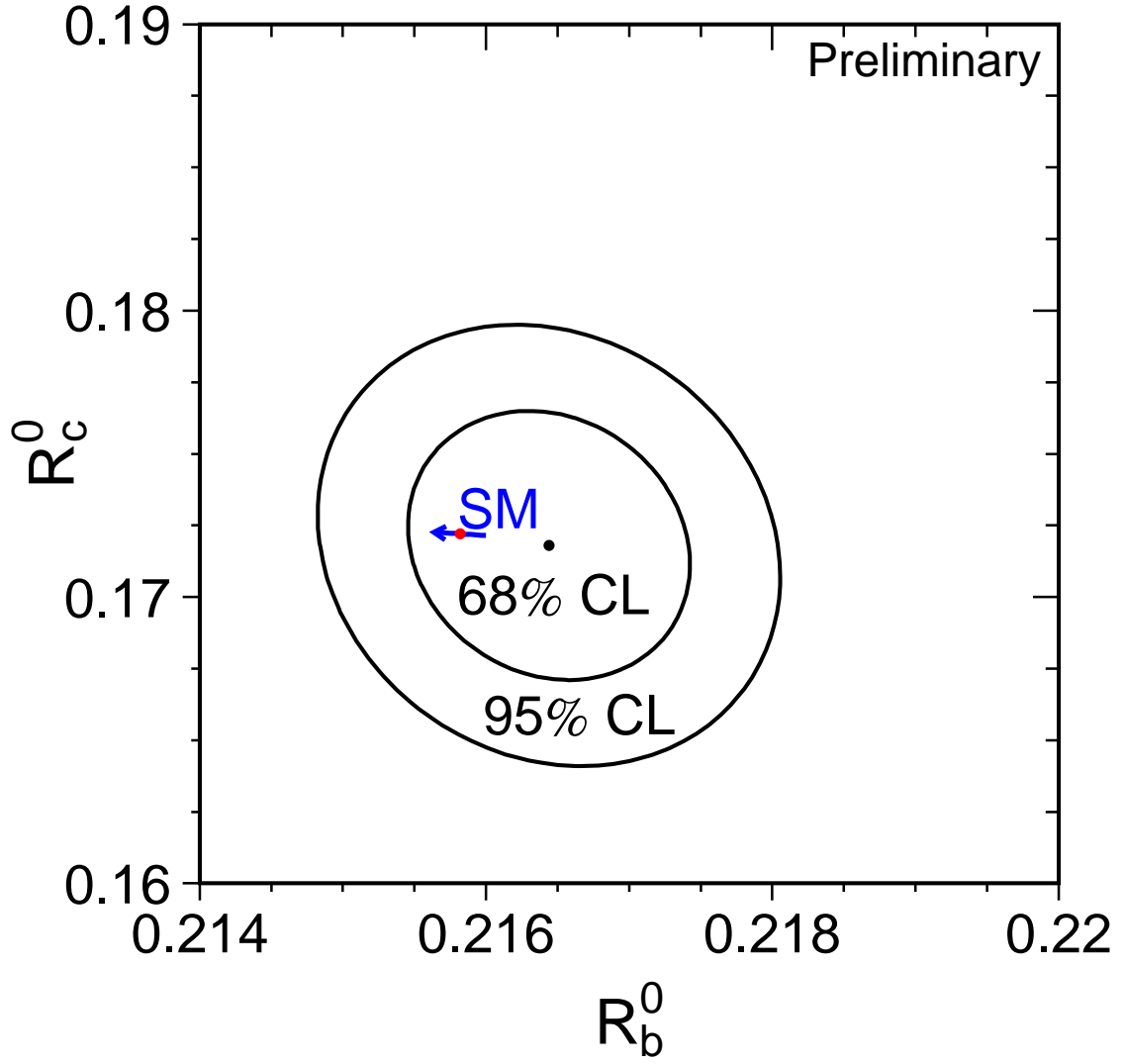


Figure 5.2: Contours in the  $(R_b^0, R_c^0)$  plane derived from the LEP+SLD data, corresponding to 68% and 95% confidence levels assuming Gaussian systematic errors. The Standard Model prediction for  $m_t = 174.3 \pm 5.1$  GeV is also shown. The arrow points in the direction of increasing values of  $m_t$ .

## Chapter 6

# The Hadronic Charge Asymmetry $\langle Q_{\text{FB}} \rangle$

### Updates with respect to summer 2002:

Unchanged w.r.t. summer 2002: All experiments have published final results which enter the combination. The final combination procedure is used, the obtained averages are final.

The LEP experiments ALEPH [61], DELPHI [62], L3 [45] and OPAL [63] provide measurements of the hadronic charge asymmetry based on the mean difference in jet charges measured in the forward and backward event hemispheres,  $\langle Q_{\text{FB}} \rangle$ . DELPHI also provides a related measurement of the total charge asymmetry by making a charge assignment on an event-by-event basis and performing a likelihood fit [62]. The experimental values quoted for the average forward-backward charge difference,  $\langle Q_{\text{FB}} \rangle$ , cannot be directly compared as some of them include detector dependent effects such as acceptances and efficiencies. Therefore the effective electroweak mixing angle,  $\sin^2 \theta_{\text{eff}}^{\text{lept}}$ , as defined in Section 15.3, is used as a means of combining the experimental results summarised in Table 6.1.

Experiment	$\sin^2 \theta_{\text{eff}}^{\text{lept}}$
ALEPH (90-94), final	$0.2322 \pm 0.0008 \pm 0.0011$
DELPHI (91-91), final	$0.2345 \pm 0.0030 \pm 0.0027$
L3 (91-95), final	$0.2327 \pm 0.0012 \pm 0.0013$
OPAL (90-91), final	$0.2326 \pm 0.0012 \pm 0.0029$
LEP Average	$0.2324 \pm 0.0012$

Table 6.1: Summary of the determination of  $\sin^2 \theta_{\text{eff}}^{\text{lept}}$  from inclusive hadronic charge asymmetries at LEP. For each experiment, the first error is statistical and the second systematic. The latter, amounting to 0.0010 in the average, is dominated by fragmentation and decay modelling uncertainties.

The dominant source of systematic error arises from the modelling of the charge flow in the fragmentation process for each flavour. All experiments measure the required charge properties for  $Z \rightarrow b\bar{b}$  events from the data. ALEPH also determines the charm charge properties from the data. The fragmentation model implemented in the JETSET Monte Carlo program [64] is used by all experiments as reference; the one of the HERWIG Monte Carlo program [65] is used for comparison. The JETSET fragmentation parameters are varied to estimate the systematic errors. The central values chosen by the experiments for these parameters are, however, not the same. The smaller of the two fragmentation errors in any pair of results is treated as common to both. The present average of  $\sin^2 \theta_{\text{eff}}^{\text{lept}}$  from  $\langle Q_{\text{FB}} \rangle$  and its associated error are not very sensitive to the treatment of common uncertainties. The ambiguities due to QCD corrections may cause changes in the derived value of



$\sin^2 \theta_{\text{eff}}^{\text{lept}}$ . These are, however, well below the fragmentation uncertainties and experimental errors. The effect of fully correlating the estimated systematic uncertainties from this source between the experiments has a negligible effect upon the average and its error.

There is also some correlation between these results and those for  $A_{\text{FB}}^{b\bar{b}}$  using jet charges. The dominant source of correlation is again through uncertainties in the fragmentation and decay models used. The typical correlation between the derived values of  $\sin^2 \theta_{\text{eff}}^{\text{lept}}$  from the  $\langle Q_{\text{FB}} \rangle$  and the  $A_{\text{FB}}^{b\bar{b}}$  jet charge measurements is estimated to be about 20% to 25%. This leads to only a small change in the relative weights for the  $A_{\text{FB}}^{b\bar{b}}$  and  $\langle Q_{\text{FB}} \rangle$  results when averaging their  $\sin^2 \theta_{\text{eff}}^{\text{lept}}$  values (Section 15.3). Thus, the correlation between  $\langle Q_{\text{FB}} \rangle$  and  $A_{\text{FB}}^{b\bar{b}}$  from jet charge has little impact on the overall Standard Model fit, and is neglected at present.

# Chapter 7

## Photon-Pair Production at LEP-II

### Updates with respect to summer 2002:

Unchanged w.r.t. summer 2002: ALEPH, L3 and OPAL have provided final results for the complete LEP-2 dataset, DELPHI up to 1999 data and preliminary results for the 2000 data.

### 7.1 Introduction

The reaction  $e^+e^- \rightarrow \gamma\gamma(\gamma)$  provides a clean test of QED at LEP energies and is well suited to detect the presence of non-standard physics. The differential QED cross-section at the Born level in the relativistic limit is given by [66,67]:

$$\left(\frac{d\sigma}{d\Omega}\right)_{\text{Born}} = \frac{\alpha^2}{s} \frac{1 + \cos^2 \theta}{1 - \cos^2 \theta}. \quad (7.1)$$

Since the two final state particles are identical the polar angle  $\theta$  is defined such that  $\cos \theta > 0$ . Various models with deviations from this cross-section will be discussed in section 7.4. Results on the  $\geq 2$ -photon final state using the high energy data collected by the four LEP collaborations are reported by the individual experiments [68]. Here the results of the LEP working group dedicated to the combination of the  $e^+e^- \rightarrow \gamma\gamma(\gamma)$  measurements are reported. Results are given for the averaged total cross-section and for global fits to the differential cross-sections.

### 7.2 Event Selection

This channel is very clean and the event selection, which is similar for all experiments, is based on the presence of at least two energetic clusters in the electromagnetic calorimeters. A minimum energy is required, typically  $(E_1 + E_2)/\sqrt{s}$  larger than 0.3 to 0.6, where  $E_1$  and  $E_2$  are the energies of the two most energetic photons. In order to remove  $e^+e^-$  events, charged tracks are in general not allowed except when they can be associated to a photon conversion in one hemisphere.

The polar angle is defined in order to minimise effects due to initial state radiation as

$$\cos \theta = \left| \sin\left(\frac{\theta_1 - \theta_2}{2}\right) \right| / \sin\left(\frac{\theta_1 + \theta_2}{2}\right),$$

where  $\theta_1$  and  $\theta_2$  are the polar angles of the two most energetic photons. The acceptance in polar angle is in the range of 0.90 to 0.96 on  $|\cos \theta|$ , depending on the experiment.

With these criteria, the selection efficiencies are in the range of 68% to 98% and the residual background (from  $e^+e^-$  events and from  $e^+e^- \rightarrow \tau^+\tau^-$  with  $\tau^\pm \rightarrow e^\pm \nu \bar{\nu}$ ) is very small, 0.1% to 1%. Detailed descriptions of the event selections performed by the four collaborations can be found in [68].

### 7.3 Total cross-section

The total cross-sections are combined using a  $\chi^2$  minimisation. For simplicity, given the different angular acceptances, the ratios of the measured cross-sections relative to the QED expectation,  $r = \sigma_{\text{meas}}/\sigma_{\text{QED}}$ , are averaged. Figure 7.1 shows the measured ratios  $r_{i,k}$  of the experiments  $i$  at energies  $k$  with their statistical and systematic errors added in quadrature. There are no significant sources of experimental systematic errors that are correlated between experiments. The theoretical error on the QED prediction, which is fully correlated between energies and experiments is taken into account after the combination.

Denoting with  $\Delta$  the vector of residuals between the measurements and the expected ratios, three different averages are performed:

1. per energy  $k = 1, \dots, 7$ :  $\Delta_{i,k} = r_{i,k} - x_k$
2. per experiment  $i = 1, \dots, 4$ :  $\Delta_{i,k} = r_{i,k} - y_i$
3. global value:  $\Delta_{i,k} = r_{i,k} - z$

The seven fit parameters per energy  $x_k$  are shown in Figure 7.1 as LEP combined cross-sections. They are correlated with correlation coefficients ranging from 5% to 20%. The four fit-parameters per experiment  $y_i$  are uncorrelated between each other, the results are given in Table 7.1 together with the single global fit parameter  $z$ .

No significant deviations from the QED expectations are found. The global ratio is below unity by 1.8 standard deviations not accounting for the error on the radiative corrections. This theory error can be assumed to be about 10% of the applied radiative correction and hence depends on the selection. For this combination it is assumed to be 1% which is of same size as the experimental error (1.0%).

Experiment	cross-section ratio
ALEPH	$0.953 \pm 0.024$
DELPHI	$0.976 \pm 0.032$
L3	$0.978 \pm 0.018$
OPAL	$0.999 \pm 0.016$
global	$0.982 \pm 0.010$

Table 7.1: Cross-section ratios  $r = \sigma_{\text{meas}}/\sigma_{\text{QED}}$  for the four LEP experiments averaged over all energies and the global average over all experiments and energies. The error includes the statistical and experimental systematic error but no error from theory.

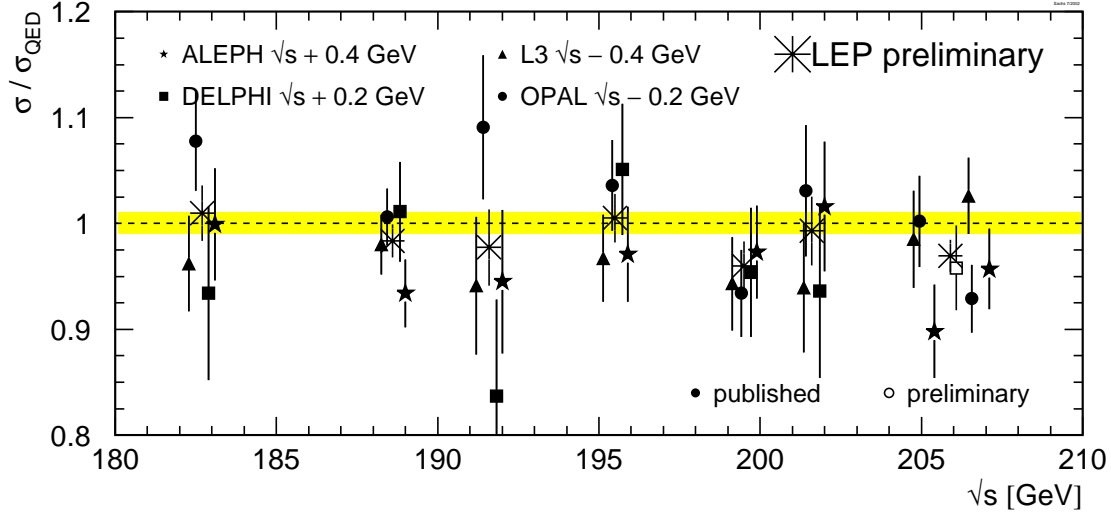


Figure 7.1: Cross-section ratios  $r = \sigma_{\text{meas}}/\sigma_{\text{QED}}$  at different energies. The measurements of the single experiments are displaced by  $\pm 200$  or  $400$  MeV from the actual energy for clarity. Filled symbols indicate published results, open symbols stand for preliminary numbers. The average over the experiments at each energy is shown as a star. Measurements between 203 and 209 GeV are averaged to one energy point. The theoretical error is not included in the experimental errors but is represented as the shaded band.

	data used		sys. error [%]		$ \cos\theta $
	published	preliminary	experimental	theory	
ALEPH	189 – 207	–	2	1	0.95
DELPHI	189 – 202	206	2.5	1	0.90
L3	183 – 207	–	2.1	1	0.96
OPAL	183 – 207	–	0.6 – 2.9	1	0.93

Table 7.2: The data samples used for the global fit to the differential cross-sections, the systematic errors, the assumed error on the theory and the polar angle acceptance for the LEP experiments.

## 7.4 Global fit to the differential cross-sections

The global fit is based on angular distributions at energies between 183 and 207 GeV from the individual experiments. As an example, angular distributions from each experiment are shown in Figure 7.2. Combined differential cross-sections are not available yet, since they need a common binning of the distributions. All four experiments give results including the whole year 2000 data-taking. Apart from the 2000 DELPHI data all inputs are final, as shown in Table 7.2. The systematic errors arise from the luminosity evaluation (including theory uncertainty on the small-angle Bhabha cross-section computation), from the selection efficiency and the background evaluations and from radiative corrections. The last contribution, owing to the fact that the available  $e^+e^- \rightarrow \gamma\gamma(\gamma)$  cross-section calculation is based on  $\mathcal{O}(\alpha^3)$  code, is assumed to be 1% and is considered correlated among energies and experiments.

Various model predictions are fitted to these angular distributions taking into account the experimental systematic error correlated between energies for each experiment and the error on the theory.

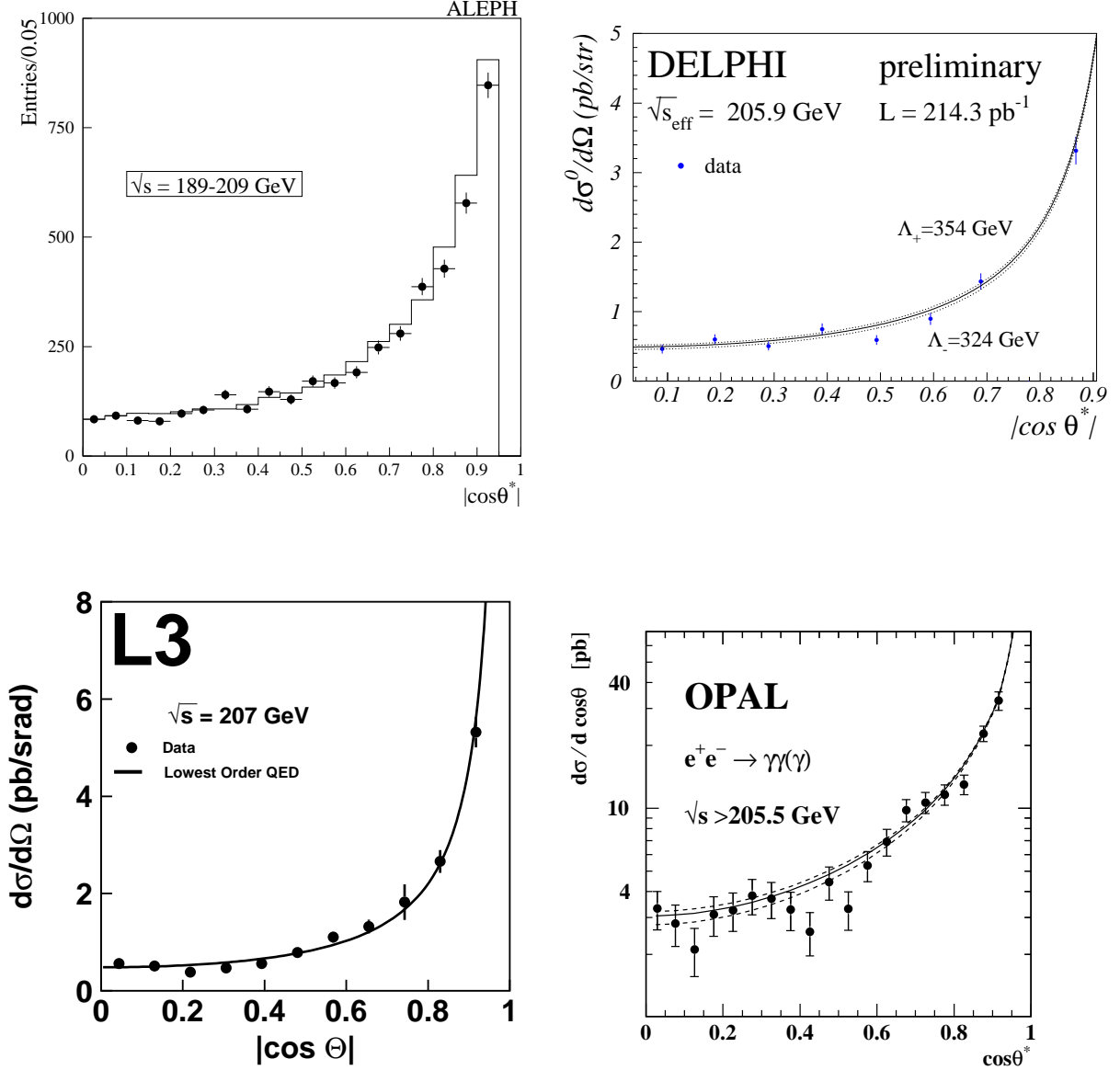


Figure 7.2: Examples for angular distributions of the four LEP experiments. Points are the data and the curves are the QED prediction (solid) and the individual fit results for  $\Lambda_{\pm}$  (dashed). ALEPH shows the uncorrected number of observed events, the expectation is presented as histogram.

A binned log likelihood fit is performed with one free parameter for the model and five fit parameters used to keep the normalisation free within the systematic errors of the theory and the four experiments. Additional fit parameters are needed to accommodate the angular dependent systematic errors of OPAL.

The following models of new physics are considered. The simplest ansatz is a short-range exponential deviation from the Coulomb field parameterised by cut-off parameters  $\Lambda_{\pm}$  [69, 70]. This leads to a differential cross-section of the form

$$\left(\frac{d\sigma}{d\Omega}\right)_{\Lambda_{\pm}} = \left(\frac{d\sigma}{d\Omega}\right)_{\text{Born}} \pm \frac{\alpha^2 \pi s}{\Lambda_{\pm}^4} (1 + \cos^2 \theta). \quad (7.2)$$

New effects can also be introduced in effective Lagrangian theory [71]. Here dimension-6 terms lead to anomalous  $ee\gamma$  couplings. The resulting deviations in the differential cross-section are similar in form to those given in Equation 7.2, but with a slightly different definition of the parameter:  $\Lambda_6^4 = \frac{2}{\alpha}\Lambda_+^4$ . While for the ad hoc included cut-off parameters  $\Lambda_\pm$  both signs are allowed the physics motivated parameter  $\Lambda_6$  occurs only with the positive sign. Dimension 7 and 8 Lagrangians introduce  $ee\gamma\gamma$  contact interactions and result in an angle-independent term added to the Born cross-section:

$$\left(\frac{d\sigma}{d\Omega}\right)_{\Lambda'} = \left(\frac{d\sigma}{d\Omega}\right)_{\text{Born}} + \frac{s^2}{16} \frac{1}{\Lambda'^6} . \quad (7.3)$$

The associated parameters are given by  $\Lambda_7 = \Lambda'$  and  $\Lambda_8^4 = m_e \Lambda'^3$  for dimension 7 and dimension 8 couplings, respectively. The subscript refers to the dimension of the Lagrangian.

Instead of an ordinary electron, an excited electron  $e^*$  with mass  $M_{e^*}$  could be exchanged in the  $t$ -channel [70, 72]. In the most general case  $e^*e\gamma$  couplings would lead to a large anomalous magnetic moment of the electron [73]. This effect can be avoided by a chiral magnetic coupling of the form

$$\mathcal{L}_{e^*e\gamma} = \frac{1}{2\Lambda} \bar{e}^* \sigma^{\mu\nu} \left[ g f \frac{\tau}{2} W_{\mu\nu} + g' f' \frac{Y}{2} B_{\mu\nu} \right] e_L + \text{h.c.} , \quad (7.4)$$

where  $\tau$  are the Pauli matrices and  $Y$  is the hypercharge. The parameters of the model are the compositeness scale  $\Lambda$  and the weight factors  $f$  and  $f'$  associated to the gauge fields  $W$  and  $B$  with Standard Model couplings  $g$  and  $g'$ . For the process  $e^+e^- \rightarrow \gamma\gamma(\gamma)$ , the following cross-section results [74]:

$$\begin{aligned} \left(\frac{d\sigma}{d\Omega}\right)_{e^*} &= \left(\frac{d\sigma}{d\Omega}\right)_{\text{Born}} \\ &+ \frac{\alpha^2 \pi}{2} \frac{f_\gamma^4}{\Lambda^4} M_{e^*}^2 \left[ \frac{p^4}{(p^2 - M_{e^*}^2)^2} + \frac{q^4}{(q^2 - M_{e^*}^2)^2} + \frac{\frac{1}{2} s^2 \sin^2 \theta}{(p^2 - M_{e^*}^2)(q^2 - M_{e^*}^2)} \right] , \end{aligned} \quad (7.5)$$

with  $f_\gamma = -\frac{1}{2}(f + f')$ ,  $p^2 = -\frac{s}{2}(1 - \cos \theta)$  and  $q^2 = -\frac{s}{2}(1 + \cos \theta)$ . Effects vanish in the case of  $f = -f'$ . The cross-section does not depend on the sign of  $f_\gamma$ .

Theories of quantum gravity in extra spatial dimensions could solve the hierarchy problem because gravitons would be allowed to travel in more than 3+1 space-time dimensions [75]. While in these models the Planck mass  $M_D$  in  $D = n + 4$  dimensions is chosen to be of electroweak scale the usual Planck mass  $M_{\text{Pl}}$  in four dimensions would be

$$M_{\text{Pl}}^2 = R^n M_D^{n+2} , \quad (7.6)$$

where  $R$  is the compactification radius of the additional dimensions. Since gravitons couple to the energy-momentum tensor, their interaction with photons is as weak as with fermions. However, the huge number of Kaluza-Klein excitation modes in the extra dimensions may give rise to observable effects. These effects depend on the scale  $M_s (\sim M_D)$  which may be as low as  $\mathcal{O}(\text{TeV})$ . Model dependencies are absorbed in the parameter  $\lambda$  which cannot be explicitly calculated without knowledge of the full theory, the sign is undetermined. The parameter  $\lambda$  is expected to be of  $\mathcal{O}(1)$  and for this analysis it is assumed that  $\lambda = \pm 1$ . The expected differential cross-section is given by [75]:

$$\left(\frac{d\sigma}{d\Omega}\right)_{M_s} = \left(\frac{d\sigma}{d\Omega}\right)_{\text{Born}} - \alpha s \frac{\lambda}{M_s^4} (1 + \cos^2 \theta) + \frac{s^3}{8\pi} \frac{\lambda^2}{M_s^8} (1 - \cos^4 \theta) . \quad (7.7)$$

## 7.5 Fit Results

Where possible the fit parameters are chosen such that the likelihood function is approximately Gaussian. The preliminary results of the fits to the differential cross-sections are given in Table 7.3. No significant deviations with respect to the QED expectations are found (all the parameters are compatible with zero) and therefore 95% confidence level limits are obtained by renormalising the probability distribution of the fit parameter to the physically allowed region. The asymmetric limits  $x_{95}^{\pm}$  on the fitting parameter are obtained by:

$$\frac{\int_0^{x_{95}^+} \Gamma(x, \mu, \sigma) dx}{\int_0^{\infty} \Gamma(x, \mu, \sigma) dx} = 0.95 \quad \text{and} \quad \frac{\int_{x_{95}^-}^0 \Gamma(x, \mu, \sigma) dx}{\int_{-\infty}^0 \Gamma(x, \mu, \sigma) dx} = 0.95, \quad (7.8)$$

where  $\Gamma$  is a Gaussian with the central value and error of the fit result denoted by  $\mu$  and  $\sigma$ , respectively. This is equivalent to the integration of a Gaussian probability function as a function of the fit parameter. The 95 % CL limits on the model parameters are derived from the limits on the fit parameters, e.g. the limit on  $\Lambda_+$  is obtained as  $[x_{95}^+(\Lambda_{\pm}^{-4})]^{-1/4}$ .

The only model with more than one free model parameter is the search for excited electrons. In this case only one out of the two parameters  $f_{\gamma}$  and  $M_{e^*}$  is determined while the other is fixed. It is assumed that  $\Lambda = M_{e^*}$ . For limits on the coupling  $f_{\gamma}/\Lambda$  a scan over  $M_{e^*}$  is performed. The fit result at  $M_{e^*} = 200\text{GeV}$  is included in Table 7.3, limits for all masses are presented in Figure 7.3. For the determination of the excited electron mass the fit cannot be expressed in terms of a linear fit parameter. For  $|f_{\gamma}| = 1$  the curve of the negative log likelihood,  $\Delta\text{LogL}$ , as a function of  $M_{e^*}$  is shown in Figure 7.4. The value corresponding to  $\Delta\text{LogL} = 1.92$  is  $M_{e^*} = 248\text{ GeV}$ .

Fit parameter	Fit result	95% CL limit [GeV]
$\Lambda_{\pm}^{-4}$	$\left(-12.5^{+25.1}_{-24.7}\right) \cdot 10^{-12} \text{ GeV}^{-4}$	$\Lambda_+ > 392$ $\Lambda_- > 364$
$\Lambda_7^{-6}$	$\left(-0.91^{+1.81}_{-1.78}\right) \cdot 10^{-18} \text{ GeV}^{-6}$	$\Lambda_7 > 831$
derived from $\Lambda_+$		$\Lambda_6 > 1595$
derived from $\Lambda_7$		$\Lambda_8 > 23.3$
$\lambda/M_s^4$	$\left(0.29^{+0.57}_{-0.58}\right) \cdot 10^{-12} \text{ GeV}^{-4}$	$\lambda = +1: M_s > 933$ $\lambda = -1: M_s > 1010$
$f_{\gamma}^4(M_{e^*} = 200\text{GeV})$	$0.037^{+0.202}_{-0.198}$	$f_{\gamma}/\Lambda < 3.9 \text{ TeV}^{-1}$

Table 7.3: The preliminary combined fit parameters and the 95% confidence level limits for the four LEP experiments.

## 7.6 Conclusion

The LEP collaborations study the  $e^+e^- \rightarrow \gamma\gamma(\gamma)$  channel up to the highest available centre-of-mass energies. The total cross-section results are combined in terms of the ratios with respect to the QED expectations. No deviations are found. The differential cross-sections are fit following different

parametrisations from models predicting deviations from QED. No evidence for deviations is found and therefore combined 95% confidence level limits are given.

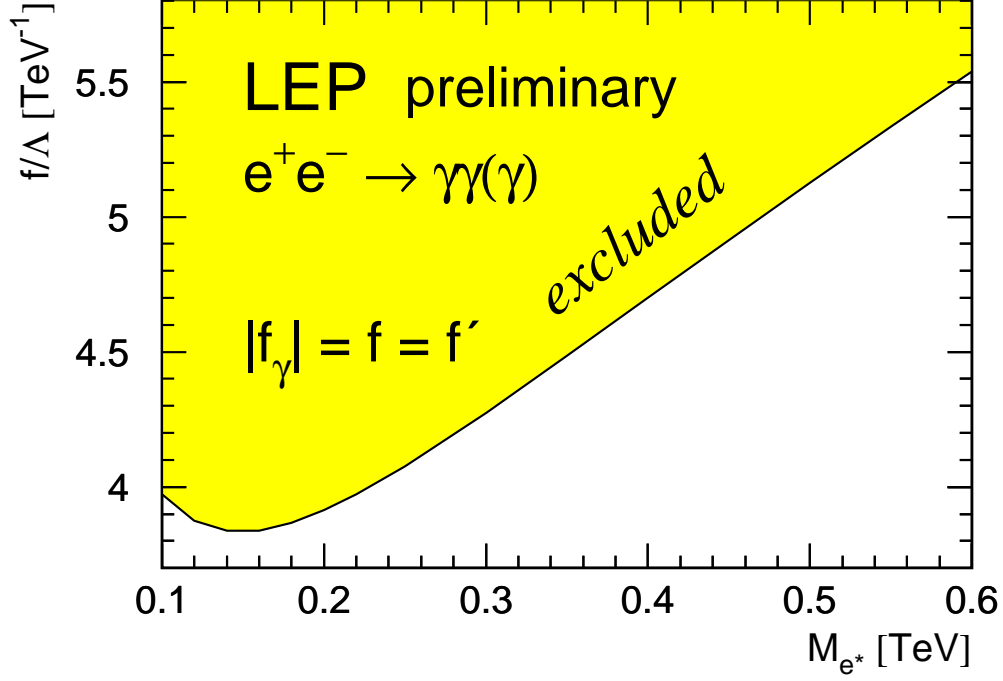


Figure 7.3: 95% CL limits on the coupling  $f_\gamma/\Lambda$  of an excited electron as a function of  $M_{e^*}$ . In the case of  $f = f'$  it follows that  $|f_\gamma| = f$ . It is assumed that  $\Lambda = M_{e^*}$ .

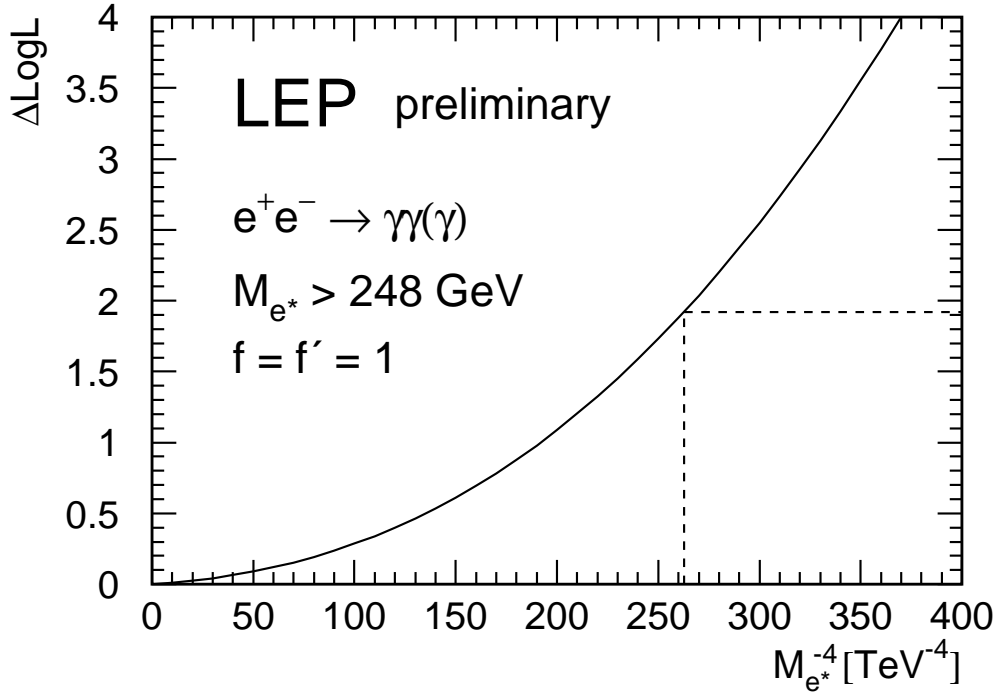


Figure 7.4: Log likelihood difference  $\Delta\text{LogL} = -\ln \mathcal{L} + \ln \mathcal{L}_{\max}$  as a function of  $M_{e^*}^{-4}$ . The coupling is fixed at  $f = f' = 1$ . The value corresponding to  $\Delta\text{LogL} = 1.92$  is  $M_{e^*} = 248$  GeV.



# Chapter 8

## Fermion-Pair Production at LEP-II

**Updates with respect to summer 2002:**

Unchanged w.r.t. summer 2002: Results are preliminary.

### 8.1 Introduction

During the LEP-II program LEP delivered collisions at energies from  $\sim 130$  GeV to  $\sim 209$  GeV. The 4 LEP experiments have made measurements on the  $e^+e^- \rightarrow f\bar{f}$  process over this range of energies, and a preliminary combination of these data is discussed in this note.

In the years 1995 through 1999 LEP delivered luminosity at a number of distinct centre-of-mass energy points. In 2000 most of the luminosity was delivered close to 2 distinct energies, but there was also a significant fraction of the luminosity delivered in, more-or-less, a continuum of energies. To facilitate the combination of the data, the 4 LEP experiments all divided the data they collected in 2000 into two energy bins: from 202.5 to 205.5 GeV; and 205.5 GeV and above. The nominal and actual centre-of-mass energies to which the LEP data are averaged for each year are given in Table 8.1.

A number of measurements on the process  $e^+e^- \rightarrow f\bar{f}$  exist and are combined. The preliminary averages of cross-section and forward-backward asymmetry measurements are discussed in Section 8.2. The results presented in this section update those presented in [76–80]. Complete results of the combinations are available on the web page [81]. In Section 8.3 a preliminary average of the differential cross-sections measurements,  $\frac{d\sigma}{d\cos\theta}$ , for the channels  $e^+e^- \rightarrow e^+e^-$ ,  $e^+e^- \rightarrow \mu^+\mu^-$  and  $e^+e^- \rightarrow \tau^+\tau^-$  is presented. In Section 8.4 a preliminary combination of the heavy flavour results  $R_b$ ,  $R_c$ ,  $A_{FB}^{b\bar{b}}$  and  $A_{FB}^{c\bar{c}}$  from LEP-II is presented. In Section 8.5 the combined results are interpreted in terms of contact interactions and the exchange of  $Z'$  bosons, the exchange of leptoquarks or squarks and the exchange of gravitons in large extra dimensions. The results are summarised in section 8.6.

There are significant changes with respect to results presented in Summer 2001 [76]:

- Changes to the combinations of results
  - updated preliminary cross-sections and leptonic forward-backward asymmetries for ALEPH
  - a new combination of preliminary differential cross-sections for  $e^+e^-$  final states

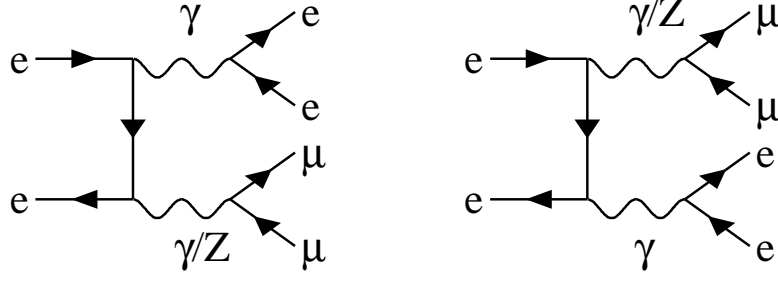


Figure 8.1: Diagrams leading to the the production of initial state non-singlet electron-positron pairs in  $e^+e^- \rightarrow \mu^+\mu^-$ , which are considered as signal in the common signal definition.

- updated preliminary differential cross-section results for  $\mu^+\mu^-$  and  $\tau^+\tau^-$  final states from ALEPH
- new preliminary heavy flavour results. Results are now averaged separately for  $b\bar{b}$  and  $c\bar{c}$  final states
- Changes to the interpretations of the combined results
  - previous results have been updated using the updated combinations
  - new interpretations of the updated data in terms of the exchange of leptoquarks
  - new interpretations of the  $e^+e^-$  final states in terms of contact interactions.

## 8.2 Averages for Cross-sections and Asymmetries

In this section the results of the preliminary combination of cross-sections and asymmetries are given. The individual experiments' analyses of cross-sections and forward-backward asymmetries are discussed in [82].

Cross-section results are combined for the  $e^+e^- \rightarrow q\bar{q}$ ,  $e^+e^- \rightarrow \mu^+\mu^-$  and  $e^+e^- \rightarrow \tau^+\tau^-$  channels, forward-backward asymmetry measurements are combined for the  $\mu^+\mu^-$  and  $\tau^+\tau^-$  final states. The averages are made for the samples of events with high effective centre-of-mass energies,  $\sqrt{s'}$ . Individual experiments have their own  $f\bar{f}$  signal definitions; corrections are applied to bring the measurements to a common signal definitions:

- $\sqrt{s'}$  is taken to be the mass of the  $s$ -channel propagator, with the  $f\bar{f}$  signal being defined by the cut  $\sqrt{s'}/s > 0.85$ .
- ISR-FSR photon interference is subtracted to render the propagator mass unambiguous.
- Results are given for the full  $4\pi$  angular acceptance.
- Initial state non-singlet diagrams [83], see for example Figure 8.1, which lead to events containing additional fermions pairs are considered as part of the two fermion signal. In such events, the additional fermion pairs are typically lost down the beampipe of the experiments, such that the visible event topologies are usually similar to a difermion events with photons radiated from the initial state.

The corrected measurement of a cross-section or a forward backward asymmetry,  $M_{\text{LEP}}$ , corresponding to the common signal definition, is computed from the experimental measurement  $M_{\text{exp}}$ ,

$$M_{\text{LEP}} = M_{\text{exp}} + (P_{\text{LEP}} - P_{\text{exp}}), \quad (8.1)$$

where  $P_{\text{exp}}$  is the prediction for the measurement obtained for the experiments signal definition and  $P_{\text{LEP}}$  is the prediction for the common signal definition. The predictions are computed with ZFITTER [84].

In choosing a common signal definition there is a tension between the need to have a definition which is practical to implement in event generators and semi-analytical calculations, one which comes close to describing the underlying hard processes and one which most closely matches what is actually measured in experiments. Different signal definitions represent different balances between these needs. To illustrate how different choices would effect the quoted results a second signal definition is studied by calculating different predictions using ZFITTER:

- For dilepton events,  $\sqrt{s'}$  is taken to be the bare invariant mass of the outgoing dilepton pair (*i.e.*, the invariant mass excluding all radiated photons).
- For hadronic events, it is taken to be the mass of the  $s$ -channel propagator.
- In both cases, ISR-FSR photon interference is included and the signal is defined by the cut  $\sqrt{s'}/s > 0.85$ . When calculating the contribution to the hadronic cross-section due to ISR-FSR interference, since the propagator mass is ill-defined, it is replaced by the bare  $q\bar{q}$  mass.

The definition of the hadronic cross-section is close to that used to define the signal for the heavy quark measurements given in Section 8.4.

Theoretical uncertainties associated with the Standard Model predictions for each of the measurements are not included during the averaging procedure, but must be included when assessing the compatibility of the data with theoretical predictions. The theoretical uncertainties on the Standard Model predictions amount to 0.26% on  $\sigma(q\bar{q})$ , 0.4% on  $\sigma(\mu^+\mu^-)$  and  $\sigma(\tau^+\tau^-)$ , 2% on  $\sigma(e^+e^-)$ , and 0.004 on the leptonic forward-backward asymmetries [83].

The average is performed using the best linear unbiased estimator technique (BLUE) [85], which is equivalent to a  $\chi^2$  minimisation. All data from nominal centre-of-mass energies of 130–207 GeV are averaged at the same time.

Particular care is taken to ensure that the correlations between the hadronic cross-sections are reasonably estimated. As in [76] the errors are broken down into 5 categories, with the ensuing correlations accounted for in the combinations:

- 1) The statistical uncertainty plus uncorrelated systematic uncertainties, combined in quadrature.
- 2) The systematic uncertainty for the final state X which is fully correlated between energy points for that experiment.
- 3) The systematic uncertainty for experiment Y which is fully correlated between different final states for this energy point.
- 4) The systematic uncertainty for the final state X which is fully correlated between energy points and between different experiments.

- 5) The systematic uncertainty which is fully correlated between energy points and between different experiments for all final states.

Uncertainties in the hadronic cross-sections arising from fragmentation models and modelling of ISR are treated as fully correlated between experiments. Despite some differences between the models used and the methods of evaluating the errors in the different experiments, there are significant common elements in the estimation of these sources of uncertainty.

New, preliminary, results from ALEPH are included in the average. The updated ALEPH measurements use a lower cut on the effective centre-of-mass energy, which makes the signal definition of ALEPH closer to the combined LEP signal definition.

Table 8.2 gives the averaged cross-sections and forward-backward asymmetries for all energies. The differences in the results obtained when using predictions of ZFITTER for the second signal definition are also given. The differences are significant when compared to the precision obtained from averaging together the measurements at all energies. The  $\chi^2$  per degree of freedom for the average of the LEP-II  $f\bar{f}$  data is 160/180. Most correlations are rather small, with the largest components at any given pair of energies being between the hadronic cross-sections. The other off-diagonal terms in the correlation matrix are smaller than 10%. The correlation matrix between the averaged hadronic cross-sections at different centre-of-mass energies is given in Table 8.3. Differences in the results with respect to previous combinations at centre-of-mass energies from 130–207 GeV [76] arise from the updates to the ALEPH results.

Figures 8.2 and 8.3 show the LEP averaged cross-sections and asymmetries, respectively, as a function of the centre-of-mass energy, together with the SM predictions. There is good agreement between the SM expectations and the measurements of the individual experiments and the combined averages. The cross-sections for hadronic final states at most of the energy points are somewhat above the SM expectations. Taking into account the correlations between the data points and also taking into account the theoretical error on the SM predictions, the ratio of the measured cross-sections to the SM expectations, averaged over all energies, is approximately a 1.7 standard deviation excess. It is concluded that there is no significant evidence in the results of the combinations for physics beyond the SM in the process  $e^+e^- \rightarrow f\bar{f}$ .

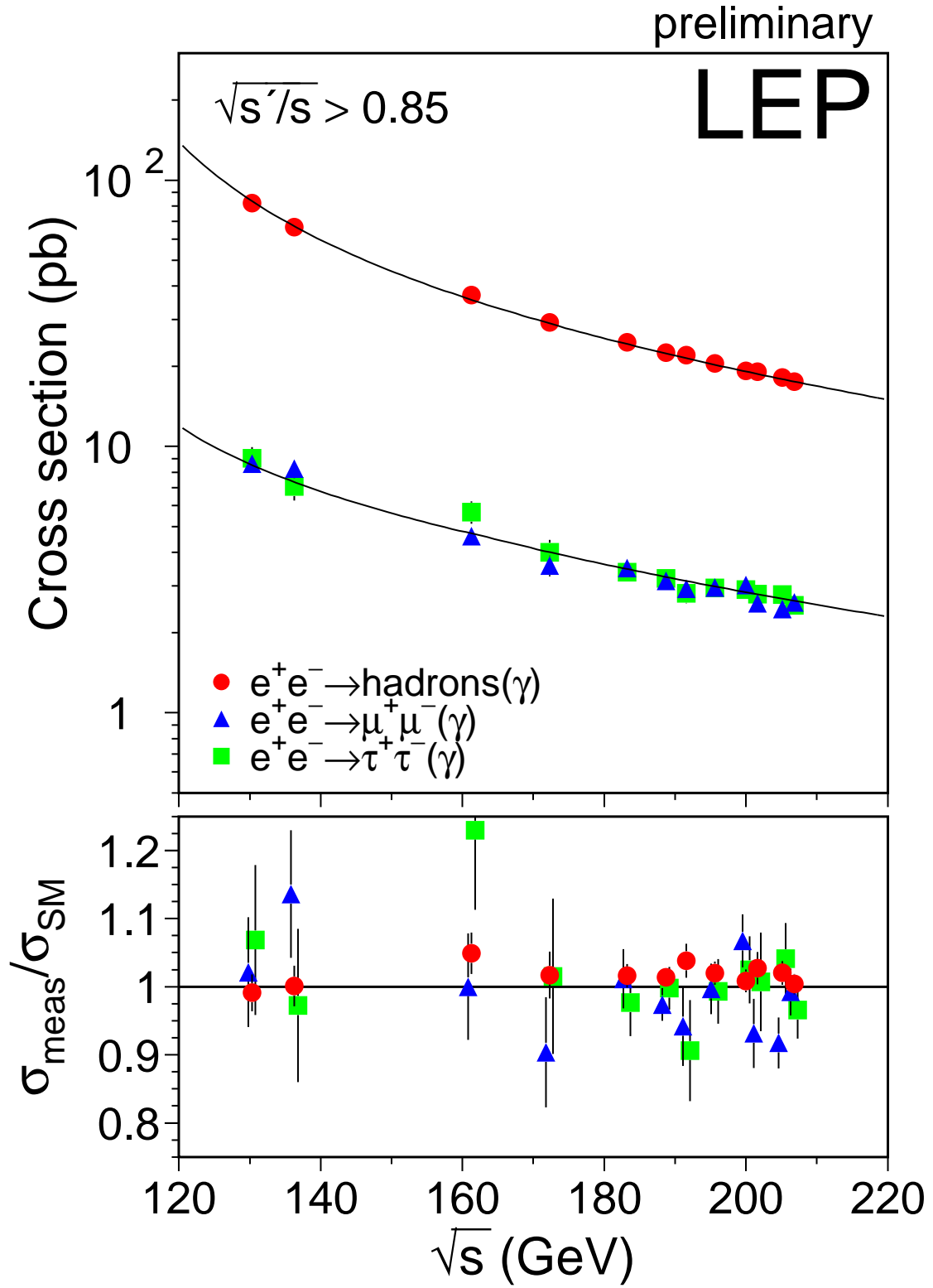


Figure 8.2: Preliminary combined LEP results on the cross-sections for  $q\bar{q}$ ,  $\mu^+\mu^-$  and  $\tau^+\tau^-$  final states, as a function of centre-of-mass energy. The expectations of the SM, computed with ZFITTER [84], are shown as curves. The lower plot shows the ratio of the data divided by the SM.

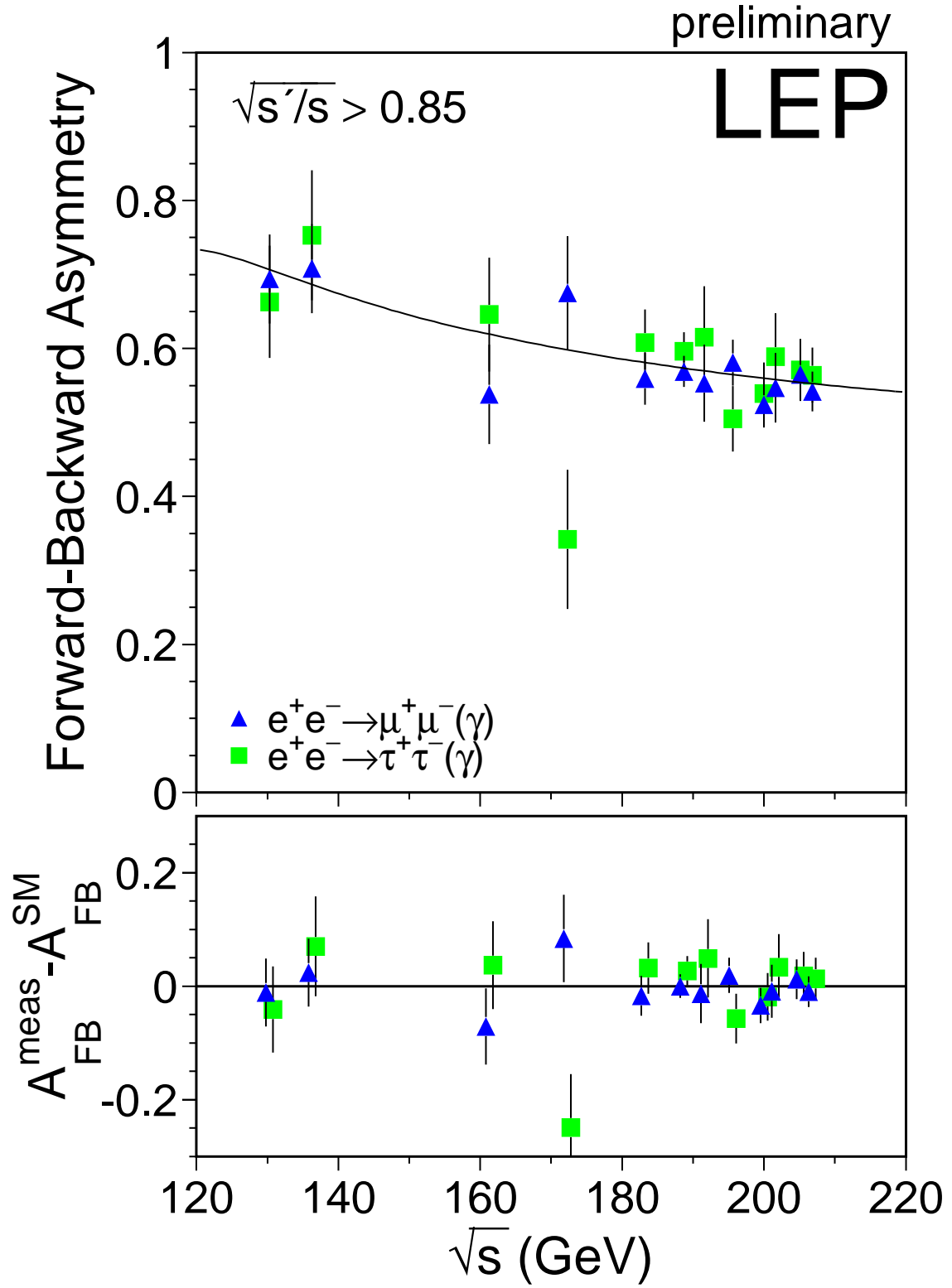


Figure 8.3: Preliminary combined LEP results on the forward-backward asymmetry for  $\mu^+\mu^-$  and  $\tau^+\tau^-$  final states as a function of centre-of-mass energy. The expectations of the SM computed with ZFITTER [84], are shown as curves. The lower plot shows differences between the data and the SM.

Year	Nominal Energy GeV	Actual Energy GeV	Luminosity $\text{pb}^{-1}$
1995	130	130.2	$\sim 3$
	136	136.2	$\sim 3$
	133*	133.2	$\sim 6$
1996	161	161.3	$\sim 10$
	172	172.1	$\sim 10$
	167*	166.6	$\sim 20$
1997	130	130.2	$\sim 2$
	136	136.2	$\sim 2$
	183	182.7	$\sim 50$
1998	189	188.6	$\sim 170$
1999	192	191.6	$\sim 30$
	196	195.5	$\sim 80$
	200	199.5	$\sim 80$
	202	201.6	$\sim 40$
2000	205	204.9	$\sim 80$
	207	206.7	$\sim 140$

Table 8.1: The nominal and actual centre-of-mass energies for data collected during LEP-II operation in each year. The approximate average luminosity analysed per experiment at each energy is also shown. Values marked with a \* are average energies for 1995 and 1996 used for heavy flavour results. The data taken at nominal energies of 130 GeV and 136 GeV in 1995 and 1997 are combined by most experiments.

$\sqrt{s}$ (GeV)	Quantity	Average value	SM	$\Delta$
130	$\sigma(q\bar{q})$	82.1 $\pm$ 2.2	82.8	-0.3
130	$\sigma(\mu^+\mu^-)$	8.62 $\pm$ 0.68	8.44	-0.33
130	$\sigma(\tau^+\tau^-)$	9.02 $\pm$ 0.93	8.44	-0.11
130	$A_{\text{FB}}(\mu^+\mu^-)$	0.694 $\pm$ 0.060	0.705	0.012
130	$A_{\text{FB}}(\tau^+\tau^-)$	0.663 $\pm$ 0.076	0.704	0.012
136	$\sigma(q\bar{q})$	66.7 $\pm$ 2.0	66.6	-0.2
136	$\sigma(\mu^+\mu^-)$	8.27 $\pm$ 0.67	7.28	-0.28
136	$\sigma(\tau^+\tau^-)$	7.078 $\pm$ 0.820	7.279	-0.091
136	$A_{\text{FB}}(\mu^+\mu^-)$	0.708 $\pm$ 0.060	0.684	0.013
136	$A_{\text{FB}}(\tau^+\tau^-)$	0.753 $\pm$ 0.088	0.683	0.014
161	$\sigma(q\bar{q})$	37.0 $\pm$ 1.1	35.2	-0.1
161	$\sigma(\mu^+\mu^-)$	4.61 $\pm$ 0.36	4.61	-0.18
161	$\sigma(\tau^+\tau^-)$	5.67 $\pm$ 0.54	4.61	-0.06
161	$A_{\text{FB}}(\mu^+\mu^-)$	0.538 $\pm$ 0.067	0.609	0.017
161	$A_{\text{FB}}(\tau^+\tau^-)$	0.646 $\pm$ 0.077	0.609	0.016
172	$\sigma(q\bar{q})$	29.23 $\pm$ 0.99	28.74	-0.12
172	$\sigma(\mu^+\mu^-)$	3.57 $\pm$ 0.32	3.95	-0.16
172	$\sigma(\tau^+\tau^-)$	4.01 $\pm$ 0.45	3.95	-0.05
172	$A_{\text{FB}}(\mu^+\mu^-)$	0.675 $\pm$ 0.077	0.591	0.018
172	$A_{\text{FB}}(\tau^+\tau^-)$	0.342 $\pm$ 0.094	0.591	0.017
183	$\sigma(q\bar{q})$	24.59 $\pm$ 0.42	24.20	-0.11
183	$\sigma(\mu^+\mu^-)$	3.49 $\pm$ 0.15	3.45	-0.14
183	$\sigma(\tau^+\tau^-)$	3.37 $\pm$ 0.17	3.45	-0.05
183	$A_{\text{FB}}(\mu^+\mu^-)$	0.559 $\pm$ 0.035	0.576	0.018
183	$A_{\text{FB}}(\tau^+\tau^-)$	0.608 $\pm$ 0.045	0.576	0.018
189	$\sigma(q\bar{q})$	22.47 $\pm$ 0.24	22.156	-0.101
189	$\sigma(\mu^+\mu^-)$	3.123 $\pm$ 0.076	3.207	-0.131
189	$\sigma(\tau^+\tau^-)$	3.20 $\pm$ 0.10	3.20	-0.048
189	$A_{\text{FB}}(\mu^+\mu^-)$	0.569 $\pm$ 0.021	0.569	0.019
189	$A_{\text{FB}}(\tau^+\tau^-)$	0.596 $\pm$ 0.026	0.569	0.018

$\sqrt{s}$ (GeV)	Quantity	Average value	SM	$\Delta$
192	$\sigma(q\bar{q})$	22.05 $\pm$ 0.53	21.24	-0.10
192	$\sigma(\mu^+\mu^-)$	2.92 $\pm$ 0.18	3.10	-0.13
192	$\sigma(\tau^+\tau^-)$	2.81 $\pm$ 0.23	3.10	-0.05
192	$A_{\text{FB}}(\mu^+\mu^-)$	0.553 $\pm$ 0.051	0.566	0.019
192	$A_{\text{FB}}(\tau^+\tau^-)$	0.615 $\pm$ 0.069	0.566	0.019
196	$\sigma(q\bar{q})$	20.53 $\pm$ 0.34	20.13	-0.09
196	$\sigma(\mu^+\mu^-)$	2.94 $\pm$ 0.11	2.96	-0.12
196	$\sigma(\tau^+\tau^-)$	2.94 $\pm$ 0.14	2.96	-0.05
196	$A_{\text{FB}}(\mu^+\mu^-)$	0.581 $\pm$ 0.031	0.562	0.019
196	$A_{\text{FB}}(\tau^+\tau^-)$	0.505 $\pm$ 0.044	0.562	0.019
200	$\sigma(q\bar{q})$	19.25 $\pm$ 0.32	19.09	-0.09
200	$\sigma(\mu^+\mu^-)$	3.02 $\pm$ 0.11	2.83	-0.12
200	$\sigma(\tau^+\tau^-)$	2.90 $\pm$ 0.14	2.83	-0.04
200	$A_{\text{FB}}(\mu^+\mu^-)$	0.524 $\pm$ 0.031	0.558	0.019
200	$A_{\text{FB}}(\tau^+\tau^-)$	0.539 $\pm$ 0.042	0.558	0.019
202	$\sigma(q\bar{q})$	19.07 $\pm$ 0.44	18.57	-0.09
202	$\sigma(\mu^+\mu^-)$	2.58 $\pm$ 0.14	2.77	-0.12
202	$\sigma(\tau^+\tau^-)$	2.79 $\pm$ 0.20	2.77	-0.04
202	$A_{\text{FB}}(\mu^+\mu^-)$	0.547 $\pm$ 0.047	0.556	0.020
202	$A_{\text{FB}}(\tau^+\tau^-)$	0.589 $\pm$ 0.059	0.556	0.019
205	$\sigma(q\bar{q})$	18.17 $\pm$ 0.31	17.81	-0.09
205	$\sigma(\mu^+\mu^-)$	2.45 $\pm$ 0.10	2.67	-0.11
205	$\sigma(\tau^+\tau^-)$	2.78 $\pm$ 0.14	2.67	-0.042
205	$A_{\text{FB}}(\mu^+\mu^-)$	0.565 $\pm$ 0.035	0.553	0.020
205	$A_{\text{FB}}(\tau^+\tau^-)$	0.571 $\pm$ 0.042	0.553	0.019
207	$\sigma(q\bar{q})$	17.49 $\pm$ 0.26	17.42	-0.08
207	$\sigma(\mu^+\mu^-)$	2.595 $\pm$ 0.088	2.623	-0.111
207	$\sigma(\tau^+\tau^-)$	2.53 $\pm$ 0.11	2.62	-0.04
207	$A_{\text{FB}}(\mu^+\mu^-)$	0.542 $\pm$ 0.027	0.552	0.020
207	$A_{\text{FB}}(\tau^+\tau^-)$	0.564 $\pm$ 0.037	0.551	0.019

Table 8.2: Preliminary combined LEP results for  $e^+e^- \rightarrow f\bar{f}$ , with cross section quoted in units of picobarn. All the results correspond to the first signal definition. The Standard Model predictions are from ZFITTEr [84]. The difference,  $\Delta$ , in the predictions of ZFITTEr for second definition relative to the first are given in the final column. The quoted uncertainties do not include the theoretical uncertainties on the corrections discussed in the text.



$\sqrt{s}$ (GeV)	130	136	161	172	183	189	192	196	200	202	205	207
130	1.000	0.071	0.080	0.072	0.114	0.146	0.077	0.105	0.120	0.086	0.117	0.138
136	0.071	1.000	0.075	0.067	0.106	0.135	0.071	0.097	0.110	0.079	0.109	0.128
161	0.080	0.075	1.000	0.077	0.120	0.153	0.080	0.110	0.125	0.090	0.124	0.145
172	0.072	0.067	0.077	1.000	0.108	0.137	0.072	0.099	0.112	0.081	0.111	0.130
183	0.114	0.106	0.120	0.108	1.000	0.223	0.117	0.158	0.182	0.129	0.176	0.208
189	0.146	0.135	0.153	0.137	0.223	1.000	0.151	0.206	0.235	0.168	0.226	0.268
192	0.077	0.071	0.080	0.072	0.117	0.151	1.000	0.109	0.126	0.090	0.118	0.138
196	0.105	0.097	0.110	0.099	0.158	0.206	0.109	1.000	0.169	0.122	0.162	0.190
200	0.120	0.110	0.125	0.112	0.182	0.235	0.126	0.169	1.000	0.140	0.184	0.215
202	0.086	0.079	0.090	0.081	0.129	0.168	0.090	0.122	0.140	1.000	0.132	0.153
205	0.117	0.109	0.124	0.111	0.176	0.226	0.118	0.162	0.184	0.132	1.000	0.213
207	0.138	0.128	0.145	0.130	0.208	0.268	0.138	0.190	0.215	0.153	0.213	1.000

Table 8.3: The correlation coefficients between averaged hadronic cross-sections at different energies.

## 8.3 Averages for Differential Cross-sections

### 8.3.1 $e^+e^-$ final state

The LEP experiments have measured the differential cross-section,  $\frac{d\sigma}{d\cos\theta}$ , for the  $e^+e^- \rightarrow e^+e^-$  channel. A preliminary combination of these results is made by performing a  $\chi^2$  fit to the measured differential cross-sections, using the statistical errors as given by the experiments. In contrast to the muon and tau channels (Section 8.3.2) the higher statistics makes the use of expected statistical errors unnecessary. The combination includes data from 189 GeV to 207 GeV from all experiments but DELPHI. The data used in the combination are summarised in Table 8.4.

Each experiment's data are binned according to an agreed common definition, which takes into account the large forward peak of Bhabha scattering:

- 10 bins for  $\cos\theta$  between 0.0 and 0.90 and
- 5 bins for  $\cos\theta$  between  $-0.90$  and 0.0

at each energy. The scattering angle,  $\theta$ , is the angle of the negative lepton with respect to the incoming electron direction in the lab coordinate system. The outer acceptances of the most forward and most backward bins for which the experiments present their data are different. The ranges in  $\cos\theta$  of the individual experiments and the average are given in Table 8.5. Except for the binning, each experiment uses their own signal definition, for example different experiments have different acollinearity cuts to select events. The signal definition used for the LEP average corresponds to an acollinearity cut of  $10^\circ$ . The experimental measurements are corrected to the common signal definition following the procedure described in Section 8.2. The theoretical predictions are taken from the Monte Carlo event generator BHWIDE [86].

Correlated systematic errors between different experiments, energies and bins at the same energy, arising from uncertainties on the overall normalisation, and from migration of events between forward and backward bins with the same absolute value of  $\cos\theta$  due to uncertainties in the corrections for charge confusion, were considered in the averaging procedure.

An average for all energies between 189–207 GeV is performed. The results of the averages are shown in Figure 8.4. The  $\chi^2$  per degree of freedom for the average is 190.8/189.

The correlations between bins in the average are well below 5% of the total error on the averages in each bin for most of the cases, and exceed 10% for the most forward bin for the energy points with the highest accumulated statistics. The agreement between the averaged data and the predictions from the Monte Carlo generator BHWIDE is good.

### 8.3.2 $\mu^+\mu^-$ and $\tau^+\tau^-$ final states

The LEP experiments have measured the differential cross-section,  $\frac{d\sigma}{d\cos\theta}$ , for the  $e^+e^- \rightarrow \mu^+\mu^-$  and  $e^+e^- \rightarrow \tau^+\tau^-$  channels for samples of events with high effective centre-of-mass energy,  $\sqrt{s'}/s > 0.85$ . A preliminary combination of these results is made using the BLUE technique. The statistical error associated with each measurement is taken as the expected statistical error on the differential cross-section, computed from the expected number of events in each bin for each experiment. Using a

Monte Carlo simulation it has been shown that this method provides a good approximation to the exact likelihood method based on Poisson statistics [78].

The combination includes data from 183 GeV to 207 GeV, but not all experiments provided data at all energies. Since [76], the ALEPH results have been updated. The data used in the combination are summarised in Table 8.6.

Each experiment's data are binned in 10 bins of  $\cos\theta$  at each energy, using their own signal definition. The scattering angle,  $\theta$ , is the angle of the negative lepton with respect to the incoming electron direction in the lab coordinate system. The outer acceptances of the most forward and most backward bins for which the four experiments present their data are different. This was accounted for as part of the correction to a common signal definition. The ranges in  $\cos\theta$  for the measurements of the individual experiments and the average are given in Table 8.7. The signal definition used corresponded to the first definition given in Section 8.2.

Correlated systematic errors between different experiments, channels and energies, arising from uncertainties on the overall normalisation are considered in the averaging procedure. Previously [76] three separate averages were performed for different centre-of-mass energies; one for 183 and 189 GeV data, one for 192–202 GeV data and for 205 and 207 GeV data, which resulted in missing correlations between measurements in different groups of energies. Now all data from all energies are combined in a single fit to obtain averages at each centre-of-mass energy yielding a full covariance matrix between the different measurements at all energies.

The results of the averages are shown in Figures 8.5 and 8.6. The correlations between bins in the average are less than 2% of the total error on the averages in each bin. Overall the agreement between the averaged data and the predictions is reasonable, with a  $\chi^2$  of 200 for 160 degrees of freedom. At 202 GeV the measured differential cross-sections in the most backward bins,  $-1.00 < \cos\theta < 0.8$ , for both muon and tau final states are above the predictions. The data at 202 GeV suffer from rather low delivered luminosity, with less than 4 events expected in each experiment in each channel in this backward  $\cos\theta$  bin. The agreement between the data and the predictions in the same  $\cos\theta$  bin is more consistent at higher energies.

$\sqrt{s}(\text{GeV})$	$e^+e^- \rightarrow e^+e^-$			
	A	D	L	O
189	P	-	P	F
192–202	P	-	P	P
205–207	P	-	P	P

Table 8.4: Differential cross-section data provided by the LEP collaborations (ALEPH, DELPHI, L3 and OPAL) for  $e^+e^- \rightarrow e^+e^-$ . Data indicated with F are final, published data. Data marked with P are preliminary. Data marked with a - were not available for combination.

Preliminary LEP Averaged  $d\sigma / d\cos\Theta (e^+e^-)$

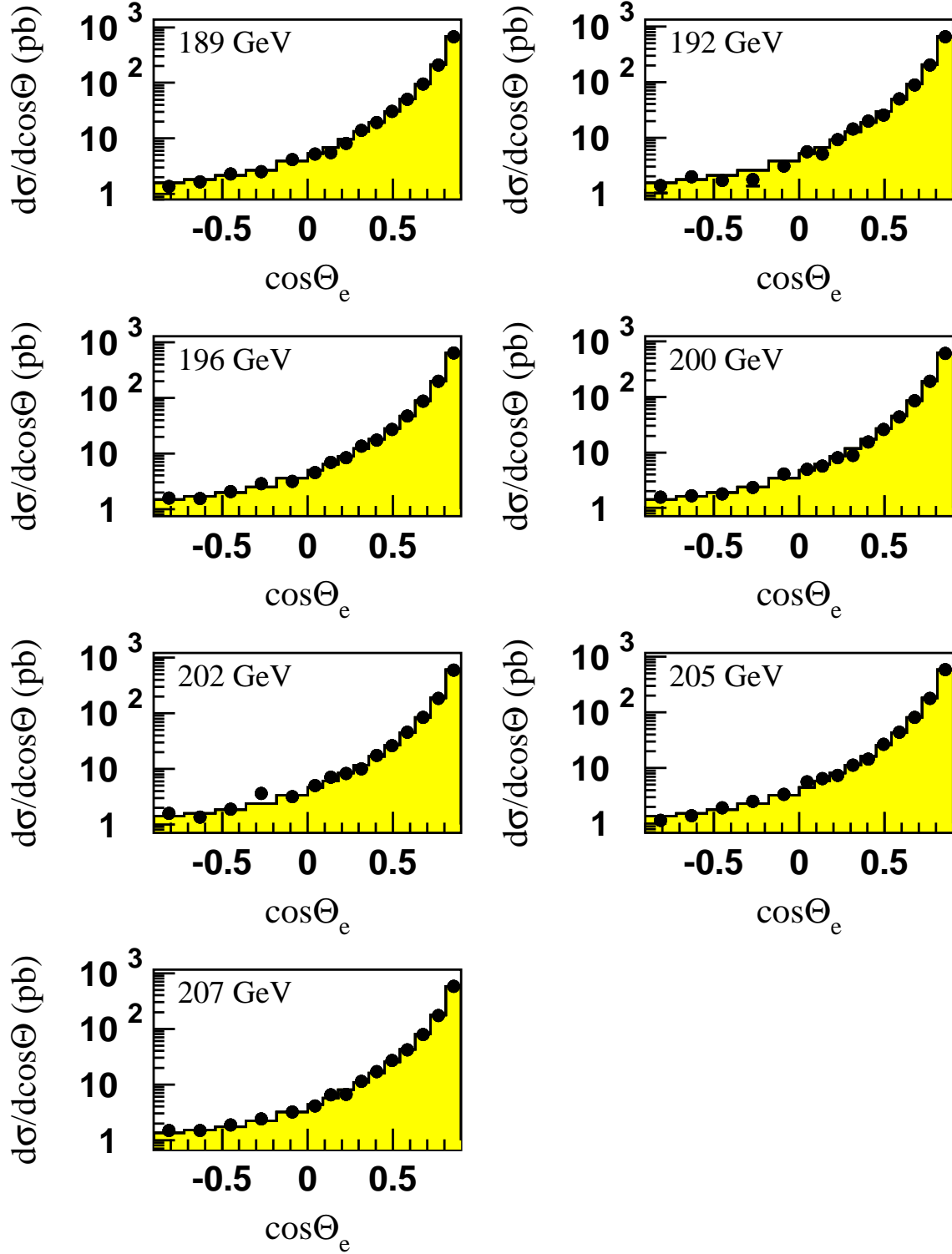


Figure 8.4: LEP averaged differential cross-sections for  $e^+e^- \rightarrow e^+e^-$  at energies of 189–207 GeV. The SM predictions, shown as solid histograms, are computed with BHWIDE [86].

Experiment	$\cos \theta_{min}$	$\cos \theta_{max}$
ALEPH ( $\sqrt{s'}/s > 0.85$ )	-0.90	0.90
L3 (acol. $< 25^\circ$ )	-0.72	0.72
OPAL (acol. $< 10^\circ$ )	-0.90	0.90
Average (acol. $< 10^\circ$ )	-0.90	0.90

Table 8.5: The acceptances for which experimental data are presented for the  $e^+e^- \rightarrow e^+e^-$  channel and the acceptance for the LEP average.

$\sqrt{s}(\text{GeV})$	$e^+e^- \rightarrow \mu^+\mu^-$				$e^+e^- \rightarrow \tau^+\tau^-$			
	A	D	L	O	A	D	L	O
183	-	F	-	F	-	F	-	F
189	P	F	F	F	P	F	F	F
192-202	P	P	P	P	P	P	-	P
205-207	P	P	P	P	P	P	-	P

Table 8.6: Differential cross-section data provided by the LEP collaborations (ALEPH, DELPHI, L3 and OPAL) for  $e^+e^- \rightarrow \mu^+\mu^-$  and  $e^+e^- \rightarrow \tau^+\tau^-$  combination at different centre-of-mass energies. Data indicated with F are final, published data. Data marked with P are preliminary. Data marked with a - were not available for combination.

Experiment	$\cos \theta_{min}$	$\cos \theta_{max}$
ALEPH	-0.95	0.95
DELPHI ( $e^+e^- \rightarrow \mu^+\mu^-$ 183)	-0.94	0.94
DELPHI ( $e^+e^- \rightarrow \mu^+\mu^-$ 189-207)	-0.97	0.97
DELPHI ( $e^+e^- \rightarrow \tau^+\tau^-$ )	-0.96	0.96
L3	-0.90	0.90
OPAL	-1.00	1.00
Average	-1.00	1.00

Table 8.7: The acceptances for which experimental data are presented and the acceptance for the LEP average. For DELPHI the acceptance is shown for the different channels and for the muons for different centre of mass energies. For all other experiments the acceptance is the same for muon and tau-lepton channels and for all energies provided.

### Preliminary LEP Averaged $d\sigma/d\cos\theta$ ( $\mu\mu$ )

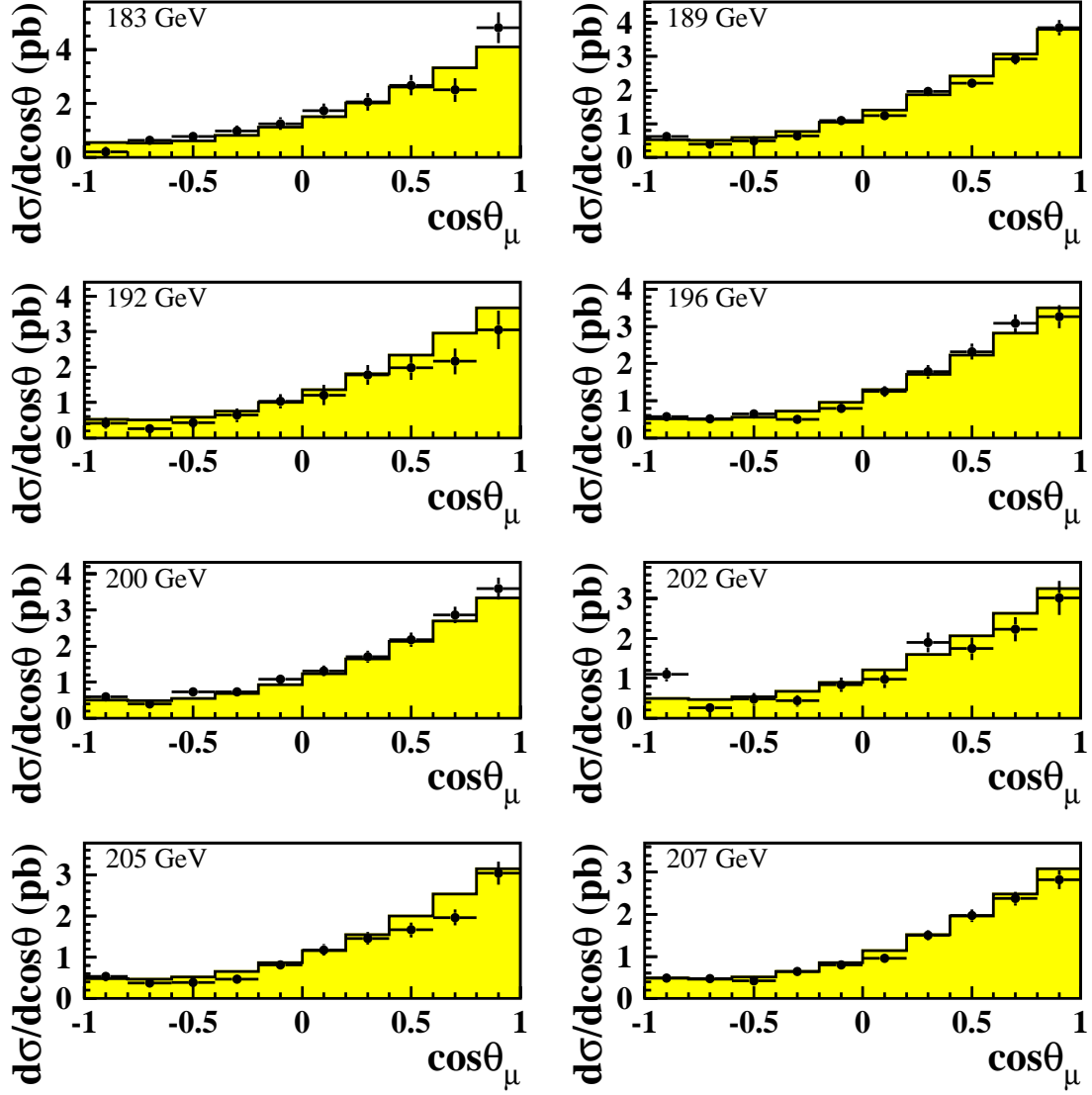


Figure 8.5: LEP averaged differential cross-sections for  $e^+e^- \rightarrow \mu^+\mu^-$  at energies of 183–207 GeV. The SM predictions, shown as solid histograms, are computed with ZFITTER [84].

### Preliminary LEP Averaged $d\sigma/d\cos\theta$ ( $\tau\tau$ )

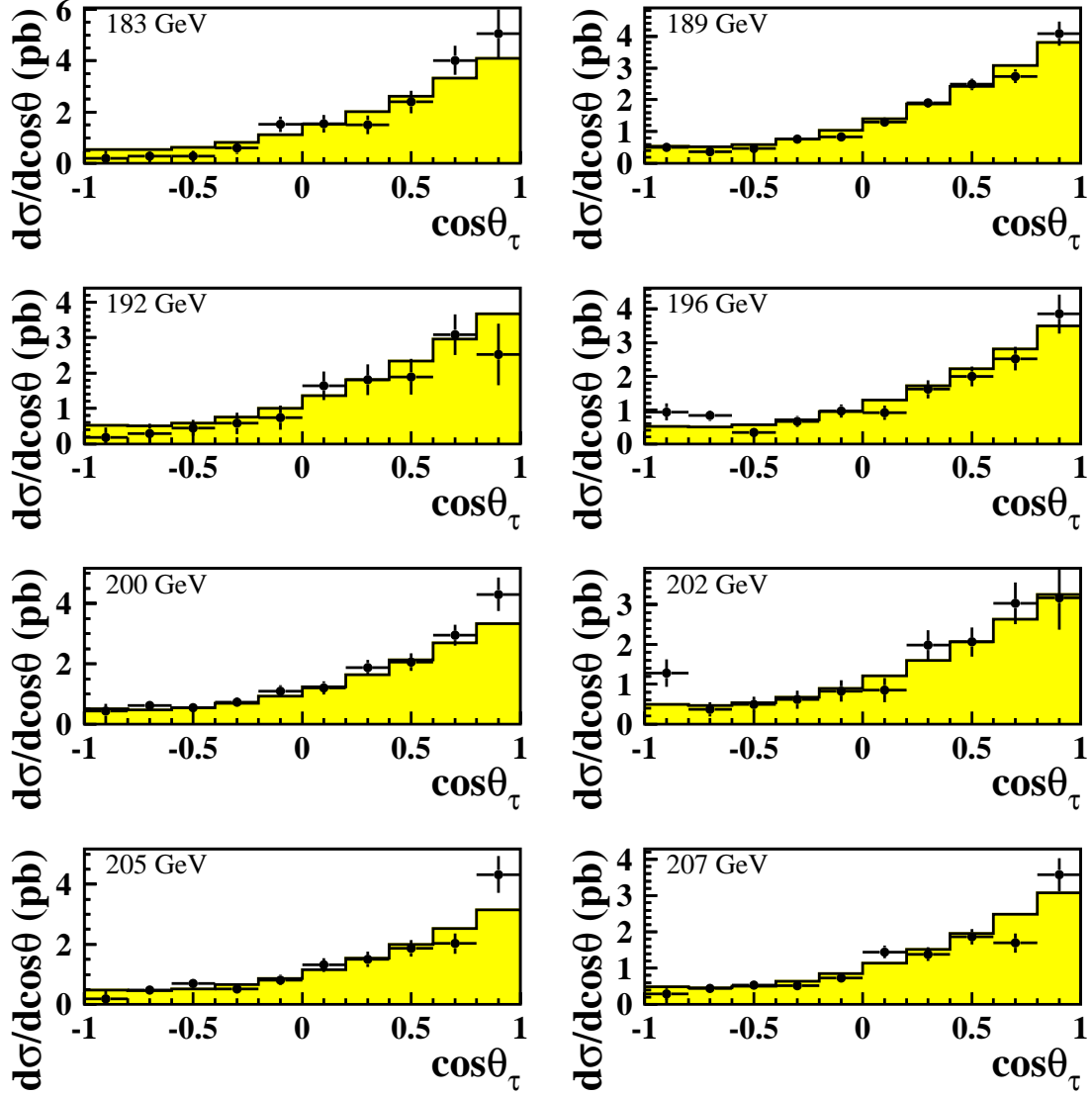


Figure 8.6: LEP averaged differential cross-sections for  $e^+e^- \rightarrow \tau^+\tau^-$  at energies of 183–207 GeV. The SM predictions, shown as solid histograms, are computed with ZFITTER [84].

## 8.4 Averages for Heavy Flavour Measurements

This section presents a preliminary combination of both published [87] and preliminary [88] measurements of the ratios cross section ratios  $R_q$  defined as  $\frac{\sigma_{q\bar{q}}}{\sigma_{\text{had}}}$  for b and c production,  $R_b$  and  $R_c$ , and the forward-backward asymmetries,  $A_{\text{FB}}^{b\bar{b}}$  and  $A_{\text{FB}}^{c\bar{c}}$ , from the LEP collaborations at centre-of-mass energies in the range of 130 GeV to 207 GeV. The averages have been updated with respect to [76]. New, preliminary, results from ALEPH on  $A_{\text{FB}}^{b\bar{b}}$  at centre-of-mass energies of 205 GeV and 207 GeV and on  $R_c$  at centre-of-mass energies of 196, 200, 205 and 207 GeV are included. Table 8.8 summarises all the inputs that have been combined so far.

A common signal definition is defined for all the measurements, requiring:

- an effective centre-of-mass energy  $\sqrt{s'} > 0.85\sqrt{s}$
- no subtraction of ISR and FSR photon interference contribution and
- extrapolation to full angular acceptance.

Systematic errors are divided into three categories: uncorrelated errors, errors correlated between the measurements of each experiment, and errors common to all experiments.

Due to the fact that  $R_c$  measurements are only provided by a single experiment and are strongly correlated with  $R_b$  measurements, it was decided to fit the b sector and c sector separately, the other flavour's measurements being fixed to their Standard Model predictions. In addition, these fitted values are used to set limits upon physics beyond the Standard Model, such as contact term interactions, in which only one quark flavour is assumed to be effected by the new physics during each fit, therefore this averaging method is consistent with the interpretations.

Full details concerning the combination procedure can be found in [89].

The results of the combination are presented in Table 8.9 and Table 8.10 and in Figures 8.7 and 8.8. The results for both b and c sector are in agreement with the Standard Model predictions of ZFITTER. The averaged discrepancies with respect to the Standard Model predictions is  $-2.08 \sigma$  for  $R_b$ ,  $+0.30 \sigma$  for  $R_c$ ,  $-1.56 \sigma$  for  $A_{\text{FB}}^{b\bar{b}}$  and  $-0.24 \sigma$  for  $A_{\text{FB}}^{c\bar{c}}$ . A list of the error contributions from the combination at 189 GeV is shown in Table 8.11.

$\sqrt{s}$ (GeV)	$R_b$				$R_c$				$A_{\text{FB}}^{b\bar{b}}$				$A_{\text{FB}}^{c\bar{c}}$			
	A	D	L	O	A	D	L	O	A	D	L	O	A	D	L	O
133	F	F	F	F	-	-	-	-	-	F	-	F	-	F	-	F
167	F	F	F	F	-	-	-	-	-	F	-	F	-	F	-	F
183	F	P	F	F	F	-	-	-	F	-	-	F	P	-	-	F
189	P	P	F	F	P	-	-	-	P	P	F	F	P	-	-	F
192 to 202	P	P	P	-	P*	-	-	-	P	P	-	-	-	-	-	-
205 and 207	-	P	P	-	P	-	-	-	P	P	-	-	-	-	-	-

Table 8.8: Data provided by the ALEPH, DELPHI, L3, OPAL collaborations for combination at different centre-of-mass energies. Data indicated with F are final, published data. Data marked with P are preliminary and for data marked with P\*, not all energies are supplied. Data marked with a - were not supplied for combination.



$\sqrt{s}$ (GeV)	$R_b$	$A_{\text{FB}}^{b\bar{b}}$
133	$0.1822 \pm 0.0132$ (0.1867)	$0.367 \pm 0.251$ (0.504)
167	$0.1494 \pm 0.0127$ (0.1727)	$0.624 \pm 0.254$ (0.572)
183	$0.1646 \pm 0.0094$ (0.1692)	$0.515 \pm 0.149$ (0.588)
189	$0.1565 \pm 0.0061$ (0.1681)	$0.529 \pm 0.089$ (0.593)
192	$0.1551 \pm 0.0149$ (0.1676)	$0.424 \pm 0.267$ (0.595)
196	$0.1556 \pm 0.0097$ (0.1670)	$0.535 \pm 0.151$ (0.598)
200	$0.1683 \pm 0.0099$ (0.1664)	$0.596 \pm 0.149$ (0.600)
202	$0.1646 \pm 0.0144$ (0.1661)	$0.607 \pm 0.241$ (0.601)
205	$0.1606 \pm 0.0126$ (0.1657)	$0.715 \pm 0.214$ (0.603)
207	$0.1694 \pm 0.0107$ (0.1654)	$0.175 \pm 0.156$ (0.604)

Table 8.9: Combined results on  $R_b$  and  $A_{\text{FB}}^{b\bar{b}}$ . Quoted errors represent the statistical and systematic errors added in quadrature. For comparison, the Standard Model predictions computed with ZFITTER [90] are given in parentheses.

$\sqrt{s}$ (GeV)	$R_c$	$A_{\text{FB}}^{c\bar{c}}$
133	-	$0.630 \pm 0.313$ (0.684)
167	-	$0.980 \pm 0.343$ (0.677)
183	$0.2628 \pm 0.0397$ (0.2472)	$0.717 \pm 0.201$ (0.663)
189	$0.2298 \pm 0.0213$ (0.2490)	$0.542 \pm 0.143$ (0.656)
196	$0.2734 \pm 0.0387$ (0.2508)	-
200	$0.2535 \pm 0.0360$ (0.2518)	-
205	$0.2816 \pm 0.0394$ (0.2530)	-
207	$0.2890 \pm 0.0350$ (0.2533)	-

Table 8.10: Combined results on  $R_c$  and  $A_{\text{FB}}^{c\bar{c}}$ . Quoted errors represent the statistical and systematic errors added in quadrature. For comparison, the Standard Model predictions computed with ZFITTER [90] are given in parentheses.

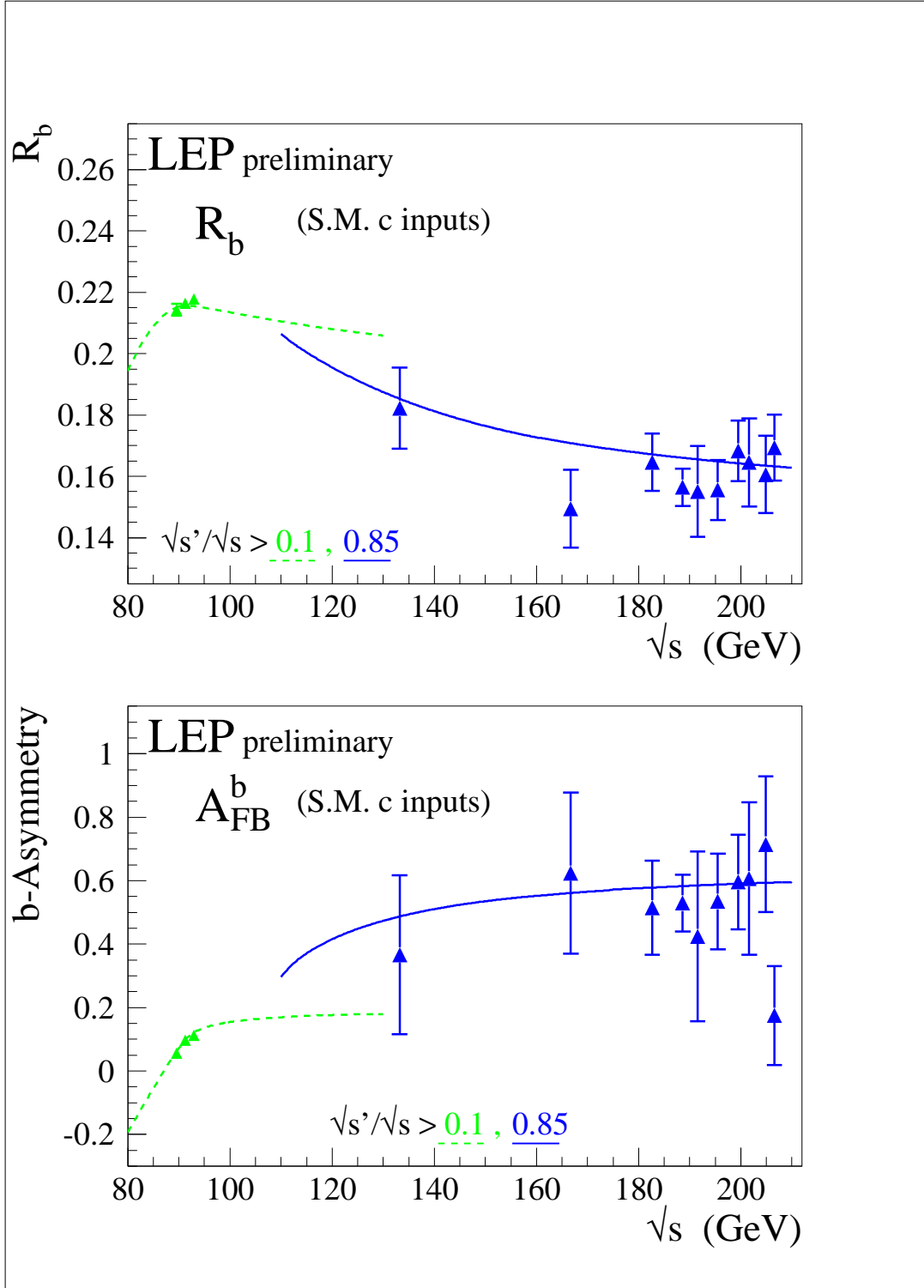


Figure 8.7: Preliminary combined LEP measurements of  $R_b$  and  $A_{FB}^{b\bar{b}}$ . Solid lines represent the Standard Model prediction for the high  $\sqrt{s}'$  selection used at LEP-II and dotted lines the inclusive prediction used at LEP-I. Both are computed with ZFITTER[90]. The LEP-I measurements have been taken from [91].

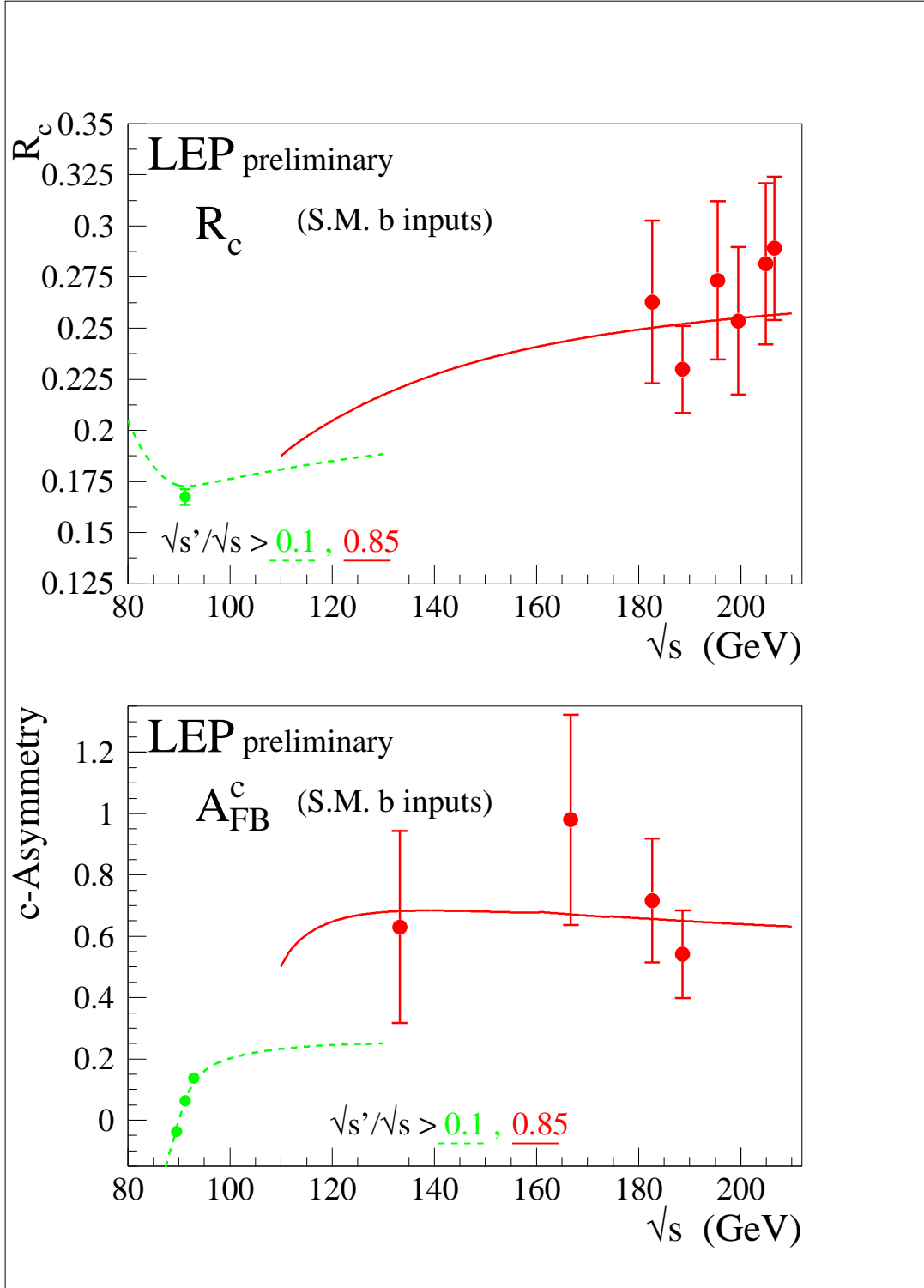


Figure 8.8: Preliminary combined LEP measurements of  $R_c$  and  $A_{FB}^{c\bar{c}}$ . Solid lines represent the Standard Model prediction for the high  $\sqrt{s'}$  selection used at LEP-II and dotted lines the inclusive prediction used at LEP-I. Both are computed with ZFITTER [90]. The LEP-I measurements have been taken from [91].

Error list	$R_b$ (189 GeV)	$A_{\text{FB}}^{\text{bb}}$ (189 GeV)	$R_c$ (189 GeV)	$A_{\text{FB}}^{\text{cc}}$ (189 GeV)
statistics	0.0057	0.084	0.0169	0.119
internal syst	0.0020	0.025	0.0109	0.042
common syst	0.0007	0.011	0.0072	0.069
total syst	0.0021	0.027	0.0130	0.081
total error	0.0061	0.089	0.0213	0.143

Table 8.11: Error breakdown at 189 GeV.

## 8.5 Interpretation

The combined measurements presented above are interpreted in a variety of models. The cross-section and asymmetry results are used to place limits on contact interactions between leptons and quarks and, using the results on heavy flavour production, on contact interaction between electrons and  $b$  and  $c$  quarks specifically. Limits on the mass of a possible additional heavy neutral boson,  $Z'$ , are obtained for a variety of models. The results update those provided in [76]. Using the combined differential cross-sections for  $e^+e^-$  final states, limits on contact interactions in the  $e^+e^- \rightarrow e^+e^-$  channel and limits on the scale of gravity in models with large extra-dimensions are presented. Limits are also derived on the masses of leptoquarks - assuming a coupling of electromagnetic strength. In all cases the Born level predictions for the physics beyond the Standard Model have been corrected to take into account QED radiation.

### 8.5.1 Contact Interactions

The averages of cross-sections and forward-backward asymmetries for muon-pair and tau-lepton pair and the cross-sections for  $q\bar{q}$  final states are used to search for contact interactions between fermions. The results are updated with respect to those given previously [76] due to updates of the averages. Limits are also given for interactions not considered before.

Following [92], contact interactions are parameterised by an effective Lagrangian,  $\mathcal{L}_{\text{eff}}$ , which is added to the Standard Model Lagrangian and has the form:

$$\mathcal{L}_{\text{eff}} = \frac{g^2}{(1+\delta)\Lambda^2} \sum_{i,j=L,R} \eta_{ij} \bar{e}_i \gamma_\mu e_i \bar{f}_j \gamma^\mu f_j, \quad (8.2)$$

where  $g^2/4\pi$  is taken to be 1 by convention,  $\delta = 1(0)$  for  $f = e$  ( $f \neq e$ ),  $\eta_{ij} = \pm 1$  or 0 for different interaction types,  $\Lambda$  is the scale of the contact interactions,  $e_i$  and  $f_j$  are left or right-handed spinors. By assuming different helicity coupling between the initial state and final state currents, a set of different models can be defined from this Lagrangian [93], with either constructive (+) or destructive (−) interference between the Standard Model process and the contact interactions. The models and corresponding choices of  $\eta_{ij}$  are given in Table 8.12. The models  $\text{LL}^\pm$ ,  $\text{RR}^\pm$ ,  $\text{VV}^\pm$ ,  $\text{AA}^\pm$ ,  $\text{LR}^\pm$ ,  $\text{RL}^\pm$ ,  $\text{V0}^\pm$ ,  $\text{A0}^\pm$  are considered here since these models lead to large deviations in  $e^+e^- \rightarrow f\bar{f}$  at LEP II. The corresponding energies scales for the models with constructive or destructive interference are denoted by  $\Lambda^+$  and  $\Lambda^-$  respectively.

For leptonic final states 4 different fits are made

- individual fits to contact interactions in  $e^+e^- \rightarrow \mu^+\mu^-$  and  $e^+e^- \rightarrow \tau^+\tau^-$  using the measured cross-sections and asymmetries,

- fits to  $e^+e^- \rightarrow \ell^+\ell^-$  (simultaneous fits to  $e^+e^- \rightarrow \mu^+\mu^-$  and  $e^+e^- \rightarrow \tau^+\tau^-$ ) again using the measured cross-sections and asymmetries,
- fits to  $e^+e^- \rightarrow e^+e^-$ , using the measured differential cross-sections.

For the inclusive hadronic final states three different model assumptions are used to fit the total hadronic cross-section

- the contact interactions affect only one quark flavour of up-type using the measured hadronic cross-sections,
- the contact interactions affect only one quark flavour of down-type using the measured hadronic cross-sections,
- the contact interactions contribute to all quark final states with the same strength.

Limits on contact interactions between electrons and  $b$  and  $c$  quarks are obtained using all the heavy flavour LEP-II combined results from 133 GeV to 207 GeV given in Tables 8.9 and 8.10. For the purpose of fitting contact interaction models to the data,  $R_b$  and  $R_c$  are converted to cross-sections  $\sigma_{b\bar{b}}$  and  $\sigma_{c\bar{c}}$  using the averaged  $q\bar{q}$  cross-section of section 8.2 corresponding to the second signal definition. In the calculation of errors, the correlations between  $R_b$ ,  $R_c$  and  $\sigma_{q\bar{q}}$  are assumed to be negligible. These results are of particular interest since they are inaccessible to  $p\bar{p}$  or  $ep$  colliders.

For the purpose of fitting contact interaction models to the data, the parameter  $\epsilon = 1/\Lambda^2$  is used, with  $\epsilon = 0$  in the limit that there are no contact interactions. This parameter is allowed to take both positive and negative values in the fits. Theoretical uncertainties on the Standard Model predictions are taken from [83].

The values of  $\epsilon$  extracted for each model are all compatible with the Standard Model expectation  $\epsilon = 0$ , at the two standard deviation level. As expected, the errors on  $\epsilon$  are typically a factor of two smaller than those obtained from a single LEP experiment with the same data set. The fitted values of  $\epsilon$  are converted into 95% confidence level lower limits on  $\Lambda$ . The limits are obtained by integrating the likelihood function in  $\epsilon$  over the physically allowed values<sup>1</sup>,  $\epsilon \geq 0$  for each  $\Lambda^+$  limit and  $\epsilon \leq 0$  for  $\Lambda^-$  limits.

The fitted values of  $\epsilon$  and their 68% confidence level uncertainties together with the 95% confidence level lower limit on  $\Lambda$  are shown in Table 8.13 for the fits to  $e^+e^- \rightarrow \ell^+\ell^-$  ( $\ell \neq e$ ),  $e^+e^- \rightarrow e^+e^-$ , inclusive  $e^+e^- \rightarrow q\bar{q}$ ,  $e^+e^- \rightarrow b\bar{b}$  and  $e^+e^- \rightarrow c\bar{c}$ . Table 8.14 shows only the limits obtained on the scale  $\Lambda$  for other fits. The limits are shown graphically in Figure 8.9.

For the VV model with positive interference and assuming electromagnetic coupling strength instead of  $g^2/4\pi = 1$ , the scale  $\Lambda$  obtained in the  $e^+e^- \rightarrow e^+e^-$  channel is converted to an upper limit on the electron size:

$$r_e < 1.4 \times 10^{-19} \text{m} \quad (8.3)$$

Models with stronger couplings will make this upper limit even tighter.

---

<sup>1</sup>To be able to obtain confidence limits from the likelihood function in  $\epsilon$  it is necessary to convert the likelihood to a probability density function for  $\epsilon$ ; this is done by multiplying by a prior probability function. Simply integrating the likelihood over  $\epsilon$  is equivalent to multiplying by a uniform prior probability function in  $\epsilon$ .

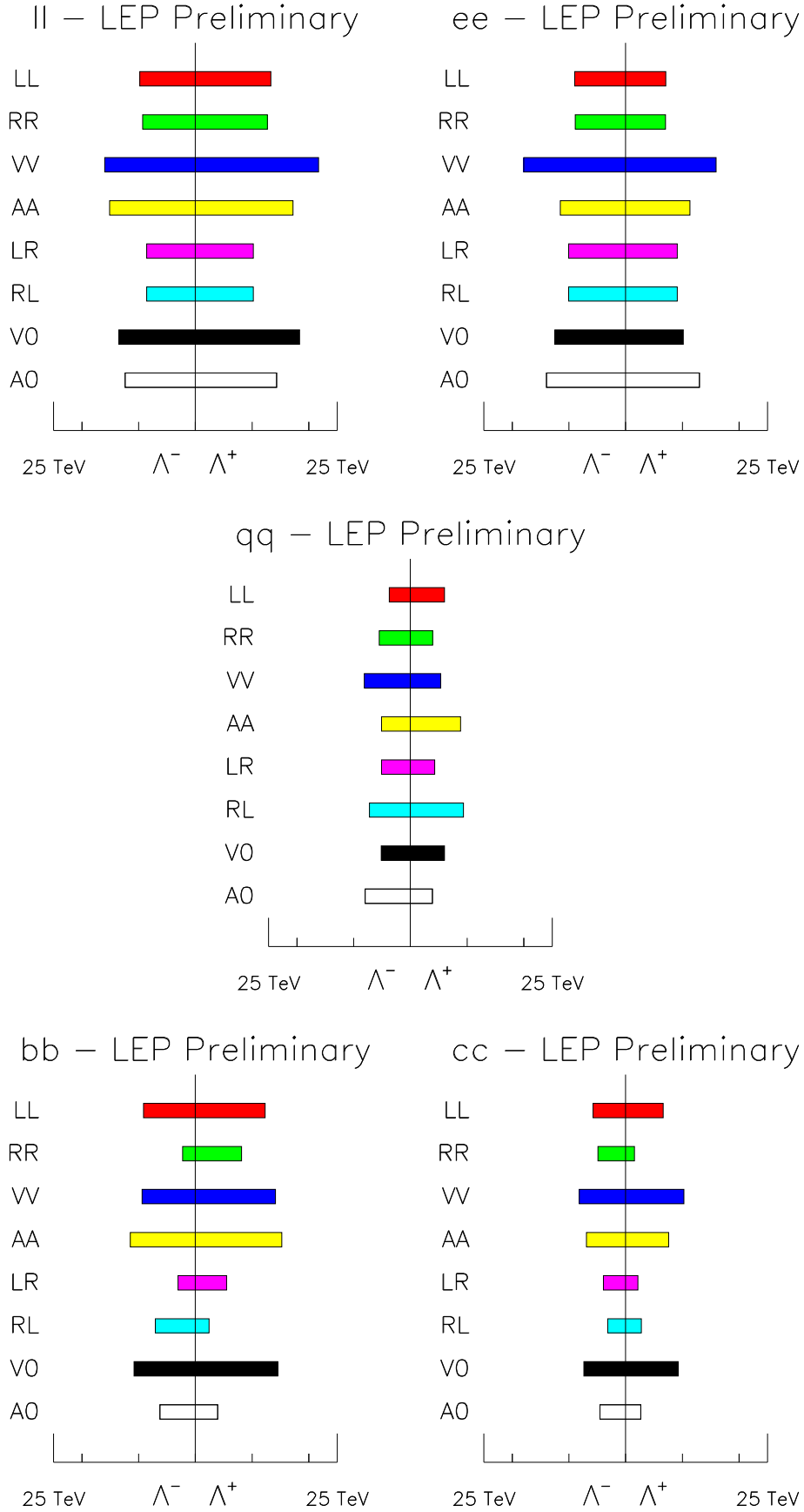


Figure 8.9: The limits on  $\Lambda$  for  $e^+e^- \rightarrow \ell^+\ell^-$  assuming universality in the contact interactions between  $e^+e^- \rightarrow \ell^+\ell^-$  ( $\ell \neq e$ ), for  $e^+e^- \rightarrow e^+e^-$ , for  $e^+e^- \rightarrow q\bar{q}$  assuming equal strength contact interactions for quarks and for  $e^+e^- \rightarrow b\bar{b}$  and  $e^+e^- \rightarrow c\bar{c}$ .

Model	$\eta_{LL}$	$\eta_{RR}$	$\eta_{LR}$	$\eta_{RL}$
$LL^\pm$	$\pm 1$	0	0	0
$RR^\pm$	0	$\pm 1$	0	0
$VV^\pm$	$\pm 1$	$\pm 1$	$\pm 1$	$\pm 1$
$AA^\pm$	$\pm 1$	$\pm 1$	$\mp 1$	$\mp 1$
$LR^\pm$	0	0	$\pm 1$	0
$RL^\pm$	0	0	0	$\pm 1$
$V0^\pm$	$\pm 1$	$\pm 1$	0	0
$A0^\pm$	0	0	$\pm 1$	$\pm 1$

Table 8.12: Choices of  $\eta_{ij}$  for different contact interaction models

### 8.5.2 Models with $Z'$ Bosons

The combined hadronic and leptonic cross-sections and the leptonic forward-backward asymmetries are used to fit the data to models including an additional, heavy, neutral boson,  $Z'$ . The results are updated with respect to those given in [76] due to the updated cross-section and leptonic forward-backward asymmetry results.

Fits are made to  $M_{Z'}$ , the mass of a  $Z'$  for models resulting from an  $E_6$  GUT and L-R symmetric models [94] and for the Sequential Standard Model (SSM) [95], which proposes the existence of a  $Z'$  with exactly the same coupling to fermions as the standard  $Z$ . LEP-II data alone does not significantly constrain the mixing angle between the  $Z$  and  $Z'$  fields,  $\Theta_{ZZ'}$ . However results from a single experiment, in which LEP-I data is used in the fit, show that the mixing is consistent with zero (see for example [96]). So for these fits  $\Theta_{ZZ'}$  was fixed to zero.

No significant evidence is found for the existence of a  $Z'$  boson in any of the models. The procedure to find limits on the  $Z'$  mass corresponds to that in case of contact interactions: for large masses the exchange of a  $Z'$  can be approximated by contact terms,  $\Lambda \propto M_{Z'}$ . The lower limits on the  $Z'$  mass are shown in Figure 8.10 varying the parameters  $\theta_6$  for the  $E_6$  models and  $\alpha_{LR}$  for the left-right models. The results for the specific models  $\chi$ ,  $\psi$ ,  $\eta$  ( $\theta_6 = 0, \pi/2, -\arctan \sqrt{5/3}$ ), L-R ( $\alpha_{LR}=1.53$ ) and SSM are shown in Table 8.15.

### 8.5.3 Leptoquarks and R-parity violating squarks

Leptoquarks (LQ) would mediate quark-lepton transitions. Following the notations in Reference [97, 98], scalar leptoquarks,  $S_I$ , and vector leptoquarks,  $V_I$  are indicated based on spin and isospin  $I$ . Leptoquarks with the same Isospin but with different hypercharges are distinguished by an additional tilde. See Reference 98 for further details. They carry fermion numbers,  $F = L + 3B$ . It is assumed that leptoquark couplings to quark-lepton pairs preserve baryon- and lepton-number. The couplings  $g_L$ ,  $g_R$ , are labelled according to the chirality of the lepton.

$\tilde{S}_{1/2}(L)$  and  $S_0(L)$  leptoquarks are equivalent to up-type anti-squarks and down-type squarks, respectively. Limits in terms of the leptoquark coupling are then exactly equivalent to limits on  $\lambda_{1jk}$  in the Lagrangian  $\lambda_{1jk} L_1 Q_j \bar{D}_k$ .

At LEP, the exchange of a leptoquark can modify the hadronic cross-sections and asymmetries,

$e^+e^- \rightarrow \ell^+\ell^-$			
Model	$\epsilon$ (TeV <sup>-2</sup> )	$\Lambda^-$ (TeV)	$\Lambda^+$ (TeV)
LL	$-0.0044^{+0.0035}_{-0.0035}$	9.8	13.3
RR	$-0.0049^{+0.0039}_{-0.0039}$	9.3	12.7
VV	$-0.0016^{+0.0013}_{-0.0014}$	16.0	21.7
AA	$-0.0013^{+0.0017}_{-0.0017}$	15.1	17.2
LR	$-0.0036^{+0.0052}_{-0.0054}$	8.6	10.2
RL	$-0.0036^{+0.0052}_{-0.0054}$	8.6	10.2
V0	$-0.0023^{+0.0018}_{-0.0018}$	13.5	18.4
A0	$-0.0018^{+0.0026}_{-0.0026}$	12.4	14.3

$e^+e^- \rightarrow e^+e^-$			
Model	$\epsilon$ (TeV <sup>-2</sup> )	$\Lambda^-$ (TeV)	$\Lambda^+$ (TeV)
LL	$0.0049^{+0.0084}_{-0.0084}$	9.0	7.1
RR	$0.0056^{+0.0082}_{-0.0092}$	8.9	7.0
VV	$0.0004^{+0.0022}_{-0.0016}$	18.0	15.9
AA	$0.0009^{+0.0041}_{-0.0039}$	11.5	11.3
LR	$0.0008^{+0.0064}_{-0.0052}$	10.0	9.1
RL	$0.0008^{+0.0064}_{-0.0052}$	10.0	9.1
V0	$0.0028^{+0.0038}_{-0.0045}$	12.5	10.2
A0	$-0.0008^{+0.0028}_{-0.0030}$	14.0	13.0

$e^+e^- \rightarrow q\bar{q}$			
Model	$\epsilon$ (TeV <sup>-2</sup> )	$\Lambda^-$ (TeV)	$\Lambda^+$ (TeV)
LL	$0.0152^{+0.0064}_{-0.0076}$	3.7	6.0
RR	$-0.0208^{+0.0103}_{-0.0082}$	5.5	3.9
VV	$-0.0096^{+0.0051}_{-0.0037}$	8.1	5.3
AA	$0.0068^{+0.0033}_{-0.0034}$	5.1	8.8
LR	$-0.0308^{+0.0172}_{-0.0055}$	5.1	4.3
RL	$-0.0108^{+0.0057}_{-0.0054}$	7.2	9.3
V0	$0.0174^{+0.0057}_{-0.0074}$	5.1	6.0
A0	$-0.0092^{+0.0049}_{-0.0041}$	8.0	3.9

$e^+e^- \rightarrow b\bar{b}$			
Model	$\epsilon$ (TeV <sup>-2</sup> )	$\Lambda^-$ (TeV)	$\Lambda^+$ (TeV)
LL	$-0.0038^{+0.0044}_{-0.0047}$	9.1	12.3
RR	$-0.1729^{+0.1584}_{-0.0162}$	2.2	8.1
VV	$-0.0040^{+0.0039}_{-0.0041}$	9.4	14.1
AA	$-0.0022^{+0.0029}_{-0.0031}$	11.5	15.3
LR	$-0.0620^{+0.0692}_{-0.0313}$	3.1	5.5
RL	$0.0180^{+0.1442}_{-0.0249}$	7.0	2.4
V0	$-0.0028^{+0.0032}_{-0.0033}$	10.8	14.5
A0	$0.0375^{+0.0193}_{-0.0379}$	6.3	3.9

$e^+e^- \rightarrow c\bar{c}$			
Model	$\epsilon$ (TeV <sup>-2</sup> )	$\Lambda^-$ (TeV)	$\Lambda^+$ (TeV)
LL	$-0.0091^{+0.0126}_{-0.0126}$	5.7	6.6
RR	$0.3544^{+0.0476}_{-0.3746}$	4.9	1.5
VV	$-0.0047^{+0.0057}_{-0.0060}$	8.2	10.3
AA	$-0.0059^{+0.0095}_{-0.0090}$	6.9	7.6
LR	$0.1386^{+0.0555}_{-0.1649}$	3.9	2.1
RL	$0.0106^{+0.0848}_{-0.0757}$	3.1	2.8
V0	$-0.0058^{+0.0075}_{-0.0071}$	7.4	9.2
A0	$0.0662^{+0.0564}_{-0.0905}$	4.5	2.7

Table 8.13: The fitted values of  $\epsilon$  and the derived 95% confidence level lower limits on the parameter  $\Lambda$  of contact interaction derived from fits to lepton-pair cross-sections and asymmetries and from fits to hadronic cross-sections. The limits  $\Lambda_+$  and  $\Lambda_-$  given in TeV correspond to the upper and lower signs of the parameters  $\eta_{ij}$  in Table 8.12. For  $\ell^+\ell^-$  ( $\ell \neq e$ ) the couplings to  $\mu^+\mu^-$  and  $\tau^+\tau^-$  are assumed to be universal and for inclusive  $q\bar{q}$  final states all quarks are assumed to experience contact interactions with the same strength.



leptons				
Model	$\mu^+\mu^-$		$\tau^+\tau^-$	
	$\Lambda_-$	$\Lambda_+$	$\Lambda_-$	$\Lambda_+$
LL	8.5	12.5	9.1	8.6
RR	8.1	11.9	8.7	8.2
VV	14.3	19.7	14.2	14.5
AA	12.7	16.4	14.0	11.3
LR	7.9	8.9	2.2	7.9
RL	7.9	8.9	2.2	7.9
V0	11.7	17.2	12.7	11.8
A0	11.5	12.4	9.8	10.8

hadrons				
Model	up-type		down-type	
	$\Lambda_-$	$\Lambda_+$	$\Lambda_-$	$\Lambda_+$
LL	6.7	10.2	10.6	6.0
RR	5.7	8.3	2.2	4.3
VV	9.6	14.3	11.4	7.0
AA	8.0	11.5	13.3	7.7
LR	4.2	2.3	2.7	3.5
RL	3.5	2.8	4.2	2.4
V0	8.7	13.4	12.5	7.1
A0	4.9	2.8	4.2	3.3

Table 8.14: The 95% confidence level lower limits on the parameter  $\Lambda$  of contact interaction derived from fits to lepton-pair cross-sections and asymmetries and from fits to hadronic cross-sections. The limits  $\Lambda_+$  and  $\Lambda_-$  given in TeV correspond to the upper and lower signs of the parameters  $\eta_{ij}$  in Table 8.12. For hadrons the limits for up-type and down-type quarks are derived assuming a single up or down type quark undergoes contact interactions.

Z' model	$\chi$	$\psi$	$\eta$	L-R	SSM
$M_{Z'}^{limit} \text{ (GeV/c}^2\text{)}$	673	481	434	804	1787

Table 8.15: The 95% confidence level lower limits on the  $Z'$  mass for  $\chi$ ,  $\psi$ ,  $\eta$ , L-R and SSM models.

as described at the Born level by the equations given in Reference 98. Using the LEP combined measurements of hadronic cross-sections, and the measurements of heavy quark production,  $R_b$ ,  $R_c$ ,  $A_{FB}^{b\bar{b}}$  and  $A_{FB}^{c\bar{c}}$ , upper limits can be set on the leptoquark's coupling  $g$  as a function of its mass  $M_{LQ}$  for leptoquarks coupling electrons to first, second and third generation quarks. For convenience, one type of leptoquark is assumed to be much lighter than the others. Furthermore, experimental constraints on the product  $g_L g_R$  allow the study leptoquarks assuming either only  $g_L \neq 0$  or  $g_R \neq 0$ . Limits are then denoted by either (L) for leptoquarks coupling to left handed leptons or (R) for leptoquarks coupling to right handed leptons.

In the processes  $e^+e^- \rightarrow u\bar{u}$  and  $e^+e^- \rightarrow d\bar{d}$  first generation leptoquarks could be exchanged in  $u$ -

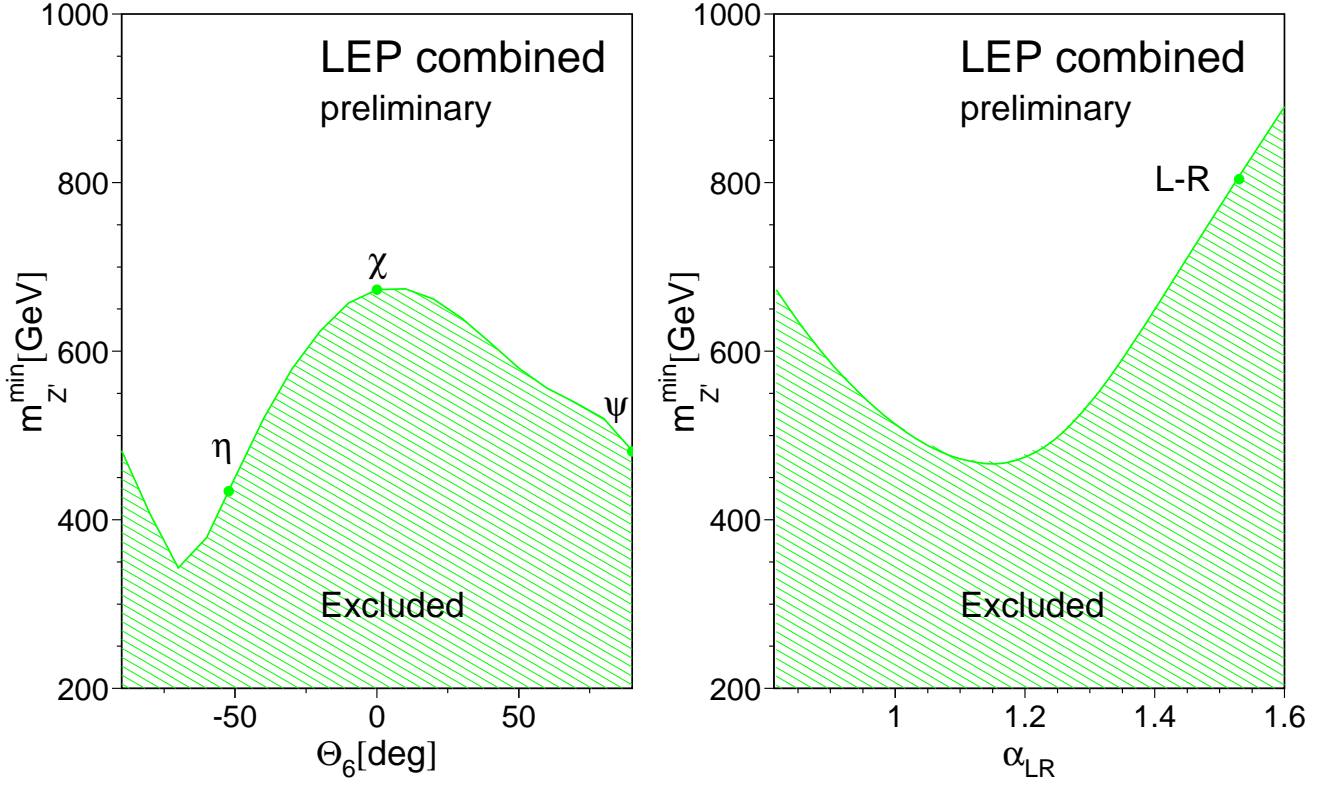


Figure 8.10: The 95% confidence level limits on  $M_{Z'}$  as a function of the model parameter  $\theta_6$  for  $E_6$  models and  $\alpha_{LR}$  for left-right models. The  $Z$ - $Z'$  mixing is fixed,  $\Theta_{ZZ'} = 0$ .

or  $t$ -channel ( $F=2$  or  $F=0$ ) which would lead to a change of the hadronic cross-section. In the processes  $e^+e^- \rightarrow c\bar{c}$  and  $e^+e^- \rightarrow b\bar{b}$  the exchange of leptoquarks with cross-generational couplings can alter the  $q\bar{q}$  angular distribution, especially at low polar angle. The reported measurements on heavy quark production have been extrapolated to  $4\pi$  acceptance, using SM predictions, from the measurements performed in restricted angular ranges, corresponding to the acceptance of the vertex-detector in each experiment. Therefore, when fitting limits on leptoquarks' coupling to the 2nd or 3rd generation of quarks, the LEP combined results for  $b$  and  $c$  sector are extrapolated back to an angular range of  $|\cos \theta| < 0.85$  using ZFITTER predictions.

The following measurements are used to constrain different types of leptoquarks

- For leptoquarks coupling electrons to 1<sup>st</sup> generation quarks, all LEP combined hadronic cross-sections at centre-of-mass energies from 130 GeV to 207 GeV are used
- For leptoquarks coupling electrons to 2<sup>nd</sup> generation quarks,  $\sigma_{c\bar{c}}$  is calculated from  $R_c$  and the hadronic cross-section at the energy points where  $R_c$  is measured. The measurements of  $\sigma_{c\bar{c}}$  and  $A_{FB}^{c\bar{c}}$  are then extrapolated back to  $|\cos \theta| < 0.85$ . Since measurements in the  $c$ -sector are scarce and originate from, at most, 2 experiments, hadronic cross-sections, extrapolated down to  $|\cos \theta| < 0.85$  are also used in the fit, with an average 10% correlated errors.
- For leptoquarks coupling electrons to 3<sup>rd</sup> generation quarks, only  $\sigma_{b\bar{b}}$  and  $A_{FB}^{b\bar{b}}$ , extrapolated back to a  $|\cos \theta| < 0.85$  are used.

The 95% confidence level lower limits on masses  $M_{LQ}$  are derived assuming a coupling of electro-

Limit on scalar LQ mass (GeV/ $c^2$ )							
	$S_0(L)$	$S_0(R)$	$\tilde{S}_0(R)$	$S_{\frac{1}{2}}(L)$	$S_{\frac{1}{2}}(R)$	$\tilde{S}_{\frac{1}{2}}(L)$	$S_1(L)$
$LQ_{1st}$	655	520	202	178	232	-	361
$LQ_{2nd}$	762	625	209	215	185	-	408
$LQ_{3rd}$	NA	NA	454	NA	-	226	1036

Limit on vector LQ mass (GeV/ $c^2$ )							
	$V_0(L)$	$V_0(R)$	$\tilde{V}_0(R)$	$V_{\frac{1}{2}}(L)$	$V_{\frac{1}{2}}(R)$	$\tilde{V}_{\frac{1}{2}}(L)$	$V_1(L)$
$LQ_{1st}$	917	165	489	303	227	176	659
$LQ_{2nd}$	968	147	478	165	466	101	687
$LQ_{3rd}$	765	167	NA	208	499	NA	765

Table 8.16: 95% confidence level lower limits on the LQ mass for leptoquarks coupling between electrons and the first, second and third generation of quarks. A dash indicates that no limit can be set and N.A denotes leptoquarks coupling only to top quarks and hence not visible at LEP.

magnetic strength,  $g = \sqrt{4\pi\alpha_{em}}$ , where  $\alpha_{em}$  is the fine structure constant. The results are summarised in Table 8.16. These results complement the leptoquark searches at HERA [99, 100] and the Tevatron [101]. Figures 8.11 and 8.12 give the 95% confidence level limits on the coupling as a function of the leptoquark mass for leptoquarks coupling electrons to the second and third generations of quarks.

#### 8.5.4 Low Scale Gravity in Large Extra Dimensions

The averaged differential cross-sections for  $e^+e^- \rightarrow e^+e^-$  are used to search for the effects of graviton exchange in large extra dimensions.

A new approach to the solution of the hierarchy problem has been proposed in [102–104], which brings close the electroweak scale  $m_{EW} \sim 1$  TeV and the Planck scale  $M_{Pl} = \frac{1}{\sqrt{G_N}} \sim 10^{15}$  TeV. In this framework the effective 4 dimensional  $M_{Pl}$  is connected to a new  $M_{Pl(4+n)}$  scale in a  $(4+n)$  dimensional theory:

$$M_{Pl}^2 \sim M_{Pl(4+n)}^{2+n} R^n, \quad (8.4)$$

where there are  $n$  extra compact spatial dimensions of radius  $\sim R$ .

In the production of fermion- or boson-pairs in  $e^+e^-$  collisions this class of models can be manifested through virtual effects due to the exchange of gravitons (Kaluza-Klein excitations). As discussed in [105–109], the exchange of spin-2 gravitons modifies in a unique way the differential cross-sections for fermion pairs, providing clear signatures. These models introduce an effective scale (ultraviolet cut-off). Adopting the notation from [105] the gravitational mass scale is called  $M_H$ . The cut-off scale is supposed to be of the order of the fundamental gravity scale in  $4+n$  dimensions.

The parameter  $\varepsilon_H$  is defined as

$$\varepsilon_H = \frac{\lambda}{M_H^4}, \quad (8.5)$$

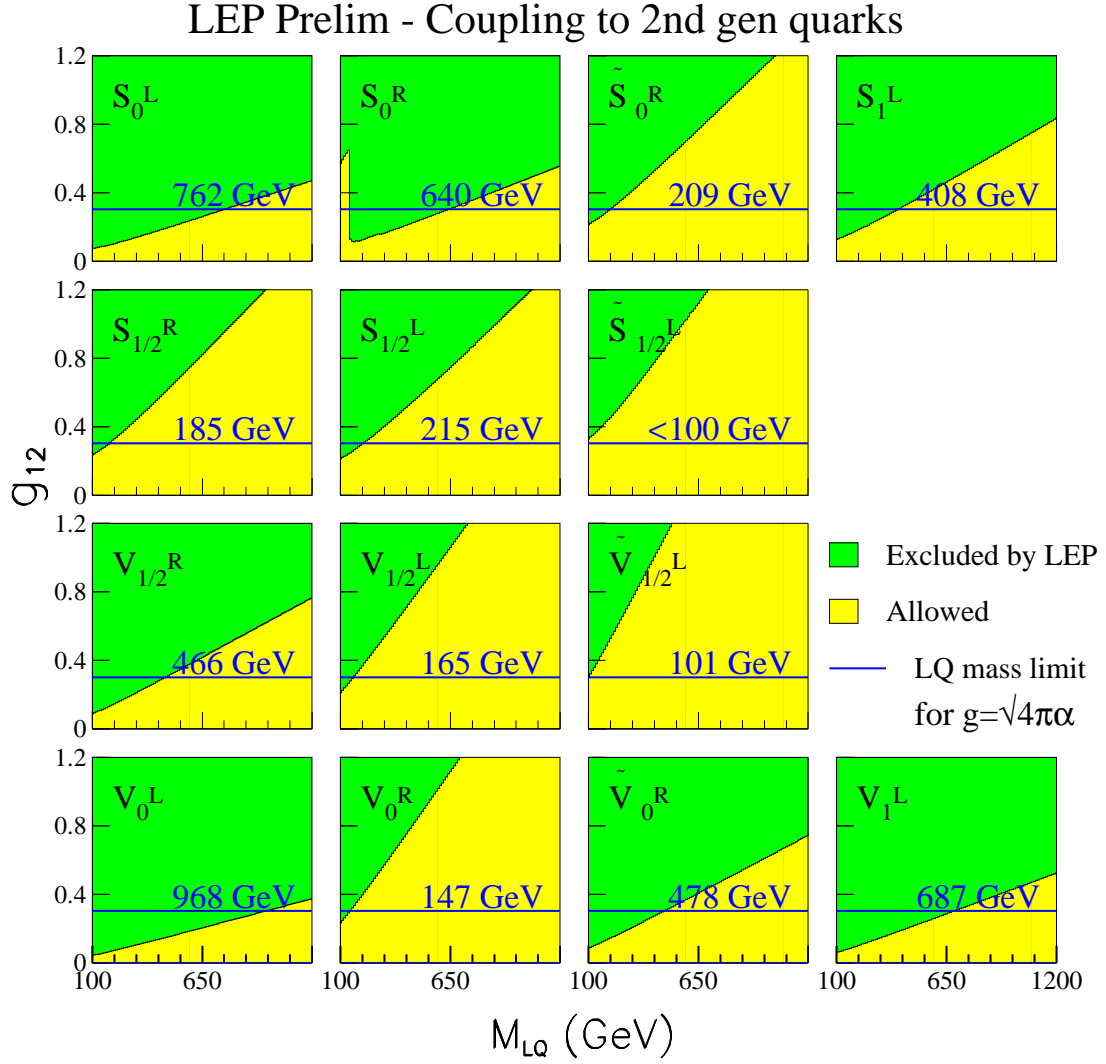


Figure 8.11: 95% confidence level limit on the coupling of leptoquarks to 2nd generation of quarks.

where the coefficient  $\lambda$  is of  $\mathcal{O}(1)$  and can not be calculated explicitly without knowledge of the full quantum gravity theory. In the following analysis we will assume that  $\lambda = \pm 1$  in order to study both the cases of positive and negative interference. To compute the deviations from the Standard Model due to virtual graviton exchange the calculations [106, 107] were used.

Theoretical uncertainties on the Standard Model predictions are taken from [83]. The full correlation matrix of the differential cross-sections, obtained in our averaging procedure, is used in the fits. This is an improvement compared to previous combined analyses of published or preliminary LEP data on Bhabha scattering, performed before this detailed information was available (see e.g. [110–112]).

The extracted value of  $\varepsilon_H$  is compatible with the Standard Model expectation  $\varepsilon_H = 0$ . The errors on  $\varepsilon_H$  are  $\sim 1.5$  smaller than those obtained from a single LEP experiment with the same data set. The fitted value of  $\varepsilon_H$  is converted into 95% confidence level lower limits on  $M_H$  by integrating the likelihood function over the physically allowed values,  $\varepsilon_H \geq 0$  for  $\lambda = +1$  and  $\varepsilon_H \leq 0$  for  $\lambda = -1$ .

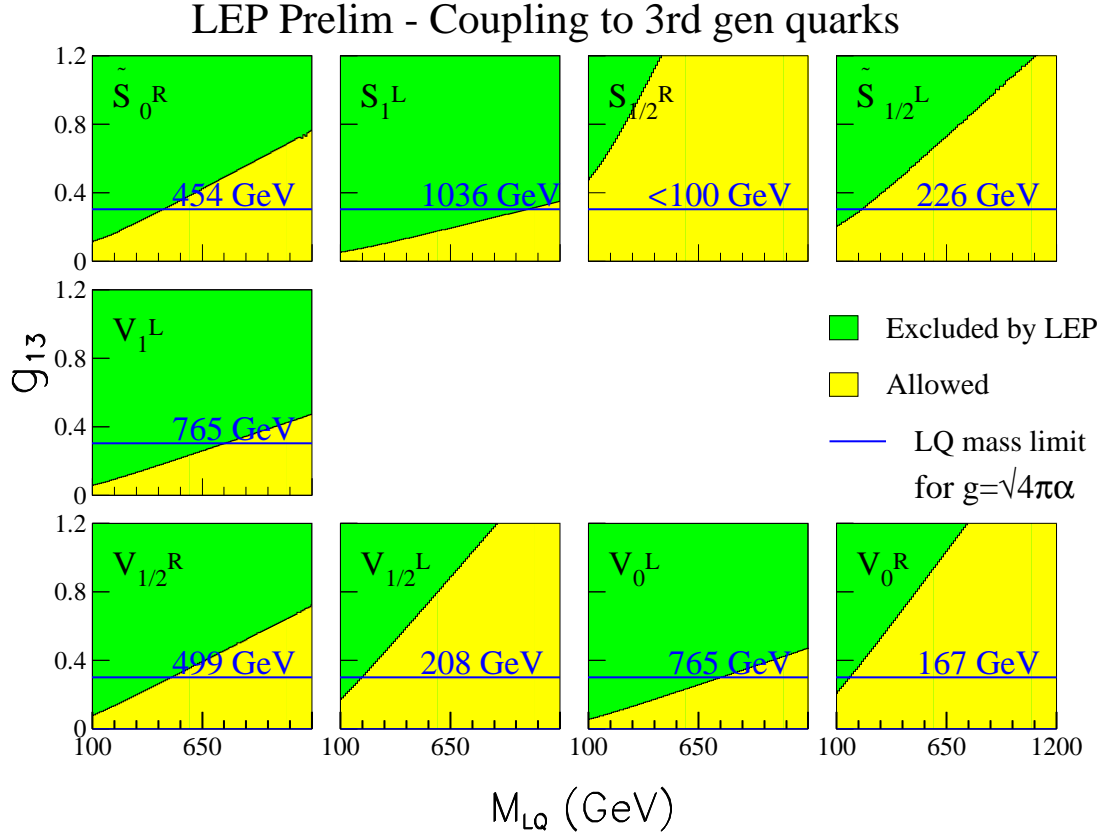


Figure 8.12: 95% confidence level limit on the coupling of leptoquarks to 3rd generation of quarks.

giving:

$$M_H > 1.20 \text{ TeV} \quad \text{for } \lambda = +1, \quad (8.6)$$

$$M_H > 1.09 \text{ TeV} \quad \text{for } \lambda = -1. \quad (8.7)$$

An example of our analysis for the highest energy point is shown in Figure 8.13.

The interference of virtual graviton exchange amplitudes with both t-channel and s-channel Bhabha scattering amplitudes makes this the most sensitive search channel at LEP. The results obtained here would not be strictly valid if the luminosity measurements of the LEP experiments, based on the very same process, are also significantly affected by graviton exchange. As shown in [110], the effect on the cross-section in the luminosity angular range is so small that it can safely be neglected in this analysis.

Preliminary LEP Averaged  $d\sigma / d\cos\Theta (e^+e^-)$

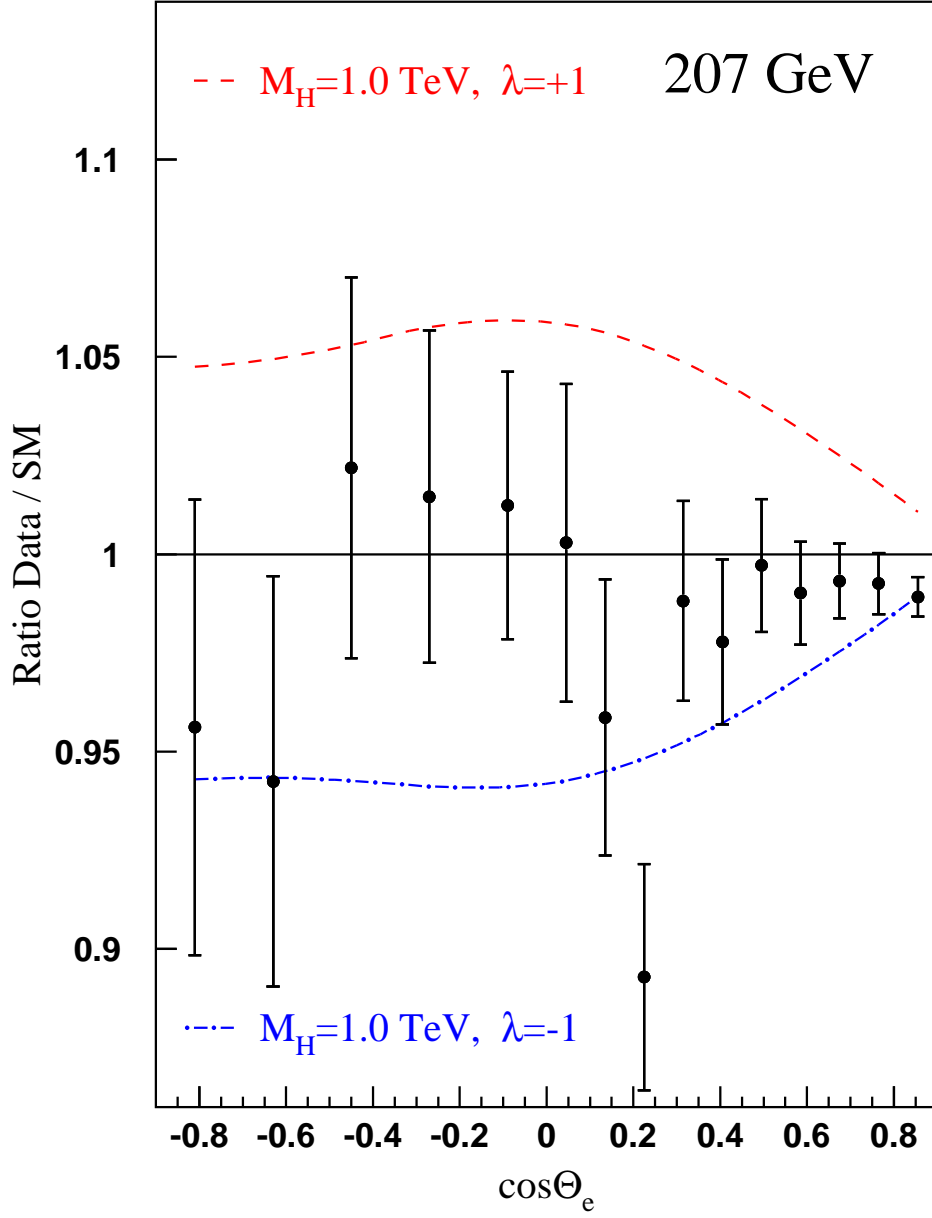


Figure 8.13: Ratio of the LEP averaged differential cross-section for  $e^+e^- \rightarrow e^+e^-$  at energy of 207 GeV compared to the SM prediction. The effects expected from virtual graviton exchange are also shown.

## 8.6 Summary

A preliminary combination of the LEP-II  $e^+e^- \rightarrow f\bar{f}$  cross-sections (for hadron, muon and tau-lepton final states) and forward-backward asymmetries (for muon and tau final states) from LEP running at energies from 130 GeV to 207 GeV has been made. The results from the four LEP experiments are in good agreement with each other. The averages for all energies are shown given in Table 8.2. Overall the data agree with the Standard Model predictions of ZFITTER, although the combined hadronic cross-sections are on average 1.7 standard deviations above the predictions. Further information is available at [81].

Preliminary differential cross-sections,  $\frac{d\sigma}{d\cos\theta}$ , for  $e^+e^- \rightarrow e^+e^-$ ,  $e^+e^- \rightarrow \mu^+\mu^-$  and  $e^+e^- \rightarrow \tau^+\tau^-$  were combined. Results are shown in Figures 8.4, 8.5 and 8.6.

A preliminary average of results on heavy flavour production at LEP-II has also been made for measurements of  $R_b$ ,  $R_c$ ,  $A_{\text{FB}}^{b\bar{b}}$  and  $A_{\text{FB}}^{c\bar{c}}$ , using results from LEP centre-of-mass energies from 130 to 207 GeV. Results are given in Tables 8.9 and 8.10 and shown graphically in Figures 8.7 and 8.8. The results are in good agreement with the predictions of the SM.

The preliminary averaged cross-section and forward-backward asymmetry results together with the combined results on heavy flavour production have been interpreted in a variety of models. Limits on the scale of contact interactions between leptons and quarks and in  $e^+e^- \rightarrow e^+e^-$  and also between electrons and specifically  $b\bar{b}$  and  $c\bar{c}$  final states have been determined. A full set of limits are given in Tables 8.13 and 8.14. The LEP-II averaged cross-sections have been used to obtain lower limits on the mass of a possible  $Z'$  boson in different models. Limits range from 340 to 1787 GeV/ $c^2$  depending on the model. Limits on the masses of leptoquarks have been derived from the hadronic cross-sections. The limits range from 101 to 1036 GeV/ $c^2$  depending on the type of leptoquark. Limits on the scale of gravity in models with large extra dimensions have been obtained from combined differential cross-sections for  $e^+e^- \rightarrow e^+e^-$ ; for positive interference between the new physics and the Standard model the limit is 1.20 TeV and for negative interference 1.09 TeV.

# Chapter 9

## Investigation of the Photon/Z-Boson Interference

**Updates with respect to summer 2002:**

Unchanged w.r.t. summer 2002: Results are preliminary.

### 9.1 Introduction

The S-Matrix ansatz provides a coherent way of describing LEP measurements of the cross-section and forward-backward asymmetries in  $s$ -channel  $e^+e^- \rightarrow f\bar{f}$  processes at centre-of-mass energies around the Z resonance, from the LEP-I program, and the measurements at centre-of-mass energies from 130 – 207 GeV from the LEP-II program.

Compared with the standard 5 and 9 parameter descriptions of the measurements at the Z [113], the S-Matrix formalism includes an extra 3 parameters (assuming lepton universality) or 7 parameters (without lepton universality) which explicitly determine the contributions to the cross-sections and forward-backward asymmetries of the interference between the exchange of a Z and a photon. The LEP-I data alone cannot tightly constrain these interference terms, in particular the interference term for hadronic cross-sections, since their contributions are small around the Z resonance and change sign at the pole. Due to strong correlations between the size of the hadronic interference term and the mass of the Z, this leads to a larger error on the fitted mass of the Z compared to the standard 5 and 9 parameter fits, where the hadronic interference term is fixed to the value predicted in the Standard Model. Including the LEP-II data leads to a significant improvement in the constraints on the interference terms and a corresponding reduction in the uncertainty on the mass of the Z. This results in a measurement of  $m_Z$  which is almost as sensitive as the standard results, but without constraining the interference to the Standard Model prediction.

This chapter describes the first, preliminary, combination of data from the full data sets of the 4 LEP experiments, to obtain a LEP combined results on the parameters of the S-Matrix ansatz. These results update those of a previous combination [114] which was based on preliminary LEP-I data and only partial statistics from the full LEP-II data set.

Different strategies are used to combined the LEP-I and LEP-II data. For LEP-I data, an average of the individual experiment's results on the S-Matrix parameters is made. This approach is rather similar to the method used to combine the results of the 5 and 9 parameter fits. To include LEP-II



data, a fit is made to LEP combined measurements of cross-sections and asymmetries above the Z, taking into account the results of the LEP-I combination of S-Matrix parameters.

In Section 9.2 the parameters of the S-Matrix ansatz are explained. In Sections 9.3.1 and 9.3.2 the average of the LEP-I data and the inclusion of the LEP-II data are described. The results are discussed in Section 9.3.3 and conclusions are drawn in Section 9.4.

## 9.2 The S-Matrix Ansatz

The S-matrix ansatz [115] is a rigorous approach to describe the cross-sections and forward-backward asymmetries in the  $s$ -channel  $e^+e^-$  annihilations under the assumption that the processes can be parameterised as the exchange of a massless and a massive vector boson, in which the couplings of the bosons including their interference are treated as free parameters.

In this model, the cross-sections can be parametrised as follows:

$$\sigma_{tot,f}^0(s) = \frac{4}{3}\pi\alpha^2 \left[ \frac{g_f^{tot}}{s} + \frac{j_f^{tot}(s - \overline{m}_Z^2) + r_f^{tot}s}{(s - \overline{m}_Z^2)^2 + \overline{m}_Z^2\overline{\Gamma}_Z^2} \right] \text{ with } f = \text{had}, e, \mu, \tau, \quad (9.1)$$

while the forward-backward asymmetries are given by:

$$A_{fb,f}^0(s) = \pi\alpha^2 \left[ \frac{g_f^{fb}}{s} + \frac{j_f^{fb}(s - \overline{m}_Z^2) + r_f^{fb}s}{(s - \overline{m}_Z^2)^2 + \overline{m}_Z^2\overline{\Gamma}_Z^2} \right] / \sigma_{tot,f}^0(s), \quad (9.2)$$

where  $\sqrt{s}$  is the centre-of-mass energy. The parameters  $r_f$  and  $j_f$  scale the Z exchange and the Z –  $\gamma$  interference contributions to the total cross-section and forward-backward asymmetries. The contribution  $g_f$  of the pure  $\gamma$  exchange was fixed to the value predicted by QED in all fits. Neither the hadronic charge asymmetry, nor the flavour tagged quark forward-backward asymmetries are considered here, which leaves 16 free parameters to described the LEP data: 14  $r_f$  and  $j_f$  parameters and the mass and width of the massive Z resonance. Applying the constraint of lepton universality reduces this to 8 parameters.

In the Standard Model the Z exchange term, the Z –  $\gamma$  interference term and the photon exchange term are given in terms of the fermion charges and their effective vector and axial couplings to the Z by:

$$\begin{aligned} r_f^{tot} &= \kappa^2 \left[ g_{Ae}^2 + g_{Ve}^2 \right] \left[ g_{Af}^2 + g_{Vf}^2 \right] - 2\kappa g_{Ve} g_{Vf} C_{Im} \\ j_f^{tot} &= 2\kappa g_{Ve} g_{Vf} (C_{Re} + C_{Im}) \\ g_f^{tot} &= Q_e^2 Q_f^2 |F_A(m_Z)|^2 \\ r_f^{fb} &= 4\kappa^2 g_{Ae} g_{Ve} g_{Af} g_{Vf} - 2\kappa g_{Ae} g_{Af} C_{Im} \\ j_f^{fb} &= 2\kappa g_{Ae} g_{Af} (C_{Re} + C_{Im}) \\ g_f^{fb} &= 0, \end{aligned} \quad (9.3)$$

with the following definitions:

$$\begin{aligned}
\kappa &= \frac{G_F m_Z^2}{2\sqrt{2}\pi\alpha} \approx 1.50 \\
C_{Im} &= \frac{\Gamma_Z}{m_Z} Q_e Q_f \operatorname{Im}\{F_A(m_Z)\} \\
C_{Re} &= Q_e Q_f \operatorname{Re}\{F_A(m_Z)\} \\
F_A(m_Z) &= \frac{\alpha(m_Z)}{\alpha},
\end{aligned} \tag{9.4}$$

where  $\alpha(m_Z)$  is the complex fine-structure constant, and  $\alpha \equiv \alpha(0)$ . The photonic virtual and bremsstrahlung corrections are included through the convolution of Equations 9.1 and 9.2 with radiator functions as in the 5 and 9 parameter fits. The expressions of the S-Matrix parameters in terms of the effective vector and axial-vector couplings given above neglect the imaginary parts of the effective couplings.

The usual definitions of the mass  $m_Z$  and width  $\Gamma_Z$  of a Breit-Wigner resonance are used, the width being  $s$ -dependent, such that:

$$\begin{aligned}
m_Z &\equiv \bar{m}_Z \sqrt{1 + \bar{\Gamma}_Z^2 / \bar{m}_Z^2} \approx \bar{m}_Z + 34.20 \text{ MeV}/c^2 \\
\Gamma_Z &\equiv \bar{\Gamma}_Z \sqrt{1 + \bar{\Gamma}_Z^2 / \bar{m}_Z^2} \approx \bar{\Gamma}_Z + 0.94 \text{ MeV}.
\end{aligned} \tag{9.5}$$

In the following fits, the predictions from the S-Matrix ansatz and the QED convolution for cross-sections and asymmetries are made using SMATASY [116], which in turn uses ZFITTER [117] to calculate the QED convolution of the electroweak kernel. In case of the  $e^+e^-$  final state,  $t$ -channel and  $s/t$  interference contributions are added to the  $s$ -channel ansatz.

## 9.3 LEP combination

In the following sections the combinations of the results from the individual LEP experiments are described: firstly the LEP-I combination, then the combination of both LEP-I and LEP-II data. The results from these combinations are compared in Section 9.3.3. Although all 16 parameters are averaged during the combination, only results for the parameters  $m_Z$  and  $j_{\text{had}}^{\text{tot}}$  are reported here. Systematic studies specific to the other parameters are ongoing.

### 9.3.1 LEP-I combination

Individual LEP experiments have their own determinations of the 16 S-Matrix parameters [118–121] from LEP-I data alone, using the full LEP-I data sets.

These results are averaged using a multi-parameter BLUE technique based on an extension of Reference 85. Sources of systematic uncertainty correlated between the experiments have been investigated, using techniques described in [113] and are accounted for in the averaging procedure and benefiting from the experience gained in those combinations.

	$m_Z$ [GeV]	$j_{\text{had}}^{\text{tot}}$	correlation
LEP-I only	$91.1925 \pm 0.0059$	$-0.084 \pm 0.324$	-0.935
LEP-I & LEP-II	$91.1869 \pm 0.0023$	$0.277 \pm 0.065$	-0.461

Table 9.1: Averaged LEP-I and LEP-II S-Matrix results for  $m_Z$  and  $j_{\text{had}}^{\text{tot}}$ .

The parameters  $m_Z$  and  $j_{\text{had}}^{\text{tot}}$  are the most sensitive of all 16 S-matrix parameters to the inclusion of the LEP-II data, and are also the most interesting ones in the context of the 5 and 9 parameter fits. For these parameters the most significant source of systematic error which is correlated between experiments comes from the uncertainty on the  $e^+e^-$  collision energy as determined by models of the LEP RF system and calibrations using the resonant depolarisation technique. These errors amount to  $\pm 3$  MeV on  $m_Z$  and  $\pm 0.16$  on  $j_{\text{had}}^{\text{tot}}$  with a correlation coefficient of  $-0.86$ . The LEP averaged values of  $m_Z$  and  $j_{\text{had}}^{\text{tot}}$  are given in Table 9.1, together with their correlation coefficient. The  $\chi^2/\text{D.O.F.}$  for the average of all 16 parameters is 62.0/48, corresponding to a probability of 8%, which is acceptable.

### 9.3.2 LEP-I and LEP-II combination

Some experiments have determined S-Matrix parameters using their LEP-I and LEP-II measured cross-sections and forward-backward asymmetries [118, 119, 122, 123]. To do a full LEP combination would require each experiment to provide S-Matrix results and would require an analysis of the correlated systematic errors on each measured parameter.

However, preliminary combinations of the measurements of forward-backward asymmetries and cross-sections from all 4 LEP experiments, for the full LEP-II period, have already been made [117] and correlations between these measurements have been estimated. The combination procedure averages measurements of cross-sections and asymmetry for those events with reduced centre-of-mass energies,  $\sqrt{s'}$ , close to the actual centre-of-mass energy of the  $e^+e^-$  beams,  $\sqrt{s}$ , removing those events which are less sensitive to the  $Z - \gamma$  interference where, predominantly, initial state radiation reduces the centre-of-mass energy to close to the mass of the  $Z$ . The only significant correlations are those between hadronic cross-section measurements at different energies, which are around 20–40%, depending on energies.

The predictions from SMATASY are fitted to the combined LEP-II cross-section and forward-backward asymmetry measurements [117]. The signal definition 1 of Reference 117 is used for the data and for the predictions of SMATASY. Theoretical uncertainties on the S-Matrix predictions for the LEP-II results and on the corrections of the LEP II data to the common signal definition are taken to be the same as for the Standard Model predictions of ZFITTER [117] which are dominated by uncertainties in the QED convolution. These amount to a relative uncertainty of 0.26% on the hadronic cross-sections, fully correlated between all LEP-II energies.

The fit also uses as inputs the averaged LEP-I S-Matrix parameters and covariance matrix. These inputs effectively constrain those parameters, such as  $m_Z$ , which are not accurately determined by LEP-II data. There are no significant correlations between the LEP-I and LEP-II inputs.

The LEP averaged values of  $m_Z$  and  $j_{\text{had}}^{\text{tot}}$  for both LEP-I and LEP-II data are given in Table 9.1, together with their correlation coefficient. The  $\chi^2/\text{D.O.F.}$  for the average of all 16 parameters is 64.4/60, corresponding to a probability of 33%, which is good.

### 9.3.3 Discussion

In the LEP-I combination the measured values of the Z boson mass  $m_Z = 91.1925 \pm 0.0059$  GeV agrees well with the results of the standard 9 parameter fit ( $91.1876 \pm 0.0021$  GeV) albeit with a significantly larger error, resulting from the correlation with the large uncertainty on  $j_{\text{had}}^{\text{tot}}$  which is then the dominant source of uncertainty on  $m_Z$  in the S-Matrix fits. The measured value of  $j_{\text{had}}^{\text{tot}} = -0.084 \pm 0.324$ , also agrees with the prediction of the Standard Model ( $0.2201^{+0.0032}_{-0.0137}$ ).

Including the LEP-II data brings a significant improvement in the uncertainty on the size of the interference between Z and photon exchange compared to LEP-I data alone. The measured value  $j_{\text{had}}^{\text{tot}} = 0.277 \pm 0.065$ , agrees well with the values predicted from the Standard Model. Correspondingly, the uncertainty on the mass of the Z in this ansatz, 2.3 MeV, is close to the precision obtained from LEP-I data alone using the standard 9 parameter fit, 2.1 MeV. The slightly larger error is due to the uncertainty on  $j_{\text{had}}^{\text{tot}}$  which amounts to 0.9 MeV. The measured value,  $m_Z = 91.1869 \pm 0.0023$  GeV, agrees with that obtained from the standard 9 parameter fits. The results are summarised in Figure 9.1.

The good agreement found between the values of  $m_Z$  and  $j_{\text{had}}^{\text{tot}}$  and their expectations provide a validation of the approach taken in the standard 5 and 9 parameter fits, in which the size of the interference between Z boson and photon exchange in the hadronic cross-sections was fixed to the Standard Model expectation.

The precision on  $j_{\text{had}}^{\text{tot}}$  is slightly better than that obtained by the VENUS collaboration [124] of  $\pm 0.08$ , which was obtained using preliminary results from LEP-I and their own measurements of the hadronic cross-section below the Z resonance. The measurement of the hadronic cross-sections from VENUS [124] and TOPAZ [125] could be included in the future to give a further reduction in the uncertainty on  $j_{\text{had}}^{\text{tot}}$ .

Work is in progress to understand those sources of systematic error, correlated between experiments, which are significant for the remaining S-Matrix parameter that have not been presented here. In particular, for  $j_e^{\text{tot}}$  and  $j_e^{\text{fb}}$ , it is important to understand the errors resulting from  $t$ -channel contributions to the  $e^+e^- \rightarrow e^+e^-$  process. These errors have only limited impact on the standard 5 and 9 parameter fits.

## 9.4 Conclusion

Results for the S-Matrix parameter  $m_Z$  and  $j_{\text{had}}^{\text{tot}}$  have been presented for LEP-I data alone and for a fit using the full data sets for LEP-I and LEP-II from all 4 LEP experiments. Inclusion of LEP-II data brings a significant improvement in the determination of  $j_{\text{had}}^{\text{tot}}$ , the fitted value  $0.277 \pm 0.065$ , agrees well with the values predicted from the Standard Model. As a result in the improvement of the uncertainty in  $j_{\text{had}}^{\text{tot}}$ , the uncertainty on the fitted value of  $m_Z$  approaches that of the standard 5 and 9 parameter fits and the measured value  $m_Z = 91.1869 \pm 0.0023$  GeV is compatible with that from the standard fits.

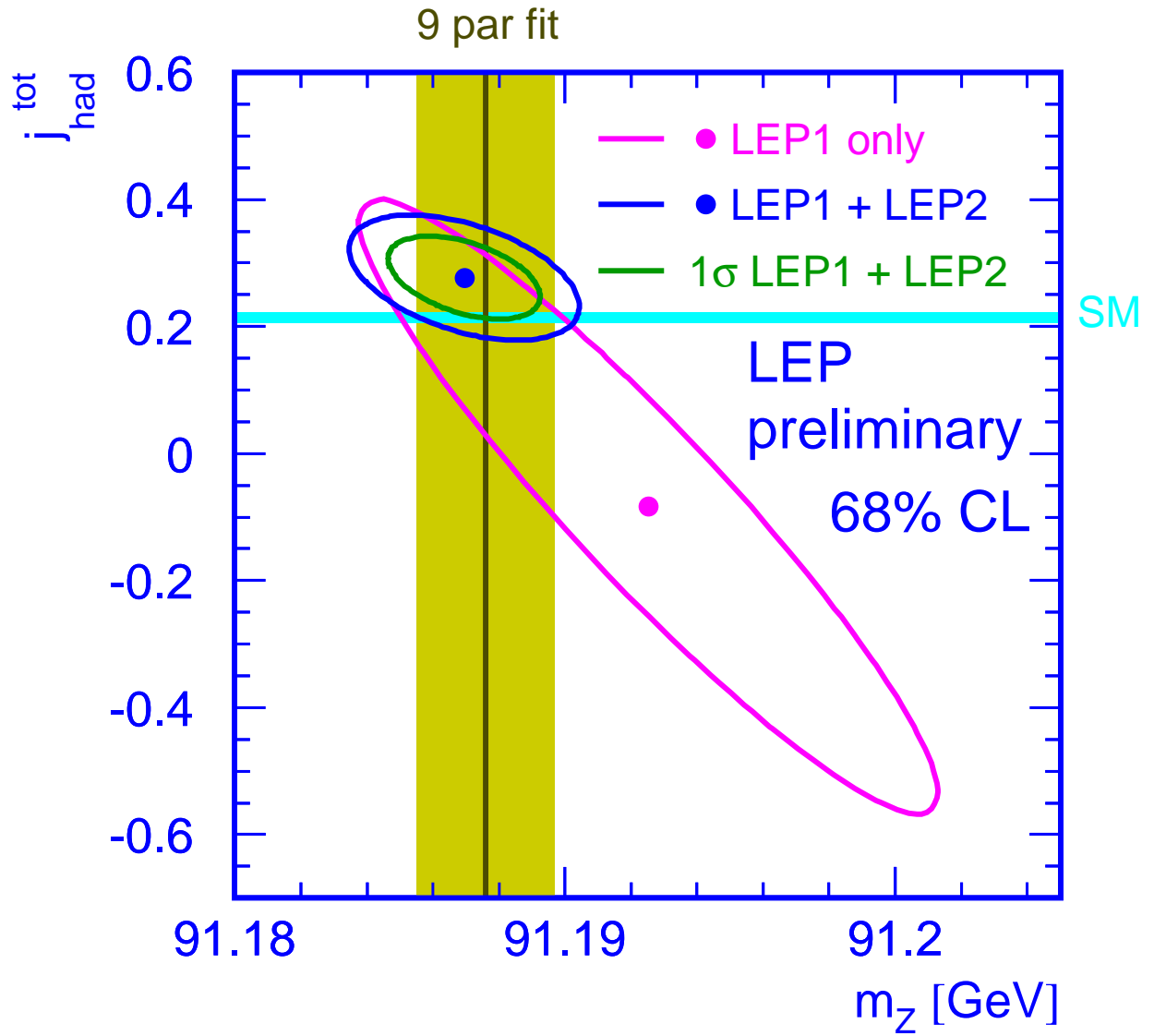


Figure 9.1: Error ellipses for  $m_Z$  and  $j_{\text{had}}^{\text{tot}}$  for LEP-I (at 39% and 68%) and the combination of LEP-I and LEP-II (at 68%).

# Chapter 10

## W and Four-Fermion Production at LEP-II

**Updates with respect to summer 2002:**

Unchanged w.r.t. summer 2002: Results are preliminary.

### 10.1 Introduction

This chapter summarises the combination of published and preliminary results of the four LEP experiments on four-fermion cross-sections for the Summer 2002 Conferences. If not stated otherwise, all presented results use the full LEP2 data sample at centre-of-mass energies up to 209 GeV and have to be considered as preliminary.

With respect to the results presented at the Winter 2002 Conferences [126], improved combination procedures for the measurements of W-pair, Z-pair and single-W cross-sections are used. This allowed to derive the average ratio of the measured cross-sections to the corresponding theoretical predictions from various models. For the first time the combination of single-Z and  $WW\gamma$  cross-sections are also presented.

The centre-of-mass energies and the corresponding integrated luminosities are provided by the experiments and are the same used for previous conferences. The LEP energy value in each point (or group of points) is the luminosity-weighted average of those values.

Cross-section results from different experiments are combined by  $\chi^2$  minimisation using the Best Linear Unbiased Estimate method described in Ref. [85], properly taking into account the correlations between the systematic uncertainties.

The detailed breakdown of systematic errors for the measurements combined in this note is described in Appendix C. Experimental results are compared with recent theoretical predictions, many of which were developed in the framework of the LEP2 Monte Carlo workshop [127].

### 10.2 W-pair production cross-section

All experiments have published final results on the W-pair (CC03 [127]) production cross-section for centre-of-mass energies from 161 to 189 GeV [128–137] and have contributed to conferences prelim-

inary measurements at  $\sqrt{s} = 192\text{--}207$  GeV. Although none of these results have been updated by the experiments for the Summer 2002 Conferences, new LEP averages of the measurements at the eight centre-of-mass energies between 183 and 207 GeV have been computed, using a new grouping of the systematic errors which improves the treatment of correlations in the combination. In particular, some of the sources of systematics which were previously considered as uncorrelated between energy or experiments are now treated as fully correlated. The total systematic errors of the experiments are unchanged with respect to previous conferences. In the new grouping fragmentation effects (both on signal and backgrounds), final state interactions in the hadronic channel (Bose-Einstein and Colour Reconnection) and the theory uncertainties on radiative corrections are now treated as 100% LEP and energy correlated. Also the part of the systematic error in the luminosity determination due to theory error in the Bhabha cross-section is now treated as fully correlated. The detailed inputs used for the combination are given in Appendix C.

The measured statistical errors are used for the combination; after building the full  $32 \times 32$  covariance matrix for the measurements, the  $\chi^2$  minimisation fit is performed by matrix algebra, as described in Ref. [138], and is cross-checked using Minuit [139].

The results from each experiment for the W-pair production cross-section are shown in Table 10.1, together with the LEP combination at each energy. All measurements assume Standard Model values for the W decay branching fractions. The results for centre-of-mass energies between 183 and 207 GeV, for which new LEP averages have been computed, supersede the ones presented in [126]: the new grouping of the systematic errors does not affect the central value of the cross-section but degrades, as expected, the total errors in each point by about 10%. The combined LEP cross-sections at the eight energies are all positively correlated, with correlations ranging from 13% to 34%. For completeness, the measurements at 161 and 172 GeV are also listed in the table.

$\sqrt{s}$ (GeV)	WW cross-section (pb)					$\chi^2/\text{d.o.f.}$
	ALEPH	DELPHI	L3	OPAL	LEP	
161.3	$4.23 \pm 0.75^*$	$3.67^{+0.99}_{-0.87}^*$	$2.89^{+0.82}_{-0.71}^*$	$3.62^{+0.94}_{-0.84}^*$	$3.69 \pm 0.45$	} 1.3 / 3
172.1	$11.7 \pm 1.3^*$	$11.6 \pm 1.4^*$	$12.3 \pm 1.4^*$	$12.3 \pm 1.3^*$	$12.0 \pm 0.7$	
182.7	$15.57 \pm 0.68^*$	$15.86 \pm 0.74^*$	$16.53 \pm 0.72^*$	$15.43 \pm 0.66^*$	$15.77 \pm 0.37$	} 25.7/24
188.6	$15.71 \pm 0.39^*$	$15.83 \pm 0.43^*$	$16.24 \pm 0.43^*$	$16.30 \pm 0.40^*$	$15.98 \pm 0.23$	
191.6	$17.23 \pm 0.91$	$16.90 \pm 1.02$	$16.39 \pm 0.93$	$16.60 \pm 0.99$	$16.74 \pm 0.50$	
195.5	$17.00 \pm 0.57$	$17.86 \pm 0.63$	$16.67 \pm 0.60$	$18.59 \pm 0.75$	$17.36 \pm 0.34$	
199.5	$16.98 \pm 0.56$	$17.35 \pm 0.60$	$16.94 \pm 0.62$	$16.32 \pm 0.67$	$16.88 \pm 0.33$	
201.6	$16.16 \pm 0.76$	$17.67 \pm 0.84$	$16.95 \pm 0.88$	$18.48 \pm 0.92$	$17.18 \pm 0.44$	
204.9	$16.57 \pm 0.55$	$17.44 \pm 0.64$	$17.35 \pm 0.64$	$15.97 \pm 0.64$	$16.76 \pm 0.33$	
206.6	$17.32 \pm 0.45$	$16.50 \pm 0.48$	$17.96 \pm 0.51$	$17.77 \pm 0.57$	$17.30 \pm 0.28$	

Table 10.1: W-pair production cross-section from the four LEP experiments and combined values at all recorded centre-of-mass energies. All results are preliminary and unpublished, with the exception of those indicated by \*. The measurements between 183 and 207 GeV have been combined in one global fit, taking into account inter-experiment as well as inter-energy correlations of systematic errors. The results for the combined LEP W-pair production cross-section at 161 and 172 GeV are taken from [140, 141] respectively.

Figure 10.1 shows the combined LEP W-pair cross-section measured as a function of the centre-of-mass energy. The experimental points are compared with the theoretical calculations from YFSWW [142] and RACOONWW [143] between 155 and 215 GeV for  $m_W = 80.35$  GeV. The two codes have been

extensively compared and agree at a level better than 0.5% at the LEP2 energies [127]. The calculations above 170 GeV, based for the two programs on the so-called leading pole (LPA) or double pole approximations (DPA) [144], have theoretical uncertainties decreasing from 0.7% at 170 GeV to about 0.4% at centre-of-mass energies larger than 200 GeV, while in the threshold region, where the codes are run in Improved Born Approximation, a larger theoretical uncertainty of 2% is assigned [145]. This theoretical uncertainty is represented by the blue band in Figure 10.1. An error of 50 MeV on the W mass would translate into additional errors of 0.1% (3.0%) on the cross-section predictions at 200 GeV (161 GeV, respectively). All results, up to the highest centre-of-mass energies, are in agreement with the considered theoretical predictions.

The agreement between the measured W-pair cross-section,  $\sigma_{\text{WW}}^{\text{meas}}$ , and its expectation according to a given theoretical model,  $\sigma_{\text{WW}}^{\text{theo}}$ , can be expressed quantitatively in terms of their ratio

$$\mathcal{R}_{\text{WW}} = \frac{\sigma_{\text{WW}}^{\text{meas}}}{\sigma_{\text{WW}}^{\text{theo}}}, \quad (10.1)$$

averaged over the measurements performed by the four experiments at different energies in the LEP2 region. The above procedure has been used to compare the measurements at the eight energies between 183 and 207 GeV to the predictions of GENTLE [146], KORALW [147], YFSWW [142] and RACOONWW [143]. The measurements at 161 and 172 GeV have not been used in the combination because they were performed using data samples of low statistics and because of the high sensitivity of the cross-section to the value of the W mass at these energies.

The combination of the ratio  $\mathcal{R}_{\text{WW}}$  is performed using as input from the four experiments the 32 cross-sections measured at each of the eight energies. These are then converted into 32 ratios by dividing them by the considered theoretical predictions, listed in Appendix C. The full  $32 \times 32$  covariance matrix for the ratios is built taking into account the same sources of systematic errors used for the combination of the W-pair cross-sections at these energies. As for the total cross-section measurement, the effect of the new grouping of the systematic is to increase the total error on  $\mathcal{R}_{\text{WW}}$  by 10%; the central values change by no more than 30% of the total error.

The small statistical errors on the theoretical predictions at the various energies, taken as fully correlated for the four experiments and uncorrelated between different energies, are also translated into errors on the individual measurements of  $\mathcal{R}_{\text{WW}}$ . The theoretical errors on the predictions, due to the physical and technical precision of the generators used, are not propagated to the individual ratios but are used when comparing the combined values of  $\mathcal{R}_{\text{WW}}$  to unity. For each of the four models considered, two fits are performed: in the first, eight values of  $\mathcal{R}_{\text{WW}}$  at the different energies are extracted, averaged over the four experiments; in the second, only one value of  $\mathcal{R}_{\text{WW}}$  is determined, representing the global agreement of measured and predicted cross-sections over the whole energy range.

The results of the two fits to  $\mathcal{R}_{\text{WW}}$  for the two models are given in Table 10.2. As already qualitatively noted from Figure 10.1, the LEP measurements of the W-pair cross-section above threshold are in very good agreement to the predictions of YFSWW and RACOONWW. In contrast, the predictions from GENTLE and KORALW are more than 2% too high with respect to the measurements; the equivalent values of  $\mathcal{R}_{\text{WW}}$  in those cases are, respectively,  $0.972 \pm 0.011$  and  $0.978 \pm 0.011$ . The main differences between these two sets of predictions come from non-leading  $\mathcal{O}(\alpha)$  electroweak radiative corrections to the W-pair production process and non-factorisable corrections, which are included (in the LPA/DPA approximation [144]) in both YFSWW and RACOONWW, but not in GENTLE and KORALW. The data clearly prefer the computations which more precisely include  $\mathcal{O}(\alpha)$  radiative corrections.



$\sqrt{s}(\text{GeV})$	$\mathcal{R}_{\text{WW}}^{\text{YFSWW}}$	$\mathcal{R}_{\text{WW}}^{\text{RACOONWW}}$
182.7	$1.026 \pm 0.024$	$1.026 \pm 0.024$
188.6	$0.982 \pm 0.014$	$0.984 \pm 0.014$
191.6	$1.010 \pm 0.030$	$1.013 \pm 0.030$
195.5	$1.031 \pm 0.020$	$1.033 \pm 0.020$
199.5	$0.992 \pm 0.019$	$0.994 \pm 0.019$
201.6	$1.006 \pm 0.026$	$1.009 \pm 0.026$
204.9	$0.979 \pm 0.019$	$0.981 \pm 0.019$
206.6	$1.009 \pm 0.016$	$1.013 \pm 0.016$
$\chi^2/\text{d.o.f}$	25.7/24	25.7/24
Average	$0.997 \pm 0.011$	$0.999 \pm 0.011$
$\chi^2/\text{d.o.f}$	35.4/31	35.4/31

Table 10.2: Ratios of LEP combined W-pair cross-section measurements to the expectations according to YFSWW [142] and RACOONWW [143]. For each of the two models, two fits are performed, one to the LEP combined values of  $\mathcal{R}_{\text{WW}}$  at the eight energies between 183 and 207 GeV, and another to the LEP combined average of  $\mathcal{R}_{\text{WW}}$  over all energies. The results of the fits are given in the table together with the resulting  $\chi^2$ . Both fits take into account inter-experiment as well as inter-energy correlations of systematic errors.

The results of the fits for YFSWW and RACOONWW are also shown in Figure 10.2, where relative errors of 0.5% on the cross-section predictions have been assumed. For simplicity in the figure the energy dependence of the theory error on the W-pair cross-section has been neglected.

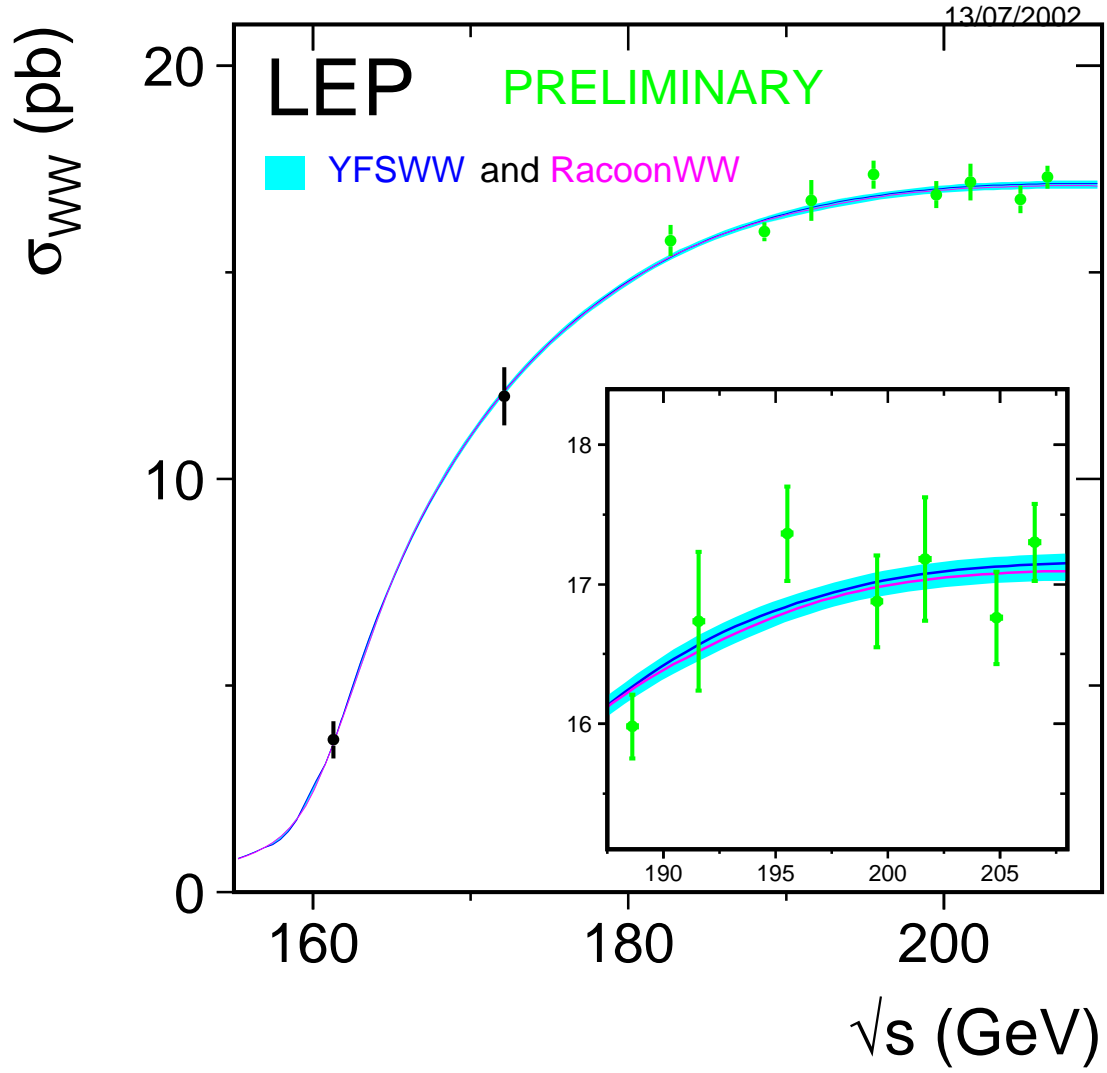


Figure 10.1: Measurements of the W-pair production cross-section, compared to the predictions of RACONWW [143] and YFSWW [142]. The shaded area represents the uncertainty on the theoretical predictions, estimated in  $\pm 2\%$  for  $\sqrt{s} < 170$  GeV and ranging from 0.7 to 0.4% above 170 GeV.

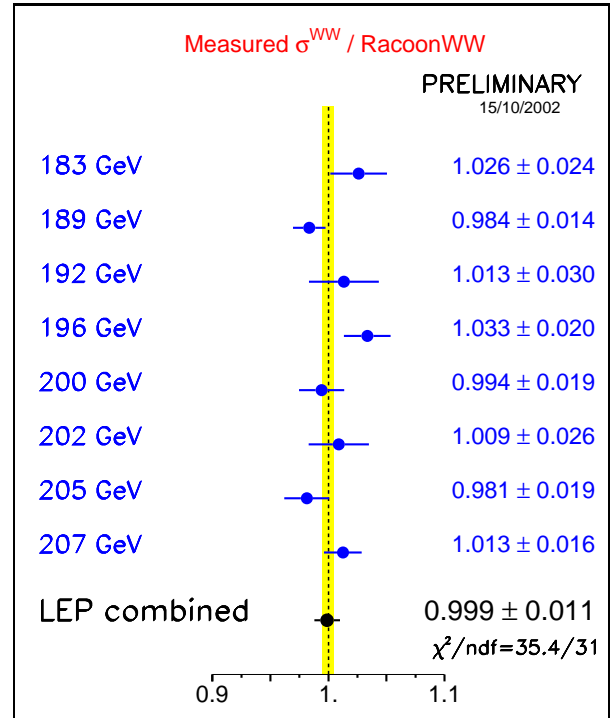
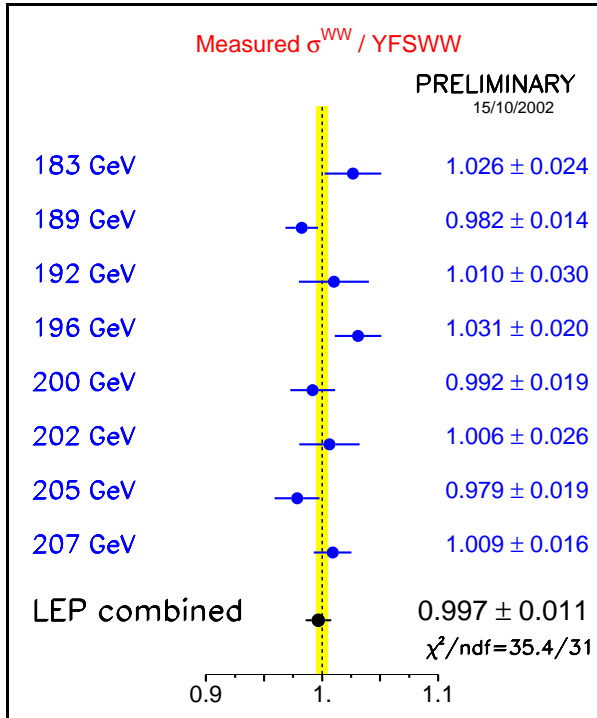


Figure 10.2: Ratios of LEP combined W-pair cross-section measurements to the expectations according to YFSWW [142] and RACOONWW [143]. The yellow bands represent constant relative errors of 0.5% on the two cross-section predictions.

### 10.3 Z-pair production cross-section

Final results of the measurements of the Z-pair production cross-section, defined as the NC02 [127] contribution to four-fermion cross-sections, have been published by ALEPH, DELPHI and OPAL at  $\sqrt{s} = 183$  and 189 GeV [148–150] and by L3 at all energies between 183 and 202 GeV [151–154]. All experiments have also contributed preliminary results for all other energies up to 207 GeV. With respect to the Winter 2002 Conferences, L3 [155] and DELPHI [156] have provided preliminary updates of their previous measurements at 205–207 GeV and 183–207 GeV, respectively.

The combination of results is performed with the same technique used for the WW cross-section. The symmetrized expected statistical error of each analysis is used, to avoid biases due to the limited number of selected events. The approach to determine the cross-section is different among the experiments: DELPHI uses a bayesian approach with the prior knowledge that the cross-section has to

$\sqrt{s}$ (GeV)	ZZ cross-section (pb)					$\chi^2/\text{d.o.f.}$
	ALEPH	DELPHI	L3	OPAL	LEP	
182.7	$0.11^{+0.16}_{-0.12}^*$	$0.40^{+0.21}_{-0.16}$	$0.31^{+0.17}_{-0.15}^*$	$0.12^{+0.20}_{-0.18}^*$	$0.22 \pm 0.08$	14.7/24
188.6	$0.67^{+0.14}_{-0.13}^*$	$0.53^{+0.12}_{-0.11}$	$0.73^{+0.15}_{-0.14}^*$	$0.80^{+0.15}_{-0.14}^*$	$0.66 \pm 0.07$	
191.6	$0.53^{+0.34}_{-0.27}$	$0.70^{+0.37}_{-0.31}$	$0.29 \pm 0.22^*$	$1.13^{+0.47}_{-0.41}$	$0.62 \pm 0.18$	
195.5	$0.69^{+0.23}_{-0.20}$	$1.08^{+0.25}_{-0.22}$	$1.18 \pm 0.26^*$	$1.19^{+0.28}_{-0.26}$	$1.00 \pm 0.12$	
199.5	$0.70^{+0.22}_{-0.20}$	$0.77^{+0.21}_{-0.18}$	$1.25 \pm 0.27^*$	$1.09^{+0.26}_{-0.24}$	$0.90 \pm 0.13$	
201.6	$0.70^{+0.33}_{-0.28}$	$0.90^{+0.33}_{-0.29}$	$0.95 \pm 0.39^*$	$0.94^{+0.38}_{-0.33}$	$0.84 \pm 0.18$	
204.9	$1.21^{+0.26}_{-0.23}$	$1.05^{+0.23}_{-0.20}$	$0.88^{+0.25}_{-0.23}$	$1.07^{+0.28}_{-0.26}$	$1.01 \pm 0.13$	
206.6	$1.01^{+0.19}_{-0.17}$	$0.97^{+0.16}_{-0.15}$	$1.23^{+0.22}_{-0.20}$	$1.07^{+0.22}_{-0.21}$	$1.03 \pm 0.10$	

Table 10.3: Z-pair production cross-section from the four LEP experiments and combined values for the eight energies between 183 and 207 GeV. All results are preliminary with the exception of those indicated by \*.

$\sqrt{s}(\text{GeV})$	$\mathcal{R}_{ZZ}^{\text{ZZTO}}$	$\mathcal{R}_{ZZ}^{\text{YFSZZ}}$
182.7	$0.855 \pm 0.325$	$0.855 \pm 0.325$
188.6	$1.014 \pm 0.112$	$1.004 \pm 0.111$
191.6	$0.794 \pm 0.226$	$0.789 \pm 0.224$
195.5	$1.111 \pm 0.134$	$1.108 \pm 0.134$
199.5	$0.920 \pm 0.126$	$0.916 \pm 0.126$
201.6	$0.833 \pm 0.175$	$0.829 \pm 0.174$
204.9	$0.967 \pm 0.126$	$0.961 \pm 0.125$
206.6	$0.974 \pm 0.095$	$0.964 \pm 0.094$
$\chi^2/\text{d.o.f.}$	14.7/24	14.7/24
Average	$0.969 \pm 0.055$	$0.962 \pm 0.055$
$\chi^2/\text{d.o.f.}$	17.6/31	17.6/31

Table 10.4: Ratios of LEP combined Z-pair cross-section measurements to the expectations according to ZZTO [158] and YFSZZ [157]. The results of the combined fits are given in the table together with the resulting  $\chi^2$ . Both fits take into account inter-experiment as well as inter-energy correlations of systematic errors.

be positive, whereas a frequentist interval is given by the other experiments. This induces a certain inconsistency in the way the ZZ cross-section combination is performed, which might lead to wrong results in the low statistics/cross-section energy points like 183 or 192 GeV. However, using private DELPHI results given in a way consistent with the other collaborations, it was verified that the effect in the combined value is negligible, both in terms of error and central values.

In addition to the results presented at the last Winter 2002 Conferences [126], the correlation in energy of some of the systematic sources is now accounted for in the combination. These include the uncertainty on the backgrounds from  $q\bar{q}$ , WW, Zee and  $W e\nu$  processes and the uncertainty on the  $b$  quark modelling.

The results of the individual experiments and the LEP averages are summarised for the different centre-of-mass energies in Table 10.3. The combination of final results at  $\sqrt{s} = 183$  and 189 GeV is the same that was given for the Summer 2000 Conferences [159]. The results above 189 GeV supersede those presented for the Winter 2002 Conferences [126], and are all preliminary with the exception of the L3 results between 192 and 202 GeV.

The measurements are shown in Figure 10.3 as a function of the LEP centre-of-mass energy, where they are compared to the YFSZZ [157] and ZZTO [158] predictions. Both these calculations have an estimated uncertainty of  $\pm 2\%$  [127]. The data do not show any significant deviation from the theoretical expectations.

In analogy with the W-pair cross-section, a value for  $\mathcal{R}_{ZZ}$  can also be determined: its definition and the procedure of the combination follows the one described in the previous section. The data are compared with the YFSZZ and ZZTO predictions; table 10.4 reports the numerical values of  $\mathcal{R}_{ZZ}$  in energy and combined, whereas figure 10.4 show them in comparison to unity, where the  $\pm 2\%$  error on the theoretical ZZ cross-section is shown as a yellow band. The experimental accuracy on the combined value of  $\mathcal{R}_{ZZ}$  is about 5.5%.

The theory predictions, the details of the experimental inputs with the the breakdown of the error contributions and the LEP combined values of the total cross-sections and the ratios to theory are reported in Appendix C.

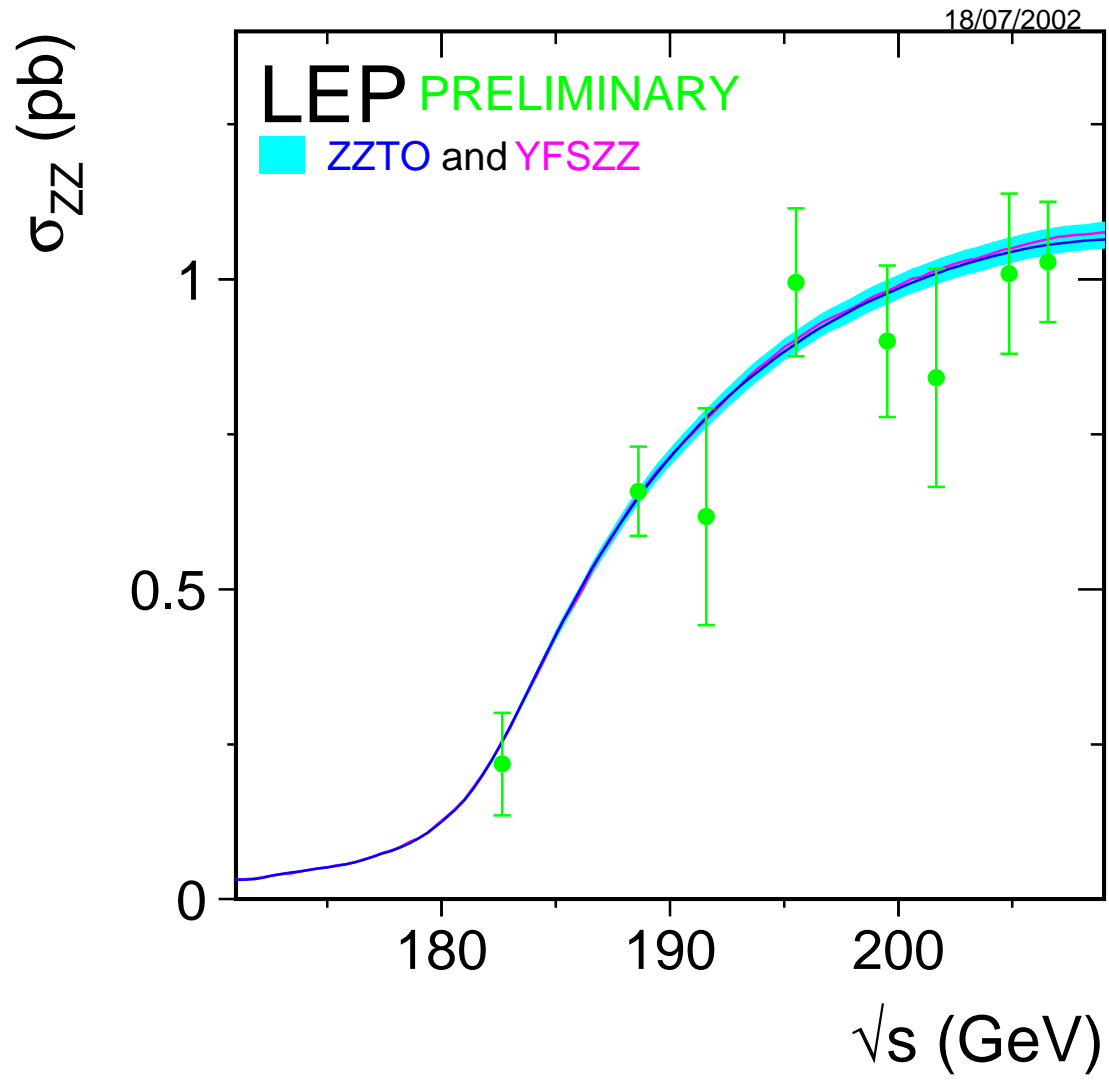


Figure 10.3: Measurements of the Z-pair production cross-section, compared to the predictions of YFSZZ [157] and ZZTO [158]. The shaded area represent the  $\pm 2\%$  uncertainty on the predictions.

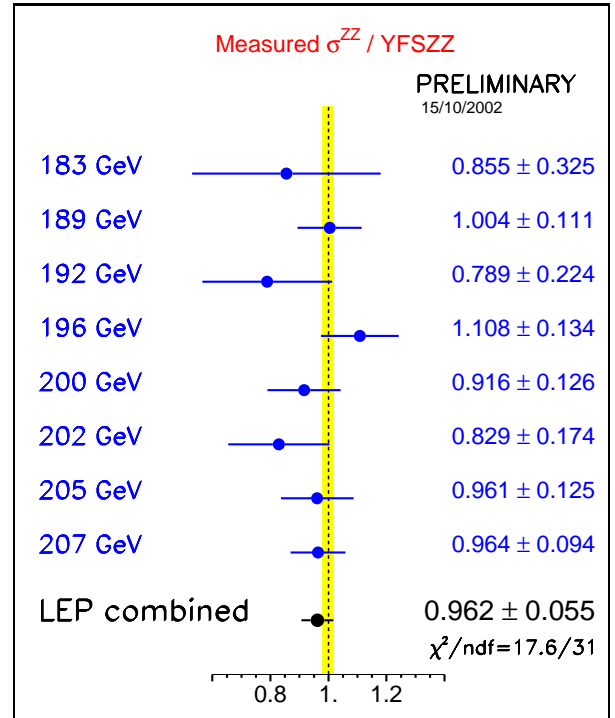
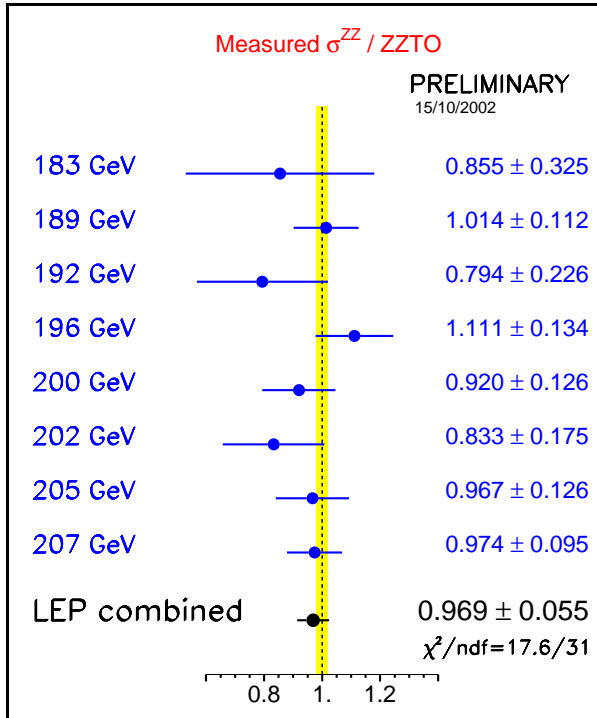


Figure 10.4: Ratios of LEP combined Z-pair cross-section measurements to the expectations according to ZZTO [158] and YFSZZ [157]. The yellow bands represent constant relative errors of 2% on the two cross-section predictions.

## 10.4 Single-W production cross-section

Single-W production at LEP2 is defined as the complete  $t$ -channel subset of Feynman diagrams contributing to  $e\nu_e\bar{f}f'$  final states, with additional cuts on kinematic variables to exclude the regions of phase space dominated by multiperipheral diagrams, where the cross-section calculation is affected by large uncertainties. The kinematic cuts used in the signal definitions are:  $m_{q\bar{q}} > 45 \text{ GeV}/c^2$  for the  $e\nu_e q\bar{q}$  final states,  $E_\ell > 20 \text{ GeV}$  for the  $e\nu_e\ell\bar{\nu}_\ell$  final states with  $\ell = \mu$  or  $\tau$ , and finally  $|\cos\theta_{e-}| > 0.95$ ,  $|\cos\theta_{e+}| < 0.95$  and  $E_{e+} > 20 \text{ GeV}$  (or the charge conjugate cuts) for the  $e\nu_e e\nu_e$  final states.

Since the Summer 2001 Conferences only L3 [160] has presented new measurements of the single-W cross-section, updating the published results corresponding to data taken at energies from 192 to 207 GeV, while none of the other results previously presented by the four experiments have been updated. These include published results by DELPHI [161] and L3 [162] and preliminary results by ALEPH [163], DELPHI [164] and OPAL [165]. The measurements performed on the small amount of data below 183 GeV, by L3 at 130–172 [166,167] and ALEPH at 161–172 GeV [168], have not been converted into the single-W common LEP definition and are absent from the tables and the following plots.

$\sqrt{s}$ (GeV)	Single-W hadronic cross-section (pb)					$\chi^2/\text{d.o.f.}$
	ALEPH	DELPHI	L3	OPAL	LEP	
182.7	$0.40 \pm 0.24^*$	—	$0.58^{+0.23}_{-0.20}^*$	—	$0.46 \pm 0.16$	12.1/16
188.6	$0.31 \pm 0.14$	$0.44^{+0.28}_{-0.25}$	$0.52^{+0.14}_{-0.13}^*$	$0.53^{+0.14}_{-0.13}$	$0.44 \pm 0.08$	
191.6	$0.94 \pm 0.44$	$0.01^{+0.19}_{-0.07}$	$0.84^{+0.44}_{-0.37}$	—	$0.69 \pm 0.25$	
195.5	$0.45 \pm 0.23$	$0.78^{+0.38}_{-0.34}$	$0.66^{+0.25}_{-0.23}$	—	$0.58 \pm 0.14$	
199.5	$0.82 \pm 0.26$	$0.16^{+0.29}_{-0.17}$	$0.37^{+0.22}_{-0.20}$	—	$0.46 \pm 0.14$	
201.6	$0.68 \pm 0.35$	$0.55^{+0.47}_{-0.40}$	$1.10^{+0.35}_{-0.36}$	—	$0.76 \pm 0.21$	
204.9	$0.50 \pm 0.25$	$0.50^{+0.35}_{-0.31}$	$0.42^{+0.25}_{-0.21}$	—	$0.45 \pm 0.16$	
206.6	$0.95 \pm 0.24$	$0.37^{+0.24}_{-0.21}$	$0.66^{+0.20}_{-0.18}$	—	$0.68 \pm 0.13$	

Table 10.5: Single-W production cross-section from the four LEP experiments and combined values for the eight energies between 183 and 207 GeV, in the hadronic decay channel of the W boson. All results are preliminary with the exception of those indicated by \*.

A new combination of LEP results at all centre-of-mass energies has been performed, taking properly into account correlations of the systematic errors in energy and among experiments, in analogy with the WW and ZZ cross-section determinations. The expected statistical errors have been used for all measurements, given the limited statistical precision of the single-W cross-section measurements. The total and the hadronic single-W cross-sections, less contaminated by  $\gamma\gamma$  interaction contributions, are combined independently; the inputs by the four LEP experiments between 183 and 207 GeV are listed in Tables 10.5 and 10.6, and the corresponding LEP combined values presented.

The LEP measurements of the single-W cross-section are shown, as a function of the LEP centre-of-mass energy, in Figure 10.5 for the hadronic decays and in Figure 10.6 for all decays of the W boson. In the two figures, the measurements are compared with the expected values from WPHACT [170] and grc4f [171]. WTO [169], which includes fermion-loop corrections for the hadronic final states, is also used in figure 10.5. As discussed more in detail in [159] and [127], the theoretical predictions are scaled upward to correct for the implementation of QED radiative corrections at the wrong energy scale  $s$ . The full correction factor of 4%, derived [127] by the comparison to the theoretical predictions from SWAP [172], is conservatively taken as a systematic error. This uncertainty dominates the  $\pm 5\%$



$\sqrt{s}$ (GeV)	Single-W total cross-section (pb)					$\chi^2/\text{d.o.f.}$
	ALEPH	DELPHI	L3	OPAL	LEP	
182.7	$0.61 \pm 0.27^*$	—	$0.80^{+0.28}_{-0.25}^*$	—	$0.68 \pm 0.19$	11.9/16
188.6	$0.45 \pm 0.15$	$0.70^{+0.30}_{-0.26}$	$0.69^{+0.16}_{-0.15}^*$	$0.67^{+0.17}_{-0.15}$	$0.60 \pm 0.09$	
191.6	$1.31 \pm 0.48$	$0.12^{+0.29}_{-0.14}$	$1.07^{+0.47}_{-0.40}$	—	$0.98 \pm 0.28$	
195.5	$0.65 \pm 0.25$	$0.90^{+0.41}_{-0.36}$	$0.93^{+0.26}_{-0.24}$	—	$0.80 \pm 0.16$	
199.5	$0.99 \pm 0.27$	$0.45^{+0.33}_{-0.20}$	$0.86^{+0.25}_{-0.23}$	—	$0.78 \pm 0.15$	
201.6	$0.75 \pm 0.36$	$1.09^{+0.52}_{-0.43}$	$1.44^{+0.44}_{-0.39}$	—	$1.06 \pm 0.23$	
204.9	$0.78 \pm 0.27$	$0.56^{+0.36}_{-0.30}$	$0.76^{+0.28}_{-0.25}$	—	$0.71 \pm 0.17$	
206.6	$1.19 \pm 0.25$	$0.58^{+0.26}_{-0.23}$	$1.04^{+0.20}_{-0.19}$	—	$0.98 \pm 0.14$	

Table 10.6: Single-W total production cross-section from the four LEP experiments and combined values for the eight energies between 183 and 207 GeV. All results are preliminary with the exception of those indicated by \*.

theoretical error currently assigned to these predictions [127, 159], represented by the shaded area in Figures 10.5 and 10.6. All results, up to the highest centre-of-mass energies, are in agreement with the theoretical predictions.

The agreement can also be appreciated in table 10.7, where the values of the ratio between measured and expected cross-section values according to the computations by **grc4f** and **WPHACT** are reported. The combination is performed accounting for the energy and experiment correlations of the systematic sources. The results are also presented in figure 10.7.

$\sqrt{s}(\text{GeV})$	$\mathcal{R}_{\text{We}\nu}^{\text{grc4f}}$	$\mathcal{R}_{\text{We}\nu}^{\text{WPHACT}}$
182.7	$1.088 \pm 0.301$	$1.122 \pm 0.310$
188.6	$0.851 \pm 0.136$	$0.877 \pm 0.140$
191.6	$1.322 \pm 0.379$	$1.362 \pm 0.391$
195.5	$1.011 \pm 0.207$	$1.042 \pm 0.214$
199.5	$0.921 \pm 0.189$	$0.949 \pm 0.194$
201.6	$1.206 \pm 0.268$	$1.242 \pm 0.276$
204.9	$0.769 \pm 0.192$	$0.792 \pm 0.198$
206.6	$1.030 \pm 0.159$	$1.061 \pm 0.163$
$\chi^2/\text{d.o.f}$	11.8/16	11.8/16
Average	$0.949 \pm 0.078$	$0.978 \pm 0.080$
$\chi^2/\text{d.o.f}$	15.8/23	15.8/23

Table 10.7: Ratios of LEP combined total single-W cross-section measurements to the expectations according to **grc4f** [171] and **WPHACT** [170]. The resulting averages over energies are also given. The averages take into account inter-experiment as well as inter-energy correlations of systematic errors.

The theory predictions and the details of the experimental inputs and the LEP combined values of the single-W cross-sections and the ratios to theory are reported in Appendix C.

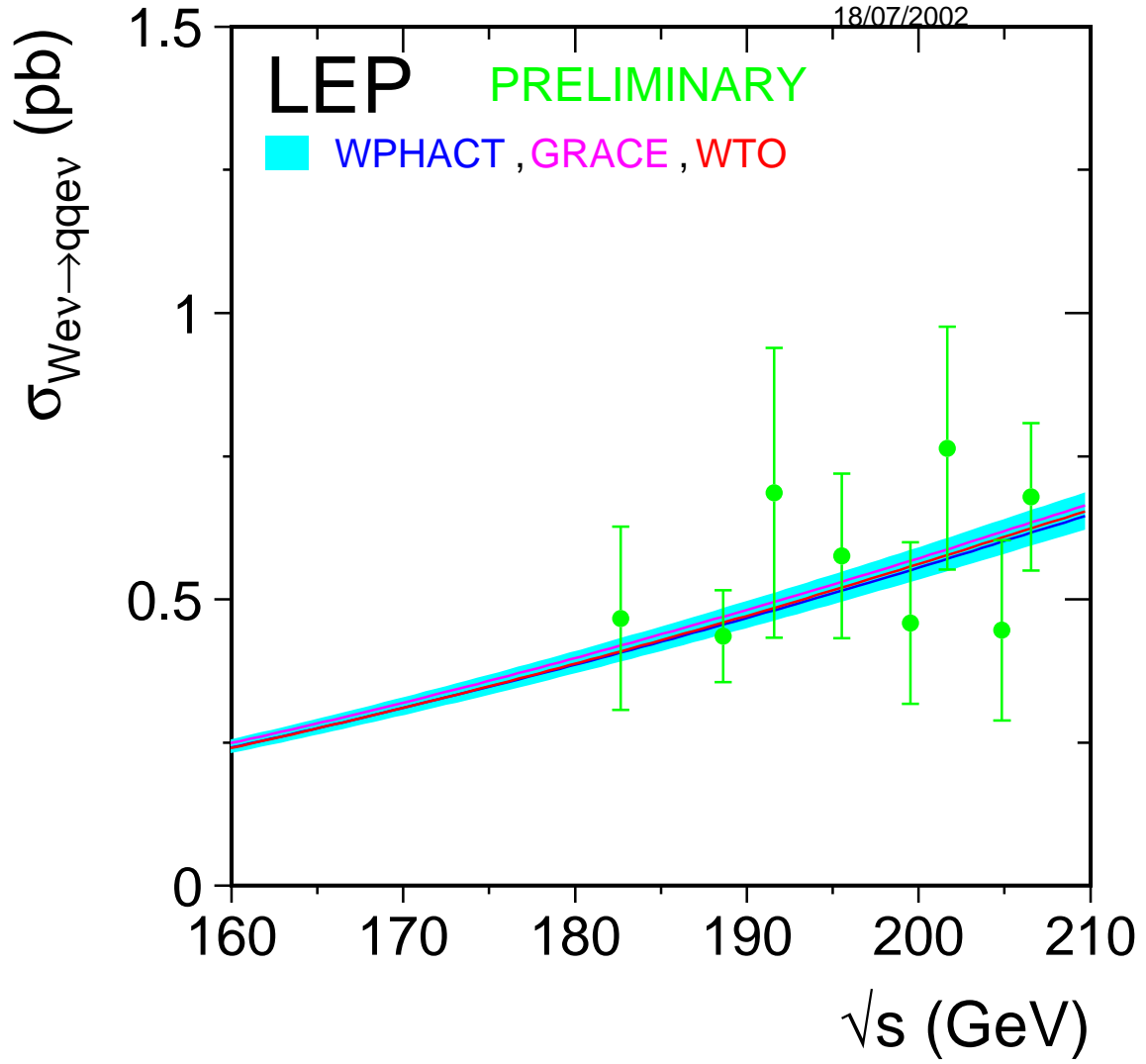


Figure 10.5: Measurements of the single-W production cross-section in the hadronic decay channel of the W boson, compared to the predictions of WTO [169], WPHACT [170] and `grc4f` [171]. The shaded area represents the  $\pm 5\%$  uncertainty on the predictions.

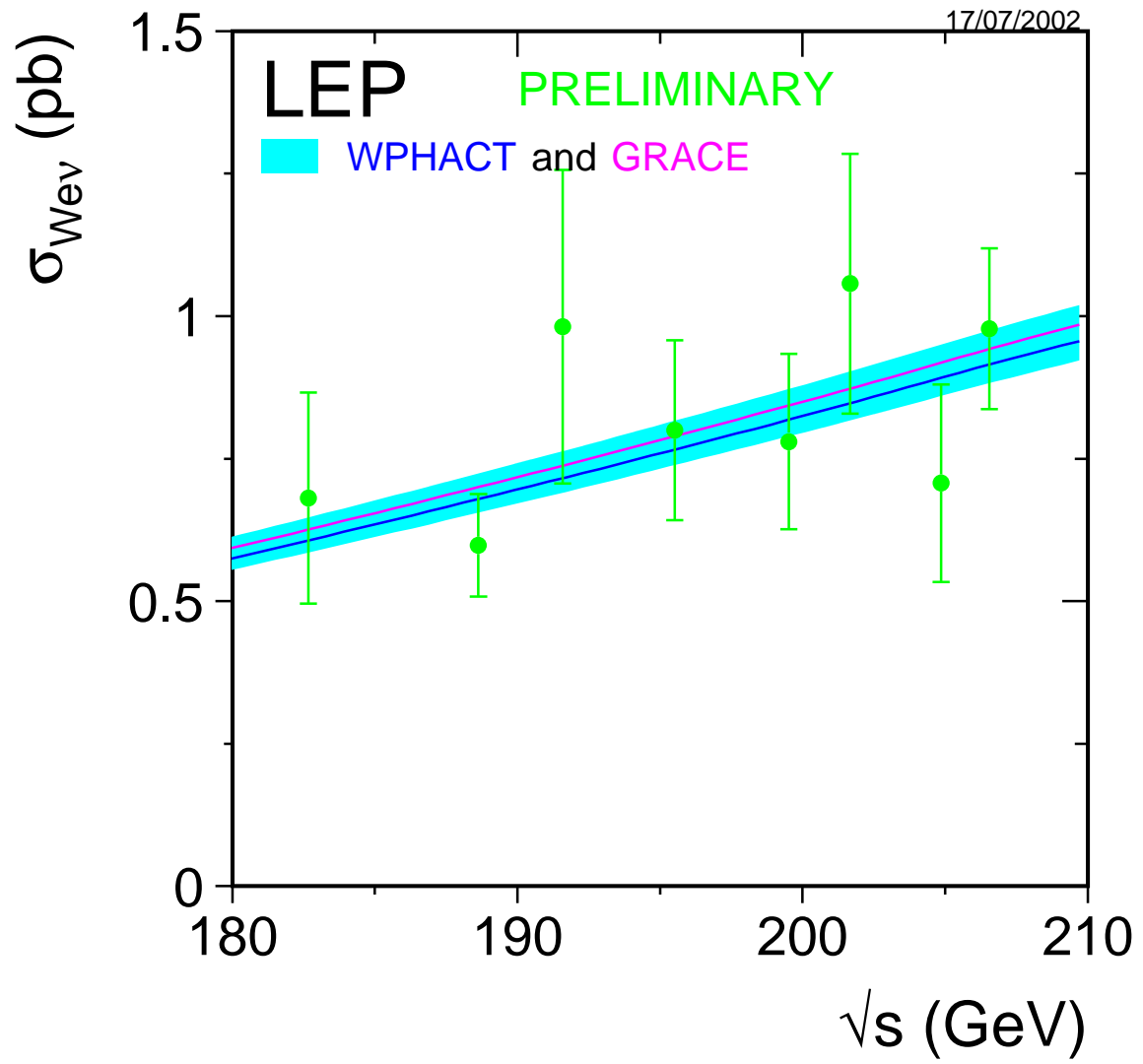


Figure 10.6: Measurements of the single-W total production cross-section, compared to the predictions of WPHACT and `grc4f`. The shaded area represents the  $\pm 5\%$  uncertainty on the predictions.

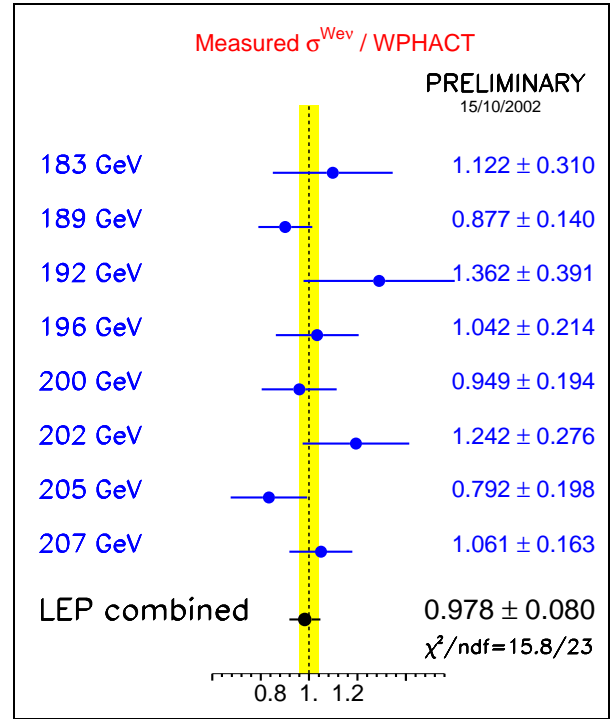
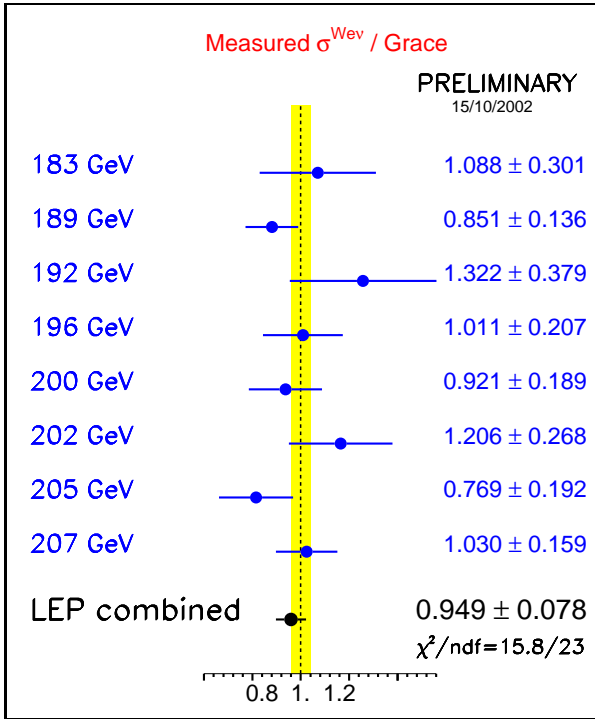


Figure 10.7: Ratios of LEP combined total single-W cross-section measurements to the expectations according to `grc4f` [171] and WPHACT [170]. The yellow bands represent constant relative errors of 5% on the two cross-section predictions.

## 10.5 Single-Z production cross-section

For the first time a LEP combination on the single-Z production cross-section has been performed using preliminary ALEPH [173], DELPHI [164] and L3 [174] inputs to the Summer 2002 Conferences. Single-Z production at LEP2 is studied considering only the  $eeq\bar{q}$ ,  $ee\mu\mu$  final states with the following phase space cuts and assuming one visible electron:  $m_{q\bar{q}}(m_{\mu\mu}) > 60 \text{ GeV}/c^2$ ,  $\theta_{e^+} < 12$  degrees,  $12 \text{ degrees} < \theta_{e^-} < 120$  degrees and  $E_{e^-} > 3 \text{ GeV}$ , with obvious notation and where the angle is defined with respect to the beam pipe, with the positron direction being along  $+z$  and the electron direction being along  $-z$ . Corresponding cuts are imposed when the positron is visible:  $\theta_{e^-} > 168$  degrees,  $60 \text{ degrees} < \theta_{e^+} < 168$  degrees and  $E_{e^+} > 3 \text{ GeV}$ .

$\sqrt{s}$ (GeV)	Single-Z hadronic cross-section (pb)					$\chi^2/\text{d.o.f.}$
	ALEPH	DELPHI	L3	OPAL	LEP	
182.7	—	$0.56^{+0.28}_{-0.23}$	$0.51^{+0.19}_{-0.16}$	—	$0.52 \pm 0.14$	7.3/8
188.6	—	$0.65^{+0.16}_{-0.15}$	$0.55^{+0.11}_{-0.10}$	—	$0.58 \pm 0.08$	
191.6	—	$0.63^{+0.40}_{-0.30}$	$0.60^{+0.27}_{-0.22}$	—	$0.61 \pm 0.18$	
195.5	—	$0.66^{+0.22}_{-0.19}$	$0.40^{+0.13}_{-0.11}$	—	$0.48 \pm 0.11$	
199.5	—	$0.57^{+0.20}_{-0.17}$	$0.33^{+0.13}_{-0.11}$	—	$0.42 \pm 0.11$	
201.6	—	$0.19^{+0.21}_{-0.16}$	$0.81^{+0.27}_{-0.23}$	—	$0.58 \pm 0.16$	
204.9	—	$0.37^{+0.18}_{-0.15}$	$0.56^{+0.16}_{-0.14}$	—	$0.49 \pm 0.12$	
206.6	—	$0.68^{+0.16}_{-0.14}$	$0.59^{+0.12}_{-0.11}$	—	$0.62 \pm 0.09$	

Table 10.8: Preliminary single-Z hadronic production cross-section from the four LEP experiments and combined values for the eight energies between 183 and 207 GeV.

	Single-Z cross-section into muons(pb)				
	ALEPH	DELPHI	L3	OPAL	LEP
Av. $\sqrt{s}$ (GeV)	196.67	197.10	—	—	196.88
$\sigma_{Zee \rightarrow \mu\mu ee}$	$0.057 \pm 0.014$	$0.070^{+0.023}_{-0.019}$	—	—	$0.063 \pm 0.011$

Table 10.9: Preliminary energy averaged single-Z production cross-section into muons from the four LEP experiments and combined values .

Tables 10.8 and 10.9 synthesize the inputs by the experiments and the corresponding LEP combinations in the hadronic and muon channel, respectively. The  $ee\mu\mu$  cross-section is already combined in energy by the individual experiments to increase the statistics of the data. The combination accounts for energy and experiment correlation of the systematic errors. The results in the hadronic channel are compared with the WPHACT and **grc4f** predictions as a function of the centre-of-mass energy and shown in figure 10.8. Table 10.10 and figure 10.9 show the preliminary values of the ratio between measured and expected cross-sections at the various energy points and the combined value; the testing accuracy of the combined value is about 8% with only two experiments contributing in the average.

The detailed breakdown of the inputs of the experiments with the split up of the systematic contribution according to the correlations for the single-Z cross-section and its ratio to theory can be found in Appendix C.

$\sqrt{s}(\text{GeV})$	$\mathcal{R}_{\text{Zee}}^{\text{grc4f}}$	$\mathcal{R}_{\text{Zee}}^{\text{WPHACT}}$
182.7	$1.016 \pm 0.268$	$1.022 \pm 0.281$
188.6	$1.064 \pm 0.180$	$1.075 \pm 0.157$
191.6	$1.102 \pm 0.333$	$1.111 \pm 0.345$
195.5	$0.848 \pm 0.195$	$0.835 \pm 0.230$
199.5	$0.699 \pm 0.224$	$0.712 \pm 0.215$
201.6	$0.976 \pm 0.267$	$0.957 \pm 0.282$
204.9	$0.799 \pm 0.215$	$0.810 \pm 0.207$
206.6	$1.021 \pm 0.212$	$1.031 \pm 0.152$
$\chi^2/\text{d.o.f}$	7.2/8	7.1/8
Average	$0.928 \pm 0.088$	$0.951 \pm 0.083$
$\chi^2/\text{d.o.f}$	10.1/15	10.3/15

Table 10.10: Ratios of LEP combined single-Z hadronic cross-section measurements to the expectations according to **grc4f** [171] and **WPHACT** [170]. The resulting averages over energies are also given. The averages take into account inter-experiment as well as inter-energy correlations of systematic errors.

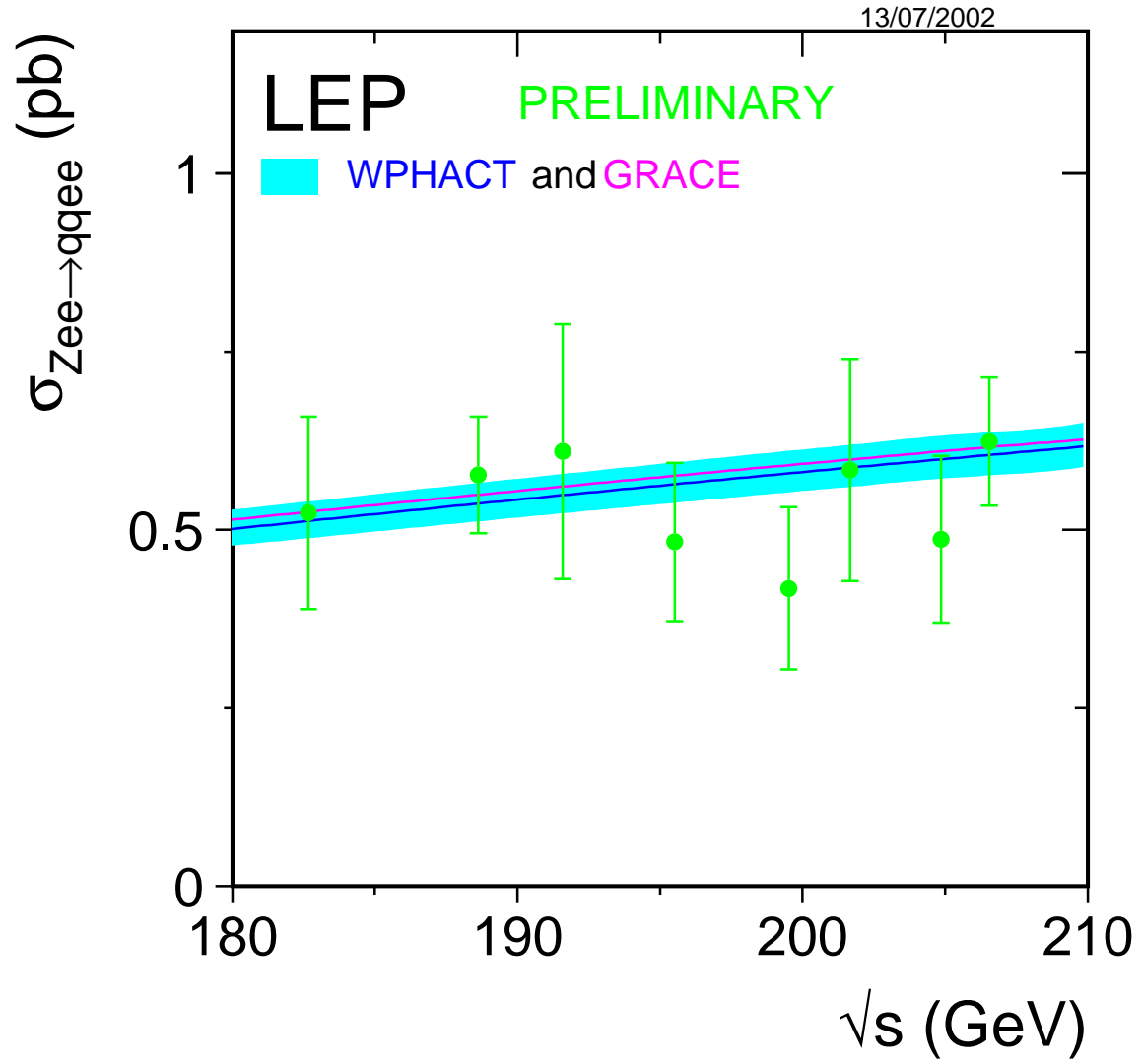


Figure 10.8: Measurements of the single-Z hadronic production cross-section, compared to the predictions of WPHACT and `grc4f`. The shaded area represents the  $\pm 5\%$  uncertainty on the predictions.

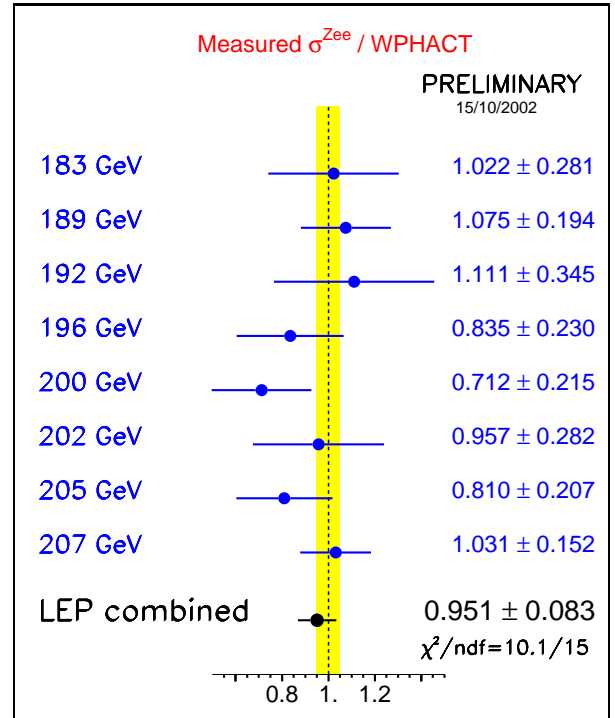
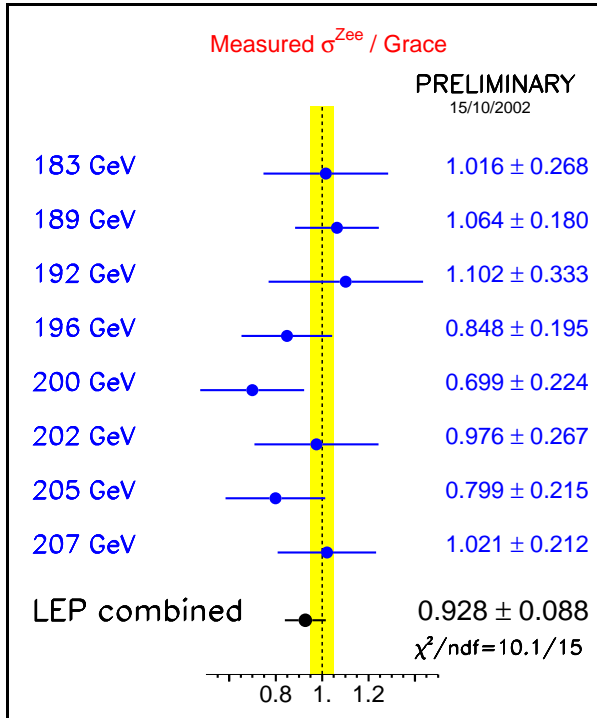


Figure 10.9: Ratios of LEP combined single-Z hadronic cross-section measurements to the expectations according to `grc4f` [171] and WPHACT [170]. The yellow bands represent constant relative errors of 5% on the two cross-section predictions.



## 10.6 $WW\gamma$ production cross-section

For the first time a LEP combination on the  $WW\gamma$  production cross-section has been performed using preliminary DELPHI [164] and L3 [174] inputs to the Summer 2002 Conferences. The signal is defined as the part of the  $WW\gamma$  process with the following cuts to the photon:  $E_\gamma > 5$  GeV,  $|\cos \theta_\gamma| < 0.95$ ,  $|\cos \theta_{\gamma,f}| < 0.90$  and  $m_W - 2\Gamma_W < m_{ff'} < m_W + 2\Gamma_W$  where  $\theta_{\gamma,f}$  is the angle between the photon and the closest charged fermion and  $m_{ff'}$  is the invariant mass of fermions from the  $W$ s.

In order to increase the statistics, the LEP combination is performed in energy intervals rather than at each energy point; they are defined according to the LEP2 running period where more statistics was accumulated. The luminosity weighted centre-of-mass per interval is determined in each experiment and then combined to obtain the corresponding value in the combination. Table 10.11 reports those energies and the cross-sections measured by the experiments, together with the combined LEP values. Figure 10.10 shows the combined data points compared with the cross-section prediction by EEWG [175]

$\sqrt{s}$ (GeV)	WW $\gamma$ cross-section (pb)				
	ALEPH	DELPHI	L3	OPAL	LEP
188.6	—	$0.07 \pm 0.08$	$0.20 \pm 0.09$	—	$0.13 \pm 0.06$
194.4	—	$0.25 \pm 0.13$	$0.17 \pm 0.10$	—	$0.20 \pm 0.08$
200.2	—	$0.42 \pm 0.13$	$0.43 \pm 0.13$	—	$0.43 \pm 0.09$
206.1	—	$0.24 \pm 0.09$	$0.13 \pm 0.08$	—	$0.18 \pm 0.06$

Table 10.11: Preliminary  $WW\gamma$  production cross-section from the four LEP experiments and combined values for the four energy bins.

## 10.7 Summary

The updated combinations of the W-pair, Z-pair and single-W cross-section measurements, based on data collected up to 209 GeV by the four LEP experiments, has been presented. For the first time new LEP combinations of single-Z and  $WW\gamma$  production cross-sections based on the same data have also been performed. All measurements agree with the theoretical predictions.

This note still reflects a preliminary status of the analyses at the time of the Summer 2002 Conferences. A definitive statement on these results must wait for publication by each collaboration. Further work for the possibility of providing a LEP combination of W angular differential distributions and other cross-sections in the neutral current sector ( $Z\gamma^*$ ,  $Z\gamma\gamma$ ) are ongoing.

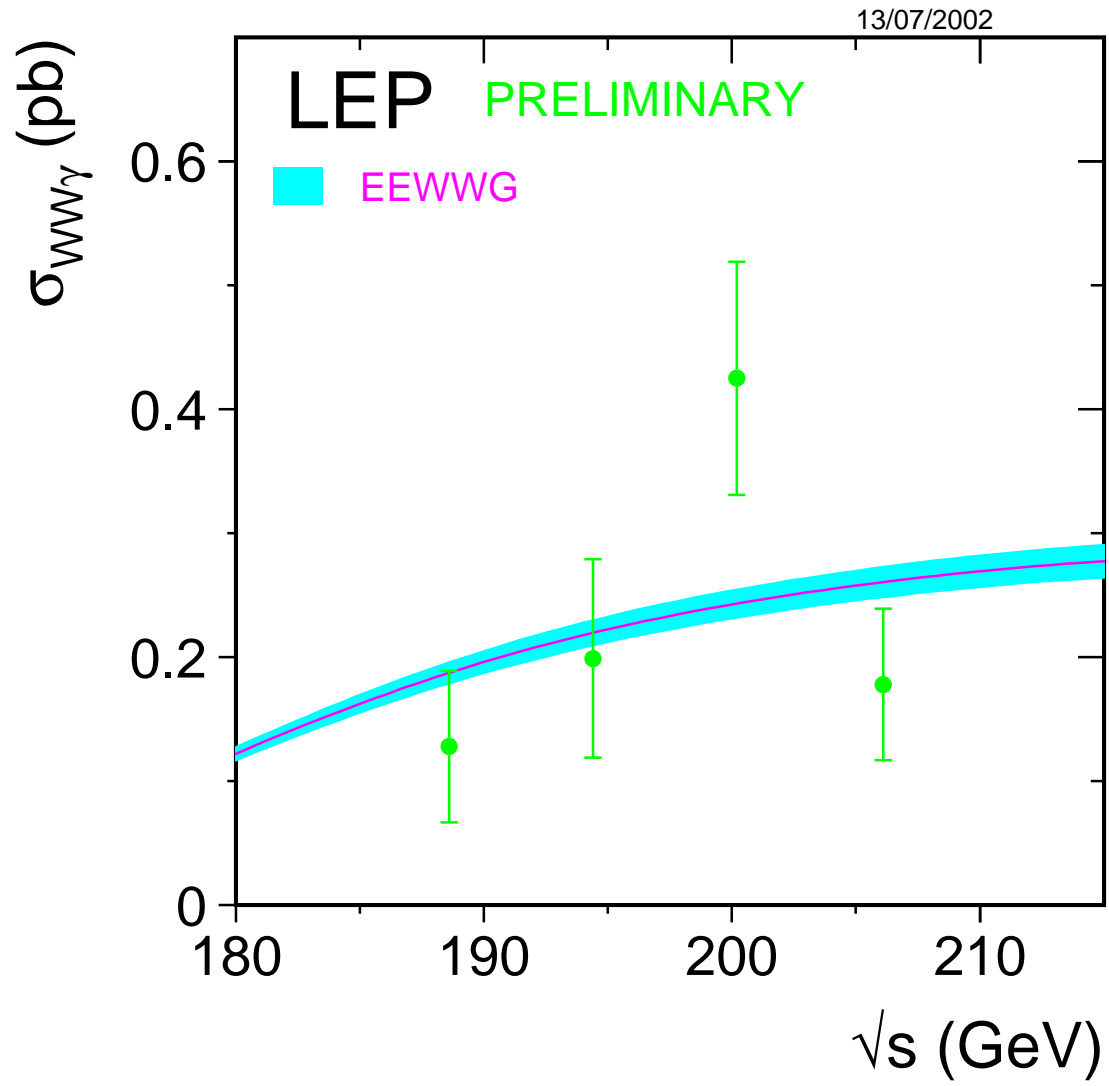


Figure 10.10: Measurements of the  $WW\gamma$  production cross-section, compared to the predictions of EEWWG [175]. The shaded area represents the  $\pm 5\%$  uncertainty on the predictions.

# Chapter 11

## Electroweak Gauge Boson Self Couplings

**Updates with respect to summer 2002:**

Unchanged w.r.t. summer 2002: Results are preliminary.

### 11.1 Introduction

During its second phase of operation, from 1996 until November 2000, the  $e^+e^-$  collider LEP at CERN steadily increased its centre-of-mass energy from 161 GeV reaching up to 209 GeV in the final year. Until the end of LEP-II operation, a total integrated luminosity of approximately  $700 \text{ pb}^{-1}$  per experiment has been recorded.

The measurement of gauge boson couplings and the search for possible anomalous contributions due to the effects of new physics beyond the Standard Model are among the principal physics aims at LEP-II [176]. Combined preliminary measurements of triple gauge boson couplings are presented here. Results from W-pair production are combined in single and also multi-parameter fits, the latter for the first time including  $O(\alpha_{em})$  corrections. A new combination of quartic gauge coupling (QGC) results for the  $ZZ\gamma\gamma$  vertex is also presented, including at this stage data from L3 and OPAL. The combination of QGCs associated with the  $WW\gamma\gamma$  vertex, including the sign convention as reported in [177, 178] and the reweighting based on [177] is foreseen for our next report. The combinations for neutral TGCs remain unchanged from our report [179] of last summer.

The W-pair production process,  $e^+e^- \rightarrow W^+W^-$ , involves charged triple gauge boson vertices between the  $W^+W^-$  and the Z or photon. During LEP-II operation, about 10,000 W-pair events were collected by each experiment. Single W ( $e\nu W$ ) and single photon ( $\nu\bar{\nu}\gamma$ ) production at LEP are also sensitive to the  $WW\gamma$  vertex. Results from these channels are also included in the combination for some experiments; the individual references should be consulted for details.

For the charged TGCs, Monte Carlo calculations (RacoonWW [180] and YFSWW [181]) incorporating an improved treatment of  $O(\alpha_{em})$  corrections to the WW production process have recently become available. These corrections affect the measurements of the charged TGCs in W-pair production. Preliminary results including these  $O(\alpha_{em})$  corrections have been submitted from all four LEP collaborations ALEPH [182], DELPHI [183], L3 [184] and OPAL [185]. LEP combinations are made for the charged TGC measurements in single-, two- and three-parameter fits.

At centre-of-mass energies exceeding twice the Z boson mass, pair production of Z bosons is

kinematically allowed. Here, one searches for the possible existence of triple vertices involving only neutral electroweak gauge bosons. Such vertices could also contribute to  $Z\gamma$  production. In contrast to triple gauge boson vertices with two charged gauge bosons, purely neutral gauge boson vertices do not occur in the Standard Model of electroweak interactions.

Within the Standard Model, quartic electroweak gauge boson vertices with at least two charged gauge bosons exist. In  $e^+e^-$  collisions at LEP-II centre-of-mass energies, the  $WWZ\gamma$  and  $WW\gamma\gamma$  vertices contribute to  $WW\gamma$  and  $\nu\bar{\nu}\gamma\gamma$  production in  $s$ -channel and  $t$ -channel, respectively. The effect of the Standard Model quartic electroweak vertices is below the sensitivity of LEP-II. Quartic gauge boson vertices with only neutral bosons, like the  $ZZ\gamma\gamma$  vertex, do not exist in the Standard Model. However, anomalous QGCs associated with this vertex are studied at LEP.

Anomalous quartic vertices are searched for in the production of  $WW\gamma$ ,  $\nu\bar{\nu}\gamma\gamma$  and  $Z\gamma\gamma$  final states. The couplings related to the  $ZZ\gamma\gamma$  and  $WW\gamma\gamma$  vertices are assumed to be different [186], and are therefore treated separately. In this report, we only combine the results for the anomalous couplings associated with the  $ZZ\gamma\gamma$  vertex. The combination of the  $WW\gamma\gamma$  vertex couplings is foreseen for the near future.

### 11.1.1 Charged Triple Gauge Boson Couplings

The parametrisation of the charged triple gauge boson vertices is described in References [176, 187–192]. The most general Lorentz invariant Lagrangian which describes the triple gauge boson interaction has fourteen independent complex couplings, seven describing the  $WW\gamma$  vertex and seven describing the  $WWZ$  vertex. Assuming electromagnetic gauge invariance as well as C and P conservation, the number of independent TGCs reduces to five. A common set is  $\{g_1^Z, \kappa_Z, \kappa_\gamma, \lambda_Z, \lambda_\gamma\}$  where  $g_1^Z = \kappa_Z = \kappa_\gamma = 1$  and  $\lambda_Z = \lambda_\gamma = 0$  in the Standard Model. The parameters proposed in [176] and used by the LEP experiments are  $g_1^Z$ ,  $\lambda_\gamma$  and  $\kappa_\gamma$  with the gauge constraints:

$$\kappa_Z = g_1^Z - (\kappa_\gamma - 1) \tan^2 \theta_W, \quad (11.1)$$

$$\lambda_Z = \lambda_\gamma, \quad (11.2)$$

where  $\theta_W$  is the weak mixing angle. The couplings are considered as real, with the imaginary parts fixed to zero. In contrast to previous LEP combinations [179, 193], we are now quoting the measured coupling values themselves and not their deviation from the Standard Model.

Note that the photonic couplings  $\lambda_\gamma$  and  $\kappa_\gamma$  are related to the magnetic and electric properties of the W-boson. One can write the lowest order terms for a multipole expansion describing the W- $\gamma$  interaction as a function of  $\lambda_\gamma$  and  $\kappa_\gamma$ . For the magnetic dipole moment  $\mu_W$  and the electric quadrupole moment  $q_W$  one obtains  $e(1 + \kappa_\gamma + \lambda_\gamma)/2m_W$  and  $-e(\kappa_\gamma - \lambda_\gamma)/m_W^2$ , respectively.

The inclusion of  $O(\alpha_{em})$  corrections in the Monte Carlo calculations has a considerable effect on the charged TGC measurement. Both the total cross-section and the differential distributions are affected. The cross-section is reduced by 1-2% (depending on the energy). Amongst the differential distributions, the effects are naturally more complex. The polar  $W^-$  production angle carries most of the information on the TGC parameters; its shape is modified to be more forwardly peaked. In a fit to data, the  $O(\alpha_{em})$  effect manifests itself as a negative shift of the obtained TGC values with a magnitude of typically -0.015 for  $\lambda_\gamma$  and  $g_1^Z$  and -0.04 for  $\kappa_\gamma$ .

### 11.1.2 Neutral Triple Gauge Boson Couplings

There are two classes of Lorentz invariant structures associated with neutral TGC vertices which preserve  $U(1)_{em}$  and Bose symmetry, as described in [188, 194].

The first class refers to anomalous  $Z\gamma\gamma^*$  and  $Z\gamma Z^*$  couplings which are accessible at LEP in the process  $e^+e^- \rightarrow Z\gamma$ . The parametrisation contains eight couplings:  $h_i^V$  with  $i = 1, \dots, 4$  and  $V = \gamma, Z$ . The superscript  $\gamma$  refers to  $Z\gamma\gamma^*$  couplings and superscript  $Z$  refers to  $Z\gamma Z^*$  couplings. The photon and the  $Z$  boson in the final state are considered as on-shell particles, while the third boson at the vertex, the  $s$ -channel internal propagator, is off shell. The couplings  $h_1^V$  and  $h_2^V$  are CP-odd while  $h_3^V$  and  $h_4^V$  are CP-even.

The second class refers to anomalous  $ZZ\gamma^*$  and  $ZZZ^*$  couplings which are accessible at LEP-II in the process  $e^+e^- \rightarrow ZZ$ . This anomalous vertex is parametrised in terms of four couplings:  $f_i^V$  with  $i = 4, 5$  and  $V = \gamma, Z$ . The superscript  $\gamma$  refers to  $ZZ\gamma^*$  couplings and the superscript  $Z$  refers to  $ZZZ^*$  couplings, respectively. Both  $Z$  bosons in the final state are assumed to be on-shell, while the third boson at the triple vertex, the  $s$ -channel internal propagator, is off-shell. The couplings  $f_4^V$  are CP-odd whereas  $f_5^V$  are CP-even.

The  $h_i^V$  and  $f_i^V$  couplings are assumed to be real and they vanish at tree level in the Standard Model.

### 11.1.3 Quartic Gauge Boson Couplings

The couplings associated with the two QGC vertices  $WW\gamma\gamma$  and  $ZZ\gamma\gamma$  are assumed to be different, and are by convention treated as separate couplings at LEP. In this report, we only combine QGCs related to the  $ZZ\gamma\gamma$  vertex. The contribution of such anomalous quartic gauge boson couplings is described by two coupling parameters  $a_c/\Lambda^2$  and  $a_0/\Lambda^2$ , which are zero in the Standard Model [195, 196]. Events from  $\nu\bar{\nu}\gamma\gamma$  and  $Z\gamma\gamma$  final states can originate from the  $ZZ\gamma\gamma$  vertex and are therefore used to study anomalous QGCs.

## 11.2 Measurements

The combined results presented here are obtained from charged and neutral electroweak gauge boson coupling measurements, and from quartic gauge boson couplings measurements as discussed above. The individual references should be consulted for details about the data samples used.

The charged TGC analyses of ALEPH, DELPHI, L3 and OPAL use data collected at LEP-II up to centre-of-mass energies of 209 GeV. These analyses use different channels, typically the semileptonic and fully hadronic  $W$ -pair decays [182–185]. The full data set is analysed by ALEPH and OPAL, whereas DELPHI presently uses all data at 189 GeV and above; L3 at this stage uses data from the semileptonic channel only. Anomalous TGCs affect both the total production cross-section and the shape of the differential cross-section as a function of the polar  $W^-$  production angle. The relative contributions of each helicity state of the  $W$  bosons are also changed, which in turn affects the distributions of their decay products. The analyses presented by each experiment make use of different combinations of each of these quantities. In general, however, all analyses use at least the expected variations of the total production cross-section and the  $W^-$  production angle. Results from  $e\nu W$  and

$\nu\bar{\nu}\gamma$  production are included by some experiments. Single  $W$  production is particularly sensitive to  $\kappa_\gamma$ , thus providing information complementary to that from  $W$ -pair production.

The  $h$ -coupling analyses of ALEPH, DELPHI and L3 use data collected up to centre-of-mass energies of 209 GeV. The OPAL measurements so far use the data at 189 GeV. The results of the  $f$ -couplings are now obtained from the whole data set above the  $ZZ$ -production threshold by all of the experiments. The experiments already pre-combine different processes and final states for each of the couplings. For the neutral TGCs, the analyses use measurements of the total cross sections of  $Z\gamma$  and  $ZZ$  production and the differential distributions: the  $h_i^V$  couplings [197–200] and the  $f_i^V$  couplings [197, 198, 201, 202] are determined.

The combination of quartic gauge boson couplings associated with the  $ZZ\gamma\gamma$  vertex is at present based on analyses of L3 [203] and OPAL [204]. The L3 analysis uses data from the  $q\bar{q}\gamma\gamma$  final state at centre-of-mass energies of 205 GeV and 207 GeV. OPAL analyses the  $\nu\bar{\nu}\gamma\gamma$  final state at centre-of-mass energies ranging from 189 GeV to 209 GeV.

### 11.3 Combination Procedure

The combination is based on the individual likelihood functions from the four LEP experiments. Each experiment provides the negative log likelihood,  $\log \mathcal{L}$ , as a function of the coupling parameters to be combined. The single-parameter analyses are performed fixing all other parameters to their Standard Model values. The two-parameter analyses are performed setting the remaining parameters to their Standard Model values. For the charged TGCs, the gauge constraints listed in Section 11.1.1 are always enforced.

The  $\log \mathcal{L}$  functions from each experiment include statistical as well as those systematic uncertainties which are considered as uncorrelated between experiments. For both single- and multi-parameter combinations, the individual  $\log \mathcal{L}$  functions are combined. It is necessary to use the  $\log \mathcal{L}$  functions directly in the combination, since in some cases they are not parabolic, and hence it is not possible to properly combine the results by simply taking weighted averages of the measurements.

The main contributions to the systematic uncertainties that are uncorrelated between experiments arise from detector effects, background in the selected signal samples, limited Monte Carlo statistics and the fitting method. Their importance varies for each experiment and the individual references should be consulted for details.

In the neutral TGC sector, the systematic uncertainties arising from the theoretical cross section prediction in  $Z\gamma$ -production ( $\simeq 1\%$  in the  $q\bar{q}\gamma$ - and  $\simeq 2\%$  in the  $\nu\bar{\nu}\gamma$  channel) are treated as correlated. For  $ZZ$  production, the uncertainty on the theoretical cross section prediction is small compared to the statistical accuracy and therefore is neglected. Smaller sources of correlated systematic uncertainties, such as those arising from the LEP beam energy, are for simplicity treated as uncorrelated.

The combination procedure for neutral TGCs, where the relative systematic uncertainties are small, is unchanged with respect to the previous LEP combinations of electroweak gauge boson couplings [179, 193]. The correlated systematic uncertainties in the  $h$ -coupling analyses are taken into account by scaling the combined log-likelihood functions by the squared ratio of the sum of statistical and uncorrelated systematic uncertainty over the total uncertainty including all correlated uncertainties. For the general case of non-Gaussian probability density functions, this treatment of the correlated errors is only an approximation; it also neglects correlations in the systematic uncertainties between the parameters in multi-parameter analyses.

In the charged TGC sector, systematic uncertainties considered correlated between the experiments are the theoretical cross section prediction (0.5% for W-pair production and 5% for single W production), hadronisation effects, the final state interactions, namely Bose-Einstein correlations and colour reconnection, and the uncertainty in the radiative corrections themselves. The latter is by convention presently taken to be the difference between Monte Carlo samples with and without the  $O(\alpha_{em})$  corrections respectively, as a reliable and applicable estimate of this uncertainty is still under study. This conservative approach makes the radiative correction uncertainty by far the dominant contribution.

In case of the charged TGCs, the systematic uncertainties considered correlated between the experiments amount to roughly 70% of the combined statistical and uncorrelated uncertainties for  $\lambda_\gamma$  and  $g_1^Z$ , while for  $\kappa_\gamma$  their contribution is equal. This means the measurement of  $\lambda_\gamma$  and  $g_1^Z$  is limited by statistics, whereas the precision in the  $\kappa_\gamma$  measurement is limited by statistical and systematic uncertainties at the same level. An improved combination procedure [205] is used for the charged TGCs. This procedure allows the combination of statistical and correlated systematic uncertainties, independently of the analysis method chosen by the individual experiments.

The combination of charged TGCs uses the likelihood curves and correlated systematic errors submitted by each of the four experiments. The procedure is based on the introduction of an additional free parameter to take into account the systematic uncertainties, which are treated as shifts on the fitted TGC value, and are assumed to have a Gaussian distribution. A simultaneous minimisation of both parameters (TGC and systematic error) is performed to the log-likelihood function.

In detail, the combination proceeds in the following way: the set of measurements from the LEP experiments ALEPH, DELPHI, OPAL and L3 is given with statistical plus uncorrelated systematic uncertainties in terms of likelihood curves:  $-\log \mathcal{L}_{stat}^A(x)$ ,  $-\log \mathcal{L}_{stat}^D(x)$ ,  $-\log \mathcal{L}_{stat}^L(x)$  and  $-\log \mathcal{L}_{stat}^O(x)$ , respectively, where  $x$  is the coupling parameter in question. Also given are the shifts for each of the five totally correlated sources of uncertainty mentioned above; each source  $S$  is leading to systematic errors  $\sigma_A^S$ ,  $\sigma_D^S$ ,  $\sigma_L^S$  and  $\sigma_O^S$ .

Additional parameters  $\Delta^S$  are included in order to take into account a Gaussian distribution for each of the systematic uncertainties. The procedure then consists in minimising the function:

$$-\log \mathcal{L}_{total} = \sum_{E=A,D,L,O} \log \mathcal{L}_{stat}^E(x - \sum_{S=DPA,\sigma_{WW},HAD,BE,CR} (\sigma_E^S \Delta^S)) + \sum_S \frac{(\Delta^S)^2}{2} \quad (11.3)$$

where  $x$  and  $\Delta_S$  are the free parameters, and the sums run over the four experiments and the five systematic errors. The resulting uncertainty on  $x$  will take into account all sources of uncertainty, yielding a measurement of the coupling with the error representing statistical and systematic sources. The projection of the minima of the log-likelihood as a function of  $x$  gives the combined log-likelihood curve including statistical and systematic uncertainties. The advantage over the scaling method used previously is that it treats systematic uncertainties that are correlated between the experiments correctly, while not forcing the averaging of these systematic uncertainties into one global LEP systematics scaling factor. In other words, the (statistical) precision of each experiment now gets reduced by its own correlated systematic errors, instead of an averaged LEP systematic error. The method has been cross-checked against the scaling method, and was found to give comparable results. The inclusion of the systematic uncertainties lead to small differences as expected by the improved treatment of correlated systematic errors, a similar behaviour as seen in Monte Carlo comparisons of these two combinations methods [206]. Furthermore, it was shown that the minimisation-based combination method used for the charged TGCs agrees with the method based on optimal observables, where systematic effects are included directly in the mean values of the optimal observables (see [206]), for any

realistic ratio of statistical and systematic uncertainties. Further details on the improved combination method can be found in [205].

In the combination of the QGCs, the influence of correlated systematic uncertainties is considered negligible compared to the statistical error, arising from the small number of selected events. Therefore, the QGCs are combined by adding the log-likelihood curves from the single experiments.

For all single- and multi-parameter results quoted in numerical form, the one standard deviation uncertainties (68% confidence level) are obtained by taking the coupling values for which  $\Delta \log \mathcal{L} = +0.5$  above the minimum. The 95% confidence level (C.L.) limits are given by the coupling values for which  $\Delta \log \mathcal{L} = +1.92$  above the minimum. Note that in the case of the neutral TGCs, double minima structures appear in the negative log-likelihood curves. For multi-parameter analyses, the two dimensional 68% C.L. contour curves for any pair of couplings are obtained by requiring  $\Delta \log \mathcal{L} = +1.15$ , while for the 95% C.L. contour curves  $\Delta \log \mathcal{L} = +3.0$  is required. Since the results on the different parameters and parameter sets are obtained from the same data sets, they cannot be combined.

## 11.4 Results

We present results from the four LEP experiments on the various electroweak gauge boson couplings, and their combination. The combined charged TGC results including  $O(\alpha_{em})$  corrections are available for the first time in two- and three-parameter fits; the single-parameter combination has been updated with the inclusion of recent results from ALEPH and OPAL [185]. The neutral TGC results remain unchanged since our last note [179]. The results quoted for each individual experiment are calculated using the methods described in Section 11.3. Therefore they may differ slightly from those reported in the individual references, as the experiments in general use other methods to combine the data from different channels, and to include systematic uncertainties. In particular for the charged couplings, experiments using a combination method based on optimal observables (ALEPH, OPAL) obtain results with small differences compared to the values given by our combination technique. These small differences have been studied in Monte Carlo tests and are well understood [206]. For the  $h$ -coupling result from OPAL and DELPHI, a slightly modified estimate of the systematic uncertainty due to the theoretical cross section prediction is responsible for slightly different limits compared to the published results.

### 11.4.1 Charged Triple Gauge Boson Couplings

The individual analyses and results of the experiments for the charged couplings are described in [182–185].

#### Single-Parameter Analyses

The results of single-parameter fits from each experiment are shown in Table 11.1, where the errors include both statistical and systematic effects. The individual  $\log \mathcal{L}$  curves and their sum are shown in Figure 11.1. The results of the combination are given in Table 11.2. A list of the systematic errors treated as fully correlated between the LEP experiments, and their shift on the combined fit result are given in Table 11.3.



## Two-Parameter Analyses

The results of two-parameter fits from the experiments participating in the combination are shown in Table 11.4, where the errors include both statistical and systematic effects. Contours at 68% and 95% confidence level for the combined fits are shown in Figure 11.2. The numerical results of the combination are given in Table 11.5.

## Three-Parameter Analysis

The results of the three-parameter fit from the experiments participating in the combination are shown in Table 11.6, where the errors include both statistical and systematic effects. Contours at 68% and 95% confidence level for the combined fit are shown in Figure 11.3. The numerical results of the combination are given in Table 11.7.

Parameter	ALEPH	DELPHI	L3	OPAL
$g_1^Z$	$1.022^{+0.033}_{-0.033}$	$1.002^{+0.041}_{-0.043}$	$0.952^{+0.053}_{-0.048}$	$0.987^{+0.037}_{-0.036}$
$\kappa_\gamma$	$0.967^{+0.091}_{-0.088}$	$0.966^{+0.106}_{-0.106}$	$0.892^{+0.099}_{-0.095}$	$0.925^{+0.087}_{-0.082}$
$\lambda_\gamma$	$0.010^{+0.034}_{-0.034}$	$0.013^{+0.048}_{-0.045}$	$-0.030^{+0.057}_{-0.054}$	$-0.065^{+0.036}_{-0.035}$

Table 11.1: The measured central values and one standard deviation errors obtained by the four LEP experiments. In each case the parameter listed is varied while the remaining two are fixed to their Standard Model values. Both statistical and systematic errors are included. The values given here differ slightly from the ones quoted in the individual contributions from the four LEP experiments, as a different combination method is used. See text in section 11.3 for details.

Parameter	68% C.L.	95% C.L.
$g_1^Z$	$0.998^{+0.023}_{-0.025}$	[0.951, 1.043]
$\kappa_\gamma$	$0.943 \pm 0.055$	[0.835, 1.052]
$\lambda_\gamma$	$-0.020 \pm 0.024$	[-0.067, 0.028]

Table 11.2: The combined 68% C.L. errors and 95% C.L. intervals obtained combining the results from the four LEP experiments. In each case the parameter listed is varied while the other two are fixed to their Standard Model values. Both statistical and systematic errors are included.

Source	$g_1^Z$	$\lambda_\gamma$	$\kappa_\gamma$
$O(\alpha_{em})$ correction	0.015	0.015	0.039
$\sigma_{WW}$ prediction	0.003	0.005	0.014
Hadronisation	0.004	0.002	0.004
Bose-Einstein Correlation	0.005	0.004	0.009
Colour Reconnection	0.005	0.004	0.010
$\sigma_{singleW}$ prediction	-	-	0.011

Table 11.3: The systematic uncertainties considered correlated between the LEP experiments in the charged TGC combination and their effect on the combined fit results.

Parameter	DELPHI [183]	L3 [184]	OPAL [185]
$g_1^Z$	$1.012^{+0.041}_{-0.045}$	$0.973^{+0.056}_{-0.059}$	$1.016^{+0.038}_{-0.042}$
$\kappa_\gamma$	$0.968^{+0.107}_{-0.107}$	$0.909^{+0.107}_{-0.102}$	$0.928^{+0.091}_{-0.084}$
$g_1^Z$	$1.000^{+0.044}_{-0.103}$	$0.838^{+0.090}_{-0.064}$	$1.076^{+0.045}_{-0.046}$
$\lambda_\gamma$	$0.013^{+0.115}_{-0.050}$	$0.121^{+0.076}_{-0.104}$	$-0.124^{+0.047}_{-0.040}$
$\kappa_\gamma$	$0.968^{+0.101}_{-0.101}$	$0.897^{+0.095}_{-0.098}$	$1.000^{+0.125}_{-0.082}$
$\lambda_\gamma$	$0.009^{+0.045}_{-0.042}$	$-0.008^{+0.095}_{-0.098}$	$-0.062^{+0.033}_{-0.046}$

Table 11.4: The measured central values and one standard deviation errors obtained by the three individual LEP experiments participating in the two-parameter combinations of the charged TGC parameters. The listed parameters are varied while the remaining one is fixed to its Standard Model value. Both statistical and systematic errors are included.

Parameter	68% C.L.	95% C.L.	Correlations
$g_1^Z$	$1.005^{+0.028}_{-0.025}$	[+0.952, +1.059]	1.00 +0.02
$\kappa_\gamma$	$0.933^{+0.061}_{-0.060}$	[+0.814, +1.058]	+0.02 1.00
$g_1^Z$	$1.029^{+0.038}_{-0.037}$	[+0.954, +1.102]	1.00 -0.47
$\lambda_\gamma$	$-0.071^{+0.038}_{-0.038}$	[-0.142, -0.002]	-0.47 1.00
$\kappa_\gamma$	$0.953^{+0.064}_{-0.058}$	[+0.836, +1.087]	1.00 +0.25
$\lambda_\gamma$	$-0.024^{+0.027}_{-0.029}$	[-0.083, +0.029]	+0.25 1.00

Table 11.5: The measured central values, one standard deviation errors and limits at 95% confidence level, obtained by combining DELPHI, L3 and OPAL for the two-parameter fits of the charged TGC parameters. Since the shape of the log-likelihood is not parabolic, there is some ambiguity in the definition of the correlation coefficients and the values quoted here are approximate. The listed parameters are varied while the remaining one is fixed to its Standard Model value. Both statistical and systematic errors are included.

Parameter	DELPHI [183]	L3 [184]	OPAL [185]
$g_1^Z$	$0.983^{+0.061}_{-0.069}$	$0.938^{+0.101}_{-0.167}$	$1.091^{+0.045}_{-0.040}$
$\kappa_\gamma$	$0.923^{+0.138}_{-0.124}$	$0.907^{+0.243}_{-0.101}$	$0.976^{+0.082}_{-0.080}$
$\lambda_\gamma$	$0.038^{+0.073}_{-0.066}$	$0.054^{+0.137}_{-0.109}$	$-0.124^{+0.038}_{-0.049}$

Table 11.6: The measured central values and one standard deviation errors obtained by the three individual LEP experiments participating in the three-parameter charged TGC combination. Both statistical and systematic errors are included.

Parameter	68% C.L.	95% C.L.	Correlations		
$g_1^Z$	$1.051^{+0.031}_{-0.032}$	$[-0.985, +1.114]$	1.00	+0.23	-0.30
$\kappa_\gamma$	$0.933^{+0.061}_{-0.059}$	$[-0.819, +1.060]$	+0.23	1.00	-0.27
$\lambda_\gamma$	$-0.067^{+0.036}_{-0.038}$	$[-0.140, +0.003]$	-0.30	-0.27	1.00

Table 11.7: The measured central values, one standard deviation errors and limits at 95% confidence level, obtained by combining DELPHI, L3 and OPAL for the three-parameter charged TGC combination. Since the shape of the log-likelihood is not parabolic, there is some ambiguity in the definition of the correlation coefficients and the values quoted here are approximate. Both statistical and systematic errors are included.

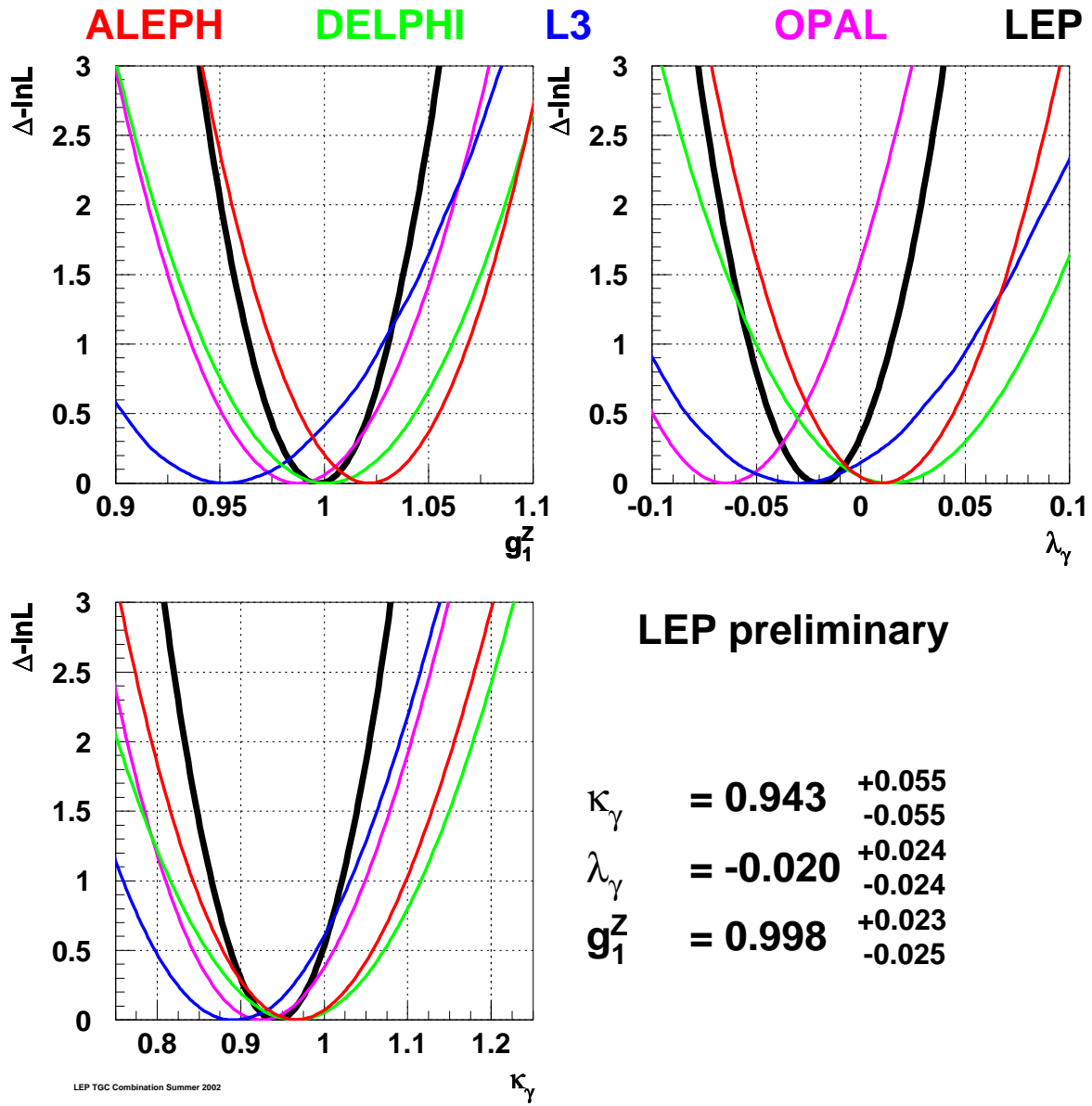


Figure 11.1: The  $\log \mathcal{L}$  curves of the four experiments (thin lines) and the LEP combined curve (thick line) for the three charged TGCs  $g_1^Z$ ,  $\kappa_\gamma$  and  $\lambda_\gamma$ . In each case, the minimal value is subtracted.

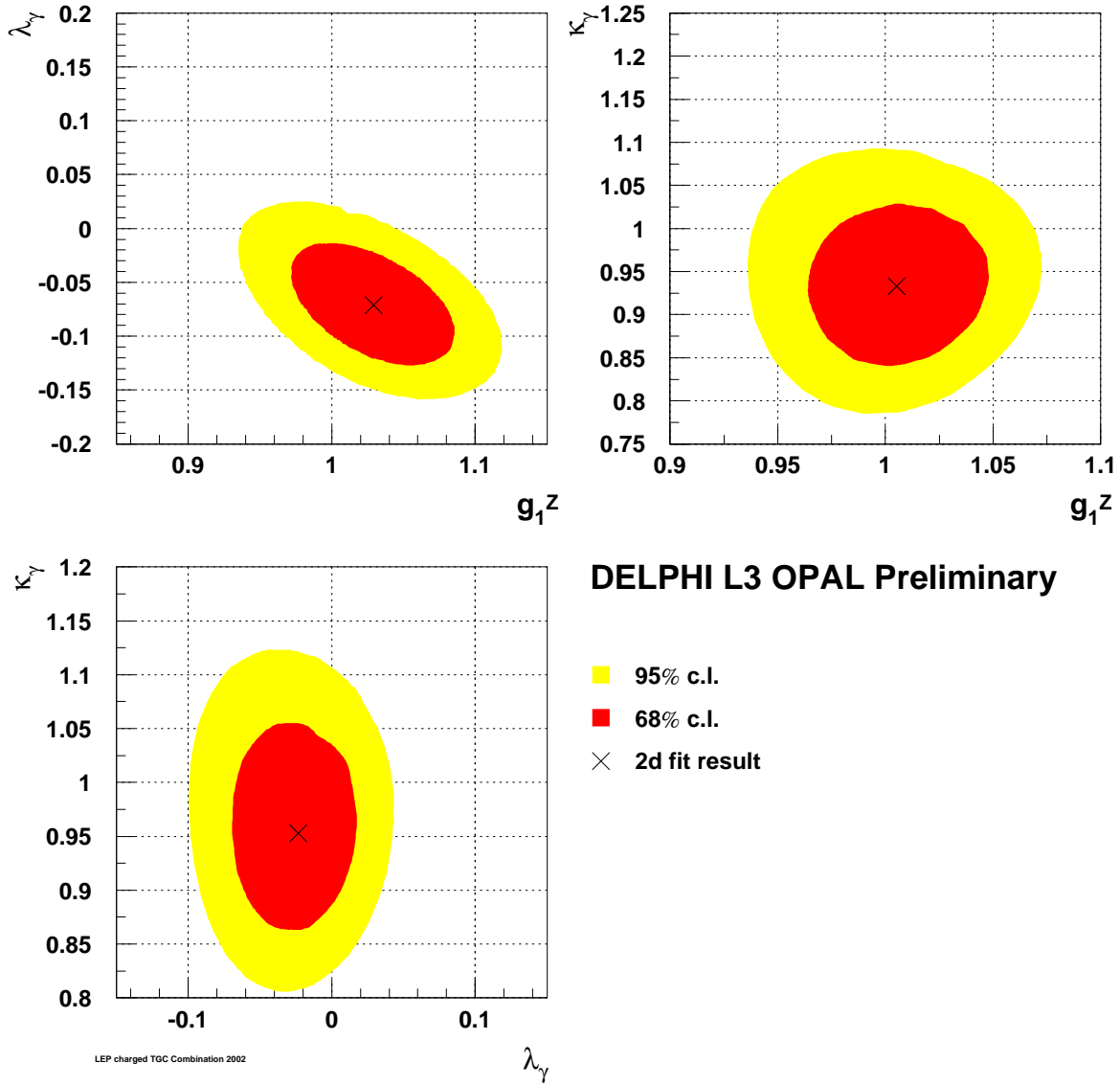


Figure 11.2: The 68% and 95% confidence level contours for the three two-parameter fits to the charged TGCs  $g_1^Z$ - $\lambda_\gamma$ ,  $g_1^Z$ - $\kappa_\gamma$  and  $\lambda_\gamma$ - $\kappa_\gamma$ . The fitted coupling value is indicated with a cross; the Standard Model value for each fit is in the centre of the grid. The contours include the contribution from systematic uncertainties, and data from DELPHI, L3 and OPAL.

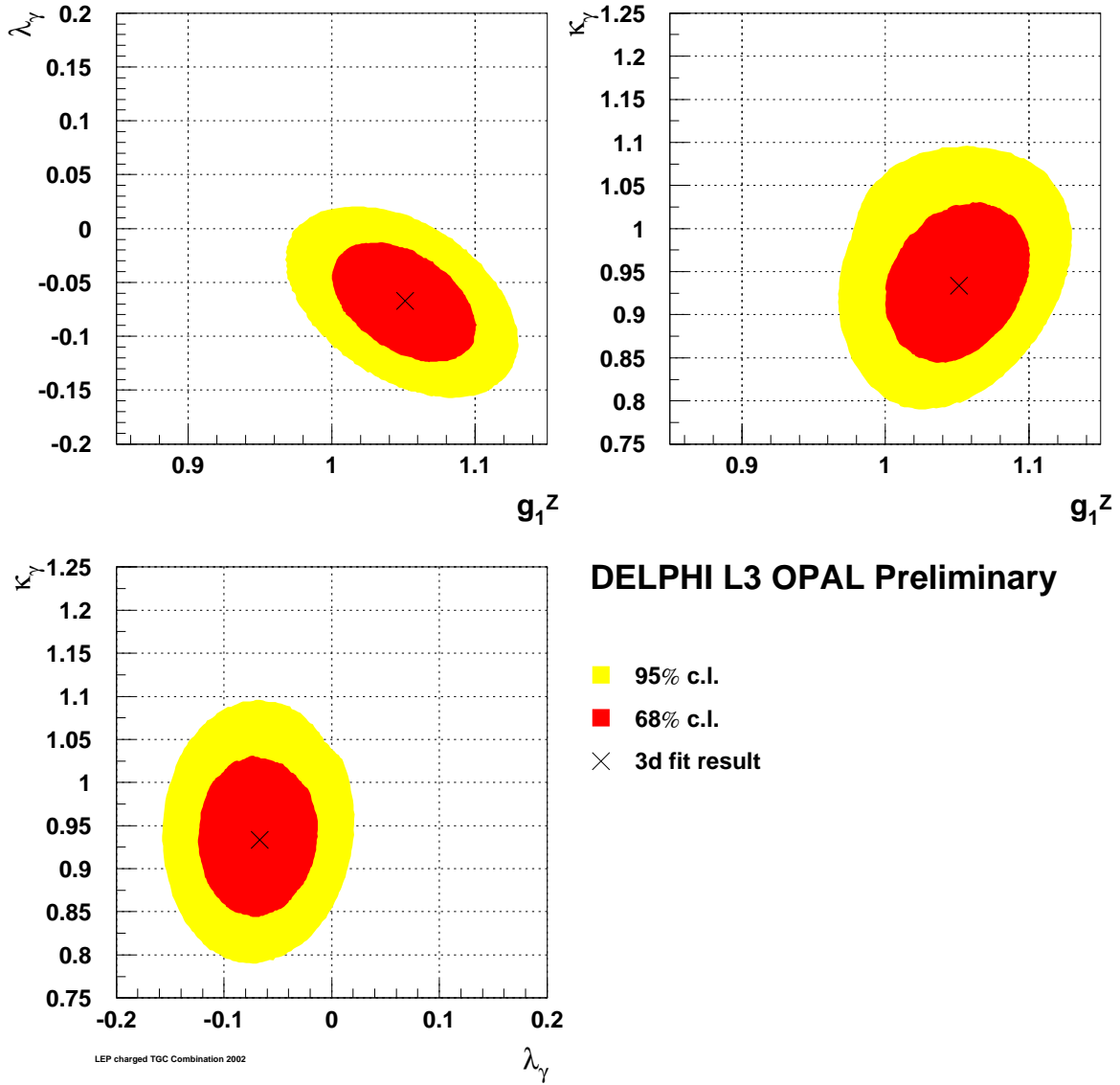


Figure 11.3: The result of the three-parameter fit, plotted in the two-dimensional planes of the three TGC pairs, with the third TGC parameter at the fitted value. In each plane, the respective 68% and 95% two-parameter confidence level contours are shown. The fitted coupling value is indicated with a cross; the Standard Model value for each fit is in the centre of the grid. The contours include the contribution from systematic uncertainties, and data from DELPHI, L3 and OPAL.

### 11.4.2 Neutral Triple Gauge Boson Couplings in $Z\gamma$ Production

The individual analyses and results of the experiments for the  $h$ -couplings are described in [197–200].

#### Single-Parameter Analyses

The results for each experiment are shown in Table 11.8, where the errors include both statistical and systematic uncertainties. The individual  $\log \mathcal{L}$  curves and their sum are shown in Figures 11.4 and 11.5. The results of the combination are given in Table 11.9. From Figures 11.4 and 11.5 it is clear that the sensitivity of the L3 analysis [199] is the highest amongst the LEP experiments. This is partially due to the use of a larger phase space region, which increases the statistics by about a factor two, and partially due to additional information from using an optimal-observable technique.

#### Two-Parameter Analyses

The results for each experiment are shown in Table 11.10, where the errors include both statistical and systematic uncertainties. The 68% C.L. and 95% C.L. contour curves resulting from the combinations of the two-dimensional likelihood curves are shown in Figure 11.6. The LEP average values are given in Table 11.11.

Parameter	ALEPH	DELPHI	L3	OPAL
$h_1^\gamma$	[−0.14, +0.14]	[−0.15, +0.15]	[−0.06, +0.06]	[−0.13, +0.13]
$h_2^\gamma$	[−0.07, +0.07]	[−0.09, +0.09]	[−0.053, +0.024]	[−0.089, +0.089]
$h_3^\gamma$	[−0.069, +0.037]	[−0.047, +0.047]	[−0.062, −0.014]	[−0.16, +0.00]
$h_4^\gamma$	[−0.020, +0.045]	[−0.032, +0.030]	[−0.004, +0.045]	[+0.01, +0.13]
$h_1^Z$	[−0.23, +0.23]	[−0.24, +0.25]	[−0.17, +0.16]	[−0.22, +0.22]
$h_2^Z$	[−0.12, +0.12]	[−0.14, +0.14]	[−0.10, +0.09]	[−0.15, +0.15]
$h_3^Z$	[−0.28, +0.19]	[−0.32, +0.18]	[−0.23, +0.11]	[−0.29, +0.14]
$h_4^Z$	[−0.10, +0.15]	[−0.12, +0.18]	[−0.08, +0.16]	[−0.09, +0.19]

Table 11.8: The 95% C.L. intervals ( $\Delta \log \mathcal{L} = 1.92$ ) measured by the ALEPH, DELPHI, L3 and OPAL. In each case the parameter listed is varied while the remaining ones are fixed to their Standard Model values. Both statistical and systematic uncertainties are included.

Parameter	95% C.L.
$h_1^\gamma$	$[-0.056, +0.055]$
$h_2^\gamma$	$[-0.045, +0.025]$
$h_3^\gamma$	$[-0.049, -0.008]$
$h_4^\gamma$	$[-0.002, +0.034]$
$h_1^Z$	$[-0.13, +0.13]$
$h_2^Z$	$[-0.078, +0.071]$
$h_3^Z$	$[-0.20, +0.07]$
$h_4^Z$	$[-0.05, +0.12]$

Table 11.9: The 95% C.L. intervals ( $\Delta \log \mathcal{L} = 1.92$ ) obtained combining the results from the four experiments. In each case the parameter listed is varied while the remaining ones are fixed to their Standard Model values. Both statistical and systematic uncertainties are included.

Parameter	ALEPH	DELPHI	L3
$h_1^\gamma$	$[-0.32, +0.32]$	$[-0.28, +0.28]$	$[-0.17, +0.04]$
$h_2^\gamma$	$[-0.18, +0.18]$	$[-0.17, +0.18]$	$[-0.12, +0.02]$
$h_3^\gamma$	$[-0.17, +0.38]$	$[-0.48, +0.20]$	$[-0.09, +0.13]$
$h_4^\gamma$	$[-0.08, +0.29]$	$[-0.08, +0.15]$	$[-0.04, +0.11]$
$h_1^Z$	$[-0.54, +0.54]$	$[-0.45, +0.46]$	$[-0.48, +0.33]$
$h_2^Z$	$[-0.29, +0.30]$	$[-0.29, +0.29]$	$[-0.30, +0.22]$
$h_3^Z$	$[-0.58, +0.52]$	$[-0.57, +0.38]$	$[-0.43, +0.39]$
$h_4^Z$	$[-0.29, +0.31]$	$[-0.31, +0.28]$	$[-0.23, +0.28]$

Table 11.10: The 95% C.L. intervals ( $\Delta \log \mathcal{L} = 1.92$ ) measured by ALEPH, DELPHI and L3. In each case the two parameters listed are varied while the remaining ones are fixed to their Standard Model values. Both statistical and systematic uncertainties are included.



Parameter	95% C.L.	Correlations	
$h_1^\gamma$	$[-0.16, +0.05]$	1.00	+0.79
$h_2^\gamma$	$[-0.11, +0.02]$	+0.79	1.00
$h_3^\gamma$	$[-0.08, +0.14]$	1.00	+0.97
$h_4^\gamma$	$[-0.04, +0.11]$	+0.97	1.00
$h_1^Z$	$[-0.35, +0.28]$	1.00	+0.77
$h_2^Z$	$[-0.21, +0.17]$	+0.77	1.00
$h_3^Z$	$[-0.37, +0.29]$	1.00	+0.76
$h_4^Z$	$[-0.19, +0.21]$	+0.76	1.00

Table 11.11: The 95% C.L. intervals ( $\Delta \log \mathcal{L} = 1.92$ ) obtained combining the results from ALEPH, DELPHI and L3. In each case the two parameters listed are varied while the remaining ones are fixed to their Standard Model values. Both statistical and systematic uncertainties are included. Since the shape of the log-likelihood is not parabolic, there is some ambiguity in the definition of the correlation coefficients and the values quoted here are approximate.

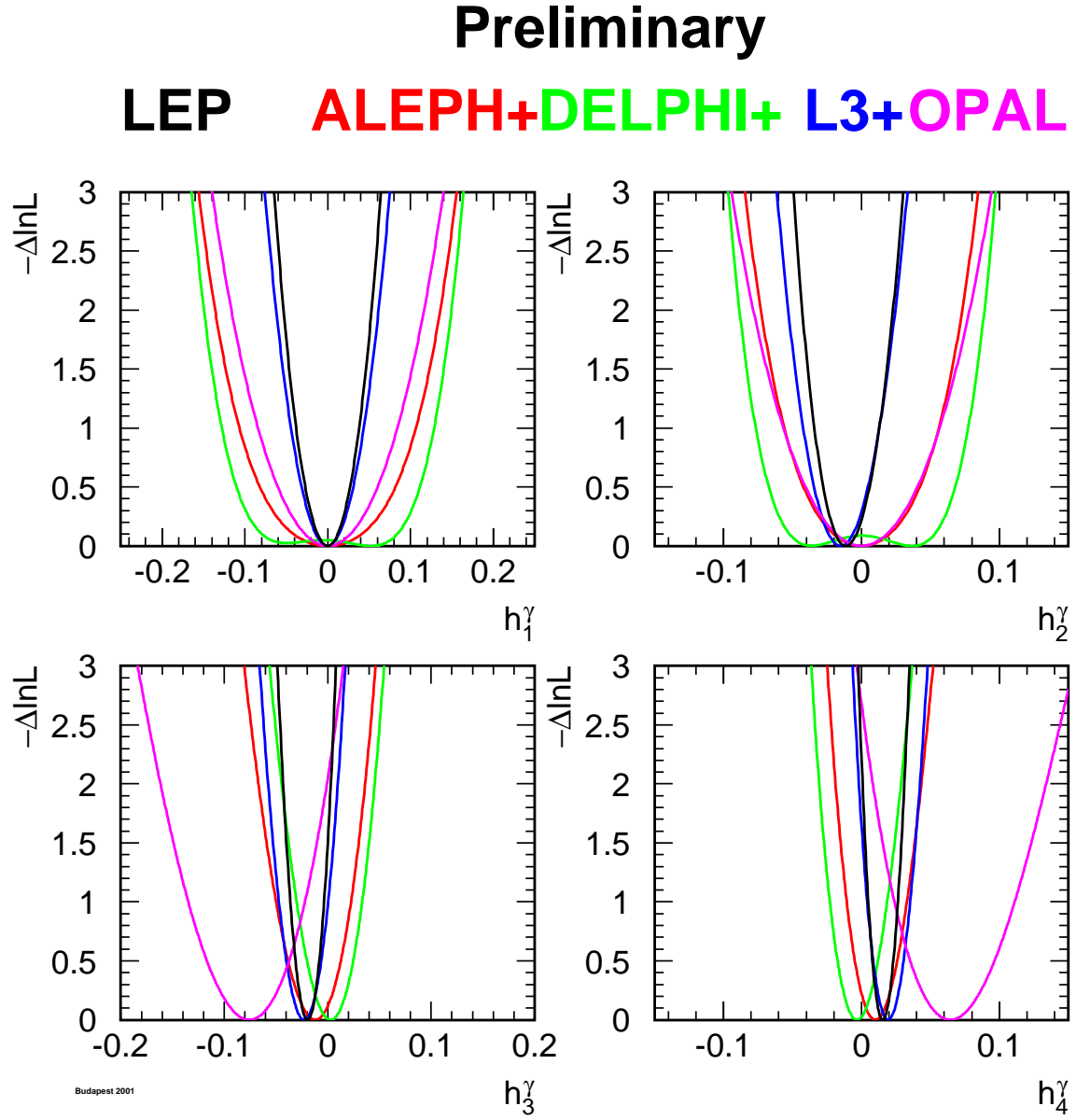


Figure 11.4: The  $\log \mathcal{L}$  curves of the four experiments, and the LEP combined curve for the four neutral TGCs  $h_i^\gamma$ ,  $i = 1, 2, 3, 4$ . In each case, the minimal value is subtracted.

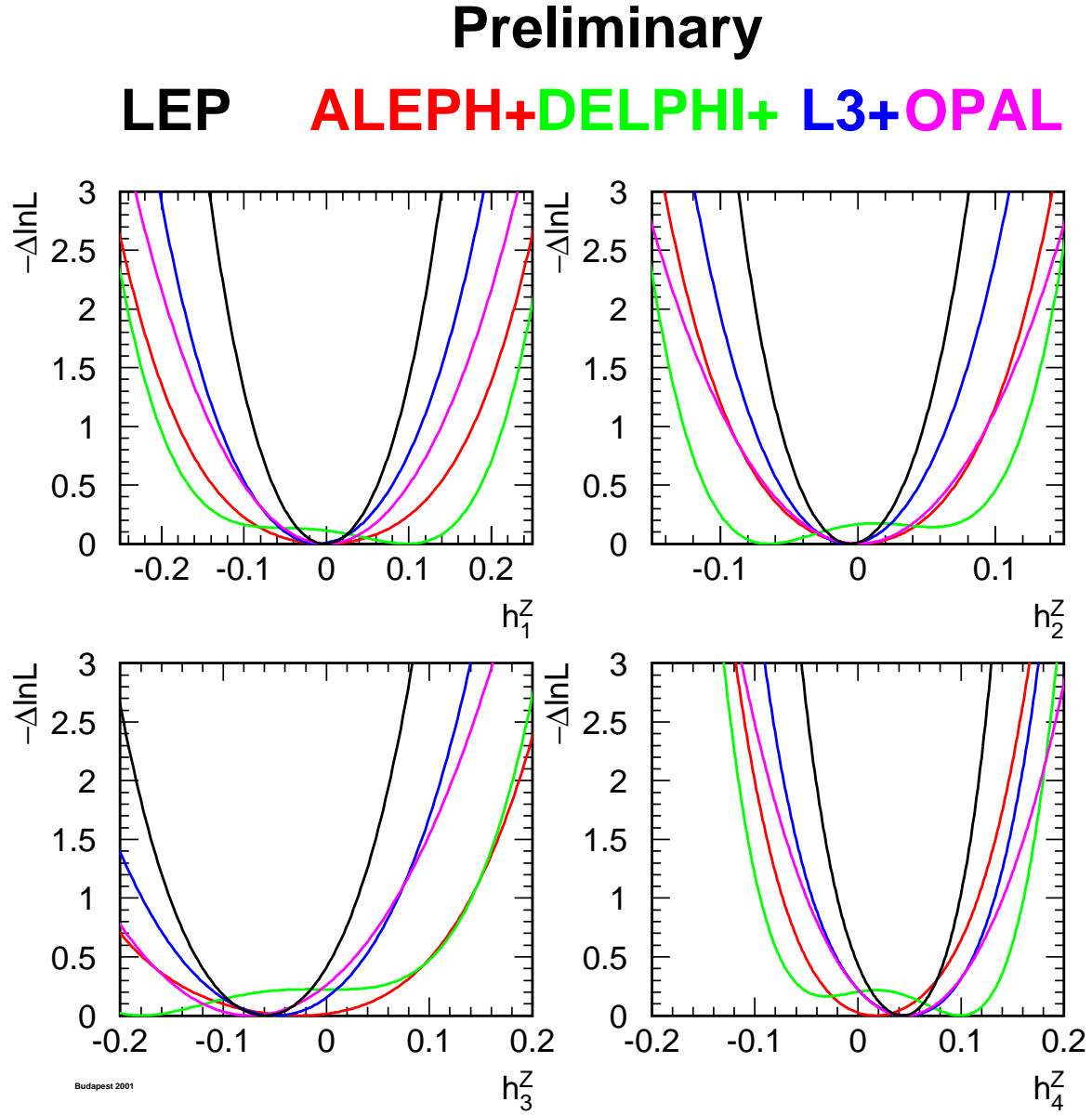


Figure 11.5: The  $\log \mathcal{L}$  curves of the four experiments, and the LEP combined curve for the four neutral TGCs  $h_i^Z$ ,  $i = 1, 2, 3, 4$ . In each case, the minimal value is subtracted.

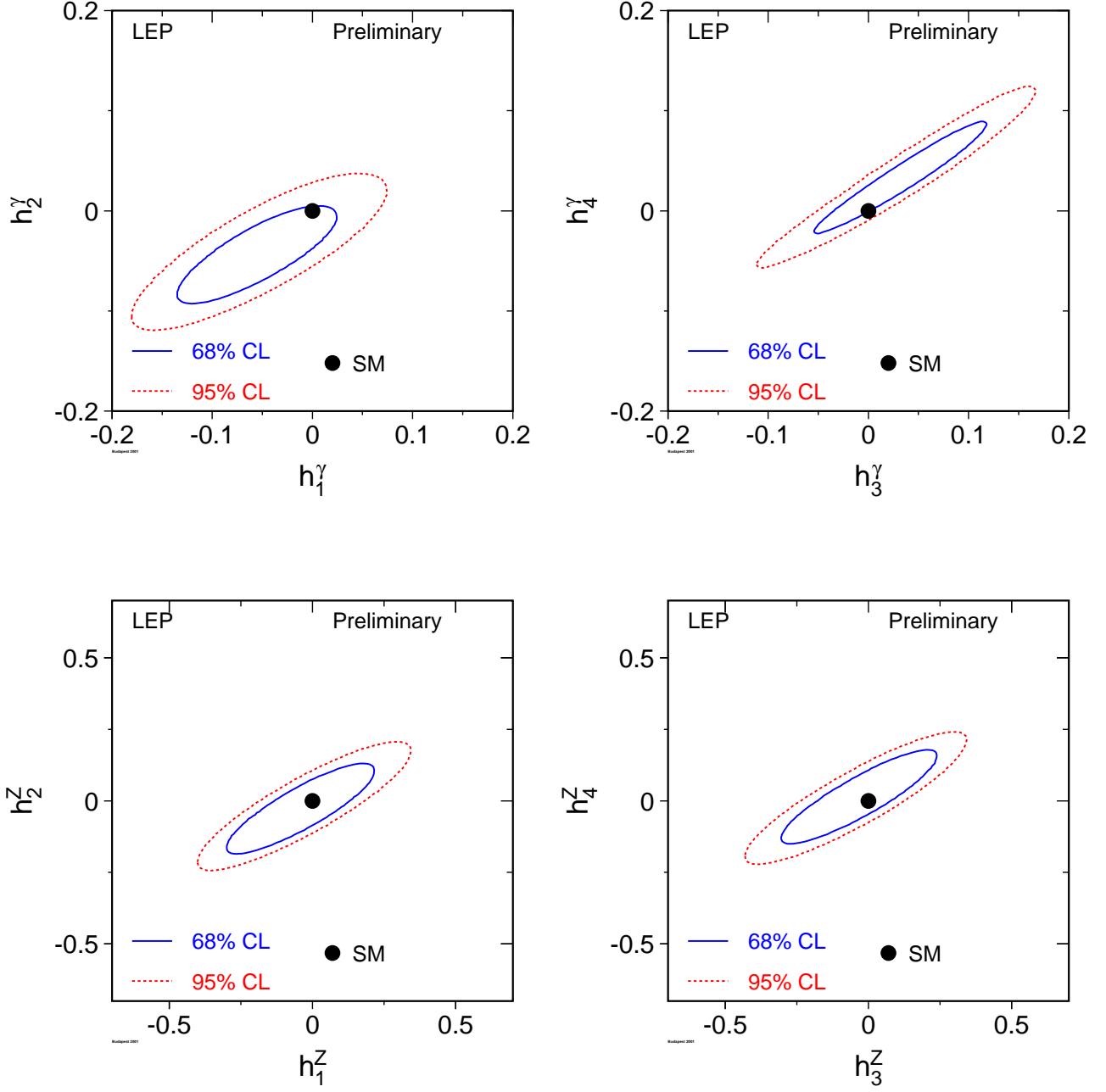


Figure 11.6: Contour curves of 68% C.L. and 95% C.L. in the planes  $(h_1^\gamma, h_2^\gamma)$ ,  $(h_3^\gamma, h_4^\gamma)$ ,  $(h_1^Z, h_2^Z)$  and  $(h_3^Z, h_4^Z)$  showing the LEP combined result.

### 11.4.3 Neutral Triple Gauge Boson Couplings in ZZ Production

The individual analyses and results of the experiments for the  $f$ -couplings are described in [197, 198, 201, 202].

#### Single-Parameter Analyses

The results for each experiment are shown in Table 11.12, where the errors include both statistical and systematic uncertainties. The individual  $\log \mathcal{L}$  curves and their sum are shown in Figure 11.7. The results of the combination are given in Table 11.13.

#### Two-Parameter Analyses

The results from each experiment are shown in Table 11.14, where the errors include both statistical and systematic uncertainties. The 68% C.L. and 95% C.L. contour curves resulting from the combinations of the two-dimensional likelihood curves are shown in Figure 11.8. The LEP average values are given in Table 11.15.

Parameter	ALEPH	DELPHI	L3	OPAL
$f_4^\gamma$	$[-0.26, +0.26]$	$[-0.26, +0.28]$	$[-0.24, +0.26]$	$[-0.36, +0.36]$
$f_4^Z$	$[-0.44, +0.43]$	$[-0.49, +0.42]$	$[-0.43, +0.41]$	$[-0.55, +0.64]$
$f_5^\gamma$	$[-0.54, +0.56]$	$[-0.48, +0.61]$	$[-0.48, +0.56]$	$[-0.82, +0.72]$
$f_5^Z$	$[-0.73, +0.83]$	$[-0.42, +0.69]$	$[-0.46, +1.2]$	$[-0.96, +0.31]$

Table 11.12: The 95% C.L. intervals ( $\Delta \log \mathcal{L} = 1.92$ ) measured by ALEPH, DELPHI, L3 and OPAL. In each case the parameter listed is varied while the remaining ones are fixed to their Standard Model values. Both statistical and systematic uncertainties are included.

Parameter	95% C.L.
$f_4^\gamma$	$[-0.17, +0.19]$
$f_4^Z$	$[-0.31, +0.28]$
$f_5^\gamma$	$[-0.36, +0.40]$
$f_5^Z$	$[-0.36, +0.39]$

Table 11.13: The 95% C.L. intervals ( $\Delta \log \mathcal{L} = 1.92$ ) obtained combining the results from all four experiments. In each case the parameter listed is varied while the remaining ones are fixed to their Standard Model values. Both statistical and systematic uncertainties are included.

Parameter	ALEPH	DELPHI	L3	OPAL
$f_4^\gamma$	$[-0.26, +0.26]$	$[-0.26, +0.28]$	$[-0.24, +0.26]$	$[-0.36, +0.36]$
$f_4^Z$	$[-0.44, +0.43]$	$[-0.49, +0.42]$	$[-0.43, +0.41]$	$[-0.54, +0.63]$
$f_5^\gamma$	$[-0.52, +0.53]$	$[-0.52, +0.61]$	$[-0.48, +0.56]$	$[-0.77, +0.73]$
$f_5^Z$	$[-0.77, +0.86]$	$[-0.44, +0.69]$	$[-0.46, +1.2]$	$[-0.96, +0.44]$

Table 11.14: The 95% C.L. intervals ( $\Delta \log \mathcal{L} = 1.92$ ) measured by ALEPH, DELPHI, L3 and OPAL. In each case the two parameters listed are varied while the remaining ones are fixed to their Standard Model values. Both statistical and systematic uncertainties are included.

Parameter	95% C.L.	Correlations
$f_4^\gamma$	$[-0.17, +0.19]$	1.00   +0.10
$f_4^Z$	$[-0.30, +0.28]$	+0.10   1.00
$f_5^\gamma$	$[-0.34, +0.38]$	1.00   -0.18
$f_5^Z$	$[-0.36, +0.38]$	-0.18   1.00

Table 11.15: The 95% C.L. intervals ( $\Delta \log \mathcal{L} = 1.92$ ) obtained combining the results from all four experiments. In each case the two parameters listed are varied while the remaining ones are fixed to their Standard Model values. Both statistical and systematic uncertainties are included. Since the shape of the log-likelihood is not parabolic, there is some ambiguity in the definition of the correlation coefficients and the values quoted here are approximate.

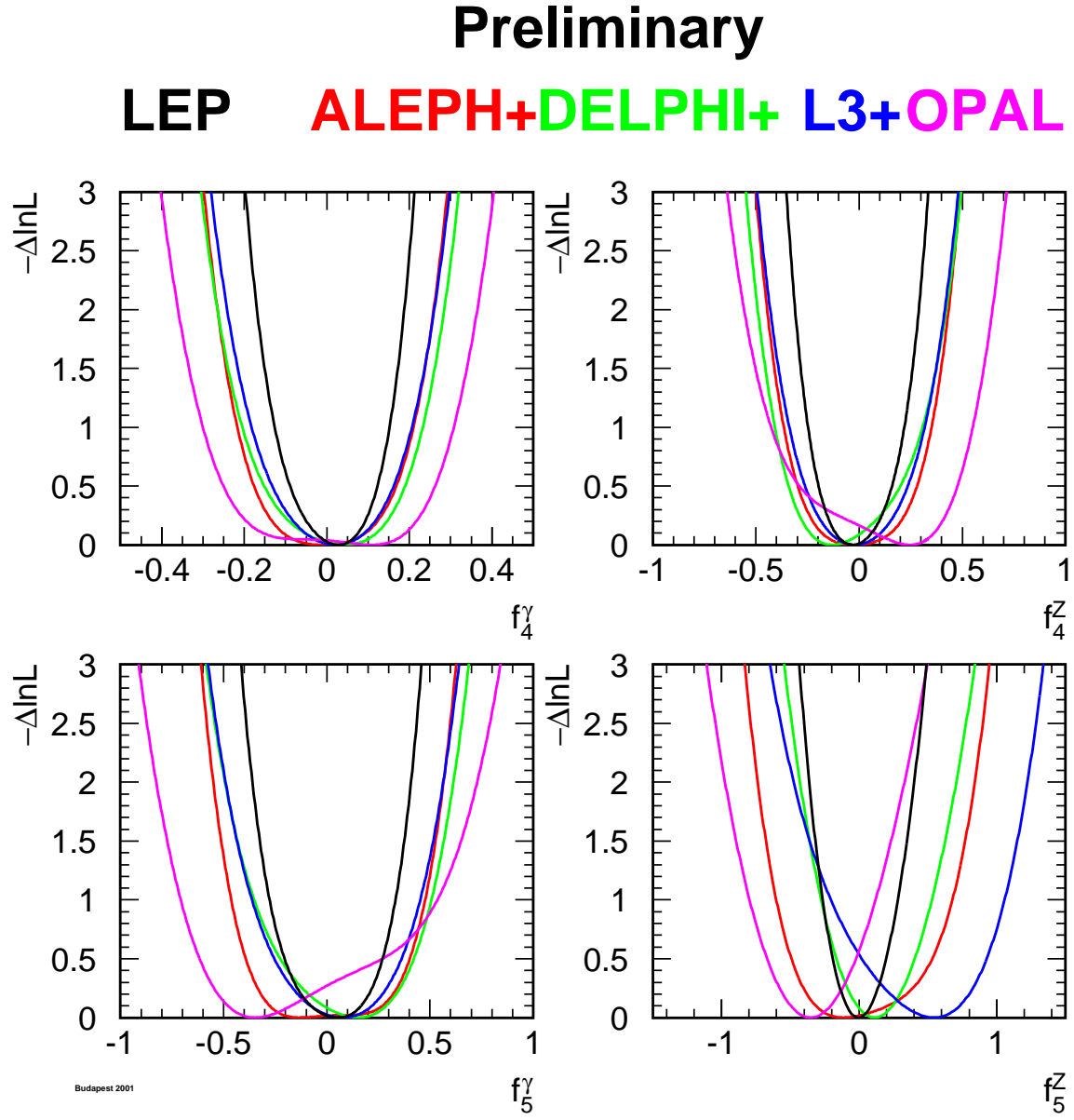


Figure 11.7: The  $\log \mathcal{L}$  curves of the four experiments, and the LEP combined curve for the four neutral TGCs  $f_i^V$ ,  $V = \gamma, Z$ ,  $i = 4, 5$ . In each case, the minimal value is subtracted.

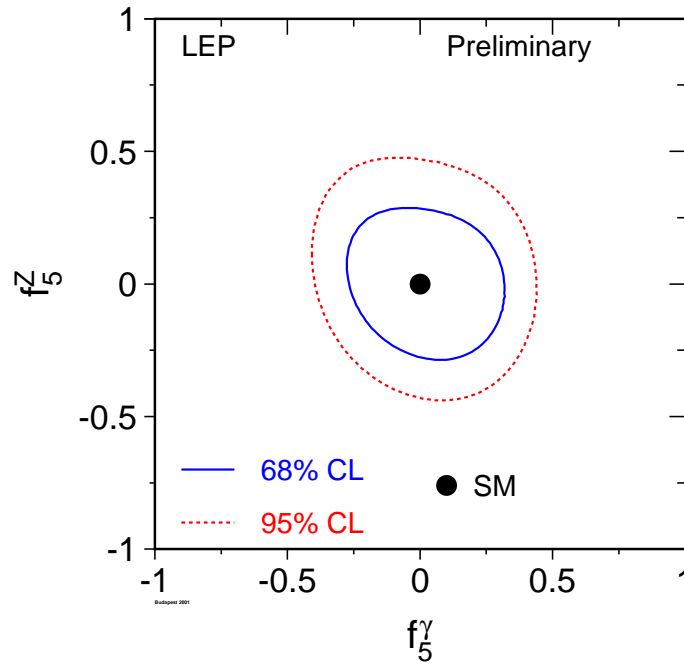
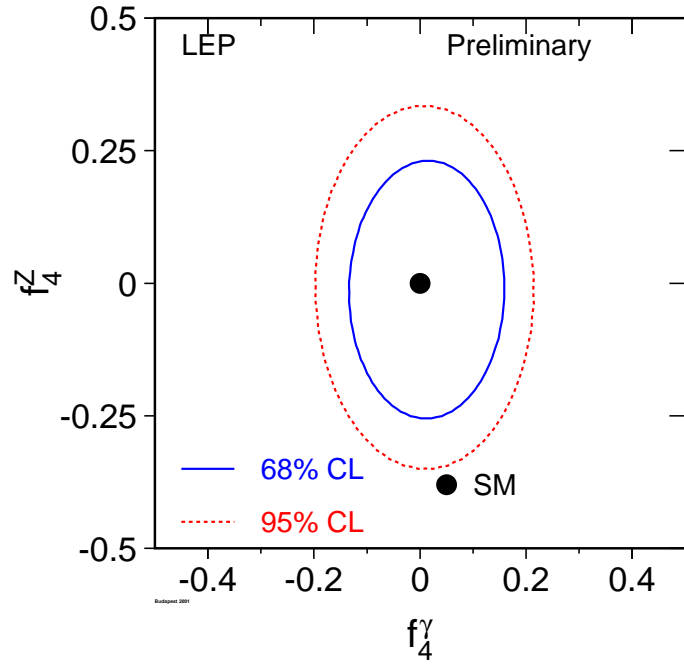


Figure 11.8: Contour curves of 68% C.L. and 95% C.L. in the plane  $(f_4^\gamma, f_4^Z)$  and  $(f_5^\gamma, f_5^Z)$  showing the LEP combined result.



#### 11.4.4 Quartic Gauge Boson Couplings

The individual numerical results from the experiments participating in the combination, and the combined result are shown in Table 11.16. The corresponding  $\log \mathcal{L}$  curves are shown in Figure 11.9. The errors include both statistical and systematic uncertainties.

Parameter	L3	OPAL	Combined
$a_c/\Lambda^2$	$[-0.037, +0.054]$	$[-0.045, +0.050]$	$[-0.033, +0.046]$
$a_0/\Lambda^2$	$[-0.014, +0.027]$	$[-0.012, +0.031]$	$[-0.009, +0.026]$

Table 11.16: The limits for the QGCs  $a_c/\Lambda^2$  and  $a_0/\Lambda^2$  associated with the  $ZZ\gamma\gamma$  vertex at 95% confidence level for L3 and OPAL, and the LEP result obtained by combining L3 and OPAL. Both statistical and systematic errors are included.

## Conclusions

Combinations of charged and neutral triple gauge boson couplings, as well as quartic gauge boson couplings associated with the  $ZZ\gamma\gamma$  vertex were made, based on results from the four LEP experiments ALEPH, DELPHI, L3 and OPAL. No significant deviation from the Standard Model prediction is seen for any of the electroweak gauge boson couplings studied. With the LEP-combined charged TGC results, the existence of triple gauge boson couplings among the electroweak gauge bosons is experimentally verified. As an example, these data allow the Kaluza-Klein theory [207], in which  $\kappa_\gamma = -2$ , to be excluded completely [208].

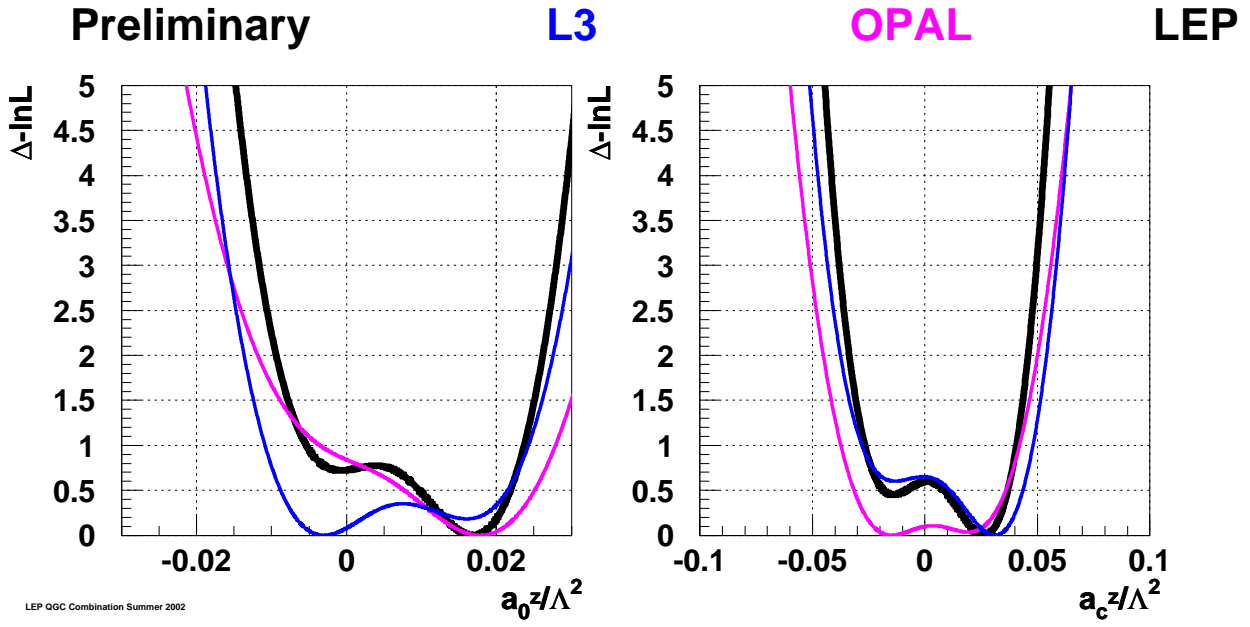


Figure 11.9: The  $\log \mathcal{L}$  curves of L3 and OPAL (thin lines) and the combined curve (thick line) for the QGCs  $a_c/\Lambda^2$  and  $a_0/\Lambda^2$ , associated with the  $ZZ\gamma\gamma$  vertex. In each case, the minimal value is subtracted.

# Chapter 12

## Colour Reconnection in W-Pair Events

**Updates with respect to summer 2002:**

Unchanged w.r.t. summer 2002: Results are preliminary.

### 12.1 Introduction

In  $W^+W^- \rightarrow q\bar{q}q\bar{q}$  events, the products of the two (colour singlet)  $W$  decays in general have a significant space-time overlap as the separation of their decay vertices,  $\tau_W \sim 1/\Gamma_W \approx 0.1$  fm, is small compared to characteristic hadronic distance scales of  $\sim 1$  fm. Colour reconnection, also known as colour rearrangement (CR), was first introduced in [209] and refers to a reorganisation of the colour flow between the two  $W$  bosons. A precedent is set for such effects by colour suppressed  $B$  meson decays, *e.g.*  $B \rightarrow J/\psi K$ , where there is “cross-talk” between the two original colour singlets,  $\bar{c}+s$  and  $c+\text{spectator}$  [209, 210].

QCD interference effects between the colour singlets in  $W^+W^-$  decays during the perturbative phase are expected to be small, affecting the  $W$  mass by  $\sim (\frac{\alpha_s}{\pi N_{\text{colours}}})^2 \Gamma_W \sim \mathcal{O}(1 \text{ MeV})$  [210]. In contrast, non-perturbative effects involving soft gluons with energies less than  $\Gamma_W$  may be significant, with effects on  $m_W \sim \mathcal{O}(10 \text{ MeV})$ . To estimate the impact of this phenomenon a variety of phenomenological models have been developed [210–215], some of which are compared with data in this note.

Many observables have been considered in the search for an experimental signature of colour reconnection. The inclusive properties of events such as the mean charged particle multiplicity, distributions of thrust, rapidity, transverse momentum and  $\ln(1/x_p)$  are found to have limited sensitivity [216–219]. The effects of CR are predicted to be numerically larger in these observables when only higher mass hadrons such as kaons and protons are considered [220]. However, experimental investigations [217, 221] find no significant gain in sensitivity due to the low production rate of such species in  $W$  decays and the finite size of the data sample.

More recently, in analogy with the “string effect” analysis in 3-jet  $e^+e^- \rightarrow q\bar{q}g$  events [222], the so-called “particle flow” method [223–225] has been investigated by all LEP collaborations [226–229]. In this, pairs of jets in  $W^+W^- \rightarrow q\bar{q}q\bar{q}$  events are associated with the decay of a  $W$ , after which four jet-jet regions are chosen: two corresponding to jets sharing the same  $W$  parent (intra- $W$ ), and two in which the parents differ (inter- $W$ ). As there is a two-fold ambiguity in the assignment of inter- $W$  regions, the configuration having the smaller sum of inter- $W$  angles is chosen.

Particles are projected onto the planes defined by these jet pairs and the particle density constructed as a function of  $\phi$ , the projected angle relative to one jet in each plane. To account for the variation in the opening angles,  $\phi_0$ , of the jet-jet pairs defining each plane, the particle densities in  $\phi$  are constructed as functions of normalised angles,  $\phi_r = \phi/\phi_0$ , by a simple rescaling of the projected angles for each particle, event by event. Particles having projected angles  $\phi$  smaller than  $\phi_0$  in at least one of the four planes are considered further. This gives particle densities,  $\frac{1}{N_{\text{event}}} \frac{dn}{d\phi_r}$ , in four regions with  $\phi_r$  in the range 0–1, and where  $n$  and  $N_{\text{event}}$  are the number of particles and events, respectively.

As particle density reflects the colour flow in an event, CR models predict a change in the relative particle densities between inter-W and intra-W regions. On average, colour reconnection is expected to affect the particle densities of both inter-W regions in the same way and so they are added together, as are the two intra-W regions. The observable used to quantify such changes,  $R_N$ , is defined:

$$R_N = \frac{\frac{1}{N_{\text{event}}} \int_{0.2}^{0.8} \frac{dn}{d\phi_r} (\text{intra} - \text{W}) d\phi_r}{\frac{1}{N_{\text{event}}} \int_{0.2}^{0.8} \frac{dn}{d\phi_r} (\text{inter} - \text{W}) d\phi_r}. \quad (12.1)$$

As the effects of CR are expected to be enhanced for low momentum particles far from the jet axis, the range of integration excludes jet cores ( $\phi_r \approx 0$  and  $\phi_r \approx 1$ ). The precise upper and lower limits are optimised by model studies of predicted sensitivity.

Each LEP experiment has developed its own variation on this analysis, differing primarily in the selection of  $W^+W^- \rightarrow q\bar{q}q\bar{q}$  events. In L3 [228] and DELPHI [227], events are selected in a very particular configuration (“topological selection”) by imposing restrictions on the jet-jet angles and on the jet resolution parameter for the three- to four-jet transition (Durham or LUCUS schemes). This selects events which are more planar than those in the inclusive  $W^+W^- \rightarrow q\bar{q}q\bar{q}$  sample and the association between jet pairs and W’s is given by the relative angular separation of the jets. The overall efficiency for selecting events is  $\sim 15\%$ . The ALEPH [226] and OPAL [229] event selections are based on their W mass analyses. Assignment of pairs of jets to W’s also follows that used in measuring  $m_W$ , using either a 4-jet matrix element [230] or a multivariate algorithm [231]. These latter selections have much higher efficiencies, varying from 45% to 90%, but lead to samples of events having a less planar topology and hence a more complicated colour flow. ALEPH also uses the topological selection for consistency checks.

The data are corrected bin-by-bin for background contamination in the inter-W and intra-W regions separately. The possibility of CR effects existing in background processes, such as  $ZZ \rightarrow q\bar{q}q\bar{q}$ , is neglected. Since the data are not corrected for the effects of event selection, momentum resolution and finite acceptance, the values of  $R_N$  measured by the experiments cannot be compared directly with one another. However, it is possible to perform a relative comparison by using a common sample of Monte Carlo events, processed using the detector simulation program of each experiment.

## 12.2 Combination Procedure

The measured values of  $R_N$  can be compared after they have been normalised using a common sample of events, processed using the detector simulation and particle flow analysis of each experiment. A variable,  $r$ , is constructed:

$$r = \frac{R_N^{\text{data}}}{R_N^{\text{no-CR}}}, \quad (12.2)$$

where  $R_N^{\text{data}}$  and  $R_N^{\text{no-CR}}$  are the values of  $R_N$  measured by each experiment in data and in a common sample of events without CR. In the absence of CR, all experiments should find  $r$  consistent with unity. The default no-CR sample used for this normalisation consists of  $e^+e^- \rightarrow W^+W^-$  events produced using the KORALW [232] event generator and hadronised using either the JETSET [64], ARIADNE [233] or HERWIG [212] model depending on the colour reconnection model being tested. Input from experiments used to perform the combination is given in terms of  $R_N$  and detailed in Appendix D.1.

### 12.2.1 Weights

The statistical precision of  $R_N$  measured by the experiments does not reflect directly the sensitivity to CR, for example the measurements of ALEPH and OPAL have efficiencies several times larger than the topological selections of L3 and DELPHI, yet only yield comparable sensitivity. The relative sensitivity of the experiments may also be model dependent. Therefore, results are averaged using model dependent weights, *i.e.*

$$w_i = \frac{(R_N^i - R_N^{i,\text{no-CR}})^2}{\sigma_{R_N}^2(\text{stat.}) + \sigma_{R_N}^2(\text{syst.})}, \quad (12.3)$$

where  $R_N^i$  and  $R_N^{i,\text{no-CR}}$  represent the  $R_N$  values for CR model  $i$  and its corresponding no-CR scenario, and  $\sigma_{R_N}^2$  are the total statistical and systematic uncertainties. To test models,  $R_N$  values using common samples are provided by experiments for each of the following models:

1. SK-I, 100% reconnected (KORALW + JETSET),
2. ARIADNE-II, inter-W reconnection rate about 22% (KORALW + ARIADNE),
3. HERWIG CR, reconnected fraction  $\frac{1}{9}$  (KORALW + HERWIG).

Samples in parentheses are the corresponding no-CR scenarios used to define  $w_i$ . In each case, KORALW is used to generate the events at least up to the four-fermion level. These special Monte Carlo samples (called “Cetraro” samples) have been generated with the ALEPH tuned parameters, obtained with hadronic Z decays, and have been processed through the detector simulation of each experiment.

### 12.2.2 Combination of centre-of-mass energies

The common files required to perform the combination are only available at a single centre-of-mass energy ( $E_{\text{cm}}$ ) of 188.6 GeV. The data from the experiments can only therefore be combined at this energy. The procedure adopted to combine all LEP data is summarised below.

$R_N$  is measured in each experiment at each centre-of-mass energy, in both data and Monte Carlo. The predicted variation of  $R_N$  with centre-of-mass energy is determined separately by each experiment using its own samples of simulated  $e^+e^- \rightarrow W^+W^-$  events, with hadronisation performed using the no-CR JETSET model. This variation is parametrised by fitting a polynomial to these simulated  $R_N$ . The  $R_N$  measured in data are subsequently extrapolated to the reference energy of 189 GeV using this function, and the weighted average of the rescaled values in each experiment is used as input to the combination.

## 12.3 Systematics

The sources of potential systematic uncertainty identified are separated into those which are correlated between experiments and those which are not. For correlated sources, the component correlated between all experiments is assigned as the smallest uncertainty found in any single experiment, with the quadrature remainder treated as an uncorrelated contribution. Preliminary estimates of the dominant systematics on  $R_N$  are given in Appendix D.1 for each experiment, and described below.

### 12.3.1 Hadronisation

This is assigned by comparison of the single sample of  $W^+W^-$  events generated using KORALW, and hadronised with three different models, *i.e.* JETSET, HERWIG and ARIADNE. The systematic is assigned as the spread of the  $R_N$  values obtained when using the various models given in Appendix D.1. This is treated as a correlated uncertainty.

### 12.3.2 Bose-Einstein Correlations

Although a recent analysis by DELPHI reports the observation of inter- $W$  Bose-Einstein correlation (BEC) in  $W^+W^- \rightarrow q\bar{q}q\bar{q}$  events with a significance of 2.8 standard deviations for like-sign pairs and 2.4 standard deviations for unlike-sign pairs [234], analyses by other collaborations [235–237] find no significant evidence for such effects, see also chapter 13. Therefore, BEC effects are only considered within each  $W$  separately. The estimated uncertainty is assigned, using common MC samples, as the difference in  $R_N$  between an intra- $W$  BEC sample and the corresponding no-BEC sample. This is treated as correlated between experiments.

### 12.3.3 Background

Background is dominated by the  $e^+e^- \rightarrow q\bar{q}$  process, with a smaller contribution from  $ZZ \rightarrow q\bar{q}q\bar{q}$  diagrams. As no common background samples exist, apart from dedicated ones for BEC analyses, experiment specific samples are used. The uncertainty is defined as the difference in the  $R_N$  value relative to that obtained using the default background model and assumed cross-sections in each experiment.

$$e^+e^- \rightarrow q\bar{q}$$

The systematic is separated into two components, one accounting for the shape of the background, the other for the uncertainty in the value of the background cross-section,  $\sigma(e^+e^- \rightarrow q\bar{q})$ .

Uncertainty in the shape is estimated by comparing hadronisation models. Experiments typically have large samples simulated using 2-fermion event generators hadronised with various models. This uncertainty is assigned as  $\pm \frac{1}{2}$  of the largest difference between any pair of hadronisation models and treated as uncorrelated between experiments.

The second uncertainty arises due to the accuracy of the experimentally measured cross-sections. The systematic is assigned as the larger of the deviations in  $R_N$  caused when  $\sigma(e^+e^- \rightarrow q\bar{q})$  is varied

by  $\pm 10\%$  from its default value. This variation was based on the conclusions of a study comparing four-jet data with models [238], and is significantly larger than the  $\sim 1\%$  uncertainty in the inclusive  $e^+e^- \rightarrow q\bar{q}$  ( $\sqrt{s'}/s > 0.85$ ) cross-section measured by the LEP2 2-fermion group. It is treated as correlated between experiments.

$$ZZ \rightarrow q\bar{q}q\bar{q}$$

Similarly to the  $e^+e^- \rightarrow q\bar{q}$  case, this background cross-section is varied by  $\pm 15\%$ . For comparison, the uncertainty on  $\sigma(ZZ)$  measured by the LEP2 4-fermion group is  $\sim 11\%$  at  $\sqrt{s} \simeq 189$  GeV. It is treated as correlated between experiments.

$$W^+W^- \rightarrow q\bar{q}\ell\nu_\ell$$

Semi-leptonic WW decays which are incorrectly identified as  $W^+W^- \rightarrow q\bar{q}q\bar{q}$  events are the third main category of background, and its contribution is very small. The fraction of  $W^+W^- \rightarrow q\bar{q}\ell\nu_\ell$  events present in the sample used for the particle flow analysis varies in the range 0.04–2.2% between the experiments. The uncertainty in this background consists of hadronisation effects and also uncertainty in the cross-section. As this source is a very small background relative to those discussed above, and the effect of either varying the cross-section by its measured uncertainty or of changing the hadronisation model do not change the measured  $R_N$  significantly, this source is neglected.

### 12.3.4 Detector Effects

The data are not corrected for the effects of finite resolution or acceptance. Various studies have been carried out, e.g. by analysing  $W^+W^- \rightarrow q\bar{q}\ell\nu_\ell$  events in the same way as  $W^+W^- \rightarrow q\bar{q}q\bar{q}$  events in order to validate the method and the choice of energy flow objects used to measure the particle yields between jets [228]. To take into account the effects of detector resolution and acceptance, ALEPH, L3 and OPAL have studied the impact of changing the object definition entering the particle flow distributions and have assigned a systematic error from the difference in the measured  $R_N$ .

### 12.3.5 Centre-of-mass energy dependence

As there may be model dependence in the parametrised energy dependence, the second order polynomial used to perform the extrapolation to the reference energy of 189 GeV is usually determined using several different models, with and without colour reconnection. DELPHI, L3 and OPAL use differences relative to the default no-CR model to assign a systematic uncertainty while ALEPH takes the spread of the results obtained with all the models with and without CR which have been used. This error is assumed to be uncorrelated between experiments.

### 12.3.6 Weighting function

The weighting function of Equation 12.3 could justifiably be modified such that only the uncorrelated components of the systematic uncertainty appear in the denominator. To accommodate this, the

average is performed using both variants of the weighting function. This has an insignificant effect on the consistency between data and model under test, e.g. for SK-I the result is changed by 0.02 standard deviations, and this effect is therefore neglected.

## 12.4 Combined Results

Experiments provide their results in the form of  $R_N$  (or changes to  $R_N$ ) at a reference centre-of-mass energy of 189 GeV by scaling results obtained at various energies using the predicted energy dependence of their own no-CR MC samples. This avoids having to generate common samples at multiple centre-of-mass energies.

The detailed results from all experiments are included in Appendix D.1. These consist of preliminary results, taken from the publicly available notes [226–229], and additional information from analysis of Monte Carlo samples. The averaging procedure itself is carried out by each of the experiments and good agreement is obtained.

An example of this averaging to test an extreme scenario of the SK-I CR model (full reconnection) is given in Appendix D.2. The average obtained in this case is:

$$r(data) = 0.969 \pm 0.011(\text{stat.}) \pm 0.009(\text{syst. corr.}) \pm 0.006(\text{syst. uncorr.}), \quad (12.4)$$

$$r(\text{SK-I } 100\%) = 0.8909. \quad (12.5)$$

The measurements of each experiment and this combined result are shown in Figure 12.1. As the sensitivity of the analysis is different for each experiment, the value of  $r$  predicted by the SK-I model is indicated separately for each experiment by a dashed line in the figure. Thus the data disagree with the extreme scenario of this particular model at a level of 5.2 standard deviations. The data from the four experiments are consistent with each other and tend to prefer an intermediate colour reconnection scenario rather than the no colour reconnection one at the level of 2.2 standard deviations in the SK-I framework.

### 12.4.1 Parameter space in SK-I model

In the SK-I model, the reconnection probability is governed by an arbitrary, free parameter,  $k_I$ . By comparing the data with model predictions evaluated at a variety of  $k_I$  values, it is possible to determine the reconnection probability that is most consistent with data, which can in turn be used to estimate the corresponding bias in the measured  $m_W$ . By repeating the averaging procedure using model inputs for the set of  $k_I$  values given in Table D.2, including a re-evaluation of the weights for each value of  $k_I$ , it is found that the data prefer a value of  $k_I = 1.18$  as shown in Figure 12.2. The 68% confidence level lower and upper limits are 0.39 and 2.13 respectively. The LEP averages in  $r$  obtained for the different  $k_I$  values are summarised in Table D.4. They correspond to a preferred reconnection probability of 49% in this model at 189 GeV as illustrated in Figure 12.3.

The small variations observed in the LEP average value of  $r$  and its corresponding error as a function of  $k_I$  (or  $P_{reco}$ ) are essentially due to changes in the relative weighting of the experiments.



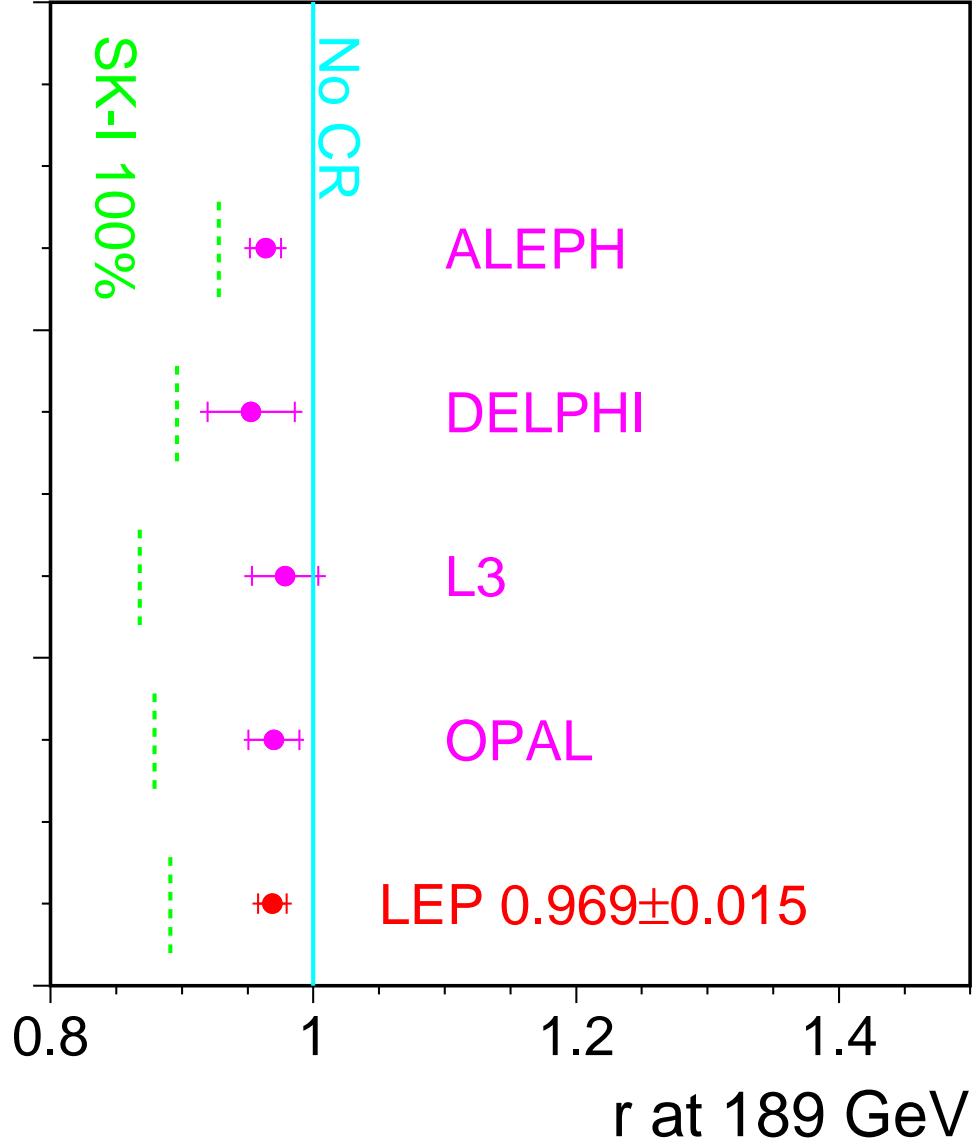


Figure 12.1: Preliminary particle flow results using all data, combined to test the limiting case of the SK-I model in which more than 99.9% of the events are colour reconnected. The error bars correspond to the total error with the inner part showing the statistical uncertainty. The predicted values of  $r$  for this CR model are indicated separately for the analysis of each experiment by dashed lines.

#### 12.4.2 ARIADNE and HERWIG models

The combination procedure has been applied to common samples of ARIADNE and HERWIG Monte Carlo models. The  $R_N$  average values obtained with these models based on their respective predicted sensitivity are summarised in Table D.5. The four experiments have observed a weak sensitivity to these colour reconnected samples with the particle flow analysis, as can be seen from Figure 12.4.

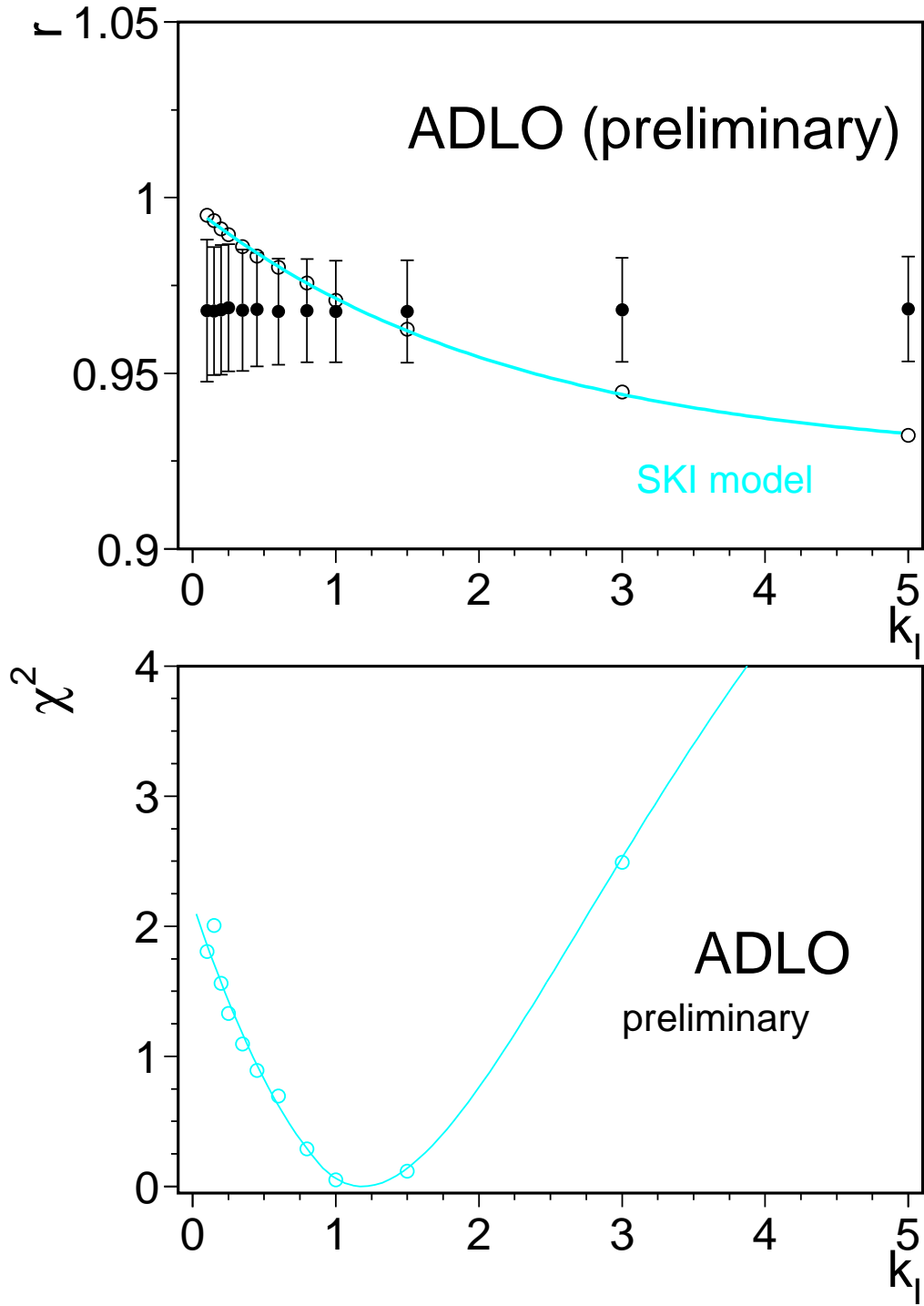


Figure 12.2: Comparison of the LEP average  $r$  values with the SK-I model prediction obtained as a function of the  $k_I$  parameter. The comparisons are performed after extrapolation of data to the reference centre-of-mass energy of 189 GeV. In the upper plot, the solid line is the result of fitting a function of the form  $r(k_I) = p_1(1 - \exp(-p_2 k_I)) + p_3$  to the MC predictions. The lower plot shows the corresponding  $\chi^2$  curve obtained from this comparison. The best agreement between the model and the data is obtained when  $k_I = 1.18$ .

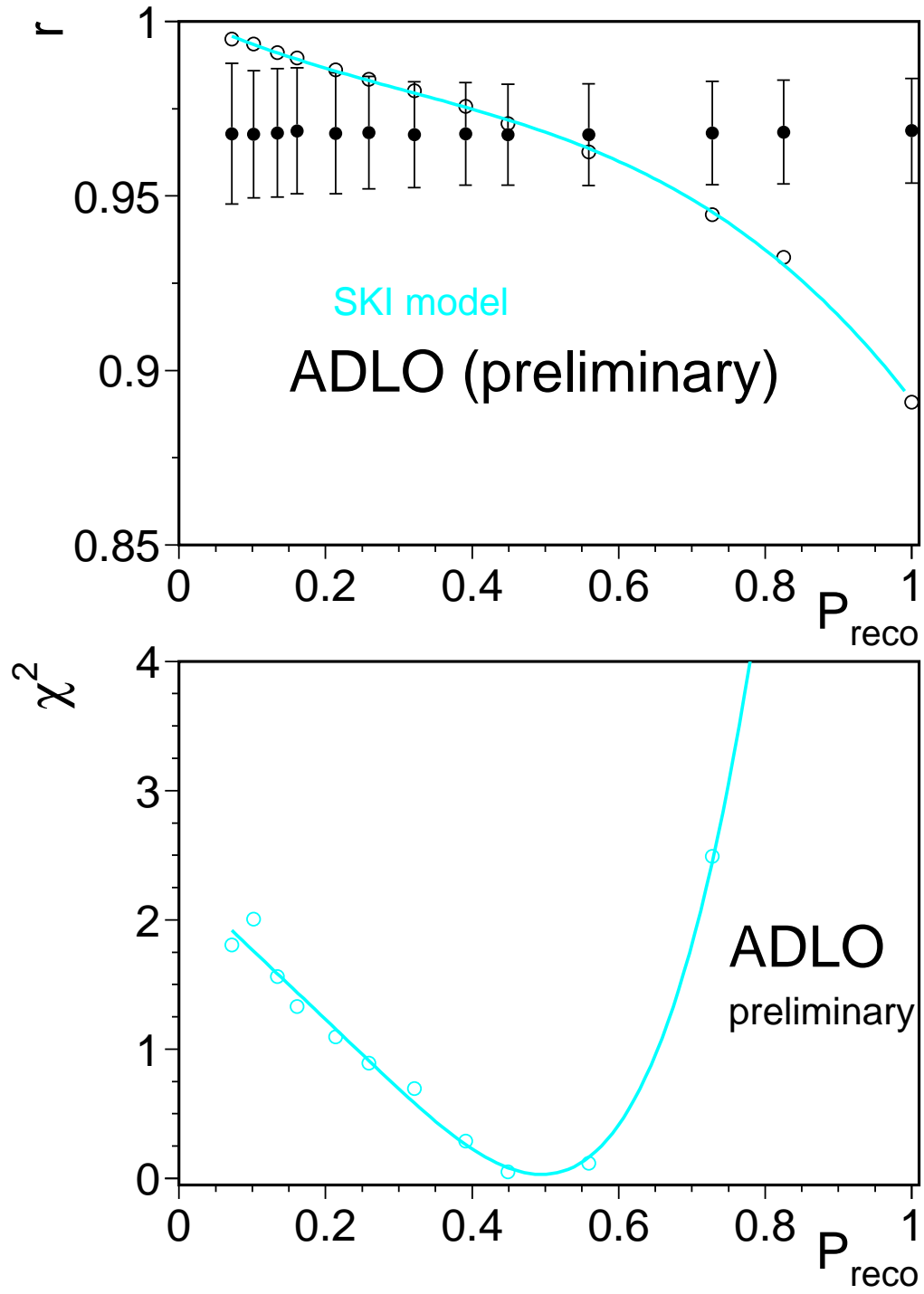


Figure 12.3: Comparison of the LEP average  $r$  values with the SK-I model prediction obtained as a function of the reconnection probability. In the upper plot, the solid line is the result of fitting a third order polynomial function to the MC predictions. The lower plot shows a  $\chi^2$  curve obtained from this comparison using all LEP data at the reference centre-of-mass energy of 189 GeV. The best agreement between the model and the data is obtained when 49% of events are reconnected in this model.

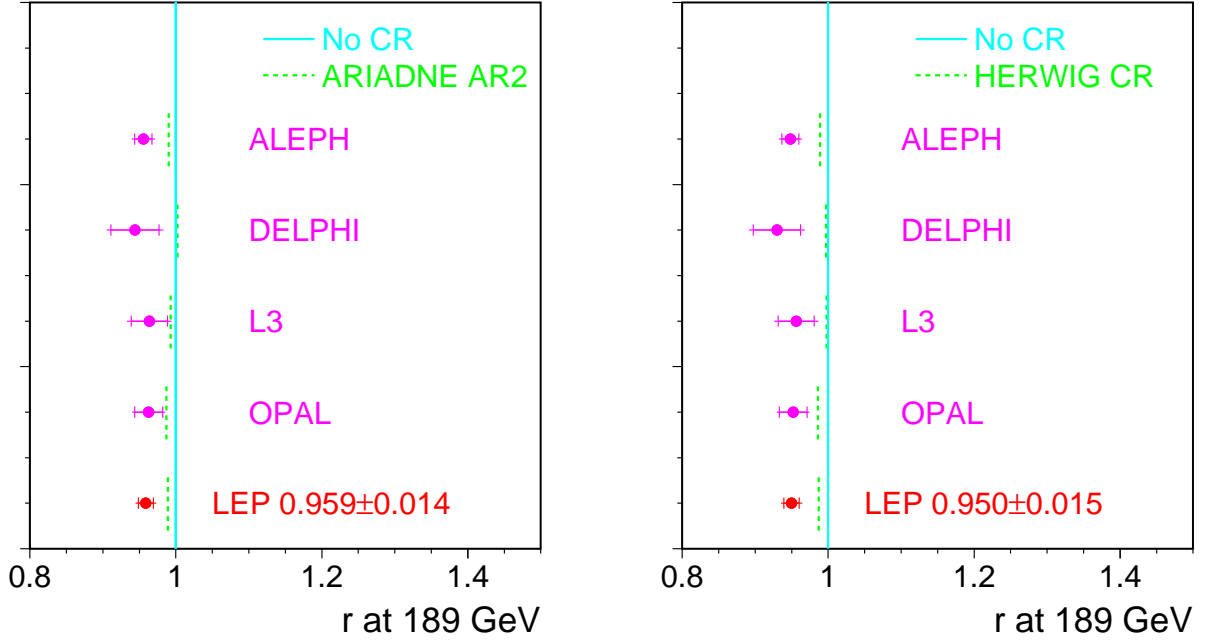


Figure 12.4: Preliminary particle flow results using all data, combined to test the ARIADNE and HERWIG colour reconnection models, based on the predicted sensitivity. The predicted values of  $r$  for this CR model are indicated separately for the analysis of each experiment by dashed lines.

## 12.5 Summary

A first, preliminary combination of the LEP particle flow results is presented, using the entire LEP2 data sample. The data disfavour by 5.2 standard deviations an extreme version of the SK-I model in which colour reconnection has been forced to occur in essentially all events. The combination procedure has been generalised to the SK-I model as a function of its variable reconnection probability. The combined data are described best by the model where 49% of events at 189 GeV are reconnected, corresponding to  $k_I = 1.18$ . The LEP data, averaged using weights corresponding to  $k_I = 1.0$ , *i.e.* closest to the optimal fit, do not exclude the no colour reconnection hypothesis, deviating from it by 2.2 standard deviations. A 68% confidence level range has been determined for  $k_I$  and corresponds to  $[0.39, 2.13]$ .

For both the ARIADNE and HERWIG models, which do not contain adjustable colour reconnection parameters, differences between the results of the colour reconnected and the no-CR scenarios are small and do not allow the particle flow analysis to discriminate between them. To test consistency between data and the no-CR models, the data are averaged using weights where the factor accounting for predicted sensitivity to a given CR model has been set to unity. The  $R_N$  values obtained with the no colour reconnection HERWIG and ARIADNE models, using the common Cetraro samples, differ from the measured data value by 3.7 and 3.1 standard deviations.

The observed deviations of the  $R_N$  values from all no colour reconnection models may indicate a possible systematic effect in the description of particle flow for 4-jet events. Independent studies of particle flow in WW semileptonic events as well as other CR-oriented analyses are required to investigate this.

# Chapter 13

## Bose-Einstein Correlations in W-Pair Events

**Updates with respect to summer 2002:**

Unchanged w.r.t. summer 2002: Results are preliminary.

### 13.1 Introduction

The LEP experiments have measured the strength of particle correlations between two hadronic systems obtained from W-pair decay occurring close in space-time at LEP-II. The work presented in this chapter is focused on so-called Bose-Einstein (BE) correlations, i.e., the enhanced probability of production of pairs (multiplets) of identical mesons close together in phase space. The effect is readily observed in particle physics, in particular in hadronic decays of the Z boson, and is qualitatively understood as a result of quantum-mechanical interference originating from the symmetry of the amplitude of the particle production process under exchange of identical mesons.

The presence of correlations between hadrons coming from the decay of a  $W^+W^-$  pair, in particular those between hadrons originating from different Ws, can affect the direct reconstruction of the mass of the initial W bosons. The measurement of the strength of these correlations can be used for the estimation of the systematic uncertainty of the W mass measurement.

### 13.2 Method

The principal method [239], called “mixing method”, used in this measurement is based on the direct comparison of 2-particle spectra of genuine hadronic WW events and of mixed WW events. The latter are constructed by mixing the hadronic parts of two semileptonic WW events (first used in [240]). Such a reference sample has the advantage of reproducing the correlations between particles belonging to the same W, while the particles from different Ws are uncorrelated by construction.

This method gives a model-independent estimate of the interplay between the two hadronic systems, for which BE correlations and also colour reconnection are considered as dominant sources. The possibility of establishing the strength of inter-W correlations in a model-independent way is rather unique; most correlations do carry an inherent model dependence on the reference sample. In the present measurement, the model dependence is limited to the background subtraction.

### 13.3 Distributions

The two-particle correlations are evaluated using two-particle densities defined in terms of the 4-momentum transfer  $Q = \sqrt{-(p_1 - p_2)^2}$ , where  $p_1, p_2$  are the 4-momenta of the two particles:

$$\rho_2(Q) = \frac{1}{N_{ev}} \frac{dn_{pairs}}{dQ} \quad (13.1)$$

Here  $n_{pairs}$  stands for number of like-sign (unlike-sign) 2-particle permutations.<sup>1</sup> In the case of two stochastically independent hadronically decaying Ws the two-particle inclusive density is given by:

$$\rho_2^{WW} = \rho_2^{W^+} + \rho_2^{W^-} + 2\rho_2^{mix}, \quad (13.2)$$

where  $\rho_2^{mix}$  can be expressed via single-particle inclusive density  $\rho_1(p)$  as:

$$\rho_2^{mix}(Q) = \int d^4p_1 d^4p_2 \rho^{W^+}(p_1) \rho^{W^-}(p_2) \delta(Q^2 + (p_1 - p_2)^2) \delta(p_1^2 - m_\pi^2) \delta(p_2^2 - m_\pi^2). \quad (13.3)$$

Assuming further that:

$$\rho_2^{W^+}(Q) = \rho_2^{W^-}(Q) = \rho_2^W(Q), \quad (13.4)$$

we obtain:

$$\rho_2^{WW}(Q) = 2\rho_2^W(Q) + 2\rho_2^{mix}(Q). \quad (13.5)$$

In the mixing method, we obtain  $\rho_2^{mix}$  by combining two hadronic W systems from two different semileptonic WW events. The direct search for inter-W BE correlations is done using the difference of 2-particle densities:

$$\Delta\rho(Q) = \rho_2^{WW}(Q) - 2\rho_2^W(Q) - 2\rho_2^{mix}(Q), \quad (13.6)$$

or, alternatively, their ratio:

$$D(Q) = \frac{\rho_2^{WW}(Q)}{2\rho_2^W(Q) + 2\rho_2^{mix}(Q)} = 1 + \frac{\Delta\rho(Q)}{2\rho_2^W(Q) + 2\rho_2^{mix}(Q)}. \quad (13.7)$$

In case of  $\Delta\rho(Q)$ , we look for a deviation from 0, while in case of  $D(Q)$ , inter-W BE correlations would manifest themselves by deviation from 1. The event mixing procedure may introduce artificial distortions, or may not fully account for some detector effects or for correlations other than BE correlations, causing a deviation of  $\Delta\rho(Q)$  from zero or D from unity for data as well as Monte Carlo without inter-W BE correlations. These possible effects are reduced by using the double ratio:

$$D'(Q) = \frac{D(Q)_{data}}{D(Q)_{MC, nointer}}, \quad (13.8)$$

where  $D(Q)_{MC, nointer}$  is derived from a MC without inter-W BE correlations.

In addition to the mixing method, ALEPH [241] also uses the double ratio of like-sign pairs ( $N_{\pi^{++},--}(Q)$ ) and unlike-sign pairs  $N_{\pi^{+-}}(Q)$  corrected with Monte-Carlo simulations not including BE effects:

$$R^*(Q) = \left( \frac{N_{\pi^{++},--}(Q)}{N_{\pi^{+-}}(Q)} \right)^{data} \bigg/ \left( \frac{N_{\pi^{++},--}(Q)}{N_{\pi^{+-}}(Q)} \right)_{noBE}^{MC}. \quad (13.9)$$

---

<sup>1</sup>For historical reasons, the number of particle permutations rather than combinations is used in formulas. For the same reason, a factor 2 appears in front of  $\rho_2^{mix}$  in eq. 13.2. The experimental statistical errors are, however, based on the number of particle pairs, i.e., 2-particle combinations.

## 13.4 Results

As examples, the distributions of  $R^*$  measured by ALEPH [241] and  $\Delta\rho$  measured by L3 [236] are shown in Figures 13.1 and 13.2, respectively. A simple combination procedure is available through a  $\chi^2$  average of the numerical results of each experiment with respect to a specific BE model under study, here based on comparisons with various (tuned) versions of the LUBOEI model [236, 241–243]. The tuning is performed by adjusting the parameters of the model to reproduce correlations in samples of  $Z^0$  and semileptonic W decays, and applying identical parameters to the modelling of inter-W correlations (so-called “full BE” scenario). In this way the tuning of each experiment takes into account detector systematics in track measurements of different experiments. However, good agreement was found between tunings used in [234, 236], and the sensitivity of the four LEP experiments to observe BE correlations between pions from the fragmentation of different Ws was found to be similar.

An important advantage of the combination procedure used here is that it allows the combination of results obtained using different analyses. The ALEPH result is based on data collected at centre-of-mass energies up to 189 GeV, while the L3 results are based on the complete LEP-2 luminosity. Since the inter-W BE correlations could be energy dependent, the results can only be combined within a model, here the LUBOEI model.

The combination procedure assumes a linear dependence of the observed size of BE correlations on various estimators used to analyse the different distributions. It was also verified that there is a linear dependence between the measured W mass shift and the values of these estimators [244]. The estimators are: the integral of the term describing the BE correlation part,  $\int \lambda \exp(-\sigma^2 Q^2)$ , when fitting the function  $\kappa(1 + \epsilon Q)(1 + \lambda \exp(-\sigma^2 Q^2))$  to the  $R^*(Q)$  distribution (ALEPH); the integral of the  $\Delta\rho(Q)$  distribution (L3); the parameter  $\Lambda$  when fitting the function  $N(1 + \delta Q)(1 + \Lambda \exp(-k^2 Q^2))$ , with  $N$  fixed to unity, to the  $D'(Q)$  distribution (L3). The size of the correlations for like-sign pairs of particles measured in terms of these estimators is compared with the values expected in the model with and without inter-W correlations in Table 13.1. For the combination of these measurements, only the uncertainties in the understanding of the background contribution in the data are treated as correlated between experiments (denoted as “corr. syst.” in Table 13.1).

Table 13.2 summarizes the normalized fractions of the model seen. Using a correlation coefficient of 0.95 between the two L3 measurements, the combination via a MINUIT fit gives:

$$\frac{\text{data} - \text{model}(\text{noBE})}{\text{model}(\text{fullBE}) - \text{model}(\text{noBE})} = 0.03 \pm 0.18, \quad (13.10)$$

where “noBE” includes correlations between decay products of each W, but not the ones between decay products of different Ws and “fullBE” includes all the correlations. A reasonable  $\chi^2/\text{dof}=0.8/2$  of the fit is observed. The measurements and their average are also shown in Figure 13.3. It can thus be seen that there is no significant evidence for BE correlations between hadrons from different W bosons.

Note that after the summer conferences 2002 whose status is reported here, the DELPHI collaboration presented new preliminary results on BE correlations [234]. Fitting the function  $N(1 + \delta Q)(1 + \Lambda \exp(-QR))$ , with  $R$  fixed by the model, to its  $D(Q)$  distribution, DELPHI finds a non-zero value of the estimator  $\Lambda$  for 2-particle correlations between like-sign particles from different W bosons at the level of 2.8 standard deviations, 1.9 standard deviations below that for a LUBOEI model with full strength correlations. DELPHI also finds a 2.4 standard deviation effect for pairs of unlike-sign particles from different W bosons, which is in agreement with the LUBOEI model with full strength correlations between particles from different W bosons.

	data–noBE	stat.	syst.	corr. syst.	fullBE–noBE	Ref.
ALEPH (fit to $R^*$ )	–0.0040	0.0062	0.0036	negligible	0.0177	[241]
L3 (fit to $D'$ )	+0.008	0.018	0.012	0.004	0.103	[236]
L3 (integral of $\Delta\rho$ )	+0.03	0.33	0.15	0.06	1.38	[236]

Table 13.1: An overview of the input values for the  $\chi^2$  combination: the difference between the measured correlations and the model without inter-W correlations (data–noBE), the corresponding statistical (stat.) and total systematic (syst.) errors, the correlated systematic error contribution (corr. syst.), and the difference between “full BE” and “no BE” scenario. In addition to the measurements made by L3 with the mixing method, the ALEPH result with the double like-sign/unlike-sign ratio  $R^*$  is given.

	fraction of the model	stat.	syst.
ALEPH (fit to $R^*$ )	–0.23	0.35	0.20
L3 (fit to $D'$ )	+0.08	0.17	0.12
L3 (integral of $\Delta\rho$ )	+0.02	0.24	0.11

Table 13.2: The measured size of correlations expressed as the relative fraction of the model with inter-W correlations.

The result of the  $\chi^2$  combination of the measurements from ALEPH and L3 can be translated into a 68% confidence level upper limit on the shift of the W mass measurements due to the BE correlations between particles from different Ws,  $\Delta m_W$ , assuming a linear dependence of  $\Delta m_W$  on the size of the correlation. For the specific BE model investigated, LUBOEI, a shift of –35 MeV in the W mass is obtained at full BE correlation strength [245]. Thus the preliminary 68% CL upper limit on the magnitude of the mass shift within the LUBOEI model is:

$$|\Delta m_W| = (0.03 + 0.18) \cdot 35 \text{ MeV} = 7 \text{ MeV} \quad (+1 \sigma \text{ limit}). \quad (13.11)$$

Further work is needed, such as: understanding the differences between the various estimators and fitting functions, including results from DELPHI and OPAL, and a generalisation to other BE models. For the time being, therefore, 35 MeV is used as an uncertainty for BE correlations in the W mass combination presented in the following chapter.



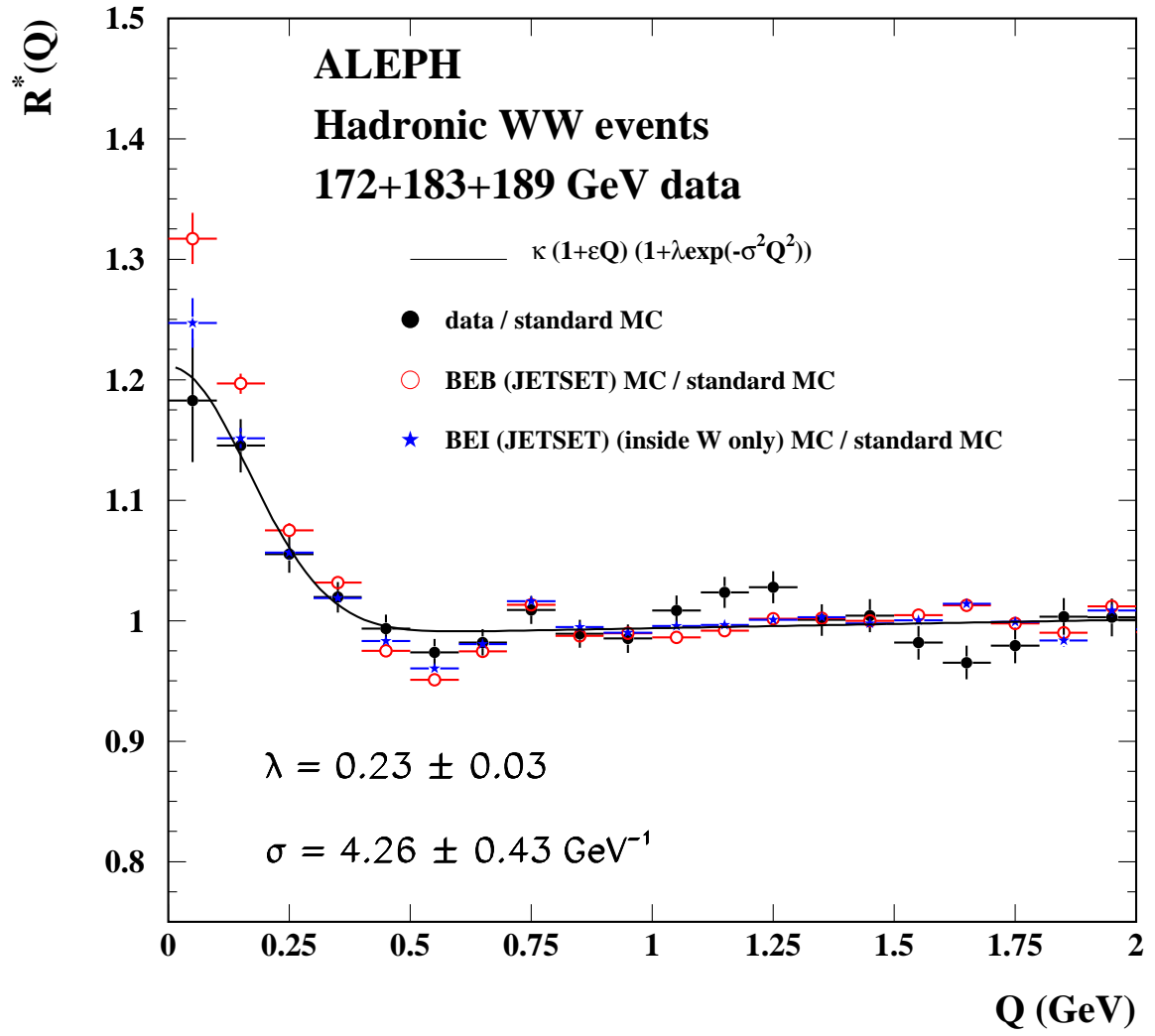


Figure 13.1: Distribution of the double ratio  $R^*$  as a function of  $Q$  as measured by the ALEPH collaboration.

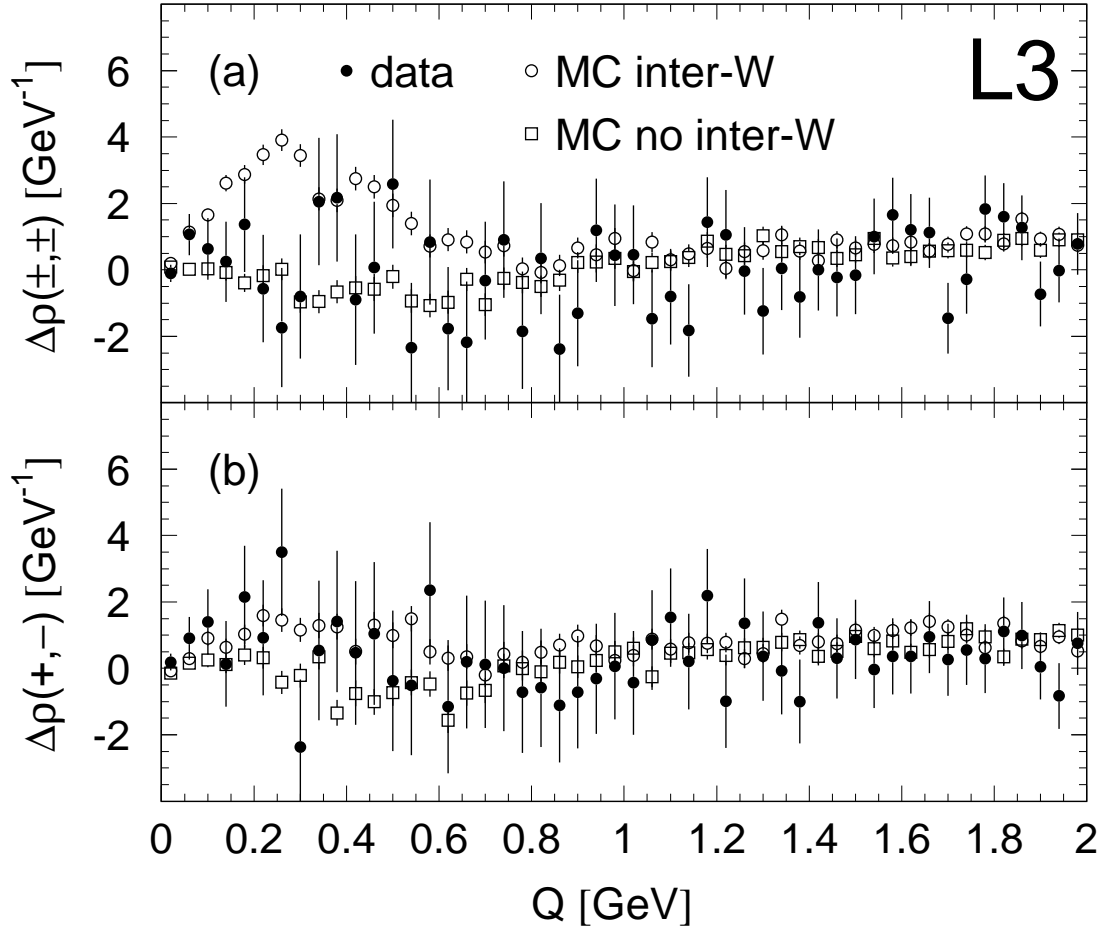


Figure 13.2: Distributions of the quantity  $\Delta\rho$  for like- and unlike-sign pairs as a function of  $Q$  as measured by the L3 collaboration.

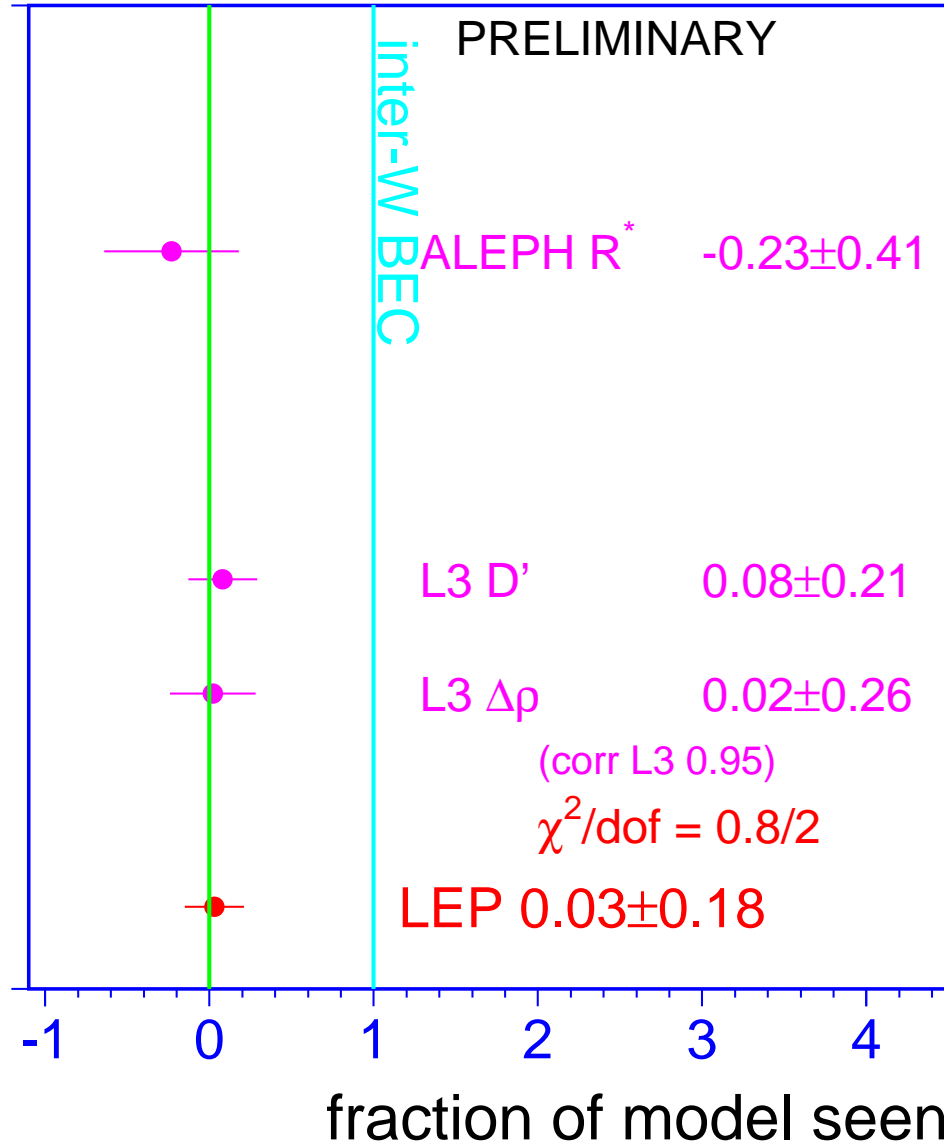


Figure 13.3:  $\chi^2$  combination of the measured size of correlations expressed as the relative fraction of the model with inter-W correlations. A correlation coefficient of 0.95 between the two L3 measurements is used.

# Chapter 14

## W-Boson Mass and Width at LEP-II

### Updates with respect to summer 2002:

New preliminary results on the mass of the W boson from ALEPH are used in the combination.

### 14.1 Introduction

The W boson mass and width results presented in this chapter are obtained from data recorded over a range of centre-of-mass energies,  $\sqrt{s} = 161 - 209$  GeV, during the 1996-2000 operation of the LEP collider. The results reported by the ALEPH, DELPHI and L3 collaborations include an analysis of the year 2000 data, and have an integrated luminosity per experiment of about  $700 \text{ pb}^{-1}$ . The OPAL collaboration has analysed the data up to and including 1999 and has an integrated luminosity of approximately  $450 \text{ pb}^{-1}$ . The ALEPH result does not include an analysis of the small amount of data (about  $10 \text{ pb}^{-1}$ ) collected in 1996 at a centre-of-mass energy of 172 GeV.

The results on the W mass and width quoted below correspond to a definition based on a Breit-Wigner denominator with an  $s$ -dependent width,  $|(s - m_W^2) + is\Gamma_W/m_W|$ .

### 14.2 W Mass Measurements

Since 1996 the LEP  $e^+e^-$  collider has been operating above the threshold for  $W^+W^-$  pair production. Initially,  $10 \text{ pb}^{-1}$  of data were recorded close to the  $W^+W^-$  pair production threshold. At this energy the  $W^+W^-$  cross section is sensitive to the W boson mass,  $m_W$ . Table 14.1 summarises the W mass results from the four LEP collaborations based on these data [246].

Subsequently LEP has operated at energies significantly above the  $W^+W^-$  threshold, where the  $e^+e^- \rightarrow W^+W^-$  cross section has little sensitivity to  $m_W$ . For these higher energy data  $m_W$  is measured through the direct reconstruction of the W boson's invariant mass from the observed jets and leptons. Table 14.2 summarises the W mass results presented individually by the four LEP experiments using the direct reconstruction method. The combined values of  $m_W$  from each collaboration take into account the correlated systematic uncertainties between the decay channels and between the different years of data taking. In addition to the combined numbers, each experiment presents mass measurements from  $W^+W^- \rightarrow q\bar{q}\ell\bar{\nu}_\ell$  and  $W^+W^- \rightarrow q\bar{q}q\bar{q}$  channels separately. The DELPHI and OPAL collaborations provide results from independent fits to the data in the  $q\bar{q}\ell\bar{\nu}_\ell$  and  $q\bar{q}q\bar{q}$  decay channels

THRESHOLD ANALYSIS [246]	
Experiment	$m_W(\text{threshold})/\text{GeV}$
ALEPH	$80.14 \pm 0.35$
DELPHI	$80.40 \pm 0.45$
L3	$80.80^{+0.48}_{-0.42}$
OPAL	$80.40^{+0.46}_{-0.43}$

Table 14.1: W mass measurements from the  $W^+W^-$  threshold cross section at  $\sqrt{s} = 161$  GeV. The errors include statistical and systematic contributions.

separately and hence account for correlations between years but do not need to include correlations between the two channels. The  $q\bar{q}\ell\bar{\nu}_\ell$  and  $q\bar{q}q\bar{q}$  results quoted by the ALEPH and L3 collaborations are obtained from a simultaneous fit to all data which, in addition to other correlations, takes into account the correlated systematic uncertainties between the two channels. The L3 result is unchanged when determined through separate fits. The systematic uncertainties in the  $W^+W^- \rightarrow q\bar{q}q\bar{q}$  channel show a large variation between experiments; this is caused by differing estimates of the possible effects of Colour Reconnection (CR) and Bose-Einstein Correlations (BEC), discussed below. The systematic errors in the  $W^+W^- \rightarrow q\bar{q}\ell\bar{\nu}_\ell$  channel are dominated by uncertainties from hadronisation, with estimates ranging from 15 to 30 MeV.

The results presented in this note differ from those in the previous combination [1] due to revised measurements from the ALEPH Collaboration [247]; otherwise the results are identical. The ALEPH measurements have been revised due to a change in their event reconstruction algorithm. This change makes the analysis less sensitive to detector simulation inaccuracies which were not taken into account in their previous preliminary result.

Experiment	DIRECT RECONSTRUCTION		
	$W^+W^- \rightarrow q\bar{q}\ell\bar{\nu}_\ell$ $m_W/\text{GeV}$	$W^+W^- \rightarrow q\bar{q}q\bar{q}$ $m_W/\text{GeV}$	Combined $m_W/\text{GeV}$
ALEPH [247]	$80.375 \pm 0.062$	$80.431 \pm 0.117$	$80.385 \pm 0.058$
DELPHI [248–251]	$80.414 \pm 0.089$	$80.374 \pm 0.119$	$80.402 \pm 0.075$
L3 [252–256]	$80.314 \pm 0.087$	$80.485 \pm 0.127$	$80.367 \pm 0.078$
OPAL [257–261]	$80.516 \pm 0.073$	$80.407 \pm 0.120$	$80.495 \pm 0.067$

Table 14.2: Preliminary W mass measurements from direct reconstruction ( $\sqrt{s} = 172 - 209$  GeV). Results are given for the semi-leptonic, fully-hadronic channels and the combined value. The  $W^+W^- \rightarrow q\bar{q}\ell\bar{\nu}_\ell$  results from the OPAL collaboration include mass information from the  $W^+W^- \rightarrow \ell\bar{\nu}_\ell\ell\bar{\nu}_\ell$  channel. The results given here differ from those in the publications of the individual experiments as they have been recalculated imposing common FSI uncertainties.

### 14.3 Combination Procedure

A combined LEP W mass measurement is obtained from the results of the four experiments. In order to perform a reliable combination of the measurements, a more detailed input than that given in Table 14.2 is required. Each experiment provided a W mass measurement for both the  $W^+W^- \rightarrow q\bar{q}\ell\bar{\nu}_\ell$  and  $W^+W^- \rightarrow q\bar{q}q\bar{q}$  channels for each of the data taking years (1996-2000) that it had analysed. In addition to the four threshold measurements a total of 36 direct reconstruction measurements are

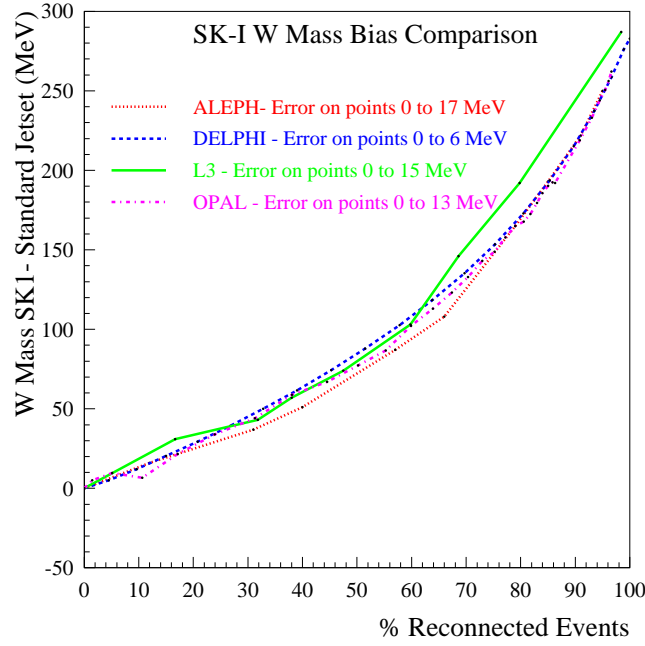


Figure 14.1: W mass bias obtained in the SK-I model of colour reconnection relative to a simulation without colour reconnection as a function of the fraction of events reconnected for the fully-hadronic decay channel at a centre of mass energy of 189 GeV. The analyses of the four LEP experiments show similar sensitivity to this effect. The points connected by the lines have correlated uncertainties increasing to the right in the range indicated.

supplied: DELPHI provided 10 measurements (1996-2000), L3 gave 8 measurements (1996-2000) having already combined the 1996 and 1997 results, ALEPH provided 8 measurements (1997-2000) and OPAL also gave 8 measurements (1996-1999). The  $W^+W^- \rightarrow \ell\bar{\nu}_\ell\ell\bar{\nu}_\ell$  channel is also analysed by the OPAL(1997-1999) collaboration; the lower precision results obtained from this channel are combined with the  $W^+W^- \rightarrow q\bar{q}\ell\bar{\nu}_\ell$  channel mass determinations.

Subdividing the results by data-taking years enables a proper treatment of the correlated systematic uncertainty from the LEP beam energy and other dependences on the centre-of-mass energy or data-taking period. A detailed breakdown of the sources of systematic uncertainty are provided for each result and the correlations specified. The inter-year, inter-channel and inter-experiment correlations are included in the combination. The main sources of correlated systematic errors are: colour reconnection, Bose-Einstein correlations, hadronisation, the LEP beam energy, and uncertainties from initial and final state radiation. The full correlation matrix for the LEP beam energy is employed [262]. The combination is performed and the evaluation of the components of the total error assessed using the Best Linear Unbiased Estimate (BLUE) technique, see Reference 85.

A preliminary study of colour reconnection has been made by the LEP experiments using the particle flow method [263] on a sample of fully-hadronic WW events, see chapter 12. These results are interpreted in terms of the reconnection parameter  $k_i$  of the SK-I model [264] and yield a 68% confidence level range of:

$$0.39 < k_i < 2.13. \quad (14.1)$$

The method was found to be insensitive to the HERWIG and ARIADNE-II models of colour recon-

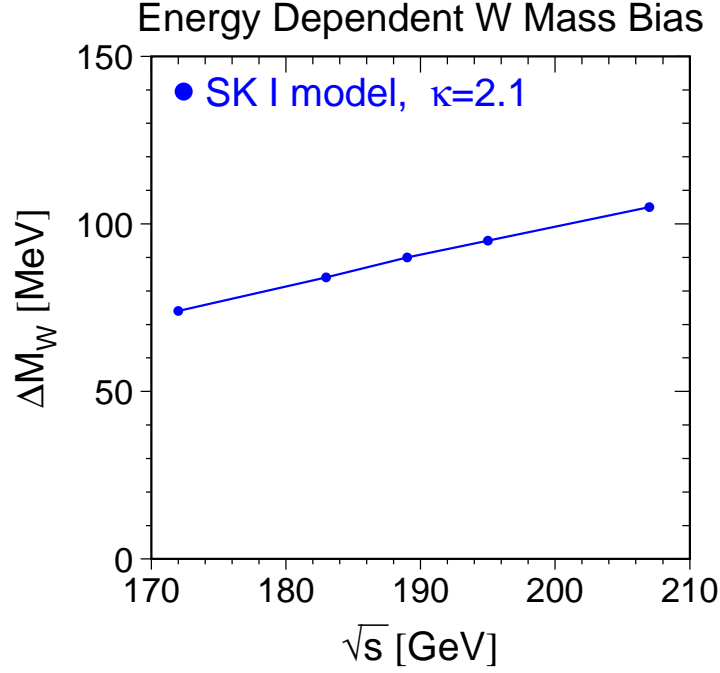


Figure 14.2: The values used in the W Mass combination for the uncertainty due to colour reconnection are shown as a function of the centre of mass energy. These values were obtained from a linear fit to simulation results obtained with the SK1 model of colour reconnection at  $k_i = 2.13$ .

nection.

Studies of simulation samples have demonstrated that the four experiments are equally sensitive to colour reconnection effects, *i.e.* when looking at the same CR model similar biases are seen by all experiments. This is shown in Figure 14.1 for the SKI model as a function of the fraction of reconnected events. For this reason a common value for all experiments of the CR systematic uncertainty is used in the combination.

For this combination, no offset has been applied to the central value of  $m_W$  due to colour reconnection effects and a symmetric systematic error has been imposed. The  $m_W$  error is set from a linear extrapolation of simulation results obtained at  $k_i = 2.13$ , the values used in the combination are: 74 MeV shift for the 1996 data at a centre-of-mass energy of 172 GeV, 84 MeV for 1997 at 183 GeV, 90 MeV for 1998 at 189 GeV, 95 MeV for 1999 at 195 GeV and 105 MeV for 2000 at 207 GeV, they are shown in Figure 14.2. Previous  $m_W$  combinations have relied upon theoretical expectations of colour reconnection effects, in which there is considerable uncertainty. This new data driven approach achieves a more robust uncertainty estimate at the expense of a significantly increased colour reconnection uncertainty. The ARIADNE-II and HERWIG models of colour reconnection have also been studied and the W Mass shift was found to be lower than that from SK1 with  $k_i = 2.13$  used for the combination.

For Bose-Einstein correlations, a similar test has been made of the respective experimental sensitivities with the LUBOEI [265] model: the experiments observed compatible mass shifts. A common value of the systematic uncertainty from BEC of 35 MeV is assumed from studies of the LUBOEI model. This value may be compared with recent direct measurements from LEP of this effect [234, 236, 266], where the observed Bose-Einstein effect was of smaller magnitude than in the LUBOEI model, see

Source	Systematic Error on $m_W$ (MeV)		
	$q\bar{q}\ell\bar{\nu}_\ell$	$q\bar{q}q\bar{q}$	Combined
ISR/FSR	8	8	8
Hadronisation	19	18	18
Detector Systematics	14	10	14
LEP Beam Energy	17	17	17
Colour Reconnection	—	90	9
Bose-Einstein Correlations	—	35	3
Other	4	5	4
Total Systematic	31	101	31
Statistical	32	35	29
Total	44	107	43
Statistical in absence of Systematics	32	28	21

Table 14.3: Error decomposition for the combined LEP W mass results. Detector systematics include uncertainties in the jet and lepton energy scales and resolution. The ‘Other’ category refers to errors, all of which are uncorrelated between experiments, arising from: simulation statistics, background estimation, four-fermion treatment, fitting method and event selection. The error decomposition in the  $q\bar{q}\ell\bar{\nu}_\ell$  and  $q\bar{q}q\bar{q}$  channels refers to the independent fits to the results from the two channels separately.

chapter 13. Hence, the currently assigned 35 MeV uncertainty is considered a conservative estimate.

## 14.4 LEP Combined W Boson Mass

The combined W mass from direct reconstruction is

$$m_W(\text{direct}) = 80.412 \pm 0.029(\text{stat.}) \pm 0.031(\text{syst.}) \text{ GeV}, \quad (14.2)$$

with a  $\chi^2/\text{d.o.f.}$  of 28.2/33, corresponding to a  $\chi^2$  probability of 70%. The weight of the fully-hadronic channel in the combined fit is 0.10. This reduced weight is a consequence of the relatively large size of the current estimates of the systematic errors from CR and BEC. Table 14.3 gives a breakdown of the contribution to the total error of the various sources of systematic errors. The largest contribution to the systematic error comes from hadronisation uncertainties, which are conservatively treated as correlated between the two channels, between experiments and between years. In the absence of systematic effects the current LEP statistical precision on  $m_W$  would be 21 MeV: the statistical error contribution in the LEP combination is larger than this (29 MeV) due to the significantly reduced weight of the fully-hadronic channel.

In addition to the above results, the W boson mass is measured at LEP from the  $10 \text{ pb}^{-1}$  per experiment of data recorded at threshold for W pair production:

$$m_W(\text{threshold}) = 80.40 \pm 0.20(\text{stat.}) \pm 0.07(\text{syst.}) \pm 0.03(E_{\text{beam}}) \text{ GeV}. \quad (14.3)$$

When the threshold measurements are combined with the much more precise results obtained from direct reconstruction one achieves a W mass measurement of

$$m_W = 80.412 \pm 0.029(\text{stat.}) \pm 0.031(\text{syst.}) \text{ GeV}. \quad (14.4)$$



The LEP beam energy uncertainty is the only correlated systematic error source between the threshold and direct reconstruction measurements. The threshold measurements have a weight of only 0.03 in the combined fit. This LEP combined result is compared with the results (threshold and direct reconstruction combined) of the four LEP experiments in Figure 14.3.

## 14.5 Consistency Checks

The difference between the combined W boson mass measurements obtained from the fully-hadronic and semi-leptonic channels,  $\Delta m_W(q\bar{q}q\bar{q} - q\bar{q}\ell\bar{\nu}_\ell)$ , is determined:

$$\Delta m_W(q\bar{q}q\bar{q} - q\bar{q}\ell\bar{\nu}_\ell) = +22 \pm 43 \text{ MeV}.$$

A significant non-zero value for  $\Delta m_W$  could indicate that CR and BEC effects are biasing the value of  $m_W$  determined from  $W^+W^- \rightarrow q\bar{q}q\bar{q}$  events. Since  $\Delta m_W$  is primarily of interest as a check of the possible effects of final state interactions, the errors from CR and BEC are set to zero in its determination. The result is obtained from a fit where the imposed correlations are the same as those for the results given in the previous sections. This result is almost unchanged if the systematic part of the error on  $m_W$  from hadronisation effects is considered as uncorrelated between channels, although the uncertainty increases by 16%:  $\Delta m_W = 19 \pm 50 \text{ MeV}$ .

The masses from the two channels obtained from this fit with the BEC and CR errors now included are:

$$\begin{aligned} m_W(W^+W^- \rightarrow q\bar{q}\ell\bar{\nu}_\ell) &= 80.411 \pm 0.032(\text{stat.}) \pm 0.030(\text{syst.}) \text{ GeV}, \\ m_W(W^+W^- \rightarrow q\bar{q}q\bar{q}) &= 80.420 \pm 0.035(\text{stat.}) \pm 0.101(\text{syst.}) \text{ GeV}. \end{aligned}$$

These two results are correlated and have a correlation coefficient of 0.18. The value of  $\chi^2/\text{d.o.f}$  is 28.2/32, corresponding to a  $\chi^2$  probability of 66%. These results and the correlation between them can be used to combine the two measurements or to form the mass difference. The LEP combined results from the two channels are compared with those quoted by the individual experiments in Figure 14.4, where the common CR and BEC errors have been imposed.

Experimentally, separate  $m_W$  measurements are obtained from the  $W^+W^- \rightarrow q\bar{q}\ell\bar{\nu}_\ell$  and  $W^+W^- \rightarrow q\bar{q}q\bar{q}$  channels for each of the years of data. The combination using only the  $q\bar{q}\ell\bar{\nu}_\ell$  measurements yields:

$$m_W^{\text{indep}}(W^+W^- \rightarrow q\bar{q}\ell\bar{\nu}_\ell) = 80.413 \pm 0.032(\text{stat.}) \pm 0.031(\text{syst.}) \text{ GeV}.$$

The systematic error is dominated by hadronisation uncertainties ( $\pm 19 \text{ MeV}$ ) and the uncertainty in the LEP beam energy ( $\pm 17 \text{ MeV}$ ). The combination using only the  $q\bar{q}q\bar{q}$  measurements gives:

$$m_W^{\text{indep}}(W^+W^- \rightarrow q\bar{q}q\bar{q}) = 80.411 \pm 0.035(\text{stat.}) \pm 0.107(\text{syst.}) \text{ GeV}.$$

where the dominant contributions to the systematic error are from CR ( $\pm 90 \text{ MeV}$ ) and BEC ( $\pm 35 \text{ MeV}$ ).

## 14.6 LEP Combined W Boson Width

The method of direct reconstruction is also well suited to the direct measurement of the width of the W boson. The results of the four LEP experiments are shown in Table 14.4 and in Figure 14.3.

Experiment	$\Gamma_W$ (GeV)
ALEPH	$2.13 \pm 0.11 \pm 0.09$
DELPHI	$2.11 \pm 0.10 \pm 0.07$
L3	$2.24 \pm 0.11 \pm 0.15$
OPAL	$2.04 \pm 0.16 \pm 0.09$

Table 14.4: Preliminary W width measurements ( $\sqrt{s} = 172 - 209$  GeV) from the individual experiments. The first error is statistical and the second systematic.

Each experiment provided a W width measurement for both  $W^+W^- \rightarrow q\bar{q}\ell\bar{\nu}_\ell$  and  $W^+W^- \rightarrow q\bar{q}q\bar{q}$  channels for each of the data taking years (1996-2000) that it has analysed. A total of 25 measurements are supplied: ALEPH provided 3  $W^+W^- \rightarrow q\bar{q}q\bar{q}$  results (1998-2000) and two  $W^+W^- \rightarrow q\bar{q}\ell\bar{\nu}_\ell$  results (1998-1999), DELPHI 8 measurements (1997-2000), L3 8 measurements (1996-2000) having already combined the 1996 and 1997 results and OPAL provided 4 measurements (1996-1998) where for the first two years the  $W^+W^- \rightarrow q\bar{q}\ell\bar{\nu}_\ell$  and  $W^+W^- \rightarrow q\bar{q}q\bar{q}$  results are already combined.

A common colour reconnection error of 65 MeV and a common Bose-Einstein correlation error of 35 MeV are used in the combination. These common errors were determined such that the same error was obtained on  $\Gamma_W$  as when using the BEC/CR errors supplied by the experiments. The change in the value of the width is only 2 MeV. The BEC and CR values supplied by the experiments were based on studies of phenomenological models of these effects, the uncertainty has not yet been determined from the particle flow measurements of colour reconnection.

A simultaneous fit to the results of the four LEP collaborations is performed in the same way as for the  $m_W$  measurement. Correlated systematic uncertainties are taken into account and the combination gives:

$$\Gamma_W = 2.150 \pm 0.068(\text{stat.}) \pm 0.060(\text{syst.}) \text{ GeV}, \quad (14.5)$$

with a  $\chi^2/\text{d.o.f.}$  of 19.7/24, corresponding to a  $\chi^2$  probability of 71%.

## 14.7 Summary

The results of the four LEP experiments on the mass and width of the W boson are combined taking into account correlated systematic uncertainties, giving:

$$\begin{aligned} m_W &= 80.412 \pm 0.042 \text{ GeV}, \\ \Gamma_W &= 2.150 \pm 0.091 \text{ GeV}. \end{aligned}$$

The statistical correlation between mass and width is small and neglected. Their correlation due to common systematic effects is under study.

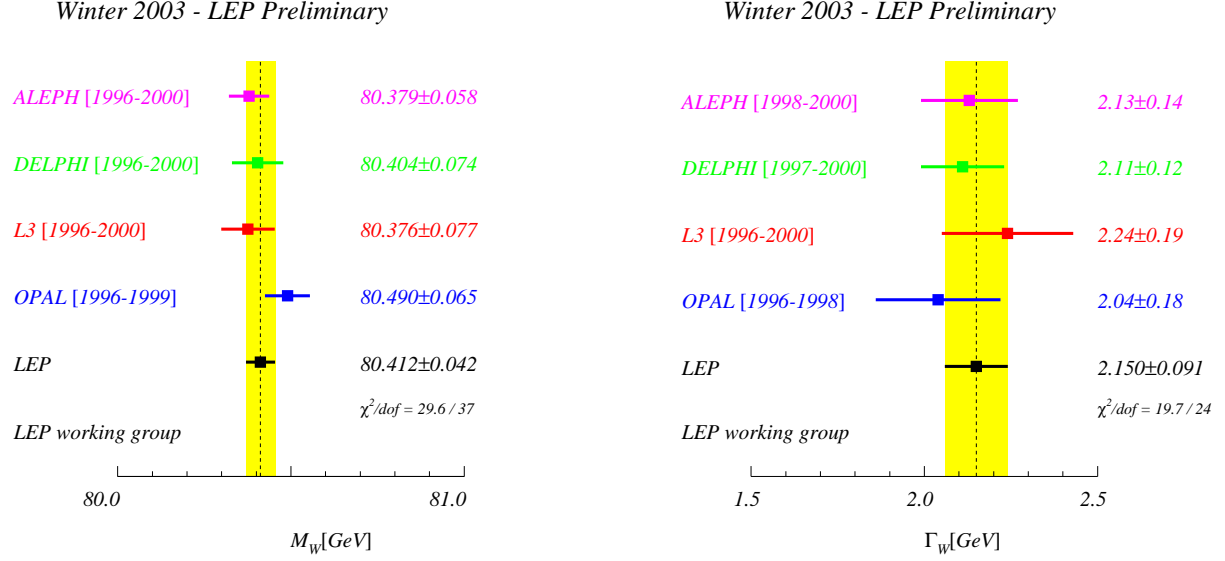


Figure 14.3: The combined results for the measurements of the W mass (left) and W width (right) compared to the results obtained by the four LEP collaborations. The combined values take into account correlations between experiments and years and hence, in general, do not give the same central value as a simple average. In the LEP combination of the  $q\bar{q}q\bar{q}$  results common values (see text) for the CR and BEC errors are used. The individual and combined  $m_W$  results include the measurements from the threshold cross section. The  $m_W$  values from the experiments have been recalculated for this plot including the common LEP CR and BEC errors.

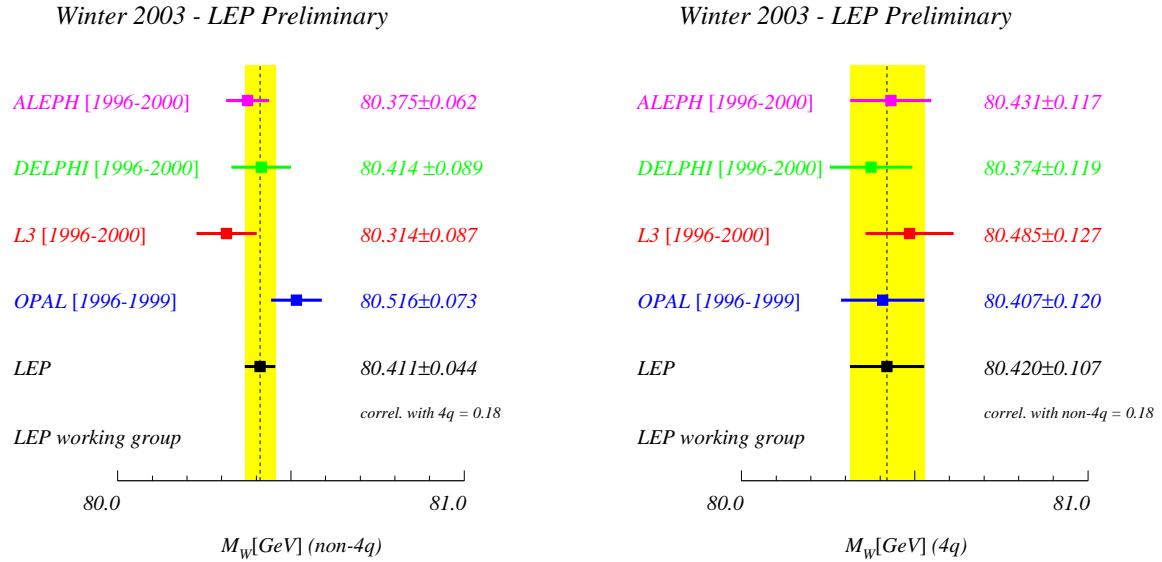


Figure 14.4: The W mass measurements from the  $W^+W^- \rightarrow q\bar{q}\ell\bar{\nu}_\ell$  (left) and  $W^+W^- \rightarrow q\bar{q}q\bar{q}$  (right) channels obtained by the four LEP collaborations compared to the combined value. The combined values take into account correlations between experiments, years and the two channels. In the LEP combination of the  $q\bar{q}q\bar{q}$  results common values (see text) for the CR and BEC errors are used. The ALEPH and L3  $q\bar{q}\ell\bar{\nu}_\ell$  and  $q\bar{q}q\bar{q}$  results are correlated since they are obtained from a fit to both channels taking into account inter-channel correlations. The  $m_W$  values from the experiments have been recalculated for this plot including the common LEP CR and BEC errors.

# Chapter 15

## Effective Couplings of the Neutral Weak Current

**Updates with respect to summer 2002:**  
 Unchanged w.r.t. summer 2002: Results are preliminary.

### 15.1 The Coupling Parameters $\mathcal{A}_f$

The coupling parameters  $\mathcal{A}_f$  are defined in terms of the effective vector and axial-vector neutral current couplings of fermions (Equation (2.4)). The LEP measurements of the forward-backward asymmetries of charged leptons (Chapter 2) and b and c quarks (Chapter 5) determine the products  $A_{\text{FB}}^{0,f} = \frac{3}{4}\mathcal{A}_e\mathcal{A}_f$  (Equation (2.3)). The LEP measurements of the  $\tau$  polarisation (Chapter 3),  $\mathcal{P}_\tau(\cos\theta)$ , determine  $\mathcal{A}_\tau$  and  $\mathcal{A}_e$  separately (Equation (3.2)). Owing to polarised beams at SLC, SLD measures the coupling parameters directly with the left-right and forward-backward left-right asymmetries (Chapters 4 and 5).

Table 15.1 shows the results for the leptonic coupling parameter  $\mathcal{A}_\ell$  from the LEP and SLD measurements, assuming lepton universality.

Using the measurements of  $\mathcal{A}_\ell$  one can extract  $\mathcal{A}_b$  and  $\mathcal{A}_c$  from the LEP measurements of the b and c quark asymmetries. The SLD measurements of the left-right forward-backward asymmetries for b and c quarks are direct determinations of  $\mathcal{A}_b$  and  $\mathcal{A}_c$ . Table 15.2 shows the results on the

	$\mathcal{A}_\ell$	Cumulative Average	$\chi^2/\text{d.o.f.}$
$A_{\text{FB}}^{0,\ell}$	$0.1512 \pm 0.0042$		
$\mathcal{P}_\tau$	$0.1465 \pm 0.0033$	$0.1482 \pm 0.0026$	0.8/1
$\mathcal{A}_\ell$ (SLD)	$0.1513 \pm 0.0021$	$0.1501 \pm 0.0016$	1.6/2

Table 15.1: Determination of the leptonic coupling parameter  $\mathcal{A}_\ell$  assuming lepton universality. The second column lists the  $\mathcal{A}_\ell$  values derived from the quantities listed in the first column. The third column contains the cumulative averages of the  $\mathcal{A}_\ell$  results up to and including this line. The  $\chi^2$  per degree of freedom for the cumulative averages is given in the last column.

	LEP ( $\mathcal{A}_\ell = 0.1482 \pm 0.0026$ )	SLD	LEP+SLD ( $\mathcal{A}_\ell = 0.1501 \pm 0.0016$ )	Standard Model fit
$\mathcal{A}_b$	$0.894 \pm 0.022$	$0.922 \pm 0.020$	$0.901 \pm 0.013$	0.935
$\mathcal{A}_c$	$0.639 \pm 0.034$	$0.670 \pm 0.026$	$0.656 \pm 0.021$	0.668

Table 15.2: Determination of the quark coupling parameters  $\mathcal{A}_b$  and  $\mathcal{A}_c$  from LEP data alone (using the LEP average for  $\mathcal{A}_\ell$ ), from SLD data alone, and from LEP+SLD data (using the LEP+SLD average for  $\mathcal{A}_\ell$ ) assuming lepton universality.

quark coupling parameters  $\mathcal{A}_b$  and  $\mathcal{A}_c$  derived from LEP measurements (Equations 5.6) and SLD measurements separately, and from the combination of LEP+SLD measurements (Equation 5.7).

The LEP extracted values of  $\mathcal{A}_b$  and  $\mathcal{A}_c$  are in agreement with the SLD measurements, but somewhat lower than the Standard Model predictions (0.935 and 0.668, respectively, essentially independent of  $m_t$  and  $m_H$ ). The combination of LEP and SLD of  $\mathcal{A}_b$  is 2.6 sigma below the Standard Model, while  $\mathcal{A}_c$  agrees well with the expectation. This is mainly because the  $\mathcal{A}_b$  value, deduced from the measured  $A_{FB}^{0,b}$  and the combined  $\mathcal{A}_\ell$ , is significantly lower than both the Standard Model and the direct measurement of  $\mathcal{A}_b$ , this can also be seen in Figure 15.1.

## 15.2 The Effective Vector and Axial-Vector Coupling Constants

The partial widths of the Z into leptons and the lepton forward-backward asymmetries (Section 2), the  $\tau$  polarisation and the  $\tau$  polarisation asymmetry (Section 3) are combined to determine the effective vector and axial-vector couplings for e,  $\mu$  and  $\tau$ . The asymmetries (Equations (2.3) and (3.2)) determine the ratio  $g_{V\ell}/g_{A\ell}$  (Equation (2.4)), while the leptonic partial widths determine the sum of the squares of the couplings:

$$\Gamma_{\ell\ell} = \frac{G_F m_Z^3}{6\pi\sqrt{2}} (g_{V\ell}^2 + g_{A\ell}^2) (1 + \delta_\ell^{QED}), \quad (15.1)$$

where  $\delta_\ell^{QED} = 3q_\ell^2\alpha(m_Z^2)/(4\pi)$ , with  $q_\ell$  denoting the electric charge of the lepton, accounts for final state photonic corrections. Corrections due to lepton masses, neglected in Equation 15.1, are taken into account for the results presented below.

The averaged results for the effective lepton couplings are given in Table 15.3 for both the LEP data alone as well as for the LEP and SLD measurements. Figure 15.2 shows the 68% probability contours in the  $g_{A\ell}$ - $g_{V\ell}$  plane for the individual lepton species. The signs of  $g_{A\ell}$  and  $g_{V\ell}$  are based on the convention  $g_{Ae} < 0$ . With this convention the signs of the couplings of all charged leptons follow from LEP data alone. The measured ratios of the e,  $\mu$  and  $\tau$  couplings provide a test of lepton universality and are shown in Table 15.3. All values are consistent with lepton universality. The combined results assuming universality are also given in the table and are shown as a solid contour in Figure 15.2.

The neutrino couplings to the Z can be derived from the measured value of the invisible width of the Z,  $\Gamma_{\text{inv}}$  (see Table 2.4), attributing it exclusively to the decay into three identical neutrino generations ( $\Gamma_{\text{inv}} = 3\Gamma_{\nu\nu}$ ) and assuming  $g_{A\nu} \equiv g_{V\nu} \equiv g_\nu$ . The relative sign of  $g_\nu$  is chosen to be in agreement with neutrino scattering data [267], resulting in  $g_\nu = +0.50068 \pm 0.00075$ .

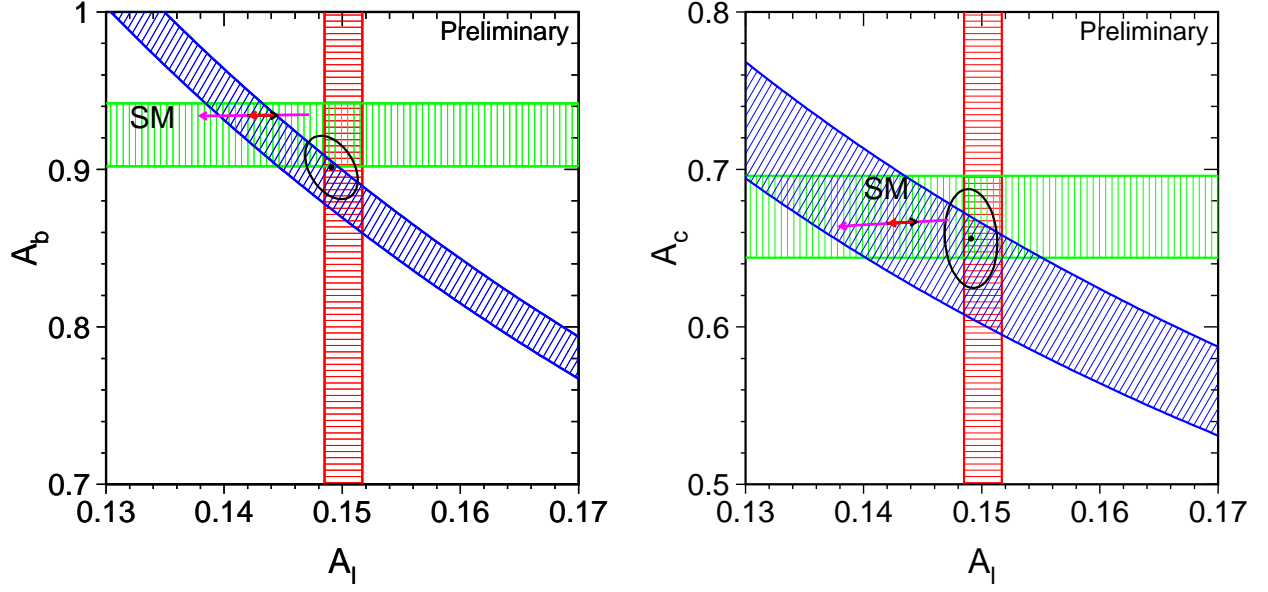


Figure 15.1: The measurements of the combined LEP+SLD  $\mathcal{A}_\ell$  (vertical band), SLD  $\mathcal{A}_b, \mathcal{A}_c$  (horizontal bands) and LEP  $A_{\text{FB}}^{0,b}, A_{\text{FB}}^{0,c}$  (diagonal bands), compared to the Standard Model expectations (arrows). The arrow pointing to the left shows the variation in the Standard Model prediction for  $m_H$  in the range  $300_{-186}^{+700}$  GeV, and the arrow pointing to the right for  $m_t$  in the range  $174.3 \pm 5.1$  GeV. Varying the hadronic vacuum polarisation by  $\Delta\alpha_{\text{had}}^{(5)}(m_Z^2) = 0.02761 \pm 0.00036$  yields an additional uncertainty on the Standard Model prediction, oriented in direction of the Higgs-boson arrow and size corresponding to the top-quark arrow. Also shown is the 68% confidence level contour for the two asymmetry parameters resulting from the joint analyses. Although the  $A_{\text{FB}}^{0,b}$  measurements prefer a high Higgs mass, the Standard Model fit to the full set of measurements prefers a low Higgs mass, for example because of the influence of  $\mathcal{A}_\ell$ .

In addition, the couplings analysis is extended to include also the heavy-flavour measurements as presented in Section 5.3. Assuming neutral-current lepton universality, the effective coupling constants are determined jointly for leptons as well as for b and c quarks. QCD corrections, modifying Equation 15.1, are taken from the Standard Model, as is also done to obtain the quark pole asymmetries, see Section 5.2.3.

The results are also reported in Table 15.3 and shown in Figure 15.3. The deviation of the b-quark couplings from the Standard Model expectation is mainly caused by the combined value of  $\mathcal{A}_b$  being low as discussed in Section 15.1 and shown in Figure 15.1.

	Without Lepton Universality:	
	LEP	LEP+SLD
$g_{Ae}$	$-0.50112 \pm 0.00035$	$-0.50111 \pm 0.00035$
$g_{A\mu}$	$-0.50115 \pm 0.00056$	$-0.50120 \pm 0.00054$
$g_{A\tau}$	$-0.50204 \pm 0.00064$	$-0.50204 \pm 0.00064$
$g_{Ve}$	$-0.0378 \pm 0.0011$	$-0.03816 \pm 0.00047$
$g_{V\mu}$	$-0.0376 \pm 0.0031$	$-0.0367 \pm 0.0023$
$g_{V\tau}$	$-0.0368 \pm 0.0011$	$-0.0366 \pm 0.0010$
	Ratios of couplings:	
	LEP	LEP+SLD
$g_{A\mu}/g_{Ae}$	$1.0001 \pm 0.0014$	$1.0002 \pm 0.0014$
$g_{A\tau}/g_{Ae}$	$1.0018 \pm 0.0015$	$1.0019 \pm 0.0015$
$g_{V\mu}/g_{Ve}$	$0.995 \pm 0.096$	$0.962 \pm 0.063$
$g_{V\tau}/g_{Ve}$	$0.972 \pm 0.041$	$0.958 \pm 0.029$
	With Lepton Universality:	
	LEP	LEP+SLD
$g_{A\ell}$	$-0.50126 \pm 0.00026$	$-0.50123 \pm 0.00026$
$g_{V\ell}$	$-0.03736 \pm 0.00066$	$-0.03783 \pm 0.00041$
$g_{\nu}$	$+0.50068 \pm 0.00075$	$+0.50068 \pm 0.00075$
	With Lepton Universality and Heavy Flavour Results:	
	LEP	LEP+SLD
$g_{A\ell}$	$-0.50126 \pm 0.00026$	$-0.50125 \pm 0.00026$
$g_{Ab}$	$-0.5166 \pm 0.0080$	$-0.5140 \pm 0.0051$
$g_{Ac}$	$+0.5002 \pm 0.0082$	$+0.5027 \pm 0.0054$
$g_{V\ell}$	$-0.03736 \pm 0.00066$	$-0.03758 \pm 0.00037$
$g_{Vb}$	$-0.319 \pm 0.013$	$-0.3231 \pm 0.0078$
$g_{Vc}$	$+0.181 \pm 0.011$	$+0.1880 \pm 0.0070$

Table 15.3: Results for the effective vector and axial-vector couplings derived from the LEP data and the combined LEP and SLD data without and with the assumption of lepton universality. Note that the results, in particular for b quarks, are highly correlated.

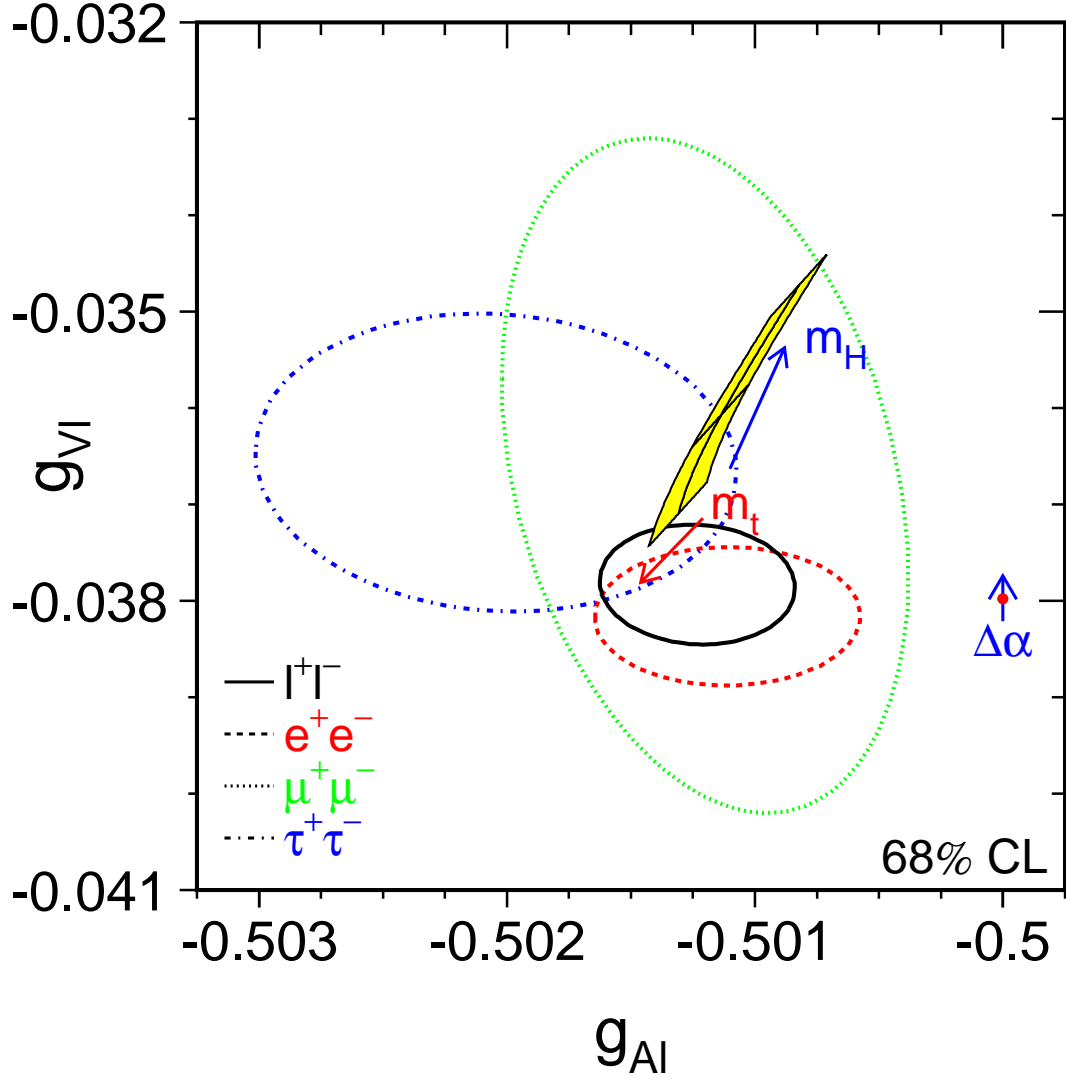


Figure 15.2: Contours of 68% probability in the  $(g_{V\ell}, g_{A\ell})$  plane from LEP and SLD measurements. The solid contour results from a fit to the LEP and SLD results assuming lepton universality. The shaded region corresponds to the Standard Model prediction for  $m_t = 174.3 \pm 5.1$  GeV and  $m_H = 300^{+700}_{-186}$  GeV. The arrows point in the direction of increasing values of  $m_t$  and  $m_H$ . Varying the hadronic vacuum polarisation by  $\Delta\alpha_{\text{had}}^{(5)}(m_Z^2) = 0.02761 \pm 0.00036$  yields an additional uncertainty on the Standard Model prediction indicated by the corresponding arrow.



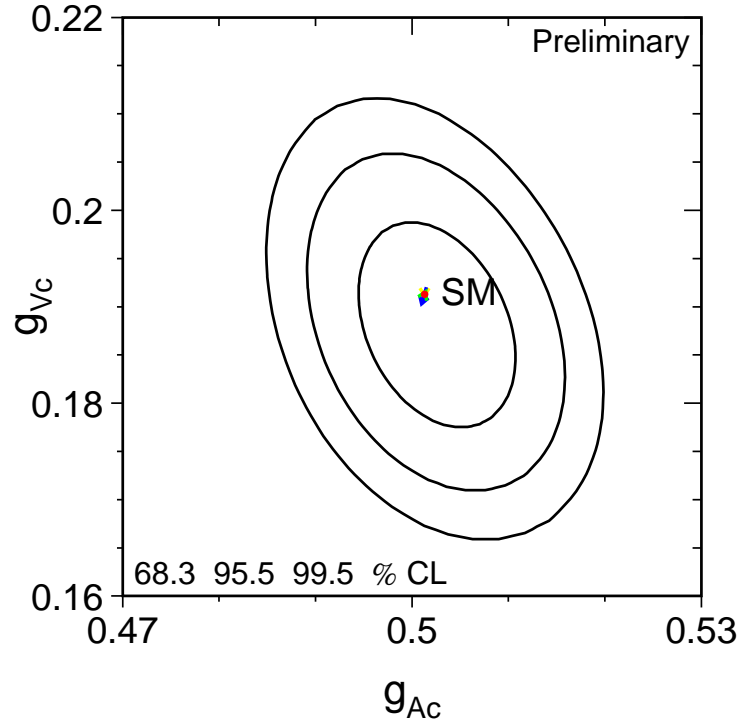
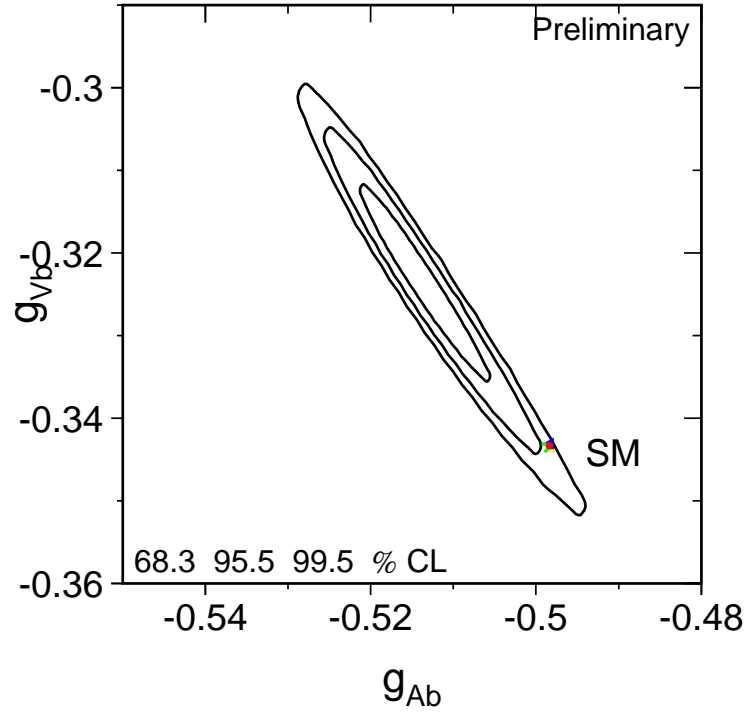


Figure 15.3: Contours of 68.3, 95.5 and 99.5% probability in the  $(g_{Vq}, g_{Aq})$  plane from LEP and SLD measurements for b and c quarks and assuming lepton universality. The dot corresponds to the Standard Model prediction for  $m_t = 174.3 \pm 5.1$  GeV,  $m_H = 300^{+700}_{-186}$  GeV and  $\Delta\alpha_{\text{had}}^{(5)}(m_Z^2) = 0.02761 \pm 0.00036$ .

### 15.3 The Leptonic Effective Electroweak Mixing Angle $\sin^2 \theta_{\text{eff}}^{\text{lept}}$

The asymmetry measurements from LEP and SLD can be combined into a single parameter, the effective electroweak mixing angle,  $\sin^2 \theta_{\text{eff}}^{\text{lept}}$ , defined as:

$$\sin^2 \theta_{\text{eff}}^{\text{lept}} \equiv \frac{1}{4} \left( 1 - \frac{g_{V\ell}}{g_{A\ell}} \right), \quad (15.2)$$

without making strong model-specific assumptions.

For a combined average of  $\sin^2 \theta_{\text{eff}}^{\text{lept}}$  from  $A_{\text{FB}}^{0,\ell}$ ,  $\mathcal{A}_\tau$  and  $\mathcal{A}_e$  only the assumption of lepton universality, already inherent in the definition of  $\sin^2 \theta_{\text{eff}}^{\text{lept}}$ , is needed. Also the value derived from the measurements of  $\mathcal{A}_\ell$  from SLD is given. We also include the hadronic forward-backward asymmetries, assuming the difference between  $\sin^2 \theta_{\text{eff}}^{\text{f}}$  for quarks and leptons to be given by the Standard Model. This is justified within the Standard Model as the hadronic asymmetries  $A_{\text{FB}}^{0,\text{b}}$  and  $A_{\text{FB}}^{0,\text{c}}$  have a reduced sensitivity to the small non-universal corrections specific to the quark vertex. The results of these determinations of  $\sin^2 \theta_{\text{eff}}^{\text{lept}}$  and their combination are shown in Table 15.4 and in Figure 15.4. The combinations based on the leptonic results plus  $\mathcal{A}_\ell$  (SLD) and on the hadronic forward-backward asymmetries differ by 2.9 standard deviations, caused by the two most precise measurements of  $\sin^2 \theta_{\text{eff}}^{\text{lept}}$ ,  $\mathcal{A}_\ell$  (SLD) dominated by  $A_{\text{LR}}^0$ , and  $A_{\text{FB}}^{0,\text{b}}$  (LEP), likewise differing by 2.9 standard deviations. This is the same effect as discussed already in sections 15.1 and 15.2 and shown in Figures 15.1 and 15.3: the deviation in  $\mathcal{A}_{\text{b}}$  as extracted from  $A_{\text{FB}}^{0,\text{b}}$  discussed above is reflected in the value of  $\sin^2 \theta_{\text{eff}}^{\text{lept}}$  extracted from  $A_{\text{FB}}^{0,\text{b}}$  in this analysis.

	$\sin^2 \theta_{\text{eff}}^{\text{lept}}$	Average by Group of Observations	Cumulative Average	$\chi^2/\text{d.o.f.}$
$A_{\text{FB}}^{0,\ell}$	$0.23099 \pm 0.00053$			
$\mathcal{A}_\ell (\mathcal{P}_\tau)$	$0.23159 \pm 0.00041$	$0.23137 \pm 0.00033$		0.8/1
$\mathcal{A}_\ell$ (SLD)	$0.23098 \pm 0.00026$		$0.23113 \pm 0.00021$	1.6/2
$A_{\text{FB}}^{0,\text{b}}$	$0.23217 \pm 0.00031$			
$A_{\text{FB}}^{0,\text{c}}$	$0.23206 \pm 0.00084$			
$\langle Q_{\text{FB}} \rangle$	$0.2324 \pm 0.0012$	$0.23217 \pm 0.00029$	$0.23148 \pm 0.00017$	10.2/5

Table 15.4: Determinations of  $\sin^2 \theta_{\text{eff}}^{\text{lept}}$  from asymmetries. The second column lists the  $\sin^2 \theta_{\text{eff}}^{\text{lept}}$  values derived from the quantities listed in the first column. The third column contains the averages of these numbers by groups of observations, where the groups are separated by the horizontal lines. The fourth column shows the cumulative averages. The  $\chi^2$  per degree of freedom for the cumulative averages is also given. The averages are performed including the small correlation between  $A_{\text{FB}}^{0,\text{b}}$  and  $A_{\text{FB}}^{0,\text{c}}$ . The average of all six results has a probability of 7.0%.

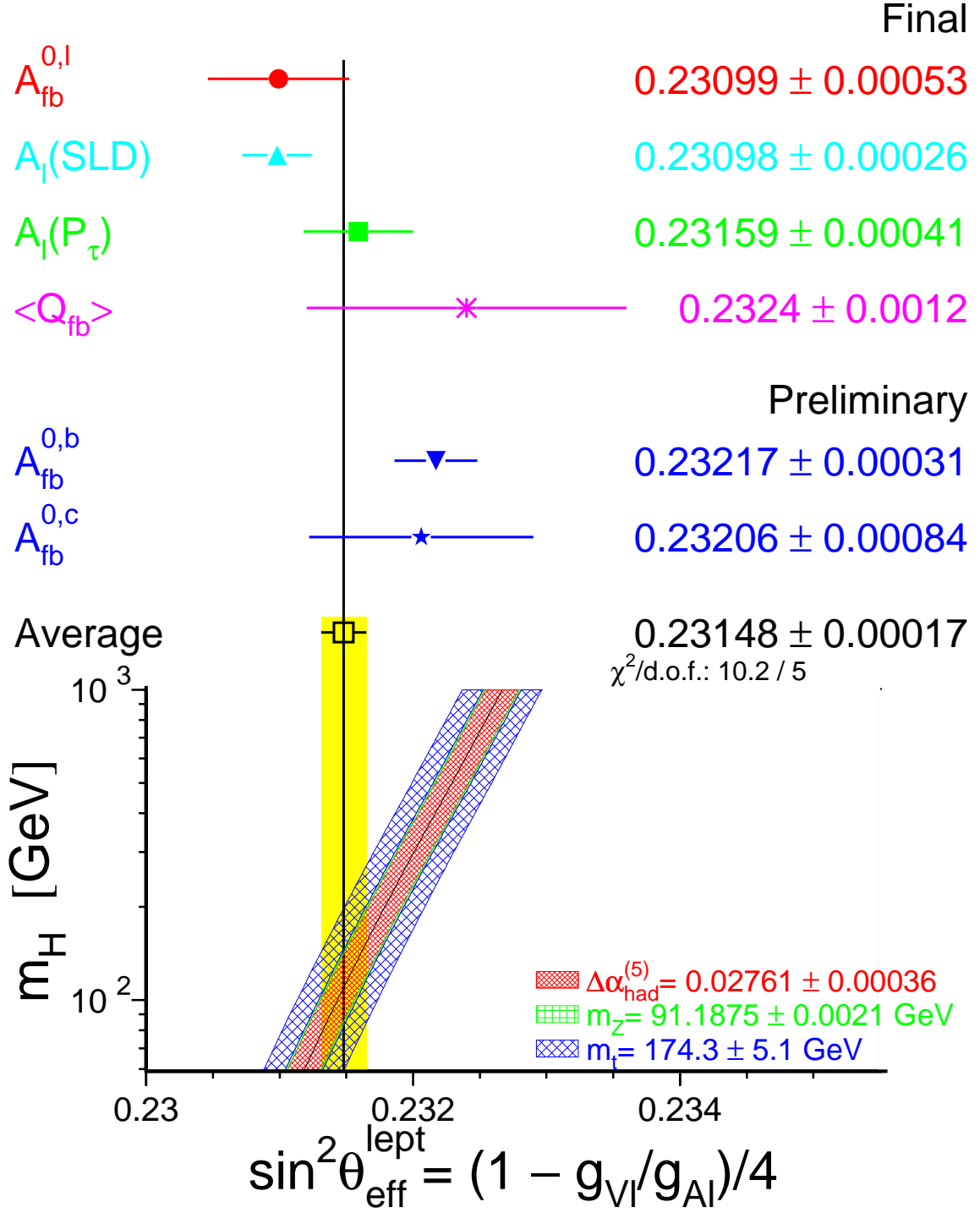


Figure 15.4: Comparison of several determinations of  $\sin^2 \theta_{\text{eff}}^{\text{lept}}$  from asymmetries. In the average, the small correlation between  $A_{FB}^{0,b}$  and  $A_{FB}^{0,c}$  is included. Also shown is the prediction of the Standard Model as a function of  $m_H$ . The width of the Standard Model band is due to the uncertainties in  $\Delta\alpha_{\text{had}}^{(5)}(m_Z^2)$  (see Chapter 16),  $m_Z$  and  $m_t$ . The total width of the band is the linear sum of these effects.

# Chapter 16

## Constraints on the Standard Model

### Updates with respect to summer 2002:

Updated preliminary and published measurements as discussed in the previous chapters are taken into account, as well as new corrections in the measurement of atomic parity violation in Caesium.

### 16.1 Introduction

The precise electroweak measurements performed at LEP and SLC and elsewhere can be used to check the validity of the Standard Model and, within its framework, to infer valuable information about its fundamental parameters. The accuracy of the measurements makes them sensitive to the mass of the top quark  $m_t$ , and to the mass of the Higgs boson  $m_H$  through loop corrections. While the leading  $m_t$  dependence is quadratic, the leading  $m_H$  dependence is logarithmic. Therefore, the inferred constraints on  $m_H$  are much weaker than those on  $m_t$ .

### 16.2 Measurements

The LEP and SLD measurements used are summarised in Table 16.1. Also shown are the results of the Standard Model fit to all results.

The final results on the W-boson mass by UA2 [268] and CDF [269,270] and DØ [271] in Run-I, and the W-boson width by CDF [272] and DØ [273] in Run-I were recently combined based on a detailed treatment of common systematic uncertainties. The results are [274]:  $m_W = 80454 \pm 59$  MeV,  $\Gamma_W = 2115 \pm 106$  MeV, with a correlation of  $-17.4\%$ . Combining these results with the updated preliminary LEP-2 measurements as presented in Chapter 14, the new preliminary world averages used in the following analyses are:

$$m_W = 80.426 \pm 0.034 \text{ GeV} \quad (16.1)$$

$$\Gamma_W = 2.139 \pm 0.069 \text{ GeV} \quad (16.2)$$

with a correlation of  $-6.7\%$ .

For the mass of the top quark,  $m_t$ , the results from CDF [275] and DØ [276] are combined<sup>1</sup>, with the result  $m_t = 174.3 \pm 5.1$  GeV. In addition, the recently published final result of the NuTeV collaboration

---

<sup>1</sup>See Reference 277 for a combination of these  $m_t$  measurements.

on neutrino-nucleon neutral to charged current cross section ratios [278], and the measurements of atomic parity violation in caesium [279, 280], with the numerical result [281] taken from a revised analysis of QED radiative corrections [281, 282] applied to the raw measurement, are included in some of the analyses shown below.

Although the  $\nu\mathcal{N}$  result is quoted in terms of  $\sin^2 \theta_W = 1 - m_W^2/m_Z^2 = 0.2277 \pm 0.0016$ , radiative corrections result in small  $m_t$  and  $m_H$  dependences<sup>2</sup> that are included in the fit. Note that the NuTeV result in terms of the on-shell electroweak mixing angle is 2.9 standard deviations higher than the expectation.

An additional input parameter, not shown in the table, is the Fermi constant  $G_F$ , determined from the  $\mu$  lifetime,  $G_F = 1.16637(1) \cdot 10^{-5} \text{GeV}^{-2}$  [283]. The relative error of  $G_F$  is comparable to that of  $m_Z$ ; both errors have negligible effects on the fit results.

## 16.3 Theoretical and Parametric Uncertainties

Detailed studies of the theoretical uncertainties in the Standard Model predictions due to missing higher-order electroweak corrections and their interplay with QCD corrections are carried out by the working group on ‘Precision calculations for the Z resonance’ [287], and more recently in [15]. Theoretical uncertainties are evaluated by comparing different but, within our present knowledge, equivalent treatments of aspects such as resummation techniques, momentum transfer scales for vertex corrections and factorisation schemes. The effects of these theoretical uncertainties are reduced by the inclusion of higher-order corrections [288, 289] in the electroweak libraries [290].

The recently calculated complete fermionic two-loop corrections on  $m_W$  [291] are currently only used in the determination of the theoretical uncertainty. Their effect on  $m_W$  is small compared to the current experimental uncertainty on  $m_W$ . However, the naive propagation of this new  $m_W$  to  $\sin^2 \theta_{\text{eff}}^{\text{lept}} = \kappa(1 - m_W^2/m_Z^2)$ , keeping the electroweak form-factor  $\kappa$  unmodified, shows a more visible effect as  $\sin^2 \theta_{\text{eff}}^{\text{lept}}$  is measured very precisely. Thus the corresponding calculations for  $\sin^2 \theta_{\text{eff}}^{\text{lept}}$  (or  $\kappa$ ) and for the partial Z widths are urgently needed; in particular since partial cancellations of these new corrections in the product  $\kappa(1 - m_W^2/m_Z^2) = \sin^2 \theta_{\text{eff}}^{\text{lept}}$  could be expected [292].

The use of the QCD corrections [289] increases the value of  $\alpha_S(m_Z^2)$  by 0.001, as expected. The effects of missing higher-order QCD corrections on  $\alpha_S(m_Z^2)$  covers missing higher-order electroweak corrections and uncertainties in the interplay of electroweak and QCD corrections and is estimated to be at least 0.002 [293]. A discussion of theoretical uncertainties in the determination of  $\alpha_S$  can be found in References 287 and 293. The determination of the size of remaining theoretical uncertainties is under continued study.

The theoretical errors discussed above are not included in the results presented in Table 16.2. At present the impact of theoretical uncertainties on the determination of Standard Model parameters from the precise electroweak measurements is small compared to the error due to the uncertainty in the value of  $\alpha(m_Z^2)$ , which is included in the results.

The uncertainty in  $\alpha(m_Z^2)$  arises from the contribution of light quarks to the photon vacuum

---

<sup>2</sup>The formula used is  $\delta \sin^2 \theta_W = -0.00022 \frac{m_t^2 - (175 \text{GeV})^2}{(50 \text{GeV})^2} + 0.00032 \ln(\frac{m_H}{150 \text{GeV}})$ . See Reference 278 for details.

	Measurement with Total Error	Systematic Error	Standard Model fit	Pull
$\Delta\alpha_{\text{had}}^{(5)}(m_Z^2)$ [284]	$0.02761 \pm 0.00036$	0.00035	0.02769	−0.2
a) <u>LEP</u> line-shape and lepton asymmetries: $m_Z$ [GeV] $\Gamma_Z$ [GeV] $\sigma_h^0$ [nb] $R_\ell^0$ $A_{\text{FB}}^{0,\ell}$ + correlation matrix Table 2.3  $\tau$ polarisation: $\mathcal{A}_\ell(\mathcal{P}_\tau)$  q $\bar{q}$ charge asymmetry: $\sin^2\theta_{\text{eff}}^{\text{lept}} (\langle Q_{\text{FB}} \rangle)$	$91.1875 \pm 0.0021$ $2.4952 \pm 0.0023$ $41.540 \pm 0.037$ $20.767 \pm 0.025$ $0.0171 \pm 0.0010$  $0.1465 \pm 0.0033$  $0.2324 \pm 0.0012$	$^{(a)}0.0017$ $^{(a)}0.0012$ $^{(b)}0.028$ $^{(b)}0.007$ $^{(b)}0.0003$  0.0016  0.0010	91.1875 2.4960 41.478 20.742 0.0164  0.1478  0.2314	0.0 −0.4 1.7 1.0 0.8  −0.4  0.8
b) <u>SLD</u> [285] $\mathcal{A}_\ell$ (SLD)	$0.1513 \pm 0.0021$	0.0010	0.1478	1.7
c) <u>LEP and SLD Heavy Flavour</u> $R_b^0$ $R_c^0$ $A_{\text{FB}}^{0,b}$ $A_{\text{FB}}^{0,c}$ $\mathcal{A}_b$ $\mathcal{A}_c$ + correlation matrix Table 5.3	$0.21644 \pm 0.00065$ $0.1718 \pm 0.0031$ $0.0995 \pm 0.0017$ $0.0713 \pm 0.0036$ $0.922 \pm 0.020$ $0.670 \pm 0.026$	0.00053 0.0022 0.0009 0.0017 0.016 0.016	0.21579 0.1723 0.1036 0.0741 0.935 0.668	1.0 −0.1 −2.4 −0.8 −0.6 0.1
d) <u>Additional</u> $m_W$ [GeV] (p $\bar{p}$ and LEP-2) $\Gamma_W$ [GeV] (p $\bar{p}$ and LEP-2) $\sin^2\theta_W$ ( $\nu\mathcal{N}$ [278]) $m_t$ [GeV] (p $\bar{p}$ [277]) $Q_W(\text{Cs})$ [286]	$80.426 \pm 0.034$ $2.139 \pm 0.069$ $0.2277 \pm 0.0016$ $174.3 \pm 5.1$ $-72.83 \pm 0.49$	  0.0009 4.0 0.39	80.386 2.093 0.2229 174.0 −72.89	1.2 0.7 2.9 0.1 0.1

Table 16.1: Summary of measurements included in the combined analysis of Standard Model parameters. Section a) summarises LEP averages, Section b) SLD results ( $\sin^2\theta_{\text{eff}}^{\text{lept}}$  includes  $A_{\text{LR}}$  and the polarised lepton asymmetries), Section c) the LEP and SLD heavy flavour results and Section d) electroweak measurements from p $\bar{p}$  colliders and  $\nu\mathcal{N}$  scattering. The total errors in column 2 include the systematic errors listed in column 3. Although the systematic errors include both correlated and uncorrelated sources, the determination of the systematic part of each error is approximate. The Standard Model results in column 4 and the pulls (difference between measurement and fit in units of the total measurement error) in column 5 are derived from the Standard Model fit including all data (Table 16.2, column 5) with the Higgs mass treated as a free parameter.

<sup>(a)</sup>The systematic errors on  $m_Z$  and  $\Gamma_Z$  contain the errors arising from the uncertainties in the LEP energy only.

<sup>(b)</sup>Only common systematic errors are indicated.

polarisation ( $\Delta\alpha_{\text{had}}^{(5)}(m_Z^2)$ ):

$$\alpha(m_Z^2) = \frac{\alpha(0)}{1 - \Delta\alpha_\ell(m_Z^2) - \Delta\alpha_{\text{had}}^{(5)}(m_Z^2) - \Delta\alpha_{\text{top}}(m_Z^2)}, \quad (16.3)$$

where  $\alpha(0) = 1/137.036$ . The top contribution,  $-0.00007(1)$ , depends on the mass of the top quark, and is therefore determined inside the electroweak libraries [290]. The leptonic contribution is calculated to third order [294] to be 0.03150, with negligible uncertainty.

For the hadronic contribution, we no longer use the value  $0.02804 \pm 0.00065$  [295], but rather the new evaluation  $0.02761 \pm 0.00036$  [284] which takes into account the recently published results on electron-positron annihilations into hadrons at low centre-of-mass energies by the BES collaboration [296]. This reduced uncertainty still causes an error of 0.00013 on the Standard Model prediction of  $\sin^2 \theta_{\text{eff}}^{\text{lept}}$ , and errors of 0.2 GeV and 0.1 on the fitted values of  $m_t$  and  $\log(m_H)$ , included in the results presented below. The effect on the Standard Model prediction for  $\Gamma_{\ell\ell}$  is negligible. The  $\alpha_S(m_Z^2)$  values for the Standard Model fits presented here are stable against a variation of  $\alpha(m_Z^2)$  in the interval quoted.

There are also several evaluations of  $\Delta\alpha_{\text{had}}^{(5)}(m_Z^2)$  [297–305] which are more theory-driven. One of the most recent of these (Reference 305) also includes the new results from BES, yielding  $0.02747 \pm 0.00012$ . To show the effects of the uncertainty of  $\alpha(m_Z^2)$ , we also use this evaluation of the hadronic vacuum polarisation. Note that all these evaluations obtain values for  $\Delta\alpha_{\text{had}}^{(5)}(m_Z^2)$  consistently lower than - but still in agreement with - the old value of  $0.02804 \pm 0.00065$ .

## 16.4 Selected Results

Figure 16.1 shows a comparison of the leptonic partial width from LEP (Table 2.4) and the effective electroweak mixing angle from asymmetries measured at LEP and SLD (Table 15.4), with the Standard Model. Good agreement with the Standard Model prediction is observed. The point with the arrow indicates the prediction if among the electroweak radiative corrections only the photon vacuum polarisation is included, which shows that LEP+SLD data are sensitive to non-trivial electroweak corrections. Note that the error due to the uncertainty on  $\alpha(m_Z^2)$  (shown as the length of the arrow) is not much smaller than the experimental error on  $\sin^2 \theta_{\text{eff}}^{\text{lept}}$  from LEP and SLD. This underlines the continued importance of a precise measurement of  $\sigma(e^+e^- \rightarrow \text{hadrons})$  at low centre-of-mass energies.

Of the measurements given in Table 16.1,  $R_\ell^0$  is one of the most sensitive to QCD corrections. For  $m_Z = 91.1875$  GeV, and imposing  $m_t = 174.3 \pm 5.1$  GeV as a constraint,  $\alpha_S = 0.1224 \pm 0.0038$  is obtained. Alternatively,  $\sigma_\ell^0$  (see Table 2.4) which has higher sensitivity to QCD corrections and less dependence on  $m_H$  yields:  $\alpha_S = 0.1180 \pm 0.0030$ . Typical errors arising from the variation of  $m_H$  between 100 GeV and 200 GeV are of the order of 0.001, somewhat smaller for  $\sigma_\ell^0$ . These results on  $\alpha_S$ , as well as those reported in the next section, are in very good agreement with recently determined world averages ( $\alpha_S(m_Z^2) = 0.118 \pm 0.002$  [306], or  $\alpha_S(m_Z^2) = 0.1178 \pm 0.0033$  based solely on NNLO QCD results excluding the LEP lineshape results and accounting for correlated errors [307]).

## 16.5 Standard Model Analyses

In the following, several different Standard Model fits to the data reported in Table 16.2 are discussed. The  $\chi^2$  minimisation is performed with the program MINUIT [139], and the predictions are calculated

with TOPAZ0 [308] and ZFITTER [37]. The somewhat increased  $\chi^2/\text{d.o.f.}$  for all of these fits is caused by the same effect as discussed in the previous chapter, namely the large dispersion in the values of the leptonic effective electroweak mixing angle measured through the various asymmetries. For the analyses presented here, this dispersion is interpreted as a fluctuation in one or more of the input measurements, and thus we neither modify nor exclude any of them. A further drastic increase in  $\chi^2/\text{d.o.f.}$  is observed when the NuTeV result on  $\sin^2 \theta_W$  is included in the analysis.

To test the agreement between the LEP data and the Standard Model, a fit to the LEP data (including the LEP-II  $m_W$  and  $\Gamma_W$  determinations) leaving the top quark mass and the Higgs mass as free parameters is performed. The result is shown in Table 16.2, column 1. This fit shows that the LEP data predicts the top mass in good agreement with the direct measurements. In addition, the data prefer an intermediate Higgs-boson mass, albeit with very large errors. The strongly asymmetric errors on  $m_H$  are due to the fact that to first order, the radiative corrections in the Standard Model are proportional to  $\log(m_H)$ .

The data can also be used within the Standard Model to determine the top quark and W masses indirectly, which can be compared to the direct measurements performed at the  $p\bar{p}$  colliders and LEP-II. In the second fit, all LEP and SLD results in Table 16.1, except the measurements of  $m_W$  and  $\Gamma_W$ , are used. The results are shown in column 2 of Table 16.2. The indirect measurements of  $m_W$  and  $m_t$  from this data sample are shown in Figure 16.2, compared with the direct measurements. Also shown are the Standard Model predictions for Higgs masses between 114 and 1000 GeV. As can be seen in the figure, the indirect and direct measurements of  $m_W$  and  $m_t$  are now in good agreement, and both sets prefer a low value of the Higgs mass.

For the third fit, the direct  $m_t$  measurement is used to obtain the best indirect determination of  $m_W$ . The result is shown in column 3 of Table 16.2 and in Figure 16.3. Also here, the indirect determination of W boson mass  $80.380 \pm 0.023$  GeV is in agreement with the combination of direct measurements from LEP-II and  $p\bar{p}$  colliders of  $m_W = 80.426 \pm 0.034$  GeV. For the next fit, (column 4 of Table 16.2 and Figure 16.4), the direct  $m_W$  and  $\Gamma_W$  measurements from LEP and  $p\bar{p}$  colliders are included to obtain  $m_t = 178_{-8}^{+11}$  GeV, in very good agreement with the direct measurement of  $m_t = 174.3 \pm 5.1$  GeV. Compared to the second fit, the error on  $\log m_H$  increases due to effects from higher-order terms.

Finally, the best constraints on  $m_H$  are obtained when all data are used in the fit. The results of this fit are shown in column 6 of Table 16.2 and Figure 16.5. While the  $\chi^2/\text{d.o.f.}$  increases by 8.8 units for the additional degree of freedom due to the NuTeV result, the fit results themselves are rather stable when excluding this measurement, as shown in column 5. In Figure 16.5 the observed value of  $\Delta\chi^2 \equiv \chi^2 - \chi^2_{\min}$  as a function of  $m_H$  is plotted for the fit including all data. The solid curve is the result using ZFITTER, and corresponds to the last column of Table 16.2. The shaded band represents the uncertainty due to uncalculated higher-order corrections, as estimated by TOPAZ0 and ZFITTER. Compared to previous analyses, its width is enlarged towards lower Higgs-boson masses due to the effects of the complete fermionic two-loop calculation of  $m_W$  discussed above. The 95% confidence level upper limit on  $m_H$  (taking the band into account) is 211 GeV. The 95% C.L. lower limit on  $m_H$  of 114.4 GeV obtained from direct searches [309] is not used in the determination of this limit. Also shown is the result (dashed curve) obtained when using  $\Delta\alpha_{\text{had}}^{(5)}(m_Z^2)$  of Reference 305.

In Figures 16.6 to 16.9 the sensitivity of the LEP and SLD measurements to the Higgs mass is shown. Besides the measurement of the W mass, the most sensitive measurements are the asymmetries, *i.e.*,  $\sin^2 \theta_{\text{eff}}^{\text{lept}}$ . A reduced uncertainty for the value of  $\alpha(m_Z^2)$  would therefore result in an improved constraint on  $\log m_H$  and thus  $m_H$ , as already shown in Figures 16.1 and 16.5. Given the constraints on the other four Standard Model input parameters, each observable is equivalent to a constraint on



the mass of the Standard Model Higgs boson. The constraints on the mass of the Standard Model Higgs boson resulting from each observable are compared in Figure 16.10. For very low Higgs-masses, these constraints are qualitative only as the effects of real Higgs-strahlung, neither included in the experimental analyses nor in the SM calculations of expectations, may then become sizeable.

	- 1 - LEP including LEP-II $m_W$ , $\Gamma_W$	- 2 - all Z-pole data	- 3 - all Z-pole data plus $m_t$	- 4 - all Z-pole data plus $m_W$ , $\Gamma_W$	- 5 - all data except NuTeV	- 6 - all data
$m_t$ [GeV]	$180^{+13}_{-11}$	$171^{+11}_{-9}$	$173.6^{+4.7}_{-4.6}$	$178^{+11}_{-8}$	$175.1^{+4.4}_{-4.3}$	$174.0^{+4.5}_{-4.4}$
$m_H$ [GeV]	$205^{+331}_{-121}$	$81^{+107}_{-40}$	$99^{+64}_{-40}$	$105^{+142}_{-55}$	$87^{+53}_{-34}$	$91^{+58}_{-37}$
$\log(m_H/\text{GeV})$	$2.31^{+0.42}_{-0.39}$	$1.91^{+0.37}_{-0.30}$	$1.99^{+0.22}_{-0.23}$	$2.02^{+0.37}_{-0.32}$	$1.94^{+0.21}_{-0.22}$	$1.96^{+0.21}_{-0.23}$
$\alpha_S(m_Z^2)$	$0.1199 \pm 0.0030$	$0.1186 \pm 0.0027$	$0.1187 \pm 0.0027$	$0.1185 \pm 0.0027$	$0.1184 \pm 0.0027$	$0.1185 \pm 0.0027$
$\chi^2/\text{d.o.f.} (P)$	11.4/9 (25%)	14.8/10 (14%)	14.9/11 (19%)	16.6/12 (17%)	16.7/14 (27%)	25.5/15 (4.4%)
$\sin^2 \theta_{\text{eff}}^{\text{lept}}$	$0.23165$ $\pm 0.00018$	$0.23145$ $\pm 0.00016$	$0.23145$ $\pm 0.00016$	$0.23138$ $\pm 0.00015$	$0.23137$ $\pm 0.00015$	$0.23142$ $\pm 0.00015$
$\sin^2 \theta_W$	$0.22313$ $\pm 0.00053$	$0.22313$ $\pm 0.00063$	$0.22299$ $\pm 0.00045$	$0.22261$ $\pm 0.00045$	$0.22270$ $\pm 0.00037$	$0.22287$ $\pm 0.00036$
$m_W$ [GeV]	$80.373 \pm 0.027$	$80.373 \pm 0.032$	$80.380 \pm 0.023$	$80.399 \pm 0.023$	$80.395 \pm 0.019$	$80.386 \pm 0.019$

Table 16.2: Results of the fits to: (1) LEP data alone, (2) all Z-pole data (LEP-1 and SLD), (3) all Z-pole data plus direct  $m_t$  determinations, (4) all Z-pole data plus direct  $m_W$  and direct  $\Gamma_W$  determinations, (5) all data (including APV) except NuTeV, and (6) all data. As the sensitivity to  $m_H$  is logarithmic, both  $m_H$  as well as  $\log(m_H/\text{GeV})$  are quoted. The bottom part of the table lists derived results for  $\sin^2 \theta_{\text{eff}}^{\text{lept}}$ ,  $\sin^2 \theta_W$  and  $m_W$ . See text for a discussion of theoretical errors not included in the errors above.

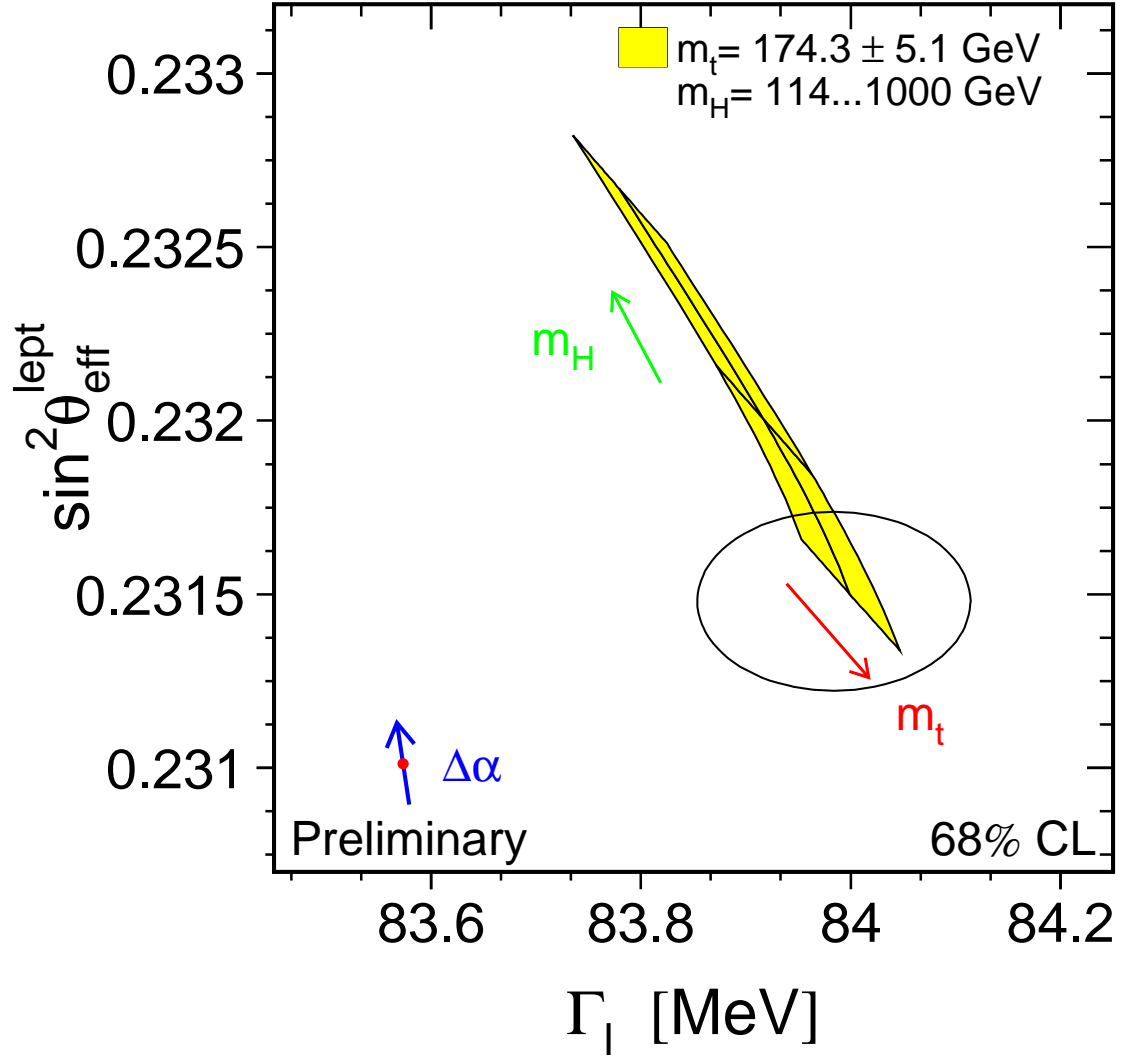


Figure 16.1: LEP-I+SLD measurements of  $\sin^2 \theta_{\text{eff}}^{\text{lept}}$  (Table 15.4) and  $\Gamma_{\ell\ell}$  (Table 2.4) and the Standard Model prediction. The point shows the predictions if among the electroweak radiative corrections only the photon vacuum polarisation is included. The corresponding arrow shows variation of this prediction if  $\alpha(m_Z^2)$  is changed by one standard deviation. This variation gives an additional uncertainty to the Standard Model prediction shown in the figure.

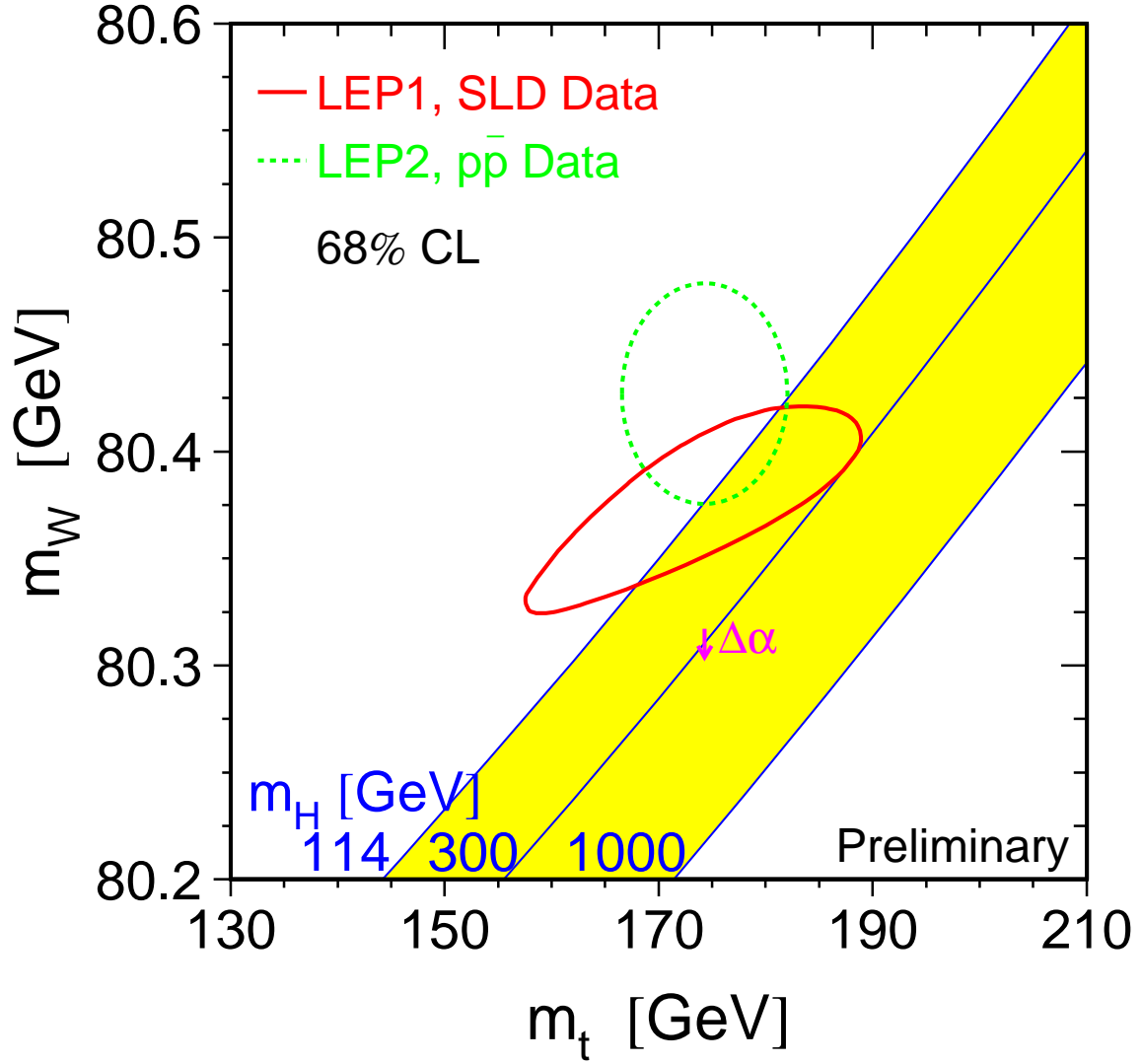


Figure 16.2: The comparison of the indirect measurements of  $m_W$  and  $m_t$  (LEP-I+ SLD data) (solid contour) and the direct measurements ( $p\bar{p}$  colliders and LEP-II data) (dashed contour). In both cases the 68% CL contours are plotted. Also shown is the Standard Model relationship for the masses as a function of the Higgs mass. The arrow labelled  $\Delta\alpha$  shows the variation of this relation if  $\alpha(m_Z^2)$  is changed by one standard deviation. This variation gives an additional uncertainty to the Standard Model band shown in the figure.